2014

Tensile Strength of Automotive Aluminum Joints Using Resistance Spot Welding, Self-Piercing Riveting and Adhesive Hybrid Joining

Luca Bertin
University of Windsor

Tensile Strength of Automotive Aluminum Joints Using Resistance Spot Welding, Self-Piercing Riveting and Adhesive Hybrid Joining

By

Luca Bertin

A Thesis
Submitted to the Faculty of Graduate Studies
through the Department of Mechanical, Automotive and Material Engineering
in Partial Fulfillment of the Requirements for
the Degree of Master of Applied Science
at the University of Windsor

Windsor, Ontario, Canada

2014

Tensile Strength of Automotive Aluminum Joints Using Resistance Spot Welding Self-Piercing Riveting and Adhesive Hybrid Joining

by

Luca Bertin

APPROVED BY:

_____

V. Stoilov
Department of Mechanical, Automotive and Material Engineering

_____

R. Bowers
Department of Mechanical, Automotive and Material Engineering

_____

J. Sokolowski, Advisor
Department of Mechanical, Automotive and Material Engineering

September 11, 2014

DECLARATION OF ORIGINALITY

I hereby certify that I am the sole author of this thesis and that no part of this thesis has been published or submitted for publication.

I certify that, to the best of my knowledge, my thesis does not infringe upon anyone's copyright nor violate any proprietary rights and that any ideas, techniques, quotations, or any other material from the work of other people included in my thesis, published or otherwise, are fully acknowledged in accordance with the standard referencing practices. Furthermore, to the extent that I have included copyrighted material that surpasses the bounds of fair dealing within the meaning of the Canada Copyright Act, I certify that I have obtained a written permission from the copyright owner(s) to include such material(s) in my thesis and have included copies of such copyright clearances to my appendix.

I declare that this is a true copy of my thesis, including any final revisions, as approved by my thesis committee and the Graduate Studies office, and that this thesis has not been submitted for a higher degree to any other University or Institution.

ABSTRACT

Increasing public demand for better fuel economy has led the automotive industry to use more aluminum components in vehicles. The present study deals with the problem of joining aluminum structural panels and examines the tensile test results of resistance spot welded and self-pierced riveted aluminum joints. It investigates the effect of combining these two technologies with the adhesive bonding technology, resulting in "hybrid joints". A "peak-by-peak" analysis approach assesses the relative contribution of each joining element to the overall performance of the joint. Stress analysis was performed to define the failure criteria for the joining elements; tentative engineering design rules are proposed. The impact of the presence of adhesive on the spot welding and riveting process has been evaluated. Optimal joining solutions are recommended.

DEDICATION

To my friend Piero Gorgi

ACKNOWLEDGEMENTS

The present work is the final outcome of a year of intense work during which I had the pleasure and the honor to work with many different people.

My biggest thanks have to go to Dr Al Conle, who guided me throughout every day work and who was instrumental in this challenging industrial research. I would like to thank my academic advisor, Dr. Jerry Sokolowski, and my committee members, Dr. Vesselin Stoilov and Dr. Randy Bowers, for the guidance they provided to me during my research. Special thanks also go to my advisor from the Politecnico di Torino Prof. Massimo Rossetto.

I wish to acknowledge the help in gathering the experimental data provided to me by my industrial tutor, Mr. Kurt Damphousse, and his colleagues from the Chrysler Technical Center, Alex Trinick from Henrob and Steve Davis from Sika.

At the end of this experience, I am glad to say that I have had fantastic people to share this year with. I thank my friends, Ashley, Fede, Fo, Giuse, Marc, Kyle, Liuk, Pheeb, Tom and Antonio for making this experience unforgettable.

I also want to thank my girlfriend Roberta, who never stopped believing in me and who made me feel like she was standing by my side even though she was 6897 km away.

Finally, big thanks go to my parents for allowing me to take part in this experience and for their continuous support.

Last but not least, I am grateful to the entire nation of Canada and its friendly people for having hosted me for an entire year and having taught me the beauty of wild nature and the passion for hockey (Go Leafs Go!), the deliciousness of maple syrup and the joyfulness of country music.

TABLE OF CONTENTS

LIST OF TABLES

LIST OF FIGURES

LIST OF ABBREVIATIONS/SYMBOLS

AW	Arc welding
CJ	Coach joint
CT	Cross-tension
EBW	Electron beam welding
EPA	US Environment Protection Agency
FEM	Finite element method
FSW	Friction-stir welding
HAZ	Heat affected zone
HV	Vickers hardness
LBW	Laser beam welding
LJ	Lap joint
NVH	Noise, Vibration, and Harshness
NA	No-Adhesive samples
OFW	Oxyfuel gas welding
RW	Resistance welding
RSW	Resistance spot welding
SPR	Self-piercing riveting
SSPR	Single-sided piercing rivet

NOMENCLATURE

d	Weld nugget diameter
d_{cr}	Critical weld nugget diameter
d_e	Rivet external diameter
d_i	Rivet internal diameter
F	Tensile testing load
I	Electric current
k	Corrective coefficient for evaluation of the effecting load carrying area, SPR joints
K	Rivet head flushness
Q	Heat released
R	Electrical Resistance
R_h	Reaction force SPR lap joints, head side
R_t	Reaction force SPR lap joints, tail side
t	Thickness of the aluminum blank
Δt	Minimum sheet thickness in a riveted joint
Δx	Minimum interlock in a riveted joint

Greek Symbols

σ_x	Normal stress in the x direction
σ_y	Normal stress in the y direction; peeling stress
σ_{cj}	Radial normal stress at the weld nugget, coach joint
σ_{ct}	Radial normal stress at the weld nugget, cross tension joint
σ_{lj}	Radial normal stress at the weld nugget, lap joint
σ_f	True ultimate fracture stress
σ_r	Normal compressive stress, SPR joints

σ_{RSW}	Plasticity corrected stress using Neuber method
$\overline{\sigma}$	Equivalent axial stress
τ_{lj}	Circumferential shear stress at the weld nugget, lap joint
τ_r	Shear stress, SPR joint
τ_{yx}	Shear stress in the x direction; shear stress in the adhesive layer

Chapter 1
Introduction

The current economic crisis is changing the scenario of the automotive world, steering research and development in a direction that began after the second Oil Crisis in the late 1970s. The performance measures that are becoming most desired by customers are no longer great acceleration, high speed and good handling, but rather low fuel consumption and low emission of pollutants and greenhouse gases. In addition, most of the main North American car manufacturers have adopted the US EPA target to increase the mileage of passenger cars and light duty trucks to 54.5 miles per gallon (23.2 km/l) by model year 2025 (Figure 1-1) [1].

Extensive modifications will be required in the design of new vehicles to achieve this highly demanding target. Simple improvement of the engine efficiency will not be enough to meet the requirement; modification of the vehicle body to improve the aerodynamic performance, and light-weighting strategies are needed.

The replacement of steel with aluminum plays a very important role. At 2,700 kg/m^3, the density of aluminum is one third that of steel. It must be specified, however, that due to the lower strength and stiffness of aluminum, aluminum components require a higher gauge thickness to carry the same load. This thickness increase does not overshadow the much lower density of aluminum and an overall 50% weight reduction can be achieved [2].

The material conversion process entails numerous challenges. This thesis will investigate an optimal solution for the joining process of aluminum alloy structural panels.

Resistance spot welding (RSW) has dominated joining of structural steel panels in the automotive industry due to its flexibility and cost effectiveness. On average, a car has about 5000 RSW joints [3]. However, RSW of aluminum alloys shows some difficulties related to the thermal and electrical properties of the material and to the presence of a tenacious oxide layer present on the blank surface.

The Self-Piercing Riveting (SPR) process was originated more than 50 years ago but is only lately growing in importance. One of the main characteristic of SPR is its ability to join both aluminum to aluminum, and aluminum to other materials. Both research and industry are increasing their attention to this technology as a joining process alternative to RSW.

Adhesive bonding is probably the most versatile solution, allowing the joining not just of aluminum components but also of components with great differences in thermal and electrical properties or in ductility. Also, adhesive bonding allows for a wider load distribution over the load transfer area and a reduction of load concentrations [4]. Additionally, adhesive joints are characterized by good stiffness and fatigue resistance and thus are often the preferred choice for tackling problems like torsional rigidity and NVH.

Adhesive bonding can be combined with RSW or SPR, to form *hybrid joints*. These joints can potentially combine all of the advantages of the two joining methods and overcome some of the issues related to adhesive bonding, e.g. the need for fixtures to hold the joint before and during the curing process of the adhesive layer.

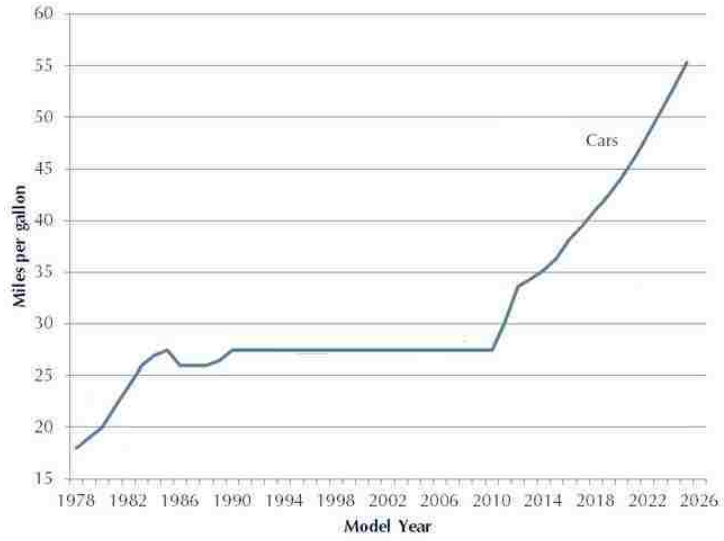

Figure 1-1. Fuel economy standard for passenger vehicles from MY 1978-2025 [1]

1.1 Thesis Objectives

The main objective of the present work is to analyze and compare the mechanical performance of RSW and SPR aluminum joints and to investigate the impact of the addition of adhesive to form hybrid joints. This study evaluates tensile test experiments that were designed and carried out at Chrysler LLC. The following outcomes have to be achieved:

1. Interpretation of the tensile test results, which included the undertaking of some additional tensile tests for clarification.
2. Determination of a suitable method for processing the data gathered from the tensile tests.

3. Analysis and comparison of obtained results and the definition of an optimal joining solution.
4. Investigation of the possibility of inferring a failure criterion for the studied joints.
5. Analysis of the impact of the presence of the adhesive layer on the RSW and the SPR process in the hybrid joints.

Chapter 2
Literature Review

Joining of two or more components can be accomplished by means of three different fundamental forces: physical forces, mechanical forces and chemical forces. The three main joining techniques based on these forces are in order: welding, mechanical joining and adhesive bonding [4].

2.1 Welding

Welding can be defined as the process of joining two or more components together by making their surfaces coalesce. About 50 different welding technologies are currently catalogued by the American Welding Society; these processes can be grouped into two main categories: fusion welding and solid state welding [5].

In fusion welding heat is supplied to the welded components causing their local melting and coalescence. The supply of heat is often combined with the application of pressure to keep the components in the proper position. The four most important fusion welding techniques are arc welding (AW), resistance welding (RW), oxyfuel gas welding (OFW) and laser and electron beam welding (LBW, EBW). In Solid state welding the coalescence of the components is achieved with the application of pressure only or with a combination of pressure and heat. The most used technique is the friction-stir welding (FSW).

The heat generated during a fusion welding process induces a modification of the microstructure of the parent material. Four different areas of a fusion welded joint can be recognized (Figure 2-1):

- Fusion zone: in this zone the melting of the material takes place; the subsequent solidification is usually characterized by a fast cooling, that leads to the formation of a fine as-cast structure; the control of the grain size is of critical importance for the resulting mechanical properties of this area [4]. In case a filler material is used the chemical composition of this region will differ from the parent material and will be a combination of the latter and the material of the filler. Similar considerations apply for welding two dissimilar materials, where the composition of the weld pool or nugget is a combination of the compositions of the two parent materials.

- Transition Zone: the transition zone is a narrow band in between the fusion zone and the heat affected zone. In this area the material is partially molten for a time short enough to prevent any mixing of the materials; thus its chemical composition is the same as the base material.
- Heat Affected Zone (HAZ): The metal in this area does not receive enough heat to reach its melting point but rather just to give rise to a series of thermally activated processes like modifications of the grain structure (recovery and recrystallization) and a re-distribution of alloying elements inside the material matrix via mechanisms of segregation and precipitation. Thus even if the chemical composition of the HAZ is the same as the base metal the heat treatment caused by the welding process can cause modifications in its properties and structure.

At a sufficient distance from the fusion zone the material is not affected at all by the welding process. The extent of these various zones and the severity of the modification in properties and metallurgy of the HAZ is function of the amount of heat supplied, the extension in time of exposure to the peak temperature, the metal thermal properties, and the cooling rate.

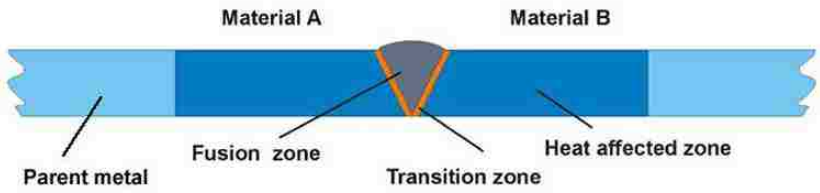

Figure 2-1. Characteristic zones of a fusion welded joint [6]

2.1.1 Resistance welding

Resistance welding is a fusion welding process in which two overlapped metal sheets are clamped between two highly-conductive electrodes (Figure 2-2); a large current is forced through the metal in a very short time, causing its heating and melting and thus allowing the coalescence of the two surfaces; this behavior is described by the Joule's law

$$Q = RI^2t \tag{2.1}$$

Where: Q is the heat released, R is the total electrical resistance, I is the current and t is the time during which the current flows.

Equation 2.1 contains in itself both two of the most important parameters used to control the process (current and time) and the main cause of variability of the process, namely the resistance. Due to Aluminum's high electrical conductivity (about three times better than steel), usually the highest contribution to the total resistance of the system is given by the contact resistance at the faying surfaces; It can be said so that resistance spot welding is a surface-critical process [4]. Figure 2-3 shows the trend of electrical resistivity for each component in the stack, highlighting both the bulk resistance and the contact resistance between each two adjacent components. It can be seen that copper electrodes have the lowest value of electrical resistance while the highest value is reached at the contact surface between the two aluminum blanks. The most-right portion of Figure 2-3 shows the trend of the temperature when the current is forced though the stack. In accordance with Equation 2.1 the areas of high electrical resistivity corresponds with the areas of high temperature and vice versa. The trend shown in Figure 2-3 is highly desirable since it allows reaching the melting temperature of the metal and starting the nugget formation at the faying surfaces without overheating the electrodes.

Another important control parameter is the clamping force. Even though the main goal of the clamping force is simply to hold properly the component to be welded, it has been shown by many authors that it contributes in controlling the phenomenon of expulsion (and thus allowing a much wider process window [7]). The phenomenon of expulsion consists in the ejection (or expulsion) of molten metal from the weld nugget (Figure 2-4) and it is usually caused by an excessive heat generation or an insufficient clamping force. Additionally, an increase in the clamping force causes a reduction the electrical resistance at the faying surfaces [8, 9]. Even though it might seem to contradict what was previously said, this reduction due to the applied force can be beneficial for the process itself; the surface electrical resistance is in fact influenced by the surface condition of the blank. The surface condition is often highly variable and the surface resistance becomes one of the biggest sources of variability and one of the most difficult parameters to control in the process of resistance welding. By increasing the clamping force and thus reducing the surface resistance the process will depend more on the bulk resistance of the material, whose value is approximately constant. It this way the robustness of the process can be increased [9].

A very useful representation often used when studying the resistance welding process is the *weld lobe diagram* (Figure 2-5): it represents the ranges of current and weld time for obtaining a proper, acceptable weld for a fixed electrode clamping force. From Equation 2.1 it can be easily understood that increasing the welding current and time the quantity of heat generated increases and so does the quantity of metal molten during the process. A higher current supplied for a longer time creates a bigger weld nugget.

In the weld lobe diagram the two boundaries for the weld spot to be considered acceptable are the expulsion condition on the upper side and the minimum nugget size on the lower side. The minimum size for the weld nugget to be considered acceptable is usually equal to 4 times the square root of the gauge of the thinnest sheet [10].

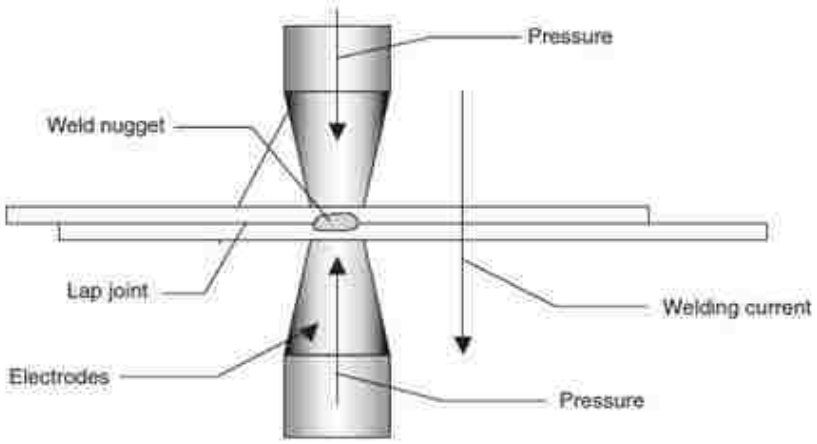

Figure 2-2. Basic scheme of spot welding process [4]

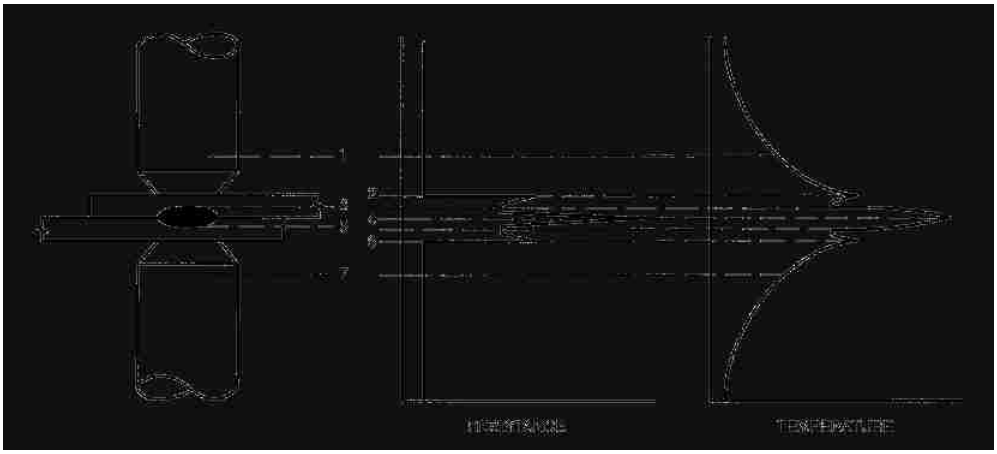

Figure 2-3. Trend of electrical resistance and temperature in the various components during RSW [11]

Figure 2-4. Expulsion of molten metal from a weld nugget [10]

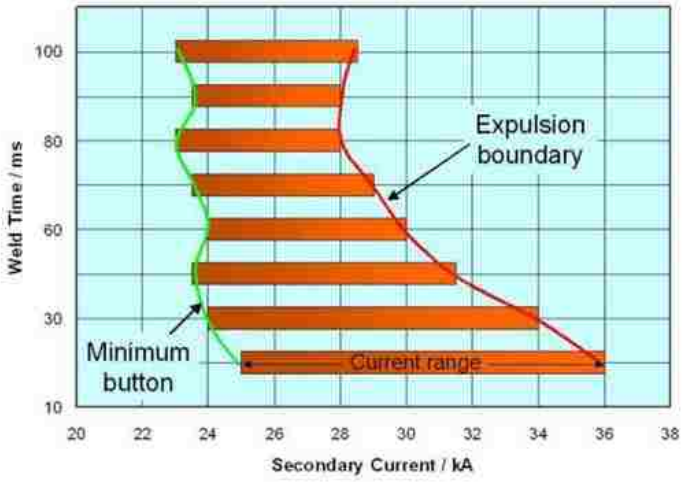

Figure 2-5. Weld lobe diagram [10]

2.1.1.1 Resistance welding of aluminum alloys

Aluminum is characterized by an excellent electrical conductivity, about three times higher than steel; for this reason a very high value of current is necessary while the welding time is usually shorter compared to steel welding (in Table 2-1 are summarized some typical welding parameters for steel and aluminum). In Section 2.1.1 it has been explained that the surface resistance at the blank's faying surfaces is usually dominant in the resistance welding process; when welding aluminum alloys this behavior is further exacerbated by the low bulk resistance of the material and the total electrical resistance of the system is almost only given by the contact resistance at the faying surfaces. An important role is thus played by the layer of aluminum oxide present at the surface of the Al blank; being highly insulating and with a high melting temperature, and being often present in a broken/non uniform status, it causes inhomogeneity in the surface resistance and consequently in the current distribution and heat generation [12]. For this reason the American Welding Society's Welding Handbook [9]

recommends removing the oxide layer and performing the welding process shortly after (8-48 hours) in order to avoid excessive re-oxidation.

Together with the necessity for a considerably high value of current, another characteristic that makes the RSW of aluminum blanks more difficult compared to steel is the reduced life of the electrodes. Copper (the material usually used for the electrodes) easily alloys with aluminum, thus wearing out very rapidly and causing not only high replacement costs, but also lower welding quality.

Table 2-1. Some typical welding parameters for steel and aluminum [10]

0.9 mm Gauge	Bare Aluminum (AA6111)	Bare Steel
Weld Time (50Hz Cycles)	3	7-10
Current Range (kA)	18.0 – 23.0	7.0 – 10.0
Force (kN)	4.1 – 5.0	1.9 – 2.6

2.1.1.2 Weldability and Welding defects

The ability of a particular component to be welded takes the name of weldability; ideally, the properties of the *weldment* (the entire joint, made of the set of the parent metals, the heat affected zone and the weld metal) should be the same as the ones of the parent metal. Actually this is usually not achievable, due to the following:

- Reduction in strength in the heat affected zone (HAZ): since RSW is one of the typologies of fusion welding all the considerations previously made apply also in this case and an annular HAZ can be observed around the nugget. In particular, the annealing effect of the welding process on the HAZ has a detrimental impact on the strength and hardness of cold-worked and solution treated alloys while it has little effect when the welded base material is in as-cast or fully annealed condition.
- Hot cracking and hot tearing: The main issue that could be encountered in the fusion zone is the hot cracking, also known as solidification cracking. Most of the alloys do not have a precise solidification temperature, but rather a solidification range between liquidus and solidus; the wider this range, the more likely is the formation of cracks during the solidification process.
- Porosity: Hydrogen solubility in molten aluminum is much higher compared to solid aluminum (about 20 times higher). This can lead to porosity problems in the molten

area during solidification. The excess of gas in the solid is released and forms pores which influence the strength of the material (Figure 2-6).

- Presence of the Oxide film: As explained in the previous paragraphs the presence of a layer of aluminum oxide on the blank surface is one of the main causes of variability of the surface resistance. In addition the oxide layer on the surface of the blank is hydroscopic and tends to absorb the ambient moisture; thus it can be a possible source of hydrogen that will in turn cause porosity in the weld nugget.

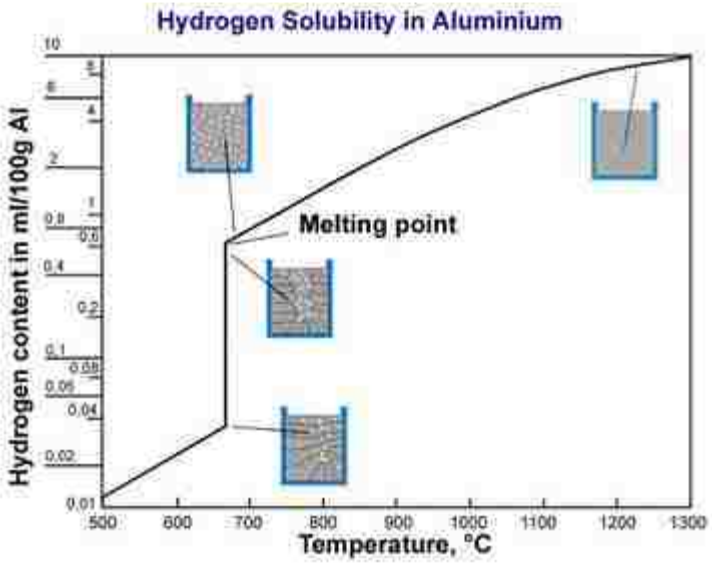

Figure 2-6. Hydrogen Solubility in Aluminum [6]

2.2 Riveting

Mechanical fastening consists in joining two or more components by means of discrete piece of hardware, call the fastener [5]. Fasteners are usually divided into two main categories: threaded and unthreaded fasteners. Screw bolts and nuts belong to the first category while rivets belong to the second.

Beside the difference on the piece of hardware itself, one of the main characteristics differentiating rivets from the vast majority of the threaded fasteners lies on the irreversibility of the riveting process; a rivet in fact is headed pin that after being inserted in a pre-drilled hole is deformed ("upset") to create the desired mechanical interlocking. This upsetting process can be either a cold or a hot working process. After the upsetting process the joint cannot be dismounted in a non-destructive way.

In Figure 2-7 the most common types of rivets are shown.

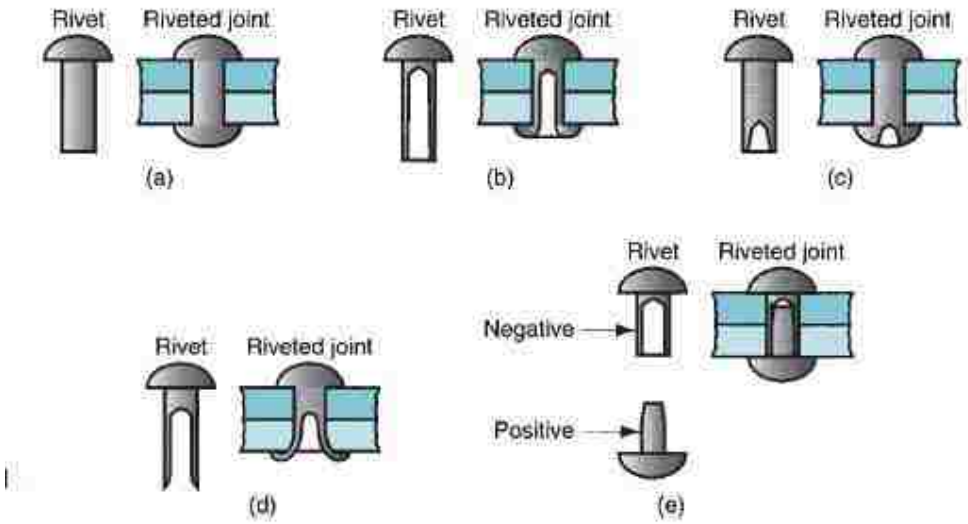

Figure 2-7. Main typologies of rivets [5] (a) solid rivet, (b) tubular rivet, (c) semi-tubular rivet, (d) bifurcated and (e) compression rivet [5]

2.2.1 Self – piercing riveting (SPR)

Self-pierce riveting is a cold forming process used to joint two or more layers of material by driving a semicircular rivet (usually made of steel) through the upper sheet, piercing (not perforating) the bottom sheet and flaring the rivet skirt under the guidance of a suitable die [13] [14] (Figure 2-8). Since there is no need to pre-drill any hole the process complications due to possible misalignments are eliminated.

The main parameters usually considered to assess the physical properties of a self-pierced riveted joint are the interlock and the minimum thickness (Figure 2-9). The interlock Δx is the horizontal distance between the outermost point on the tip of the rivet leg and the point where the same rivet leg has pierced through the top sheet. The interlock is the main responsible for the mechanical strength of the joint. The minimum thickness Δt is measured at the point where the greatest thinning of the lower sheet has happened and its location can vary. A minimum sheet thickness is necessary to guarantee the complete insulation of the rivet legs from any external agent thus preventing it from corroding. A commonly suggested minimum value for Δt is 0.2mm [15].

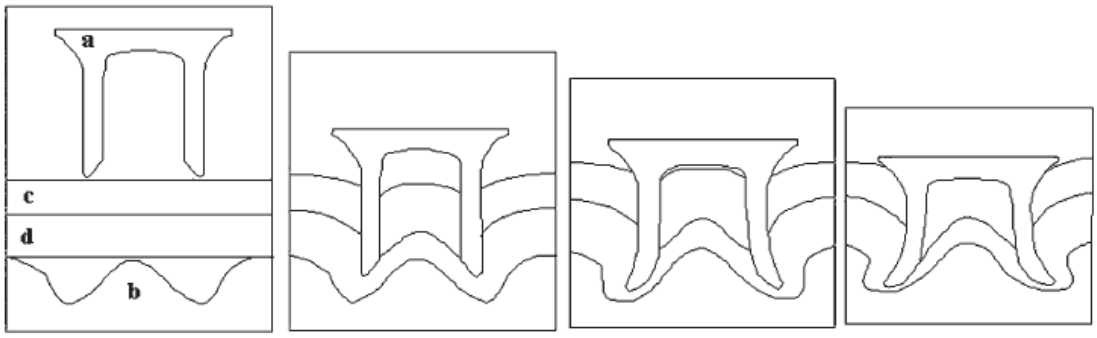

Figure 2-8. Schematic representation of riveting process. On the left-most side of the figure: (a) rivet, (b) and (c) sheet metals and (d) die [14]

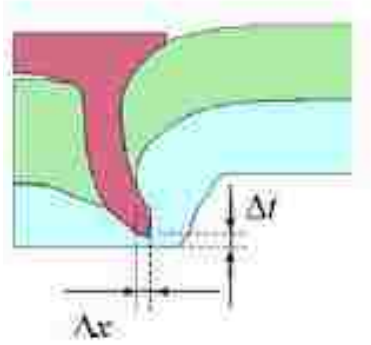

Figure 2-9. Interlock and minimum thickness [16]

2.2.1.1 Design of a riveting process

In the design of a self-riveting process the material to be riveted and the thickness of the stack need to be analyzed first. In this regard two basic rules have to be met [15];

- The bottom sheet of the stack needs to be ductile enough to allow the rivet flaring. An elongation greater than 15% is generally recommendable.
- The ratio between the thickness of the two sheets (usually referred as thin-to-thick ratio or thick-to-thin ratio depending on whether the thicker sheet is at the bottom or at the top) should be carefully chosen. It is usually advised to use a thicker material for the bottom sheet, so as to allow a sufficient flaring of the rivet skirt. In case the joint design mandates that the top sheet has to be thicker, the thinner sheet must exceed 33% of the total joint thickness [15].

When designing the rivet joint five variables are to be considered (Figure 2-10) [15];

- Rivet diameter: the two most common diameter dimensions are 3 mm and 5 mm. 3 mm rivets are usually used for non-structural joints.

- Rivet length: the rivet length has to be selected as function of the stack thickness. As a general rule usually the length is 3 mm longer than the total stack thickness. Shorter rivets can be selected when the top sheet is thicker than the bottom one or when the flaring is restrained by the limited ductility of the bottom sheet or the die profile. Vice versa a thick and ductile bottom sheet allows the use of a longer rivet.
- Rivet hardness: the rivet hardness must be chosen as function of the material hardness; the harder the material the harder the rivet needed. In addition, the longer the rivet the higher the rivet hardness required to retain the columnar strength of the legs. Usually boron-alloyed steels are used for rivets since the hardness can be properly controlled by means of a heat treatment.
- Die diameter: should be selected in accordance with the rivet length. In general the volume of the die should match with the volume of the rivet.
- Die profile: the die profile is chosen in accordance with the ductility of the bottom material; the lower the material ductility, the shallower the die profile used.

When these five variables are properly considered a joint close to ideal joint is obtained (Figure 2-11). It can be seen that an ideal self-pierced riveted joint is characterized by a good contact between head and surface of the sheet, a symmetrical flaring of the rivet legs that lock into the bottom sheet without cracking and the complete encapsulation of the bottom sheet in the joint button.

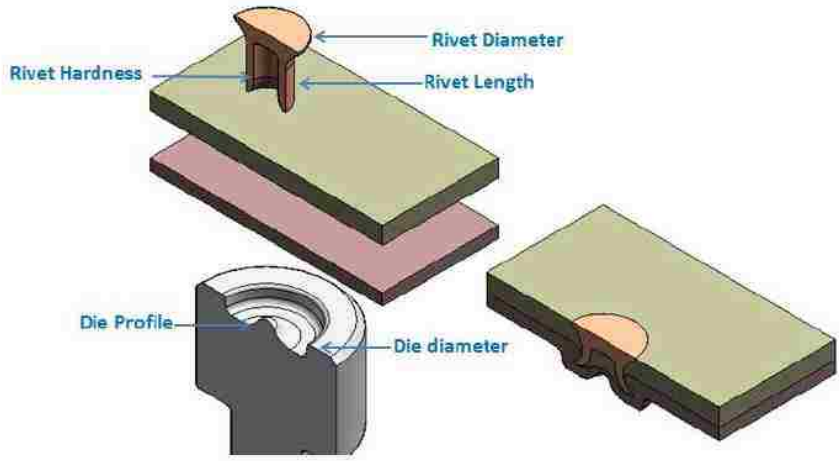

Figure 2-10. Most important variables in the riveting process [15]

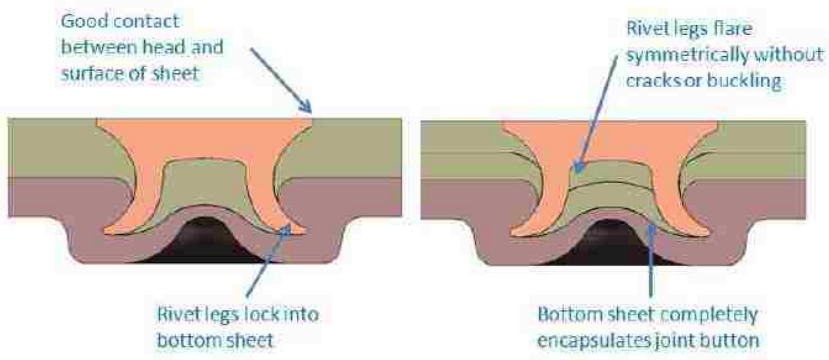

Figure 2-11. Main Characteristics of an ideal riveted Joint [15]

2.2.1.2 Self-piercing riveting of Aluminum

The self-pierce riveting process is almost completely independent from the surface condition (as long as the material hardness or ductility is not influenced) and does not depend on the electrical and thermal conductivity of the joined material. All the main issues listed for the RSW process are thus virtually eliminated with SPR. In addition the relatively good ductility and low hardness of aluminum make it a material highly suitable for being joined with the SPR technology.

One of the main concerns related with the riveting of aluminum joints is represented by the galvanic corrosion; as mentioned before the vast majority of the rivets are made of steel. Consequently a protective coating has to be applied to the rivet to avoid the onset of galvanic corrosion.

Hoang et al. [16] studied the possibility of substituting steel rivets with aluminum rivets. They compared both numerically and experimentally the mechanical behavior of aluminum T-joints riveted with steel and with aluminum rivets; they noticed that the strength of the two types of riveted joints is comparable while the elongation obtained at joint failure is much higher for the steel rivets. The authors justified these results by explaining that aluminum rivets absorb less energy than steel rivets.

2.2.1.3 Joint quality inspection

In the previous paragraphs it has been explained that the most important variables to quantify the quality of a riveted joint are the interlock and the minimum thickness. Unfortunately the only way to directly measure them is to section the rivet, thus destroying permanently the joint [15].

Measuring the variation of the rivet head flushness *("K")* can give important information about the interlock and the minimum thickness [15]. The relationship among these variables is described in Figure 2-12: in the middle is shown an "ideal joint", with the head flush with the blank; on the left it can be seen that a positive value of flushness correlates with a lower penetration of the rivet and thus a reduced interlock while when the rivet is pressed too deeply inside the blank (Figure 2-12 (c)) the minimum sheet thickness reduces to zero.

In addition, a non-proper value of the rivet flushness can cause the following issues

- In case of incomplete rivet penetration (too high rivet head, K_H) the achieved mechanical interlock is reduced (Figure 2-12 (a)).
- An excessive rivet penetration (too low rivet head, K_L) is often associated with a "coining effect of the top sheet" which may cause premature failure, and a reduced value of minimum thickness.

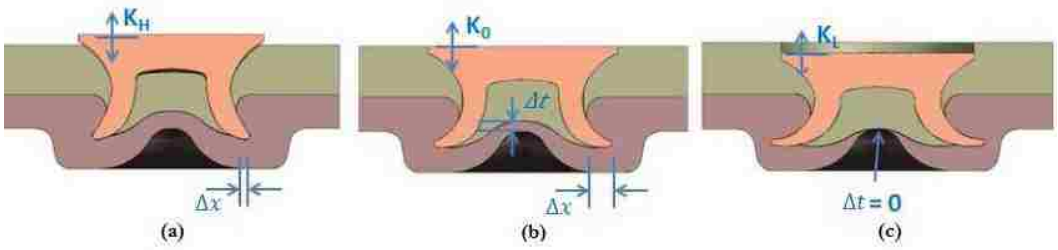

Figure 2-12. Relationship between rivet head flushness and minimum thickness and interlock [15]

2.3 Adhesive Bonding

Adhesive bonding is a permanent joining method in which two components (called in this case "adherends") are held together by a filler material, the "adhesive" which is able to create the surface attractive force responsible for the joint effectiveness [4].

2.3.1 Cohesion vs. Adhesion: Forces and Failure Modes

An adhesively bonded joint is characterized by two main forces, namely cohesion force and adhesion force (Figure 2-13). Adhesive force arises between the adhesive and the adherends; on the other side the cohesive force links together the molecules of the adhesive

As in a chain, the final strength is limited by the strength of the weakest link. Thus it can be easily understood the vital importance of both the forces involved.

The failure mode of an adhesive joint strictly relates to the presence of these two different forces simultaneously; two predominant failure modes exist: adhesive failure and cohesive failure [4].

- Cohesive failure results into the separation inside the adhesive itself, and a visible layer of adhesive will be present on both the adherends (Figure 2-14 a).
- Adhesive failure instead is the failure at the interface between adhesive and adherends or at a boundary layer in the proximity of this interface. Bikermann's theory [17] claims that if the bond is properly made it will fail cohesively either inside the adhesive or in the adherends and it will not fail at the interface between the adhesive and the adherent. If adhesive failure happens, it is actually due to the presence of a boundary layer close to the actual interface whose force is much lower. The presence of this layer is due to factors like contamination of the adherends, air trapped inside the bond, weakly attached oxide layer. Thus the presence of adhesive failure usually indicated an inadequate surface preparation [4] [18](Figure 2-14 c).
- More rarely cohesive failure can happen in the adherends; in this case it takes the name of "coherent failure of substrate" (Figure 2-14 b).
- Often both failure mechanisms take place at the same time and the failure is often expressed as a percentage of cohesive or adhesive modes. This failure mode is known as "mixed mode" failure (Figure 2-14 d).

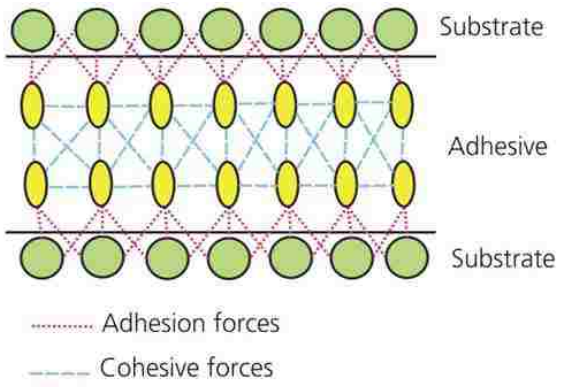

Figure 2-13. Schematic illustration of adhesive and cohesive forces in an adhesively bonded joint [19]

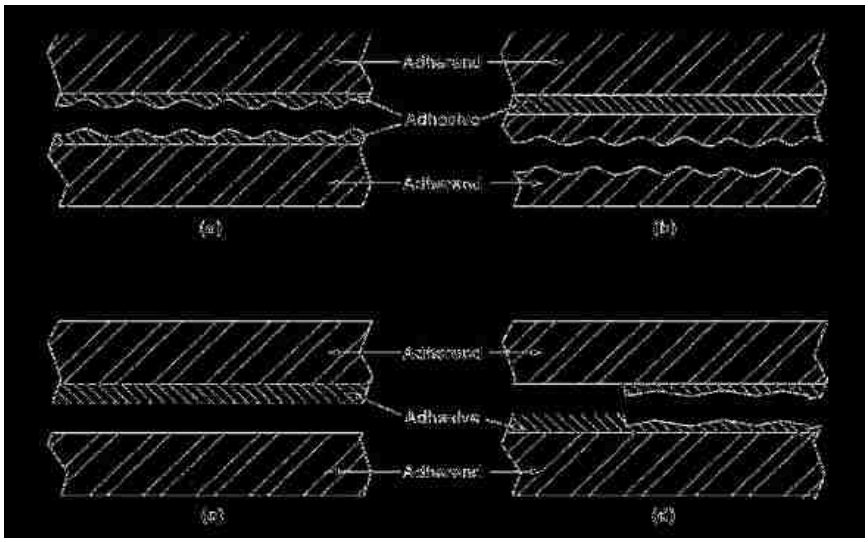

Figure 2-14. Schematic illustration of the most common failure modes in an adhesive joint: (a) cohesive failure, (b) coherent failure of substrate, (c) adhesive failure, (d) mixed mode failure [4]

2.3.2 Curing process

Adhesives are usually applied to the area to be joined in the liquid state. Before they are able to bear any load they have to undergo a chemical process known as a "curing process". During this process the adhesive solidifies and crosslinks, that means that the molecules of the adhesive develop strong covalent bonds responsible for the final strength of the adhesive. Depending on the nature of the adhesive, the curing reaction can be triggered by different factors like pressure, heat, UV light or moisture [20].

The curing process in most of the cases is not instantaneous and requires some time, known as "curing time" or "setting time". The curing time is clearly a big disadvantage for the manufacturing process. One of the most common solutions adopted in the automotive industry is to take advantage of the paint bake process for curing the adhesive with then no need for an additional cycle designed specifically for the adhesive setting. This requires however the use of adhesives with curing temperature and times similar to the paint bake cycle.

2.3.3 Adhesive joint design

The optimal joint design is dictated by the nature of the adhesive and by the geometry of the adherends; it has to be kept in mind that the adhesive is not acting at a single point like a fastener but rather on a surface; thus it is usually desirable to maximize the contact surface [4].

The final strength of a joint is mainly determined by the following factors [4]:

- Joint loading mode (Figure 2-15)
- Joint geometry and dimension
- Mechanical properties of adhesive and adherent
- Presence of impurities
- Extension of the contact area and degree of wetting

Joint loading mode: adhesive joints behave much differently according to the kind of load applied; ordered from the most favorable to the least favorable the joint loading modes that can be found in an adhesive joint are:

- Compression
- Shear
- Tension
- Cleavage
- Peel

Shear load acts parallel to the surface of the joint and distributes over the entire surface area thus leading to optimal performances of the adhesive.

In both peel and cleavage loading the applied load is neither parallel to the plane as in pure shear nor perpendicular to it as in pure tension/compression; in these kinds of load the stress is virtually concentrated on an edge where separation starts. This edge moves "inward" to the joint causing its failure. The main difference between peel and cleavage is that in the former case one or both of the adherends is able to deform causing an even higher stress concentration at the adhesive-adherends interface. When both the adherends are rigid the joint undergoes cleavage stress. A typical case of cleavage stress is induced when an offset tensile load is applied.

The above discussion indicates that the joint geometry should be designed in such a way that the adhesive works in its more favorable condition, namely shear. One of the preferred solutions is thus the lap joint that combines a large application area with a very simple joint design

In the majority of the cases however a unique load mode is not found, but rather a combination of two or more [4]. When a simple lap joint is pulled in a tension test the load path is not aligned with the joining surface and some stress non-uniformities are present;

thus the joint tends to rotate and the loading mode is no more purely shear. In fact the adherends have to withstand both tension and bending while the adhesive is loaded both in shearing and in peeling mode. A mixed stress state thus develops that is a combination of tension stress (perpendicular to the adhesion plane) and shear stress (parallel to the adhesion plane) [21] (Figure 2-16).

Similarly a tensile load can actually induce some degree of peel or cleavage as a consequence of bending of the adherents or asymmetries in the joints [4].

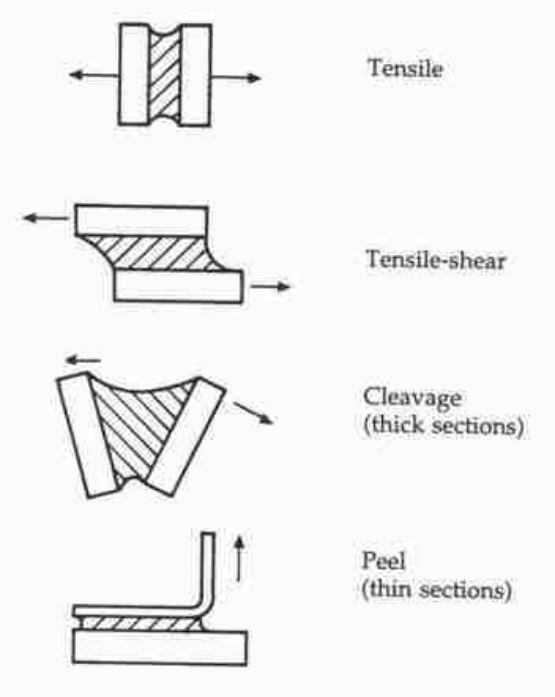

Figure 2-15. Schematic illustration of the most common loading modes [22]

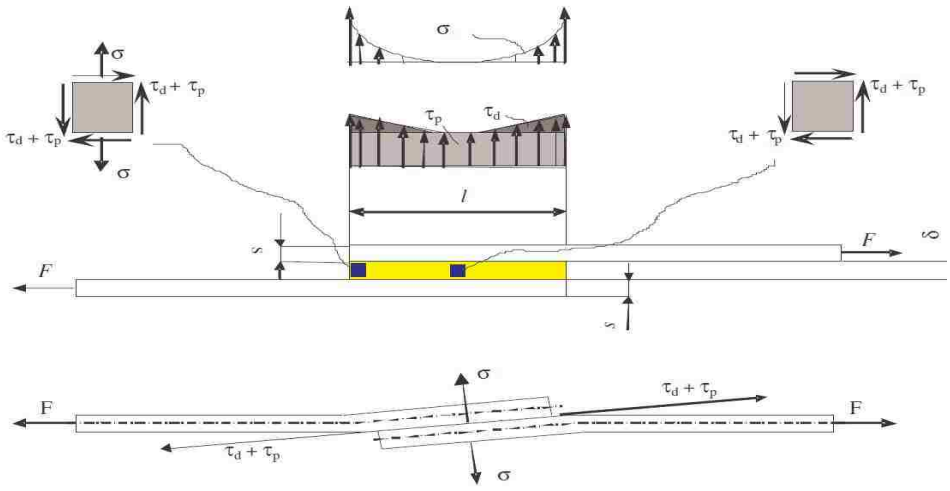

Figure 2-16. Stress distribution in a single lap joint. In addition to the shear stress τ_p due to the moving parts a shear stress component τ_d and a normal peeling stress σ arise respectively due to the deformation of the adherends and the bending moment [21]

2.4 Hybrid Joints

When two materials are joined with both adhesive bonding and RSW or SPR, the joint usually takes the name of "hybrid joint". More specifically the combination of riveting and adhesive bonding is called "rivet-bonding" while when welding is combined with adhesive it is referred as "weld-bonding". Hybrid joints potentially take advantage of all the benefits of each one of the joining method used and at the same time solves the two main problems of adhesive bonded joints; in a hybrid joint in fact the peeling load will be hold mainly by the weld nugget or by the rivet. In addition the nugget/rivet will keep the two components in position preventing any relative motion until the adhesive is completely cured.

Two different techniques exist for the application of the adhesive layer in a spot-welded joint [23]:

- With the flow-in technique the joint is first welded and subsequently the adhesive is applied. This method uses a low viscosity adhesive able to propagate into the narrow cavity at the overlap between the two sheets.
- In weld-through mode the adhesive is applied first and then the welding process takes places. This technique allows for the use of higher viscosity adhesives. It has been reported however that the considerable heat generated by the welding

process can actually degrade the adhesive in a region around the spot weld, thereby decreasing its load bearing capability.

Similar considerations apply to the rivet-bonded joints. In order not to deteriorate the quality of the interlocking only pump-able adhesive should be used [15]; during the riveting process the presence of an excessively rigid adhesive layer can hinder the flaring of the rivet legs and thus decrease the quality of the interlock.

By combining adhesive bonding with welding or riveting the following advantages can be obtained [23] [24] [25] [26] [27] [28]:

- High static strength
- Improved fatigue strength
- Better sealing properties
- Improved corrosion resistance
- Reduced manufacturing costs since no fixture is needed before and during the curing process
- Noise damping capacity

2.5 Evaluation and comparison of welding, riveting and adhesive bonding

In the previous sections of Chapter 2 the characteristics of the welding, riveting and adhesive bonding joining process have been analyzed individually and the main characteristics of the hybrid joints have been introduced. In the remaining sections of Chapter 2 these technologies will be compared on the basis of their mechanical properties, the stress distribution over the joining area and of the failure mode. Lastly, the failure criterions proposed by some authors will be analyzed.

2.5.1 Mechanical Properties

In this section the work of different authors aimed at evaluating the tensile strength of the previously described joining methods is analyzed. Given that this thesis deals with the mechanical properties of structural joints in static load test the fatigue performance will be just briefly mentioned.

2.5.1.1 SPR

Porcaro et al. [29] investigated the behavior of SPR under different loading conditions and with aluminum sheets of different thicknesses and different heat treatment of the material. The authors tested both a T-peel joint and a U-joint at 3 different configurations, namely from pure shear ($\theta = 0^0$) to pure tension ($\theta = 90^o$) (Figure 2-17).

In Figure 2-18 are represented the curves of force-displacement for the peeling test (b) and for the U-shape coupon as function of the loading angles (a). The cases analyzed here consider joints made with sheet of same gauge (2+2 mm). It can be seen that by increasing the angle (so changing from shear loading to tensile loading) the peak strength and the stiffness decreased, while the maximum elongation increased. In other words the joint exhibits the highest strength but the lowest elongation when loaded in pure shear. By comparing the two graphs shown in Figure 2-18 it is evident that the riveted Joint is much weaker when loaded in peeling mode, with a maximum achieve load that is about half compared to pure tension and almost five times lower than in pure shear.

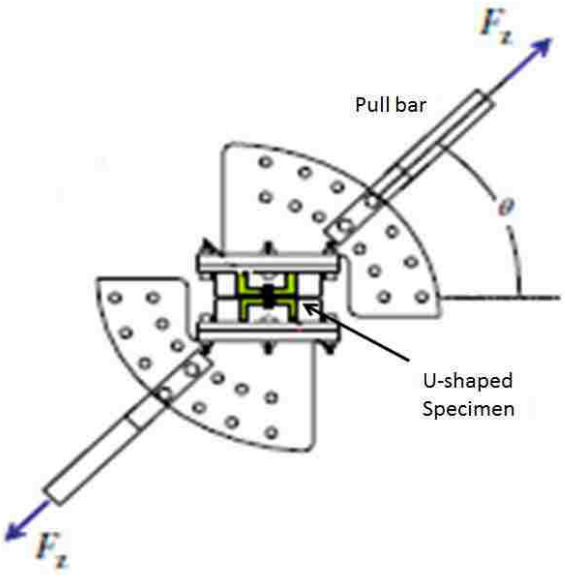

Figure 2-17. U-shaped specimen and fixture to allow varying the loading mode [29]

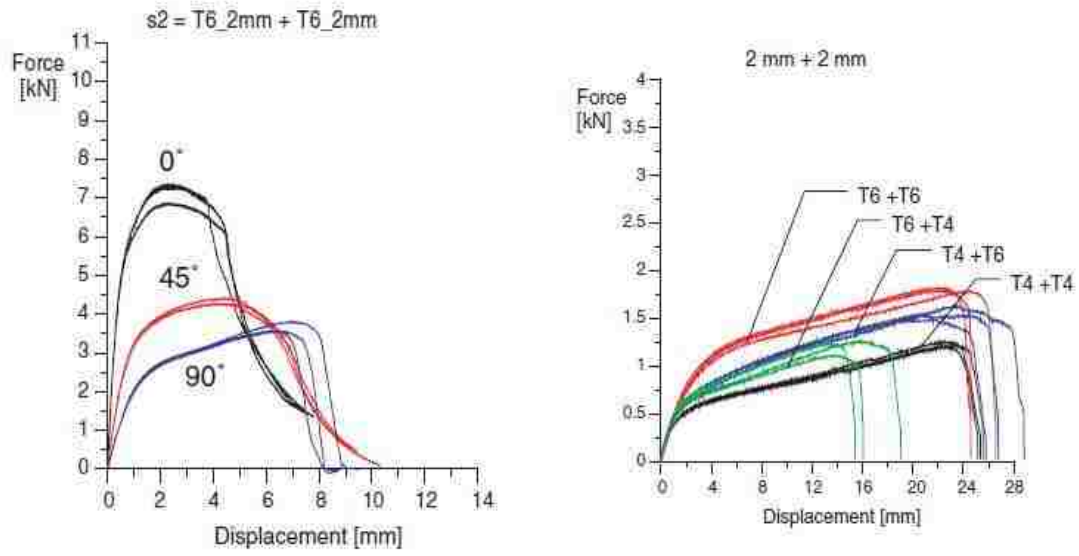

Figure 2-18. Force-displacement curve for the tensile test of U-shaped specimens (a) and T-peel specimen (b) [29]

2.5.1.2 RSW

Darwish [30] studied and compared the properties of a welded lap joint; in particular he analyzed the strength of the joint and relation with the nugget size. In the joint preparation four different parameters were varied: welding current, electrode clamping force, welding time and sheet thickness. The thicknesses used in this research are 1mm and 2 mm and the material used is a commercially pure aluminum alloy. The results show an increase in the strength of the joint with the nugget size. The author then repeated all the tests adding adhesive to the joints; interestingly the correlation between nugget dimension and load to failure is more evident for the welded joints than the hybrid ones. This fact clearly indicates that the adhesive is carrying part of the load and thus the importance of the nugget dimension is reduced.

A similar study was carried out by Radakovic and Tumuluru [31] who investigated the impact of the nugget dimension and sheet thickness on the strength of steel cross tension joints. Different nugget sizes were produced by varying the welding current. The obtained results show that the final strength of the joint is influenced both by the sheet thickness and by the weld nugget dimensions; in particular, the thicker the material and the bigger the weld nugget the higher the load that the joint is able to hold. The authors also noticed that of the two parameters the sheet thickness was the one with the larger impact (Figure 2-19, Figure

2-20). Even though all these experiments were conducted on steel joints, the information obtained is valuable as well for this study on aluminum joints. The described behavior is in fact believed to be a function of the joint geometry and of the stress distribution and concentration around the weld nugget (see also Section 2.5.2). The use of a different material will probably vary the obtained results but not the observed trends.

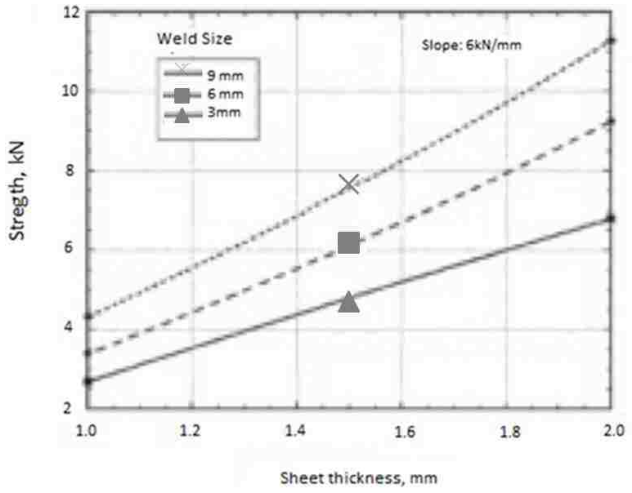

Figure 2-19. Joint strength as a function of the sheet thickness [31]

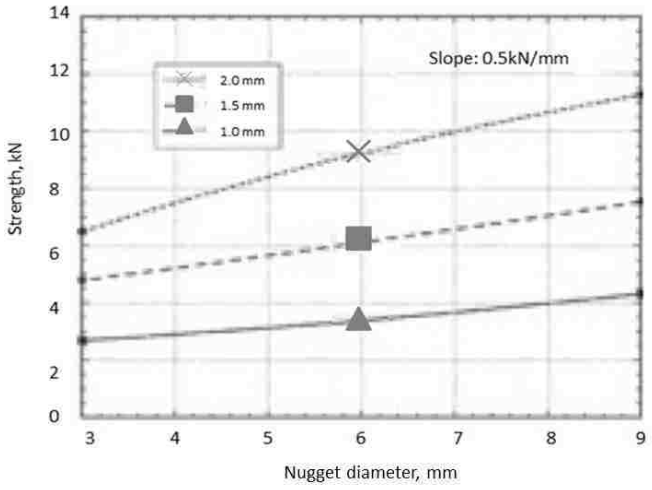

Figure 2-20. Joint strength as a function of the nugget thickness [31]

2.5.1.3 SPR vs. RSW

He et al. [13] summarized in their work the research of many other authors and concluded that in general the static strength of SPR and RSW is comparable while SPR outperform RSW under fatigue stresses (Figure 2-21). When aluminum joints are considered a dependence on the sheet thickness is usually observed; in particular some studies [32]

pointed out that the strength of RSW was higher than that of SPR in lap shear and t-peel joints made of stacks of 3 mm thick sheet while for thinner stacks (1.2 mm) and for unequal thicknesses the strength of SPR was usually higher.

While the trend of the static strength is not very clear, almost all the authors quoted by He et al. agree that fatigue strength of SPR is higher than RSW. A possible reason for this behavior can be found analyzing the area surrounding the weld nugget and the rivet; while in the former case the HAZ shows a lower strength, in the latter the area surrounding the rivet has been work-hardened by the riveting process. An enhancement of both the static and especially the fatigue strength of the joint can be achieved with the use of hybrid joints [13]. The experimental results obtained by Chang[1] [26] shows that the addition of adhesive elongates the fatigue life of a RSW lap-joint by almost two orders of magnitude and the static strength of about 40%.

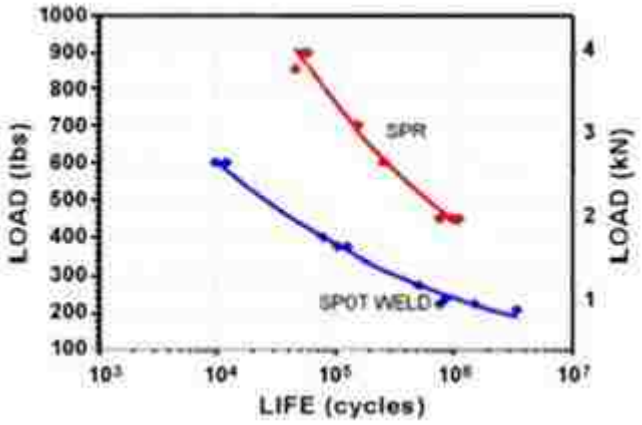

Figure 2-21. Comparison of the fatigue strength of self-pierce riveted and spot welded lap joints [13]

Extensive experimental studies aimed at comparing the mechanical properties of RSW and SPR aluminum joints have been carried out by Han et al. [33] and by Briskham et al. [34]. Han et al. [33] used in their study three joint configurations (lap shear, t-peel and cross-tension), three different blank thicknesses and different combinations of welding and riveting parameters, namely:

- 1 mm thick blank: 3 different nugget sizes[2] and 1 rivet-die combinations.
- 2 mm thick blank: 2 different nugget sizes2 and 2 rivet-die combinations.

[1] Steel components used

[2]In the study by Han et al. [33] for each thickness the current was varied to obtained different nugget sizes; the nugget size is expressed as function of "RT" in Figure 2-22, that is the square root of the thickness of the sheet (see also Section 2.1.1)

- 3 mm thick blank: 1 nugget size2 and 2 rivet-die combinations.

The following conclusions can be drawn from their study (Figure 2-22):

- Varying the welding and riveting parameters has a significant impact on the joint strength and energy absorbed; in particular the influence of the nugget size is function of the joint geometry, being the maximum for the lap shear and the minimum for the t-peel.
- High variability of the obtained results can be noticed in RSW. The authors attribute this effect to differences in nugget properties and diameter that in turn are caused by inhomogeneity of the surface condition; as explained in Section 2.1.1, RSW is sensitive to the surface condition of the material to be joined. On the other hand the authors noticed a high consistency of the SPR process, proved by a low variability of the obtained results.
- T-peel: for both the joining techniques the strength obtained in peel joints is lower compared to lap shear of cross tension. SPR has higher strength than RSW in t-peel joint and increasing the nugget size the obtained increase in the strength for RSW in rather limited and not as significant as in lap shear. The gap between RSW and SPR is even greater in term of the energy absorption at maximum load.
- Lap Shear: Increasing the nugget size has a beneficial effect on the strength of RSW joints that, especially in the thinnest stack, can achieve strength higher that SPR. The energy absorbed at maximum load for RSW was comparable to SPR for the thinnest stack but lower for the two thicker stacks. If instead the energy at joint failure is consider SPR always outperforms RSW thank to a much greater elongation at failure [33].
- Cross-tension: the increase in the nugget dimension proved to be beneficial from 4RT to 5RT but detrimental from 5RT to 6RT. The authors attributed this behavior to a higher results variability induced by the occurrence of the phenomenon of expulsion in numerous samples. In general the two joining methods proved to be comparable in this configuration, with RSW outperforming SPR in the energy absorption at maximum load for the thicker stack.

Briskham et al. [34] did a similar study comparing the mechanical properties of riveted and welded lap shear and t-peel joints and obtained similar results to Han et al. [33]. Some of

the obtained results are summarized in Figure 2-23 and Figure 2-24. From the reported load-displacement curve it can be seen that the maximum load obtained with SPR is slightly higher compared with RSW. Keeping in mind that the energy absorbed during the joint deformation is equal to the area under the load-displacement curve it can be seen that it is much higher for SPR, especially if the energy until final fracture is considered.

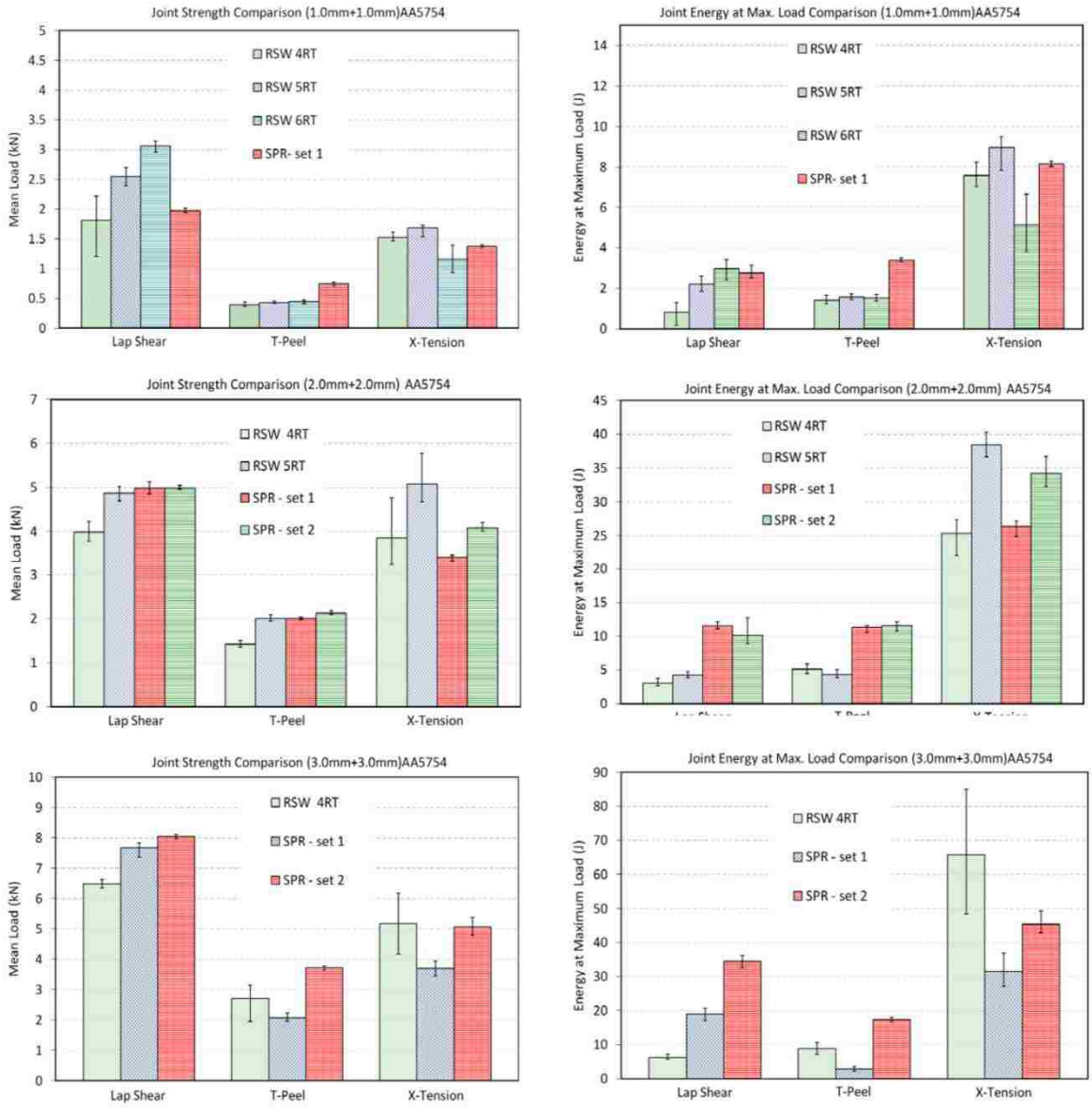

Figure 2-22. Comparison of the strength (left) and the energy absorbed (right) at maximum load for lap shear, coach peel and cross-tension and for three different stack thicknesses [33]

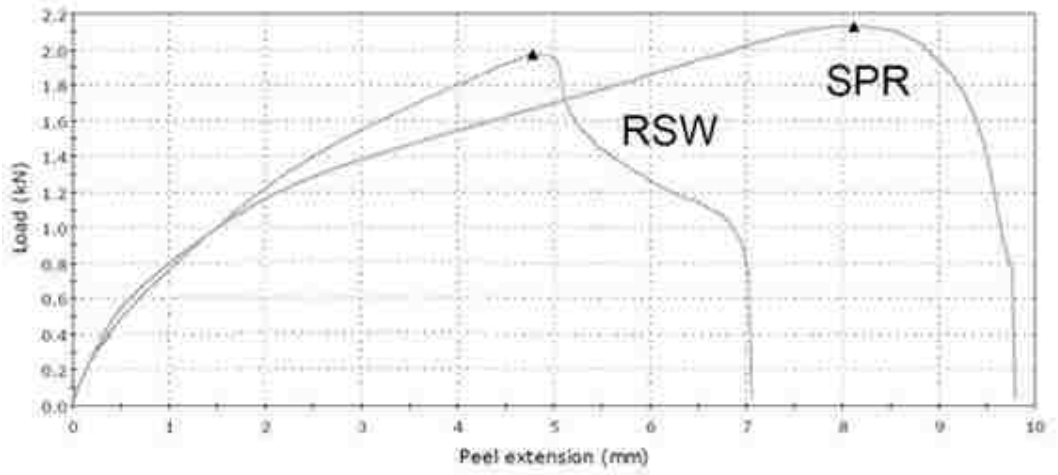

Figure 2-23. T-peel load-displacement curves [34]

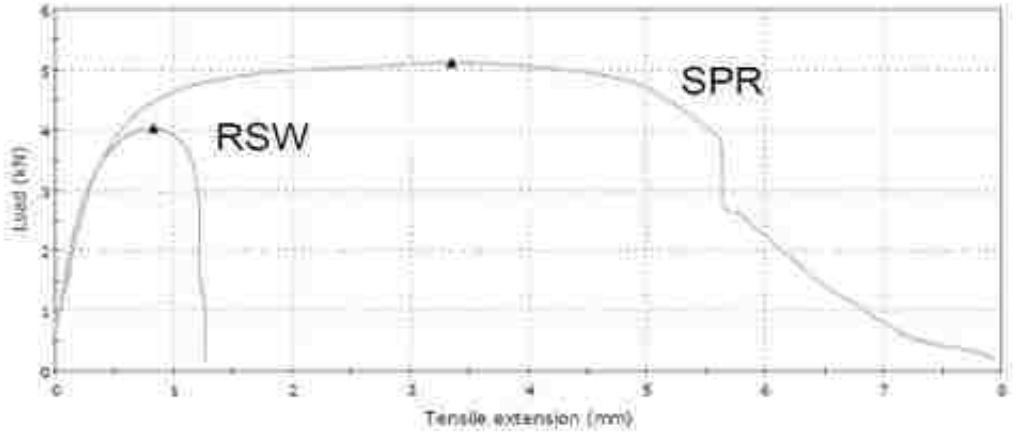

Figure 2-24. Lap-shear load-displacement curves [34]

2.5.1.4 Hybrid Joint Performance

As already mentioned in Section 2.4 the simultaneous use of adhesive together with RSW or SPR is a very promising solution under many different points of view, from the static to the fatigue strength to the vibration dampening and the corrosion resistance.

Briskham et al. [34] in their comparison between welded and riveted joints compared as well the strength of weld-bonded and rivet-bonded joints. Adding the adhesive, the strength of the lap joint was greatly increased while the difference between weld-bonded and riveted bonded was quite low (Figure 2-25 left). Alternatively the influence of adding adhesive on the T-peel joint is much more reduced, especially for the SPR; the weld-bonded joint instead behaved better than the welded joint, reducing thus the gap with the riveted joint.

As mentioned in Section 2.5.1.2 also in the study carried out by Darwish [30] the weld-bonded lap joint showed a higher maximum force compared to the simply-welded joint. In addition the author studied the capability of the joint to damp down vibrations and noticed a benefit from the addition of adhesive to the traditional joint.

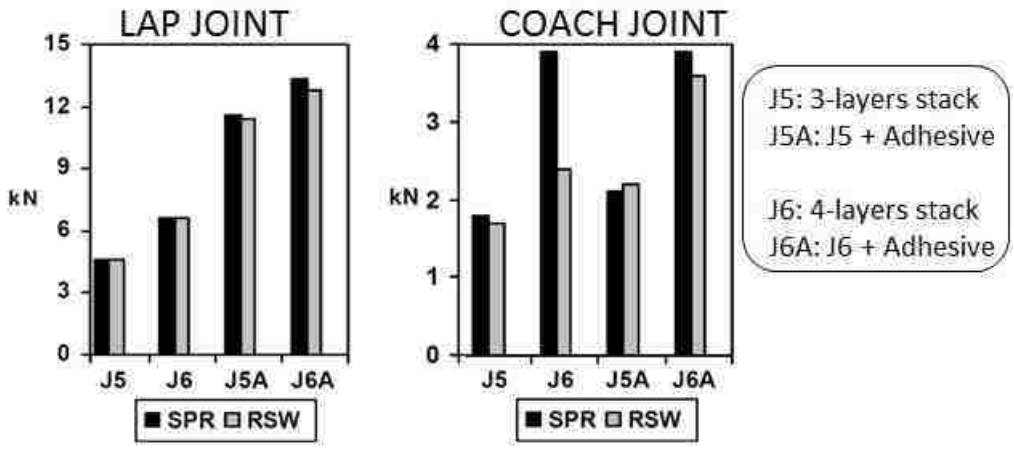

Figure 2-25. Schematic comparison of the strength of lap shear (left) and coach joint (right) joints with (J5A and J6A) and without (J5 and J6) adhesive [34]

Bartczak et al. [35] compared the properties of welded, adhesive-bonded and weld-bonded lap and t-peel joints (Figure 2-25) by performing both a finite element method (FEM) analysis to study the stress distribution inside the joint (see Section 2.5.2) and an experimental test to quantify the load-bearing capacity of these three joining solutions[3]. The experimental results showed that the adhesive bonded joint is stronger that the spot welded joint in shear mode while the opposite result is obtained in tearing mode. The addition of adhesive to the spot welded joint did not show any significant increase in the joint strength compared to the two traditional joining techniques as far as the strength of the joint is concerned. The energy absorbed at joint fracture was instead greatly increased, particularly compared to the adhesive-bonded joint. Lastly the authors pointed out the "two-stage" nature of the load deflection curve of the weld-bonded shearing joint; after a first peak due the adhesive yielding the load partly drops and then rises again until the yielding of the nugget (Figure 2-26). The two different loading modes were characterized by different trends of load-deflection: for the lap joint (shearing mode) the final displacement is quite

[3] Steel components are studied in this research. As said in Section 2.5.1.2 only the trend of the results should be considered and not the numerical values obtained.

limited but a high value of load is attained. Opposite behavior is noticed for the t-peel (tearing mode), where much higher values of displacement were achieved but the maximum obtained strength was about half compared to the shearing mode.

A similar observation is made by Moroni [25] that describes the load-displacement curve for rivet-bonded joints as made of two regions: a first region characterized by a high stiffness where most of the load is carried by the adhesive; then after adhesive breakage the load is carried by the rivet and the result is a low stiffness peak. For this reason the final energy absorbed is almost equal to the sum of the two simple joining methods [25].

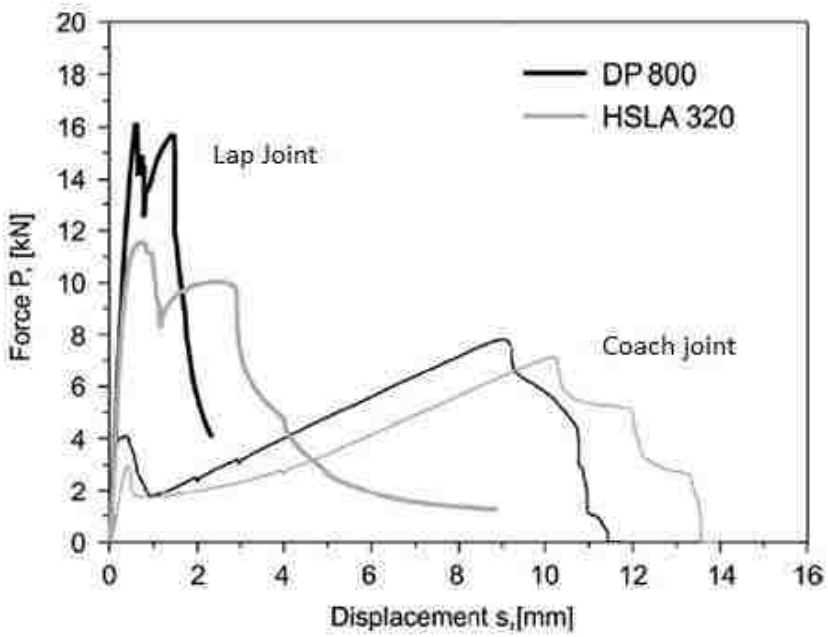

Figure 2-26. Load-displacement curve of a weld-bonded joint loaded in shearing (thick line) and in tearing (thin line) mode [35]

The interesting conclusion that can be drawn from the research of Bartczak et al. is that if the only objective is to increase the maximum load of a lap joint the most suitable solution is adhesive-bonding, followed by weld-bonding and last comes welding. However, once the yielding load of the adhesive layer is reached the fracture propagates rapidly with almost null energy absorption. For this latter goal weld-bonding is then the best performing joining method; after the failing of the adhesive layer the nugget still holds the joints in position allowing greater energy absorption. This is particularly true when the adhesive yields under peeling load.

Liu et al. [36] explained the lower tensile performance in shear of weld-bonding compared to adhesive bonding by saying that in shear load the adhesive bonding technique is the most effecting and the addition of any other element reduces the surface contact area of the adhesive and consequently the joint strength. The authors investigated the properties of a variation of the rivet-bonded joint, in which the traditional self-piercing rivet is replaced by a single-sided piercing rivet (SSPR). They main goal of the authors of this research was to find a technique suitable for keeping the adhesive bonded joint in the proper position before the curing process. In addition, the tensile tests done in this research indicated that even though the strength of a SSPR lap joint is lower compared to a SPR lap joint, when combined with adhesive the result is opposite. As can be seen in Figure 2-27 the area over which the adhesive was pushed away by the riveting process with the SPR is much bigger compared with SSPR, and thus the strength recorded is higher for the latter case. Additionally the authors tested the effect of the increase in overlap area on the shear strength of the joint. The increase in overlap resulted in an increase in the joint strength; however the shear stress, calculated as the peak load divided by the area was actually lower for the sample with the bigger overlap, as expressed by the following relation

$$\tau = ke^{-\lambda l} \tag{2.2}$$

Where τ is the shear stress, l the length of the overlap and k and λ are coefficients related with the material properties. The decreasing trend of the shear stress at the increase of the overlap length means that the strength does not increase linearly with the overlap area but at a lower rate; this fact could be explained by the variation in the stress distribution inside the overlap area [23] [35] (see Section 2.5.2).

This is agreement with the results obtained by Lucic et al [21].

The length of the overlap has a very important role in determining the strength of the joint; as a general rule, increasing the overlap length the strength of the joint can be increased. When the overlap is too small the joint strength is limited to a value lower than the yield point of the material; in this situation thus the bending induced by the deformation of the material is quite limited and the joint fails mainly in shear. By increasing the overlap length the load held by the adhesive-adherent interface grows until reaching the yield point of the adherend; at this point deformation of the material start from the end of the overlapping regions [21]. The author suggests that the point where the adhesion strength

matches the yield point of the material can be considered as the optimal overlap dimension for maximum strength; increasing it over this value will have the only effect of increasing material bending and the final fracture stress will be lower (Figure 2-28).

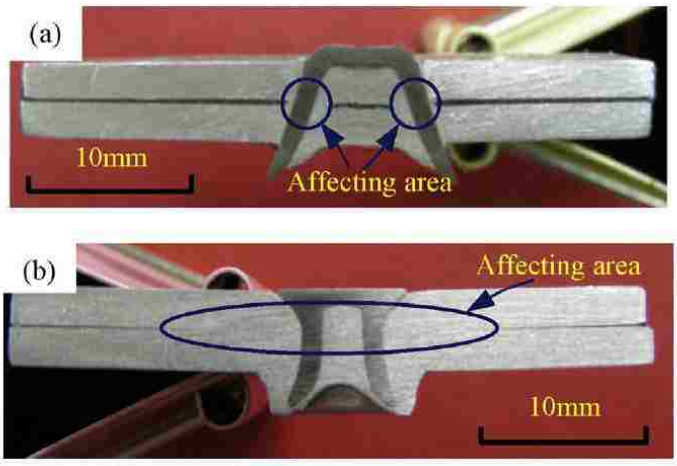

Figure 2-27. Cross-section of a SSPR (a) and a SPR (b) joints [36]

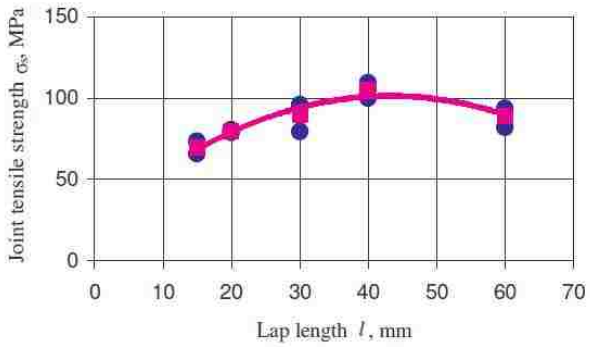

Figure 2-28. Variation of adhesive bonded joint strength as function of the overlap length [21]

Moroni et al. [25] analyzed the effect of numerous variables on the performance of simple and hybrid lap joints. In particular, adhesive bonded, welded and weld-bonded joint were tested for homogeneous joints (same thickness for both the joined component) while the riveted, rivet-bonded and adhesive bonded were compared with heterogeneous joints (thus joining two blanks of different thickness). The variables considered in this research are: material thickness, weld pitch, operating temperature, and the effect of an ageing cycle. The effect of these variables on the joint strength and energy absorbed has been summarized

Table 2-2. The results obtained with the heterogeneous joint are similar to the one of the homogeneous joint and thus only the latter ones have been reported.

Table 2-2. Brief summary of the results obtained by Moroni [25]

	Measured quantity	Variable 1	Variable 2	Comments
Figure 2-29	Force	Thickness	Weld Pitch	RSW = increasing thickness and decreasing the pitch the strength increases.
				Bonded = little increase in strength with thickness.
				Hybrid = better than RSW in joining thin sheets and/or with high pitch.
Figure 2-30	Force	Temperature		RSW: independent of temperature
				Bonded: Severe strength drop with increase in temperature
				Hybrid: Sensitivity to Temperature is halved; the minimum strength corresponds to the strength of the welded joint.
Figure 2-31	Force	Thickness	Temp.	Bonded: greater dependence on operating temperature and highly sensitive to ageing cycle.
				Hybrid: increasing the thickness and decreasing the temperature the strength increases. Independent on the ageing cycle
Figure 2-32	Stiffness	Thickness	Pitch	RSW = high stiffness for low pitch and high thickness.
				Bonded = much higher stiffness than welded. As thickness is increase slightly stiffer.
				Hybrid = slightly stiffer than adhesive bonded
Figure 2-33	Stiffness	Temperature		RSW: the stiffness of the joint is independent of the temperature.
				Bonded: High dependence on temperature. Except for the maximum temperature the bonded joint is stiffer than the RSW joint
				Hybrid: Reduced dependence on temperature. Highest value of stiffness.
Figure 2-34	Energy	Weld Pitch	Thickness	RSW: Maximum energy absorption for maximum thickness and minimum pitch.
				Bonded: Energy absorbed increases with thickness
				Hybrid: Same trend as bonded, much higher value of energy absorbed.

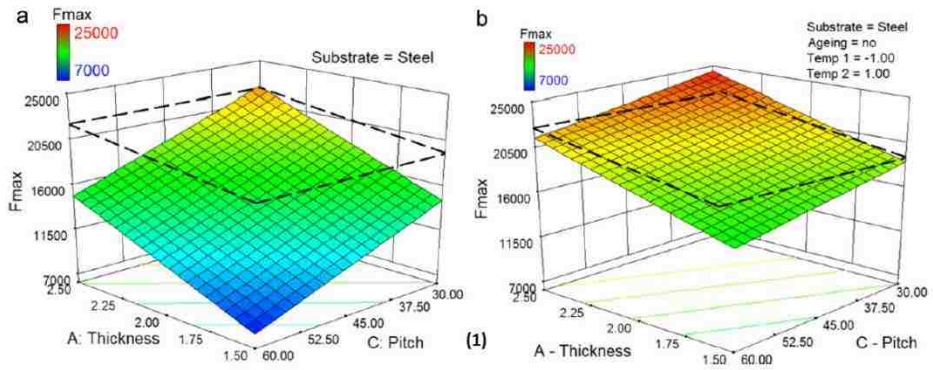

Figure 2-29. Strength at room temperature as a function of thickness and pitch of (a) spot welded and (b) weld-bonded steel joints. Dotted lines refer to bonded joints [25]

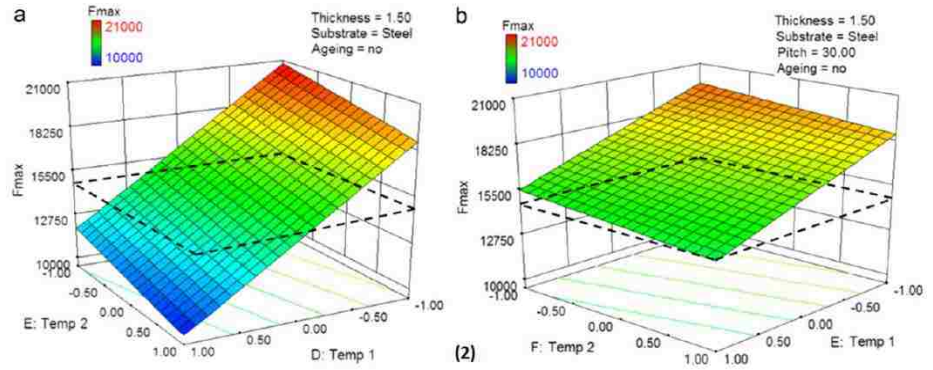

Figure 2-30. Strength as a function of temperature of (a) bonded and (b) 1.5 mm-thick, 30 mm pitch weld-bonded steel joints. Dotted lines refer to spot welded joints [25][4]

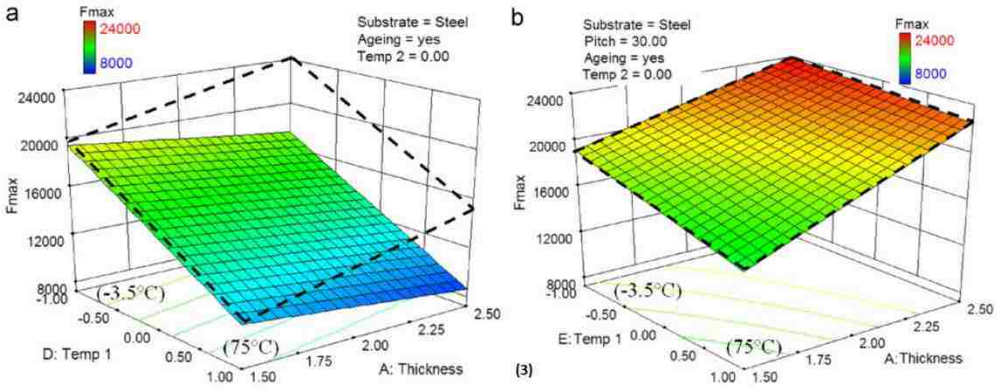

Figure 2-31. Strength as function of ageing of: (a) bonded and (b) weld-bonded steel joints. Dotted lines refer to non-aged condition [25]

[4] The convention used for the temperature is the following:
Temp1 = Temp2 = -1 = -30°C
Temp1 = -1, Temp2 = 1 = 23 °C
Temp1 = 1, Temp2 = -1 = 60 °C
Temp1 = Temp2 = 1 = 90°C

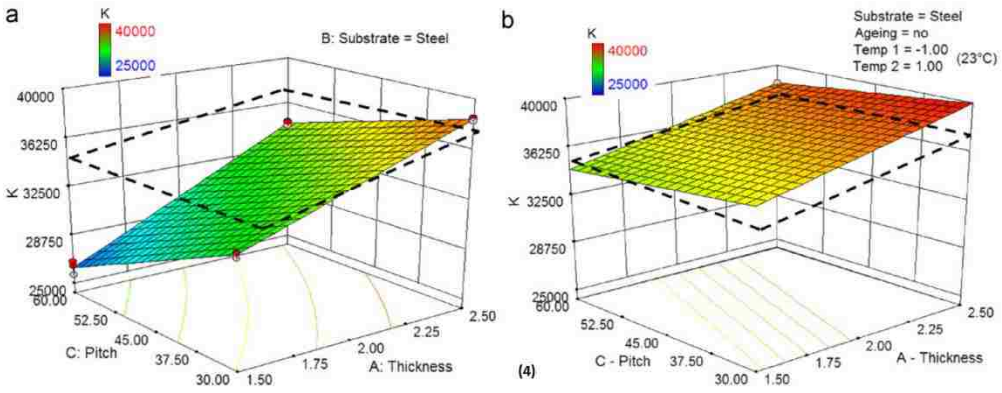

Figure 2-32. Stiffness behavior at room temperature as a function of thickness and pitch of: (a) spot welded and (b) weld-bonded steel joints. Dotted lines refer to bonded joints [25]

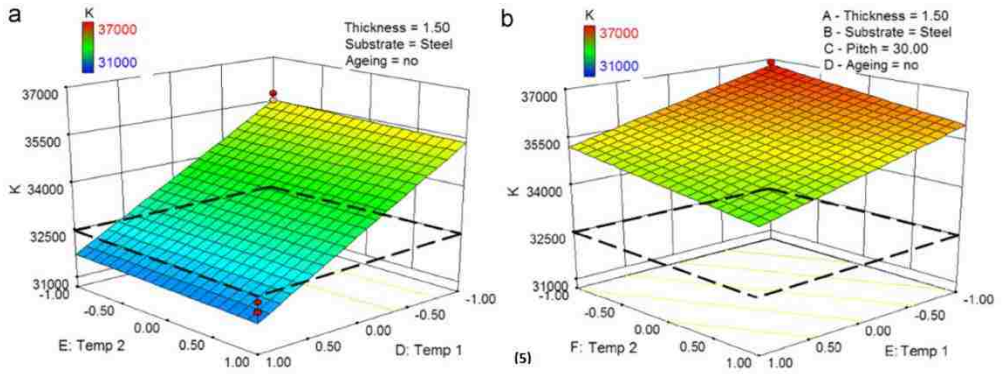

Figure 2-33. Stiffness as a function of temperature of: (a) bonded and (b) 1.5 mm-thick, 30 mm pitch weld-bonded steel joints. Dotted lines refer to spot welded joints [25]

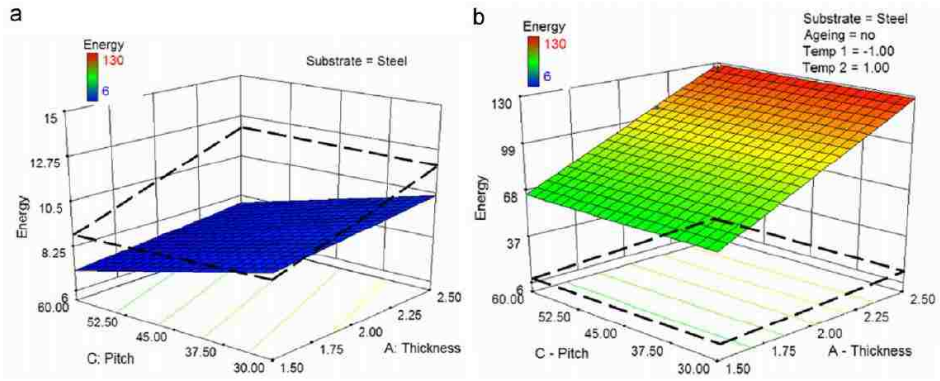

Figure 2-34. Energy absorption at room temperature as a function of thickness and pitch of: (a) spot welded and (b) weld-bonded steel joints. Dotted lines refer to bonded joints [25]

2.5.2 Stress distribution

In order to explained the mechanical properties of the joints analyzed in Section 2.5.1 many authors studied the distribution of stress inside the joint when subjected to a tensile load. Many factors however contribute in making this analysis quite complex; given the geometries of the joint the loading line is always not aligned with the components and this gives rise to bending moments and joint rotations and distortion; the latter effect is also consequence of the not infinite rigidity of the components of the joints. As a result for example in a lap joint in addition to shear loading some peel and cleavage loading arise. Some simplified theories to study the stress distribution inside an adhesive bonded lap joint have been developed by Volkerson and Goland and Reissner (Section 2.5.4.1).

The most popular solution used nowadays to perform the stress analysis of the joints is to use Finite Element Analysis, which allows taking into account all the complexity factors previously mentioned. Most of the authors concentrate their attention on studying the stress distribution on steel lap shear joints and on understanding the effect of using hybrid joint and to vary the joints parameters (overlap length, adhesive thickness and mechanical properties etc.) [21] [23] [24] [26] [30] [35] [37] . More rarely the same analysis was conducted for coach joints [38] [39]. As mentioned in Section 2.5.1.2 the information collected by these authors are still valuable for this thesis even when the considered material is different since the stress distribution is mainly determined by the geometry of the joint, the joining method used and the loading condition.

Al-Samhan and Darwish [24] and Chang [26] investigated the difference in stress distribution in adhesive bonded, welded and weld-bonded steel lap joints. In this study the stresses have been calculated along the midline of the spot weld, adhesive bonded and weld-bonded joint. The stresses calculated are σ_x, σ_y, τ_{yx}; σ_x is responsible for the tensile deformation of the plates, τ_{yx} for its angular deformation and σ_y controls the tearing fracture of the joint.

Figure 2-35shows the distribution of σ_x, σ_y, τ_{yx} for the three analyzed joining solution. Immediately evident is the incredibly high stress concentration at the periphery of the weld nugget for the welded joint. The normal stress σ_x reached a stress-concentration factor (calculated as the peak stress over the average stress) of 16.7 [26] and it is 160% higher than the maximum stress for the weld-bonded case. The trend of σ_y is due to the asymmetric

transmission of the load that causes the adherends rotation. This is also the reason for the presence of a compressive load in the inner areas of the weld nugget [23]. Lastly the shear load τ_{yx} shows as well a very high load concentration at the nugget periphery but a null stress at the nugget center. Away from the weld nugget the stress is always null for a spot-welded joint.

The distributions of the normal stresses σ_x and σ_y in the adhesive-bonded joints shows a maximum at the edges of the overlap area where the two adherends tend to separate while it is null over all the central portion of the joint. The shear stress τ_{yx} has a convex shape where again the maximum is registered at the edges of the overlap but in this case same shear stress is present over the entire joining area.

The stress distribution of the weld-bonded joint shows some aspects of both the welded and the adhesive-bonded joint. The normal stress σ_x has the same increase at the end of the overlap area as the adhesive-bonded and an area of higher stress in correspondence to the weld nugget; the stress at the weld nugget is anyway much lower compared to the peak reached in the case of the spot welded joint. The trend for σ_y and τ_{yx} is instead almost identical to the adhesive-bonded, showing an increase at the edges of the overlap and being null at the joint's center. This reduction of the peak stress given by the presence of the adhesive is the reason for the better mechanical performance of the weld-bonded joint. The adhesive contributes in fact in distributing homogeneously the stress over the entire overlapping surface and thus the highest values registered for the stress were more limited. Intuitively, the higher the stress the higher the deformation of the joint; thus the weld bonded joint will experience a much lower deformation compared to the spot welded one [35].

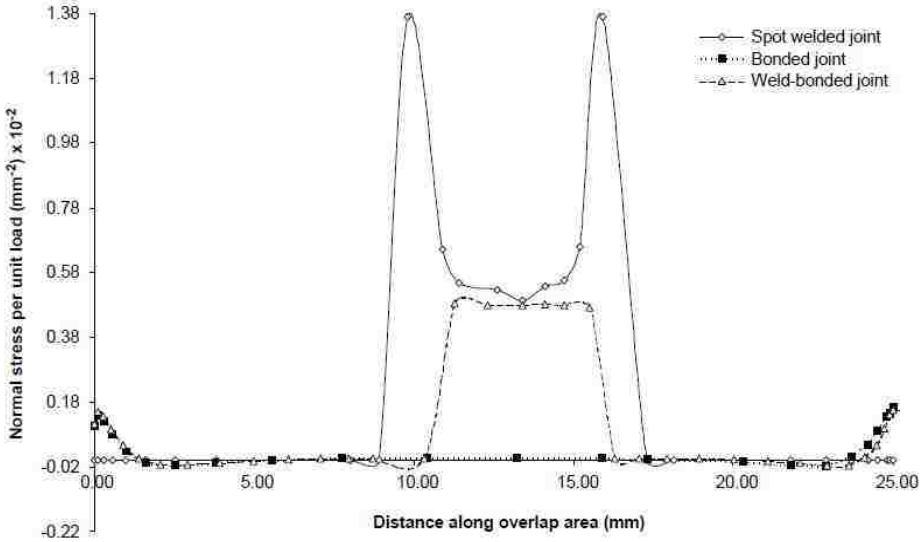

Figure 2-35. Distribution of normal stress σ_x along the overlap area for the three joining methods [24]

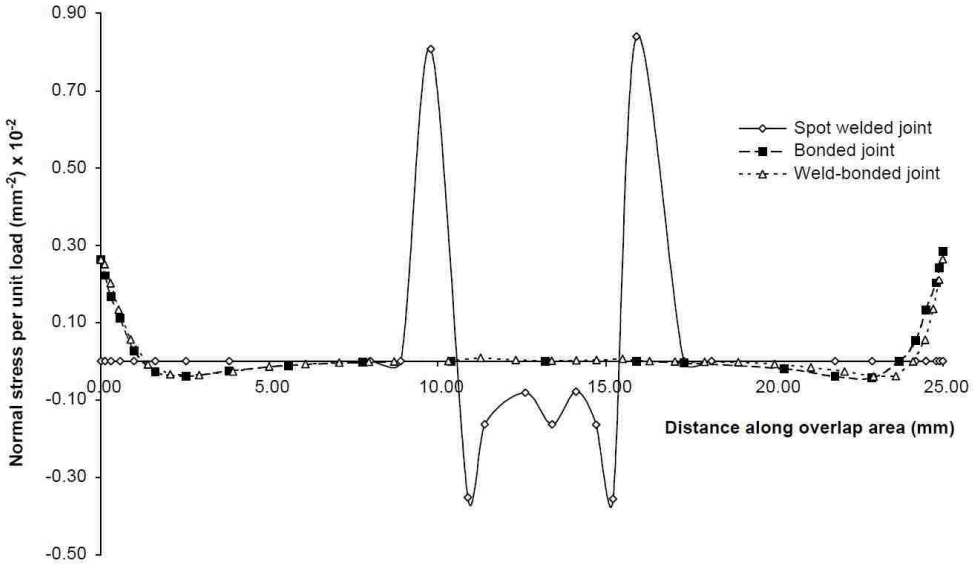

Figure 2-36. Distribution of normal stress σ_y along the overlap area for the three joining methods [24]

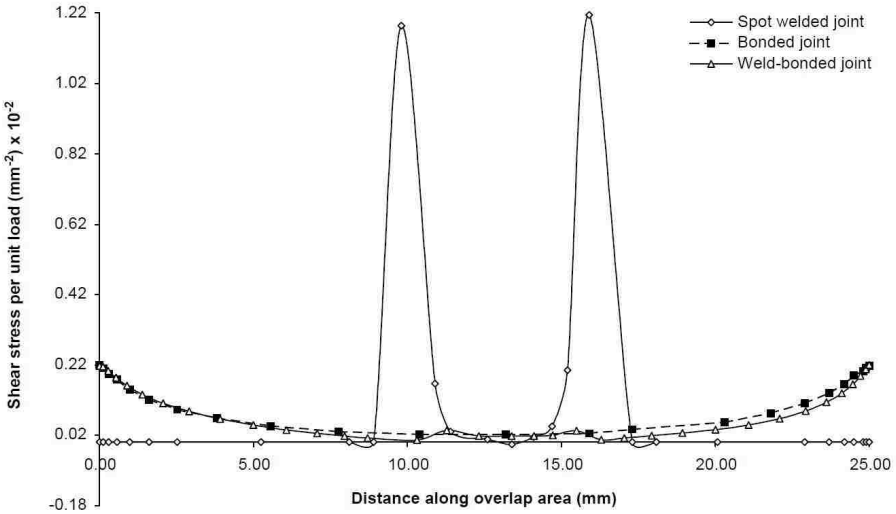

Figure 2-37. Distribution of shear stress τ_{yx} along the overlap area for the three joining methods [24]

The stress distribution shown and explained in the previous paragraphs is influenced also by the joint design parameters; Campilho et al. [23] and Bartczak et al. [35] investigated the variation of the stress distribution corresponding to a variation in the length of the overlap in steel lap joints. The variation of σ_y and τ_{yx} by varying the overlap length from 15mm to 60 mm in a weld-bonded lap joint is shown in Figure 2-38. As a general rule it can be said that the larger the overlap, the higher the load it can bear, the more it is similar to an adhesive-bonded joint. On the other hand if the overlap area is reduced part of the load is carried by the weld nugget and thus the stress distribution resembles the one for the spot welded joint. In particular, Campihlo et al. [23] justified the observed behavior for the shear stress explaining that the stiffness of the weld nugget is higher by two orders of magnitude compared to the adhesive; thus the weld nugget plays an important role in transmitting the load in a region where bonded joints are usually lightly loaded. In addition it can be noticed that increasing the overlap length the stress is more concentrated at the edges of the overlap. Bartczak noticed the same behavior with adhesive-bonded joints; even though in his research the absolute value of the stress at the overlap edge was unchanged; increasing the overlap reduced the stress at the center progressively, and thus the stress gradient from the center to the edges of the overlap increased [35]. This variation in stress distribution is the reason for the non-linear increase in the strength of the adhesive bonded joint with the increase of the overlap area, as described by Liu et al. [36] and Lucic et al. [21] in Section 2.5.1.4.

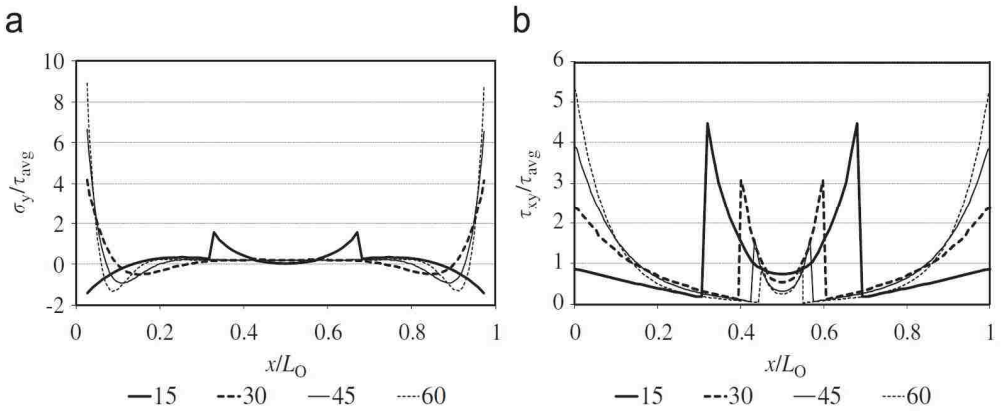

Figure 2-38. Influence of overlap length on the normal stress σ_y and the shear stress τ_{yx} of a weld-bonded joint [23]

Chang et al. [27] studied by means of FEM how the stress concentration at the weld nugget and at the edges of the overlap varies as function of the adhesive layer thickness and of the adhesive elastic modulus. Figure 2-39 show the effect of the adhesive elastic modulus on the stress concentration at the edges of the overlap and at the weld nugget. It can be seen that in general the normal stress σ_x at the overlap edge is maximum in the mid-section and then decreases toward the side of the sample (the y-axis is in this case aligned with the sample width). By increasing the elastic modulus of the adhesive the stress concentration at the overlap edge is reduced. The shear stress τ_{zx}[5] instead shows an opposite behavior; in fact a less stiff adhesive allows greater deformation thus reducing the shear stress [27].

A very stiff adhesive allows to evenly distribute the radial stress at the nugget perimeter, keeping also its value limited while the lower the stiffness the higher the stress at the stress concentration points and the more uneven the stress distribution. The shear stress at the nugget shows the same behavior where the magnitude of the stress is concerned but its distribution is always fairly homogeneous. In other words the stiffer the adhesive, the more load it carries while the lower the stiffness the more the load is born by the nugget; thus the former case will eventually lead to adhesive failure while the second to a nugget failure.

The adhesive layer has usually a thickness in between 0.1 - 1.0 mm; its variation has the same effect of the variation in elastic modulus; in particular an increase in thickness causes an increase in the stress loading at the weld nugget and in the normal stress at the edge σ_x but reduced the shear stress τ_{zx} at the edge, similarly to a decrease in stiffness. A decrease in

[5] Equivalent to τ_{yx} in [23] and [35]. Different reference frame orientation used.

thickness will instead have the same effect as an increase in the adhesive stiffness (Figure 2-40).

The authors conclude by stating that an increase in the adhesive stiffness and a reduction of its layer is generally recommendable for increasing the performance of the joint.

Lastly Darwish et al. [37] analyzed the effect of the adherend properties by comparing the stress concentration in aluminum joint and in steel one. The results showed that even though at the weld nugget the stress distribution is the same, at the edges of the overlap the lower stiffness of aluminum caused the stress concentration reach values almost 4.5 times higher compared to steel. This last graph is particularly important for the purpose of this thesis for two reasons; first of all it gives the indication that the most critical point in weld-bonded lap joints will probably be the overlap edge. Secondly it validates the hypothesis previously formulated that the variation of the joined material will affect only the absolute value of the stress at each point but not its trend inside the joint; thus all the graphs of stress distribution previously showed can give valid information on the stress distribution inside the joint independently from the joined material.

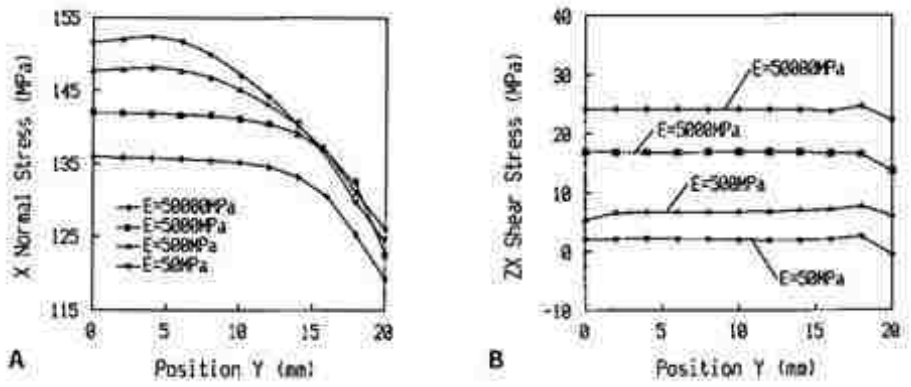

Figure 2-39. Distribution of the normal stress (left) and of the shear stress (b) at the overlap edge along the width of the sample as function of the adhesive elastic modulus [27]

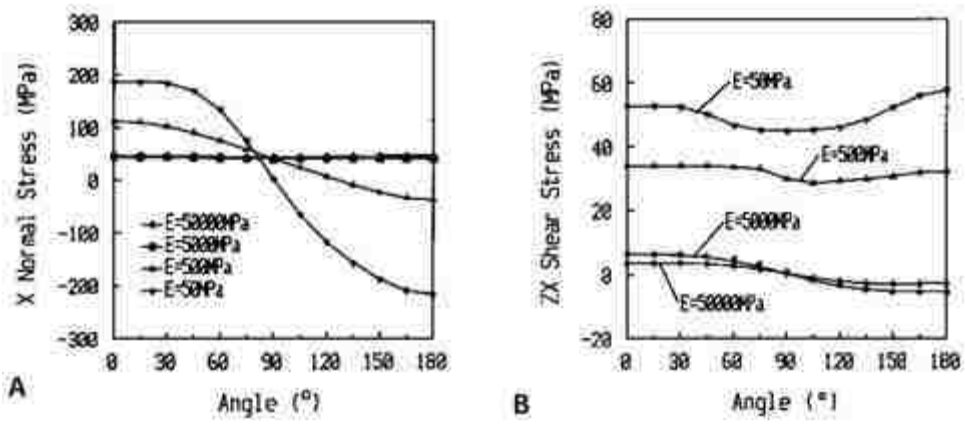

Figure 2-40. Angular distribution of normal stress (left) and shear stress (right) at the periphery of the weld nugget as function of the adhesive elastic modulus [27]

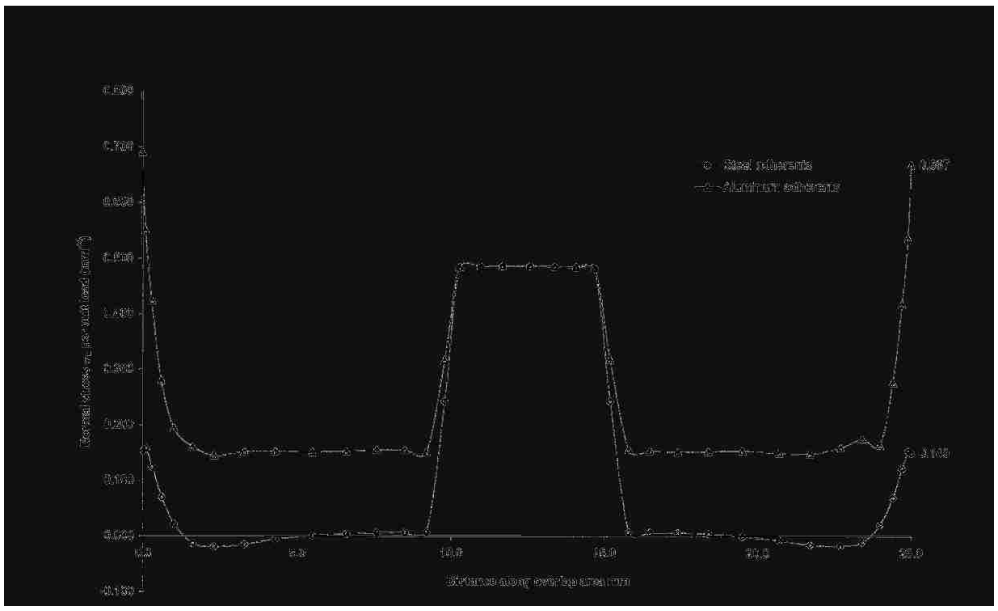

Figure 2-41. Comparison of the stress distribution in aluminum and steel weld-bonded joints [37]

2.5.3 Failure analysis

Together with the analysis of the stress distribution important information can be obtained by performing a failure analysis of the tested joint, which consists in observing the failure mode and in studying the factors that caused it [33].

Especially when adhesive-bonded or hybrid joints are used this analysis can be crucial; Davis and Bond [18] claim that in most of the cases joint failure is due to the lack of effective surface preparation or a non-proper joint design. Overlooking the importance of failure analysis has often lead in the past to errors in the identification of the issues during

the joint design and the manufacturing process, to the use of inappropriate testing methods and often to the attribution of non-satisfactory performance of bonded joints to the adhesive itself rather than to its misuse [18]. The characteristic failure modes of an adhesive-bonded joint have been already analyzed in Section 2.3.1. Davis and Bond summarized them as follow [18]:

- Failure of the adherends: this failure mode is typically obtained with good quality bond of thin adherends.
- Cohesive Failure: this failure is characterized by the presence of adhesive on the matching faces of both the adherends. Cohesive failure is usually caused by poor joint design: insufficient overlap or excessive peel stresses. When a good quality bond of thin adherends is obtained usually no fatigue failure is obtained; when thicker adhesive joints are loaded in fatigue, failure always occurs in cohesive mode.
- Adhesion failure: the adhesion failure is characterized by the complete absence of adhesive on one of the bonding surface. The cause of this failure mode is an inadequate surface preparation that leads to the hydration of the chemical bond between the adhesive and the substrate material. When aluminum is adhesively bonded the presence of the aluminum oxide at the surface can be the cause of the disbonding and failing of the joint. Lastly, the curing of the adhesive prior to the complete formation of chemical bonding with the substrate can lead to adhesion failure.

Depending on the loading mode and on the nugget/rivet size two main failure modes can be observed for both RSW and SPR; welded joints can fail either for "nugget pulled-out" (Figure 2-42a) of the opposing sheet or "nugget shearing" (Figure 2-42b) while rivet joint fail either for "rivet tail pulled out" (Figure 2-42c) or for "rivet head pull out" (Figure 2-42d) [29] [33]. Han et al. [33] and Porcaro et al. [29] studied the occurrence of each failure mode as function of the loading condition (or joint geometry), the sheet thickness and nugget size. The obtained results are ordered and summarized below per joint geometry.

Lap Joint:

As mentioned in Section 2.5.1.3 Han et al. [33] used three different stacks and investigated the influence of the nugget dimension. Two different failure modes were observed in the RSW joint, 1mm+1mm thickness stack. When a low value of current was

used a smaller nugget was obtained ($4\sqrt{t}$) and the failure happened as nugget shearing while with higher values of current and consequently bigger nugget sizes ($5\sqrt{t}$ and $6\sqrt{t}$) nugget pull-out was observed. A smaller nugget has a lower penetration and thus it is not able to withstand the same shear load of the parent material and it eventually fails. On the other side since a bigger nugget has a much higher penetration the parent material left surrounding the nugget is considerably thinner and when subjected to shear load it fails and causes the pull out of the undamaged weld nugget. Increasing the stack thickness the amount of parent material surrounding the nugget is usually strong enough to sustain a higher load than the nugget, which will then fail by shearing. Chao [40] derived a set of analytical expression for predicting the failure mode in Cross-Tension and Lap shear loading mode based on the calculation of a "critical diameter", below which the weld nugget is sheared. Sun et al. [41] obtained a similar expression for the critical diameter, taking into account also of the porosity inside the weld nugget.

It is important to remember that the area surrounding the weld nugget corresponds to the Heat Affected Zone (HAZ) thus its strength can be lower compared to the sheet material before welding (see Section 2.1). Darwish and Dekhial [42] investigated the relationship between the micro-hardness of the material at the HAZ and the strength of the joints and found a correlation between these quantities.

SPR lap joint failed in the same way for all the three thicknesses considered, namely by rivet tail pull-out. This kind of failure indicates that the strength of the joint is governed by the mechanical interlock at the lower sheet, so in general it can be said that the higher the achieved interlock the higher the joint strength [33]. In addition it is important to specify that a partial tilting of the rivet, which in turn caused the partial tearing of the upper sheet, was observed (Figure 2-43). Atzeni et al. [43] explain that due to the loading path non-linearity a rotation of the rivet around an axis perpendicular to the joint axis is induced. Since the steel rivet is harder than the aluminum components its head penetrates inside the sheet causing its partial tearing [43].

Briskham et al. [34] indicate the higher deformation needed for the rivet tilting and pull-out compared with nugget shearing as the reason for the higher energy absorption measured in the tensile test of the SPR joints compared to the RSW joints (see Section 2.5.1.3).

Coach Joint:

All the RSW coach joints failed by nugget pulled out; this suggests that the weakest point of a joint in this loading configuration is tearing strength of the material at the HAZ surrounding the nugget [33].

Two different failure modes were observed for the SPR joint: for the thinnest stack rivet-tail pull-out was observed while increasing the thickness of the material the strength of the interlock increased and exceeded the tearing strength of the material and caused the failure by "rivet-head pull-out" [33].

Cross-tension Joint:

For this case all the SPR samples failed as "rivet-tail pull-out" and all the RSW failed as "nugget pull-out".

Radakovic and Rumuluru [31] investigated in more deph the failure dynamics of a RSW cross-tension joint and indicated the testing mode as the main cause for the occurrence of this failure mode; in a cross tension test the samples are blocked to the crosshead is such a way that no lateral motion is allowed; thus a large tensile load is induced in addition to the bending moment (a clear proof of this is the ovalization of the holes drilled to attach the sample to the grip fixtures). Under this condition the stress acting at the weld nugget is actually mainly perpendicular to the loading direction and this will eventually lead to the crack propagation and the weld pull out. For this reason this failure mode was observed for all the analyzed cases, independently from the nugget size.

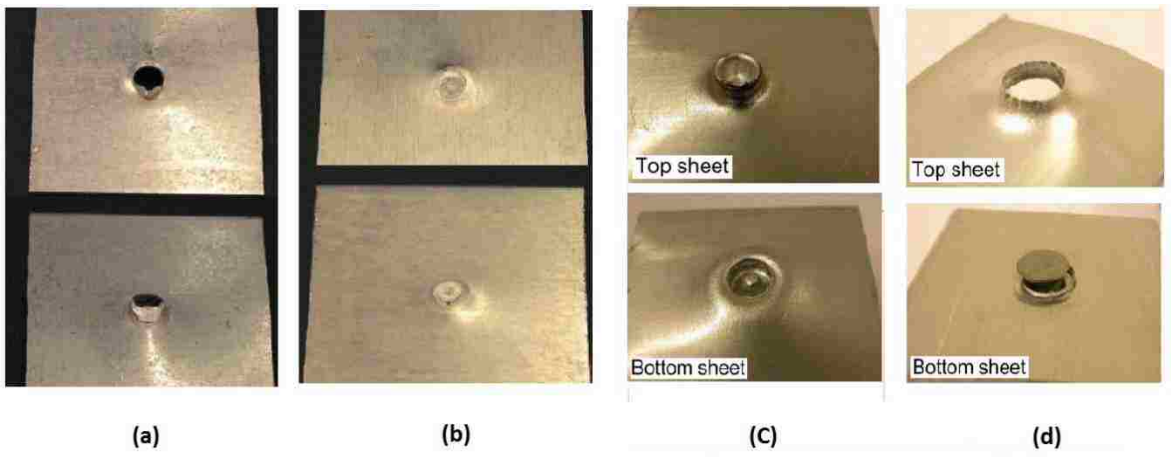

Figure 2-42. Most common failure mode in welded and riveted joints: (a) nugget pulled-out, (b) nugget shearing, (c) rivet tail pull-out (d) rivet head pull-out [29] [33]

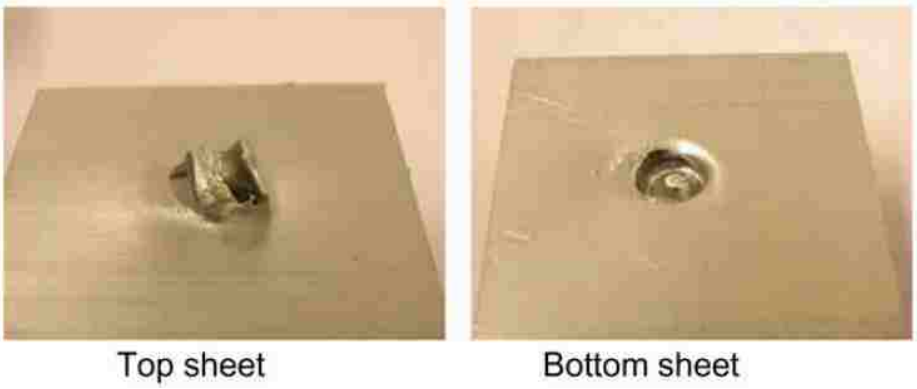

Figure 2-43. Typical Failure mode of SPR lap joint: partial tilting and rivet tail pull-out can be observed [29]

2.5.4 Failure criterion

Accurate prediction of the strength of a joint is a fundamental step for the design of a structural joint. The capability of defining a simple failure criterion based both on the stress analysis and on the joint fracture mechanisms is then crucial. Even though spot welding has been used extensively in the past decades a unique method for assessing the joint strength does not exists [44]. The same considerations apply for adhesive bonding; in particular many authors [45] [46] claim that one of the main reasons behind the limited diffusion of adhesive bonding technology is the lack of a simple and reliable method for predicting the joint strength.

As mentioned in Section 2.5.2 the stress analysis of structural joints is usually dealt with Finite Element Models due to the complexity of the stress fields, often characterized by singularity points. However three-dimensional finite element analyses for determining the stress intensity at the bond line and at the weld nugget are computationally expensive and time-consuming and an analytical solution for rapid prediction of the joint strength would be valuable for the engineering design process [44, 47]. Figure 2-44 is represents a basic scheme of the joint design process.

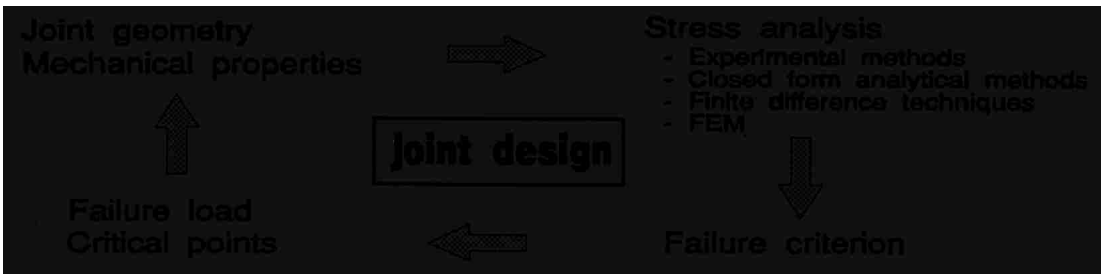

Figure 2-44. Basic scheme of the joint design process [48]

2.5.4.1 Adhesive bonded joints

The majority of the authors that studied the stress distribution inside adhesive bonded joints focused their attention to single lap joints loaded in tension. The main reasons lying behind this choice are the vast utilization of this geometry in the industry and simplicity and convenience for testing [48].

Most of the analytical theories developed are based on the following assumptions and simplifications [48]:

- The joint has square edges (no spew fillet)
- The applied load is low, so no plastic deformation is induced either in the adherends or in the adhesive. I.e. an elastic analysis is carried out.
- The calculated stress is the average value over the thickness; the stress distribution actually varies through the thickness but this variation is not considered.
- The problem is considered as two dimensional, as the variation of stress over the width is neglected.
- The stress singularity points are not taken into account.

Given the listed assumptions, the stress calculation in the adhesive layer is then limited to the shear stress τ_{xy}, the peel stress σ_y and the longitudinal direct stress σ_x (Figure 2-45).

Additionally, given that the longitudinal elongation of the adhesive and the adherends are the same for continuity, and that the elastic modulus of the adhesive is much lower, the longitudinal stress σ_x is often neglected.

The easiest approach for the calculation of the stresses in an adhesively bonded lap-joint is to assume infinitely rigid adherends and pure shear as the only stress in the adhesive layer. The resulting stress thus is constant over the entire overlap and equal to

$$\tau = \frac{F}{bl} \tag{2.2}$$

Where: F is the applied load, b is the joint width and l is the joint length (Figure 2-46 a).

A first refinement in this calculation was introduced by Volkerson in 1938. In his "shear lag" theory elastic adherends are assumed. Due to the non-uniform deformation of the metal sheets the resulting stress distribution is more concentrated at the edges of the overlap (Figure 2-46 b), reaching a peak stress equal to

$$\frac{\tau_{max}}{\tau_{avg}} = \left(\frac{P}{2}\right)^{\frac{1}{2}} coth\left(\frac{P}{2}\right)^{\frac{1}{2}} \quad (2.3)$$

Where τ_{avg} is the average shear stress calculated as in Equation 2.2 and P is given by

$$P = \frac{Gl^2}{Et_1t_2} \quad (2.4)$$

Where: G is the adhesive shear modulus, l is the length of the overlap, E is the adherends Young's modulus, t_1 the adherends thickness and t_2 the adhesive thickness.

The main limitation of the shear-lag theory is that it fails to take into account the bending moment that arises from the misalignment of the two loads applied. This bending moment also induces a rotation of the adherends that further changes the position of the load line and thus of the value of the bending moment itself. These factors were included in the analysis by Goland and Reissner, who first took into account the stress induced by the bending moment and proposed the use of a coefficient, k to account for the variation of the bending moment induced by the adherends rotation (Figure 2-47) [4]. Goland and Reissner also proposed an analytical expression for the calculation of the peeling stress σ_y that is not considered in the theory by Volkerson. A similar analysis was proposed also by Hart and Smith [48].

Figure 2-45. Normal, peel and shear stress in the adhesive [48]

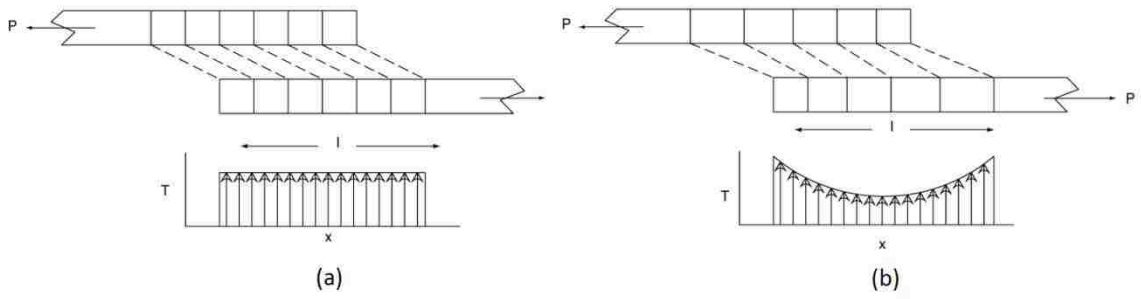

Figure 2-46. Shear stress distribution in bonded lap joint with infinitely rigid adherends (a) and with elastic adherends (Volkerson's "shear lag theory") (b) [4]

Figure 2-47. Bending moment in the lap joint before (left) and after (right) the deformation of the adherends [48]

The theories by Hart and Smith and by Goland and Reissner are the basis of a large number of works by numerous authors aimed at calculating the stress distribution in the overlap area. All these theories are based on the assumptions previously made in this Section and on the following equations [48]:

- Equilibrium equations to relate the stress in the adhesive and in the adherends.
- Compatibility requirements connecting the displacement of the adherends to the adhesive strain at the edges of the overlaps.
- Hooke's law for relating stresses and strains in the adherends and in the adhesive.
- Thin plate theory for calculating the adherends transverse displacement given the adherend stress.

Among the many developed theories the one proposed by Bigwood and Crocombe [46] is briefly analyzed here. As indicate by Goglio et al. [45] and by van Ingen [48] this model conjugates both simplicity and the ability of predicting the behavior of virtually any joint configuration. The overlapping portion of the joint is modelled as a three-layered sandwich beam at which ends a set of axial, transversal and bending moment loads are applied; by varying these end loads the stress generated by any loading condition and joint geometries

can be evaluated (Figure 2-48). The shear stress τ_{xy} and peeling stress σ_y distribution are calculated from Equations 2.5 and 2.6

$$\frac{d^3\tau_{yx}}{dx^3} - K_6^2 \frac{d\tau_{yx}}{dx} = 0 \tag{2.5}$$

$$\frac{d^4\sigma_y}{dx^4} + 4K_5^4\sigma_y = 0 \tag{2.6}$$

Where: K_5 and K_6 depends on the material properties and on the joint geometries. The solution of the Equations (2.5) and (2.6) are

$$\tau_{yx} = B_1 \cosh(K_6 x) + B_2 \sinh(K_6 x) + B_3 \tag{2.7}$$

$$\begin{aligned}\sigma_y = {} & A_1 \cos(K_5 x)\cosh(K_5 x) + A_2 \cos(K_5 x)\sinh(K_5 x) \\ & + A_3 \sin(K_5 x)\cosh(K_5 x) + A_4 \sin(K_5 x)\sinh(K_5 x)\end{aligned} \tag{2.8}$$

Where: A_i and B_i are functions of the applied loading condition.

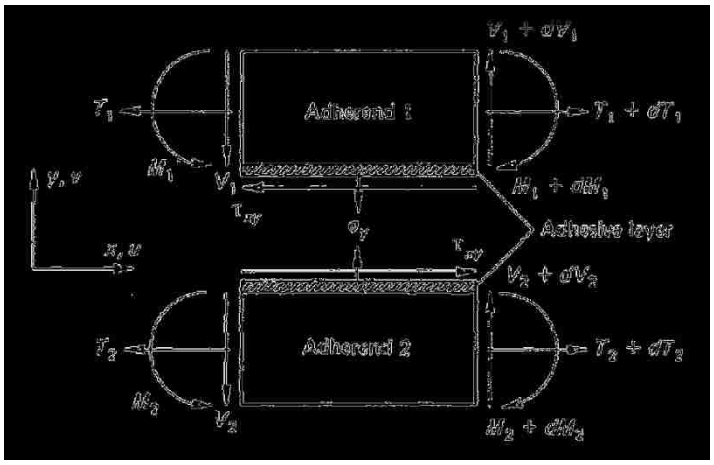

Figure 2-48. Adherend-adhesive sandwich under general loading condition [46]

2.5.4.2 Spot welded joints

As mentioned in Section 2.5.4 a unique failure criterion for the prediction of the nugget strength as function of its geometrical characteristics and of the loading condition is still not available. Numerous efforts have been presented for calculating the stresses and the stress intensity factors at the weld nuggets. The most common methodology used is to evaluate the stress distribution from the failure mode and the failure load of experimental tests. Chao [44]

chose the cross-tension and the lap shear geometry as representative cases for opening and shear loading conditions. By means of detailed fractographs the author concluded that the cross-tension joint failure is actually characterized by shearing of the metal through the thickness at the Heat Affected Zone (HAZ) around the nugget that result into nugget pull-out. He assumed a harmonic stress distribution around the nugget [44].

Figure 2-49. Stress distribution at the weld nugget in cross tension loading mode [44]

A similar approach was taken by Sun et al. [41]; in their study however they considered the stress as uniformly distributed over the weld nugget lateral surface. When instead the nugget was sheared ("interfacial failure mode") the stress was calculated as the load divided by the cross sectional area of the nugget as expressed in Equation 2.9

$$\sigma = \frac{F_{IF}}{\pi \frac{D^2}{4} f} \tag{2.9}$$

Where: σ is the failure stress, $F_{IF}$the failure load, D the nugget diameter and f is a coefficient to account for the reduction in the effective load carrying area due to the presence of porosity in the nugget.

Zhang [47] approximated the weld nugget as a circular rigid inclusion and found some simple analytical expressions to approximate the nominal stress at the weld nugget. He applied this approach to the most common joint geometries, namely lap shear (tensile shear), cross tension and coach-peel and calculated the radial normal stress at the weld nugget for all three joints and the circumferential shear stress at the nugget in the tensile-shearing mode (see Section 5.1).

In addition to the testing of the aforementioned joint geometries a common practice is to use U-shaped and square-cup specimens (Figure 2-50) [44] [49] [50]. The biggest difference between these two geometries can be noticed when loaded in pure opening mode; while for the cup-specimen the load is distributed uniformly around the nugget (bi-axial opening) with the U-shaped specimen the load is more concentrated at the two extremes of the nugget with a distribution similar to the cross tension joint (uniaxial loading).

The main advantage of these specimen geometries is the possibility to load the weld nugget under a wide range of combinations of shearing and opening load; in particular this is possible by using fixture geometry as shown in Figure 2-17. Lin et al. [50] decomposed the external load into an opening (N) and a shearing (S) component acting at the weld nugget Figure 2-51. By imposing the equilibrium conditions at the weld nugget and employing the Von Mises criterion the author formulated the failure criterion reported in Equation 2.10

$$\bar{N}^2 + \alpha\bar{S}^2 = 1 \qquad (2.10)$$

Where: α is a function of the thickness of the sheet and of the nugget diameter and $\bar{N}$ and $\bar{S}$ are the opening and shearing load normalized with respect to the yield strength of the material. Figure 2-52 shows that the formulated failure criterion predicts the experimental results.

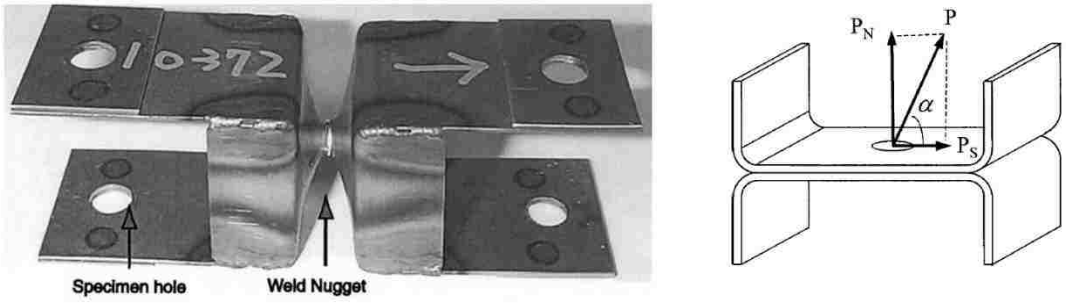

Figure 2-50. Square-cup (left) and U-shaped specimens (right) [44] [50]

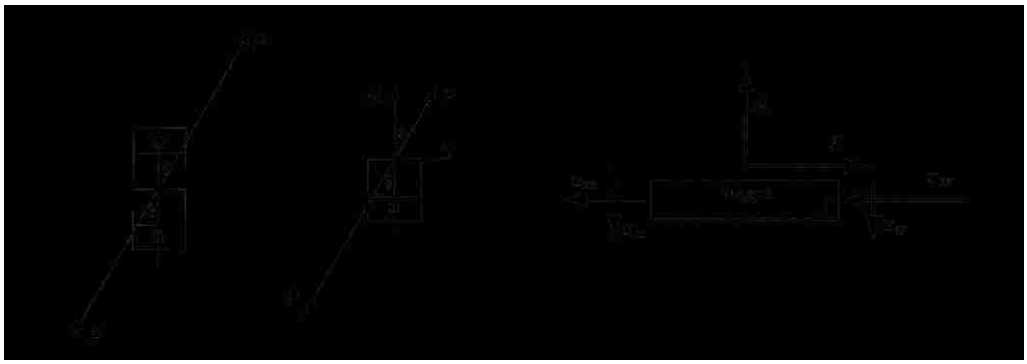

Figure 2-51. The external load is decomposed into an opening (N) and a shear (S) load [50]

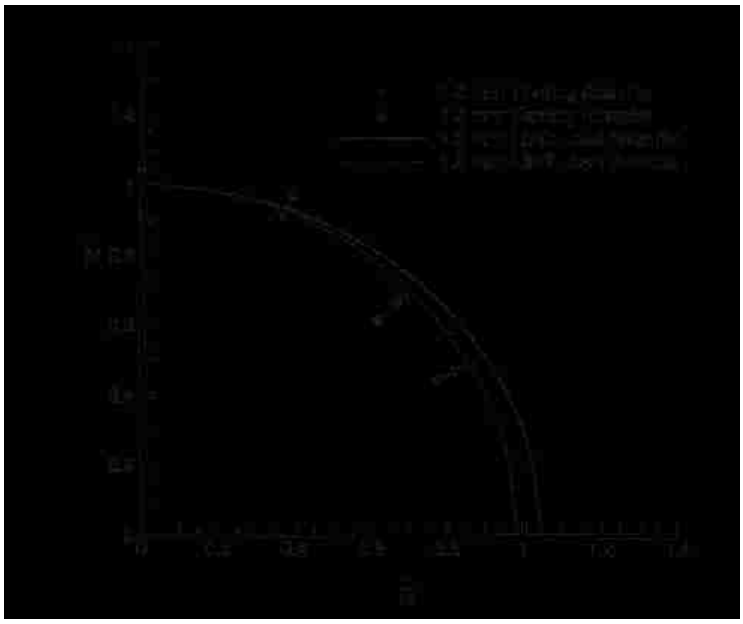

Figure 2-52. Comparison of the experimental results with the quadratic failure contour [50]

2.5.4.3 Riveted joints

The availability of analytical techniques for estimating and predicting the strength of a riveted joint is much more limited; given in fact the even more complicated distribution of stress compared to welded joints, its analysis is almost always assessed by means of Finite Element Models.

The simplest case can be probably considered to be the cross tension joint; Sun et al. [51] analyzed this geometry and proposed a simple model for predicting the failure mode. In their calculation the load was homogeneously distributed over the entire flared area of the rivet skirt on one side and on the flared area of the rivet head on the other side. When taking into account of these geometrical quantities and of the material(s) used the model is able to

predict whether the head or the tail of the rivet will be pulled out. The rivet head and tail pull-out load are expressed respectively by Equations 2.11 and 2.12 as

$$F_h^T \approx \eta_h \beta_h t_1 \pi D_h \sigma_h \quad (2.11)$$

$$F_t^T \approx \eta_t \beta_t t_{eff} \pi D_c \sigma_t \quad (2.12)$$

where F_h^T and F_t^T are the rivet head and tail pull-out loads, t_1 is the thickness of the upper sheet, t_{eff} is the effective material thickness on the tail side, D_h and D_c are the rivet head and tail diameters, σ_h and σ_t are the yield strengths of the upper and lower blanks and η_h, β_h, η_t and β_t are coefficient to account for the ductility of the blanks (for ductile materials $\eta_h = \beta_h = \eta_t = \beta_t = 1$) (Figure 2-53). The calculation of the strength on the two sides of the rivet will then indicate which side is the weakest and more likely to fail.

Porcaro et al. [29] conducted a study very similar to the one by Lin [50] described in Section 2.5.4.2 they tested U-shaped riveted joints at different angles and they proposed the failure criterion in Equation 2.13[6]

$$\left(\frac{N}{N_u}\right)^a + \left(\frac{S}{S_u}\right)^b = 1 \quad (2.13)$$

Where: N and S are the component of the load respectively normal and parallel to the rivet head and N_u and S_u are respectively the maximum normal force in pure tension and pure shear condition.

No analytical formulas were instead found in the literature for assessing the strength of riveted lap and coach-peel joints.

[6] The values of the coefficients a and b were not provided in the Journal Article [29]

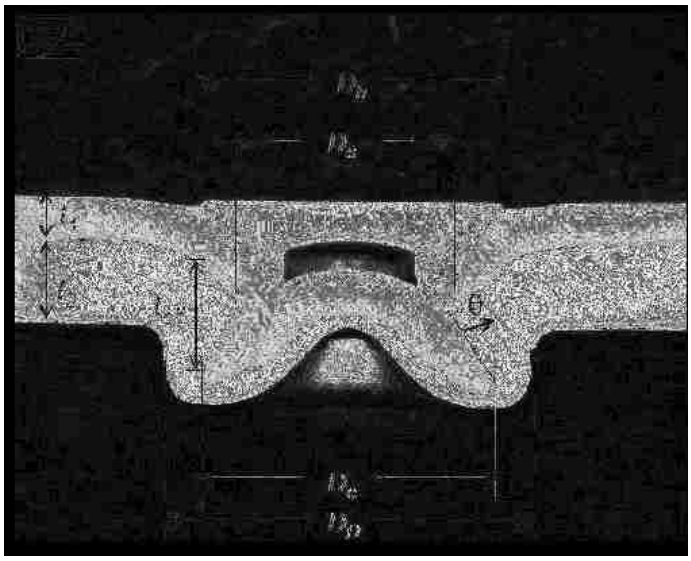

Figure 2-53. Cross section of a rivet and geometrical quantities used for strength estimation [51]

Chapter 3
Experimental Procedure

3.1 Experimental Design

This chapter describes the experiment designed at Chrysler LLC to verify the static strength of aluminum structural joints.

The joint geometries adopted and the matrix of the experimental variables are shown respectively in Figure 3-1 and Table 3-1. Five samples were prepared per experimental condition shown in Table 3-1, for a total of 180 samples. An additional three samples were prepared for the conditions highlighted in orange in Table 3-1 were prepared for video-recording of the tensile tests by a video camera synchronized with the testing machine.

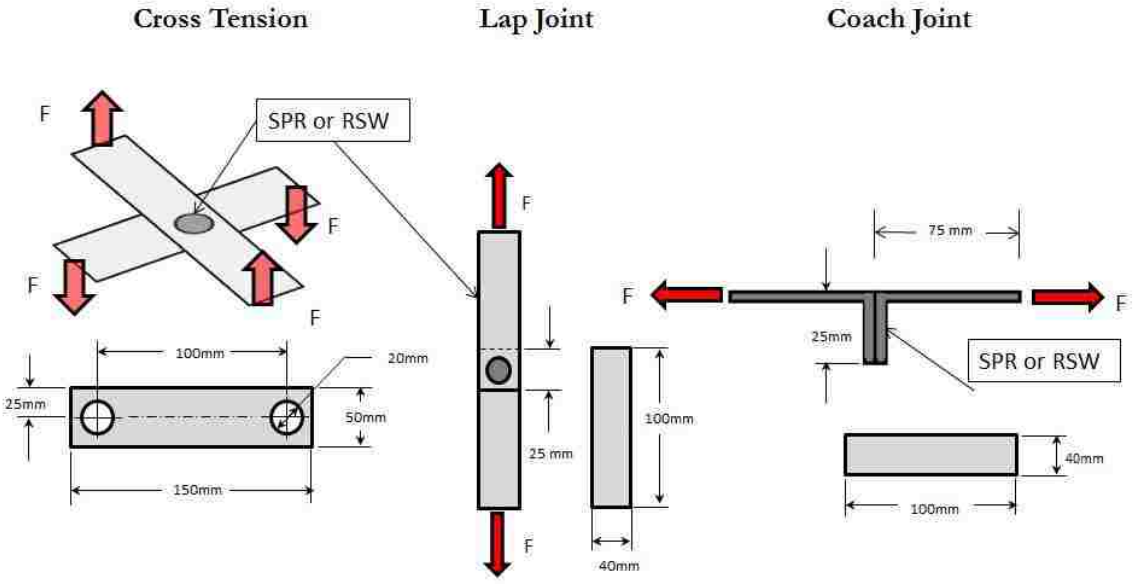

Figure 3-1. Joint geometries adopted in the design of experiment.

Table 3-1. Matrix of the experimental variables. Highlighted in orange are the geometries of the samples additionally prepared for video recording the tensile tests.

Material: MS8580 – A95182 (AA5182)					
Thickness = 1.3 mm			Thickness = 1.75 mm		
Joining Method	**Joint Geometry**	**Adhesive**	**Joining Method**	**Joint Geometry**	**Adhesive**
RSW	Coach	No	**RSW**	Coach	No
		SikaPower 497			SikaPower 497
		Dow BetaMate 1620US			Dow BetaMate 1620US
	Lap	No		Lap	No
		SikaPower 497			SikaPower 497
		Dow BetaMate 1620US			Dow BetaMate 1620US
	Cross - Tension	No		Cross - Tension	No
		SikaPower 497			SikaPower 497
		Dow BetaMate 1620US			Dow BetaMate 1620US
SPR	Coach	No	**SPR**	Coach	No
		SikaPower 497			SikaPower 497
		Dow BetaMate 1620US			Dow BetaMate 1620US
	Lap	No		Lap	No
		SikaPower 497			SikaPower 497
		Dow BetaMate 1620US			Dow BetaMate 1620US
	Cross - Tension	No		Cross- Tension	No
		SikaPower 497			SikaPower 497
		Dow BetaMate 1620US			Dow BetaMate 1620US
Number of sample per condition		**5**	**Number of sample per condition**		**5**
Total number of samples		**90**	**Total number of samples**		**90**

3.2 Material

The material used in this investigation is the aluminum alloy AA5182-O. Its nominal chemical composition and mechanical properties are given in Table 3-2 and Table 3-3. According to the International Alloy Designation System (IADS) classification, AA5182 belongs to the 5000 series of the wrought aluminum alloys. Its main alloying element is

magnesium; it is a strain-hardenable, non-heat-treatable alloy. This latter information is particularly useful for assessing the properties of the hybrid joints, which have to undergo a curing process at moderate temperature. No significant modifications of the mechanical properties are expected due to this heating.

Table 3-2: Chemical Composition AA5182 [52]

AA 5182									
Element	Al	Mn	Mg	Cr	Si	Ti	Zinc	Cu	Fe
%wt	95.2	0.35	4.5	≤ 0.1	≤ 0.2	≤ 0.1	≤0.25	≤0.15	≤0.35

Table 3-3: Mechanical Properties AA5182-O [52]

Mechanical Properties AA5182-O	
Tensile Strength, Ultimate	275 MPa
Tensile Strength, Yield	130 MPa
Elongation at Break	21 %
Modulus of Elasticity	69.6 GPa
Shear Modulus	26.0 GPa
Shear Strength	150 MPa
Poisson Ratio	0.330

3.3 Sample preparation

Both the coach and the lap joints were prepared with aluminum sheet blanks, 100-mm long and 40-mm wide, using the fixture shown in Figure 3-2 (a). The hole visible in the fixture allowed the welding and riveting gun to reach the material and accomplish the welding process. For the preparation of the lap joints, Figure 3-2 (b), the blanks were positioned on the fixture is such a way that they overlapped only over the hole for a length of 25 mm, as specified in Figure 3-1. For the coach joint preparation, the blanks were placed on the same side of the fixture completely overlapped, Figure 3-2 (c). Then a manual vise was used to bend the two blanks to approximately 90^{o} at a distance of 25 mm from the right edge obtaining the final shape shown in Figure 3-1. This manual procedure did not allow for control of the final radius of curvature. The impact of this deviation from a consistent ideal geometry will be illustrated in Section 4.1.4.

Sample preparation of the cross-tension joints is shown in Figure 3-3; the coupon shape and dimensions are shown in Figure 3-1. The fixture has four pins, which match the holes at the extremes of the coupons to be joined and allow control of the relative alignment and positioning of the coupons. The hole in the middle of the fixture is not visible; it allows the welding/riveting gun to reach the component.

For the preparation of the hybrid joints, glue was spread manually over the overlapping area before the welding/riveting process.

Figure 3-2. Sample preparation; (a) fixture for coach and lap joint. (b) lap joint (c) coach joint.

Figure 3-3. Sample preparation; cross tension geometry.

The characteristic parameters of the welding, riveting, curing process and of the tensile tests are summarized in Table 3-4.

The same welding schedule and electrode geometry were used for both stack thicknesses. A pre-heating cycle was added when welding the hybrid joints in order to displace the adhesive from the area affected by the welding process. Different rivets and dies were used for the two different sheet thicknesses; no modifications to the riveting process were introduced for joining the hybrid samples.

The times and temperature for the curing cycle were selected to simulate the car paint baking process, during which the adhesive curing process takes place on the assembly line.

Table 3-4: RSW process parameters.

Welding Process							
Adhesive	Clamping force [lbs]	Preheat	Cool	Weld time	Weld Current [kA]	Hold	Electrode
no	950	-	-	4 cycles	32	2 cycles	3/4" ball nose with 4.8mm face
yes	950	2 cycles at 5 KA	2 cycles	4 cycles	32	2 cycles	

Table 3-5. SPR process parameters.

Riveting Process						
Sheet thickness [mm]	Rivet type	Rivet dimension (length [mm] x diameter [mm])	Die type	Die Diameter [mm]	Riveting speed [mm/s]	Riveting force [kN]
1.3	AS	5 x 5	DZ09-025	9	225	48
1.75	AT	6 x 5	DP09-200	9	255	51

Table 3-6. Adhesive bonding curing cycle.

Adhesive Curing Cycle				
Heating 1	Cooling 1	Heating 2	Cooling 2	Heating 3
350˚F (177˚C), 30 min	2 hours	350˚F (177˚C), 30 min	2 hours	280˚F (138˚C), 30 min

Table 3-7. Tensile test parameters.

Tensile Test		
Equipment	Load Rate [in./minute]	Jaw separation [in.]
Tinius Olsen 30k Testing Machine	0.2	2.46

3.4 Methodologies for data processing and analysis

In Chapter 4 the results of the experimental tests are presented and analyzed. It is divided into three main subsections, one per joint geometry. The results are grouped by "joint geometry type": all the joints with the same geometry and "traditional" (RSW or SPR) joining method, both with and without the addition of adhesive, i.e., all the RSW coach joints 1.3mm and 1.75 mm thick, are considered as a "group" and analyzed together.

For each group a brief interpretation of the tensile test load-displacement curves is presented first, to outline the influence of material thickness and joining method on the behaviour of the specimens behave when tested. Two methodologies have been followed. The first method compares the curves obtained in a single group by superimposing the results obtained with and without the adhesive. This superposition allows an understanding of the effect of the adhesive. The failure mode hypotheses that arise from such a superposition are then verified by observation of additional tensile tests using a video-camera synchronized with the tensile test machine.

Following this interpretation, the results are presented and analyzed. The quantities calculated in the analysis are the load, the displacement, the energy absorbed and the initial loading stiffness during the tensile test. The comparison of the results is carried out by means of a "peak-by-peak" approach, as explained in Section 4.1.1.1. The results are then analyzed by mean of a failure mode analysis and, only for the RSW joints, by correlating the load with the measured weld nugget size. Finally, possible deviations from ideal sample preparation and testing conditions are presented and their impact is analyzed. The load – displacement curves for all the tested samples are reported in Appendix A.

In Chapter 5 the stress at failure of the joining elements are calculated from the load at failure by means of analytical formulae. In particular, the models proposed by Zhang [47] and by Bigwood and Crocombe [46] are utilized for the calculation of the failure stress of the weld nugget and of the adhesive layer respectively. A new analytical method is presented for the calculation of the stress at failure in the SPR joints. The results obtained from the analytical calculation are then compared both to investigate the possibility of defining a universal failure criterion, as well as to infer design rules for designing of the studied joints.

Chapter 6 analyzes the impact of the adhesive layer on the RSW and SPR process. The weld nugget porosity and the microhardness in the HAZ and the fused zone in the hybrid joints are compared to the welded-only sample values to highlight possible effects of the

adhesive layer. For the riveted-only and the rivet-bonded joints, the impact of the adhesive layer on the rivet interlock will be analyzed by comparing relevant cross-sections.

Chapter 4
Results

4.1 Coach Joint

4.1.1 Coach Joint RSW

4.1.1.1 Tensile test data interpretation – Coach Joint RSW

Figure 4-1 shows three typical load-displacement curves for the 1.3mm RSW coach joint. The result for the no-adhesive (NA) test resembles the one obtained by Briskham [34] shown in Figure 2-23. The load increases linearly until reaching a maximum, then after a partial load drop the elongation proceeds at almost constant load until the final failure. The weld nugget is the only joining element, and a crack is expected to start at the point of maximum stress concentration at the weld nugget. The subsequent load drop and the plateau correspond to the crack propagation until final failure. In particular, knowing that all of the welded coach joints failed in "nugget pull-out" mode, Section 4.1.1.6, it can be said that the crack is propagating in the HAZ surrounding the weld nugget, Section 2.5.3.

The two batches of samples glued with SIKAPOWER497 and DOW BETAMATE 1620S show the effect of adding adhesive to the spot welded joint. Both have a clear peak after a few millimeters of deflection that was not present in the NA case. Corroboration of this hypothesis comes from a review of the literature, wherein the researchers agree that the increase in the joint stiffness is one of the advantages of the addition of adhesive [23, 24, 25, 26, 28]. Bartczak et al. [35] pointed out in their study the presence of two clearly distinguished peaks in the load-deflection curve of hybrid joints. They indicated the adhesive yielding and the nugget yielding as the causes for the two peaks respectively, Figure 2-26.

The initial load rise of the hybrid joints is very steep and ends in a peak attributed to adhesive yielding. The fracture then begins propagating in the adhesive layer, as manifested by a load drop. The load drop, however, is stopped after few millimeter of deformation when the majority of the load transfers to the weld nugget. Beyond this point on the shape of the curve of the hybrid joints is very similar to the welded joints. Final deformation of

the hybrid joint is increased because the adhesive still present at the extremity of the overlap holds the load after the nugget has completely failed.

The video recording of the coach joint tensile tests confirmed the failure sequence described in the previous paragraph. Figure 4-3(a) shows the un-deformed shaped of the coach joint sample; Figure 4-3 (b), (c) and (d) show the deformation of the sample before the maximum load, at the maximum load, and during the crack propagation immediately before the final joint failure. Comparing Figure 4-3 (b) and Figure 4-3 (c), it can be seen that the joint is progressively "opening" starting from the joint curvature toward the weld nugget. Once the tip of the split reaches the nugget its translation is temporarily stopped, until the maximum load is reached and the nugget starts to fail, Figure 4-3 (c). In Figure 4-3 (d), the joint is highly deformed, and the nugget has been almost entirely pulled out. Even though the nugget itself cannot be clearly distinguished, the hole left by the nugget in the upper sheet can be seen.

Figure 4-4 shows the progression of the tensile test for a 1.3mm thick RSW coach joint with the addition of the Dow adhesive. Compared to the no-adhesive sample, no variation from the un-deformed shape is noticeable until the first peak, Figure 4-4 (a) and (b)). Figure 4-4 (c) shows the test sample after the first peak; a crack propagating inside the adhesive layer is visible. Figure 4-4 (d) resembles Figure 4-3 (c) and illustrates the deformation of the joint at the second load peak, shortly before the weld nugget starts to fail. Figure 4-4 (e) shows the sample before the joint final failure. In this case, however, the nugget has been completely pulled out and the two components are held together only by the adhesive left on the tip of the overlap. The superimposition of three curves of the 1.75mm RSW Coach Joint, Figure 4-2, depicts this "three-peak" shape.

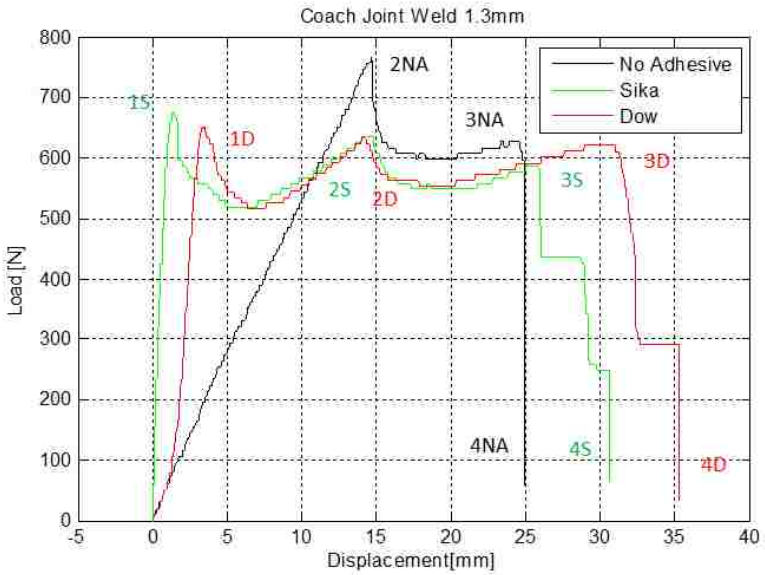

Figure 4-1. Results Interpretation; Curve superimposition for the 1.3 mm Coach Joint RSW.

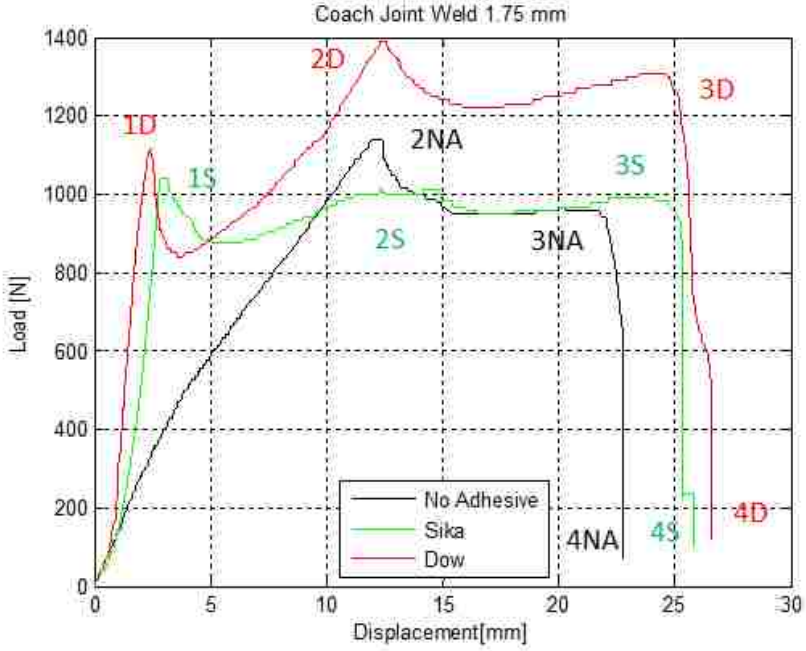

Figure 4-2. Results Interpretation; Curve superimposition Coach Joint Weld 1.75mm.

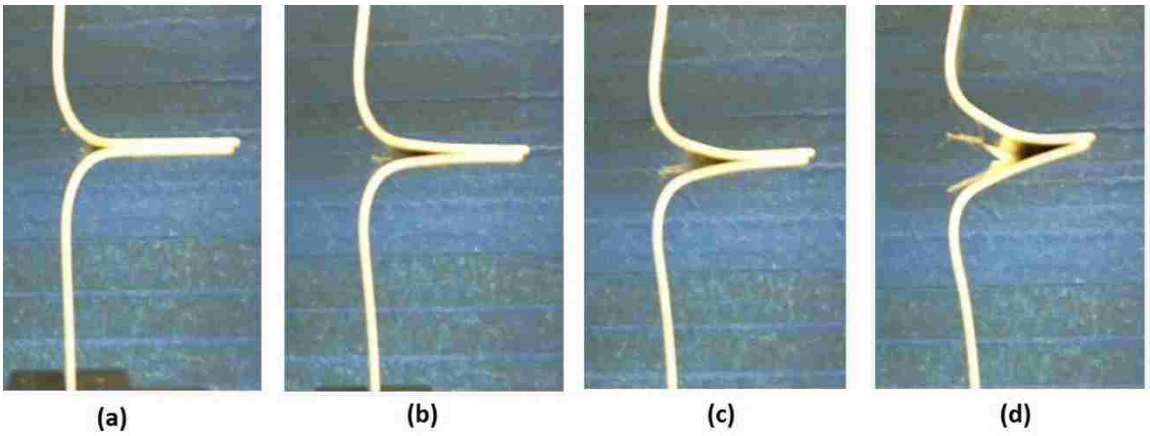

Figure 4-3. Tensile test of a 1.3 mm thick welded coach joint, No adhesive; un-deformed shape (a), deformed shape before the nugget yielding (b), at maximum load (nugget yielding) (c) and during crack propagation, before final failure (d).

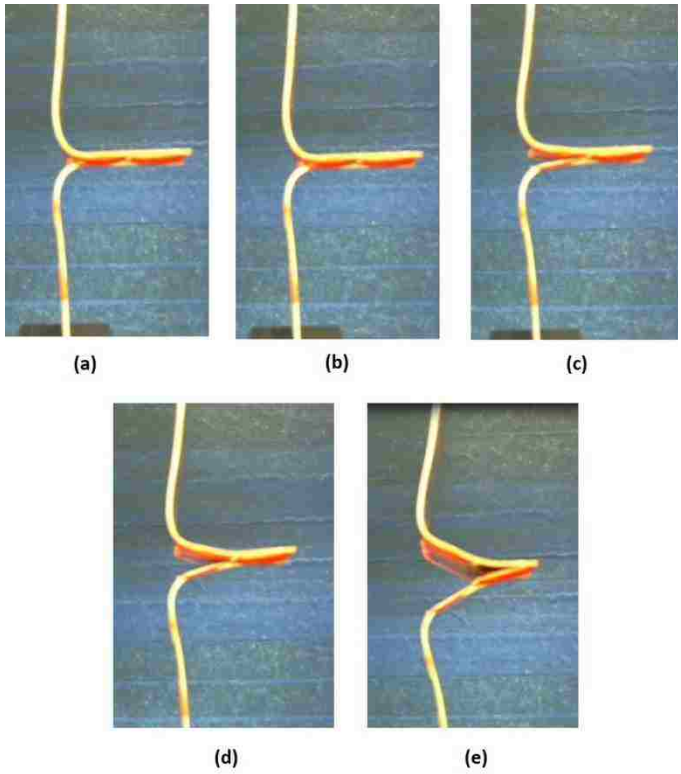

Figure 4-4. Tensile test of a 1.3 mm thick welded coach joint with DOW adhesive; un-deformed shape (a), shape before the adhesive yielding (b), shape after the adhesive yielding and before nugget yielding (b), shape at nugget yielding (d) and during crack propagation, before final failure (e).

Based on this analysis, the following relevant points and regions have been highlighted for all the tested samples:

- RSW only (No-Adhesive, NA): Nugget yielding and final failure of the joint (2 NA, 3 NA and 4 NA in Figure 4-1 and Figure 4-2).

- RSW + Adhesive (SIKAPOWER497): Adhesive Yielding, Nugget yielding and final failure of the joint (1S, 2S, 3S and 4S in Figure 4-1and Figure 4-2).
- RSW + Adhesive (DOW BETAMATE 1620US): Adhesive Yielding, Nugget yielding and final failure of the joint (1D, 2D, 3D and 4D in Figure 4-1 and Figure 4-2).

The tensile test load, displacement, and energy were calculated at each one of these highlighted relevant points; the stiffness of the joint was tabulated. Data processing was accomplished with an EXCEL® spreadsheet and Matlab ® code.

4.1.1.2 Load vs Displacement – Coach Joint RSW

The results for load and displacement of the RSW Coach Joint Weld group are summarized in Figure 4-5, Figure 4-6, Table 4-1[7], and Table 4-2. Appendix A reports the load – displacement curves for all the tested samples.

The points indicated in Figure 4-5, Figure 4-6 show the average performance of the five tested samples at the previously highlighted peaks and the error bars indicate the standard deviation of the five measurements. It is important to mention that the dashed lines connecting the points in Figure 4-5 and Figure 4-6 do not represent the real behavior of the load-displacement lines. They are used to make the diagrams easier to read.

The average load held at the adhesive yielding peaks 1S and 1D in the Sika and Dow joints is comparable for both stack thicknesses. The results obtained at this peak for the Sika samples showed a high variability with the thinner stack, and a low variability with the thicker stack. An opposite trend was noticed with Dow samples. The increment in sheet thickness gave both joints a significant increase in load at the first peak, close to 65%. The lower deformation experience by the adherends due to the increase in their cross section causes a more favorable loading condition of the adhesive layer. As noted in Figure 2-15, the thicker the section of the coupons, the more the loading mode can be described as a cleavage loading; while the thinner the section, the more it can be equated to peel. The elongation at the first peak was similar for both hybrid joints; its increment as function of the variation of sheet thickness was less significant compared to the load, especially for the Dow samples.

[7] Note: in this table and the following tables, the standard deviation of the joint properties is expressed as a percentage of the average value.

The weld nugget of the 1.3 mm joints yielded on average at a higher load for the welded–only samples (635 N) compared to the hybrid ones (583 N and 552 N for Sika and Dow); however, the variability of these results was large enough to make it impossible to state which case showed the best performance. The load carried by the nugget in the two hybrid cases is comparable; the samples glued with SIKAPOWER 497 showed a slightly higher variability. An explanation for the high variability, both at the adhesive peak and at the nugget peak is given in Section 4.1.1.6. It is interesting to note that, on average, the 1.3 mm thick hybrid samples showed a higher load at the adhesive peak than at the nugget peak.

The 1.75 mm Dow samples showed the highest load at the second peak; for the thicker stack the load held by the hybrid joints at the second peak is about equal (Sika) or higher (Dow) than the first peak. The second peak showed a comparable increase in load as function of the increase in thickness for Sika and no-adhesive samples (74% and 69%), and an even greater increase for Dow samples (109%). Among the factors contributing to this increase, an important role is played by the weld nugget size variation which is analyzed in Section 4.1.1.5. In addition the increase in thickness can significantly reduce the loading at the nugget. The portion of the overlap area from the curvature to the weld nugget can be modelled with good approximation as a beam loaded in bending. As such, the larger the cross section of the coupon, the lower the stress because of the bending moment that the weld nugget will have to sustain.

Table 4-1 also shows that, on average, the nugget yielding peak benefits more than the adhesive yielding peak from the increase in thickness. The same trend was noticed by Moroni et al. [25]. The load held by the 1.3 mm joints before final failure, the third peak values in Table 4-1 is comparable for all the tested joints. The elongation, Table 4-2, is on average larger for the hybrid joints. In addition, the drop in load after this point is almost vertical for the no-adhesive samples, meaning an instantaneous breakage; while for the hybrid joints, the load drop is more gradual. This difference can be attributed to the presence of the adhesive surrounding the weld nugget and at the tip of the overlap, Figure 4-4 (e). The adhesive is able to slightly delay the propagation of the crack around the nugget, which guarantees a larger average displacement at the third peak, and to avoid the sudden breakage that the NA samples have experienced. Some additional displacement is then gained after complete nugget failure while the crack propagates through the final portion of adhesive. The benefit to the final elongation by the presence of the adhesive was reduced

with the thicker stack. The drop in load after the third point was comparable for all the cases; for the Dow samples, almost no additional elongation was obtained after the third peak. The NA and Sika samples show a very similar load at the third point, while the Dow samples performed better on average.

In summary, the hybrid samples did not show any particular increase in strength compared to the NA samples. An increase in elongation above the NA joints was observed at the last peak and at final failure of the joint. This additional elongation could be highly beneficial for the energy absorption in conditions such as crash. Finally, the two adhesives showed similar performance.

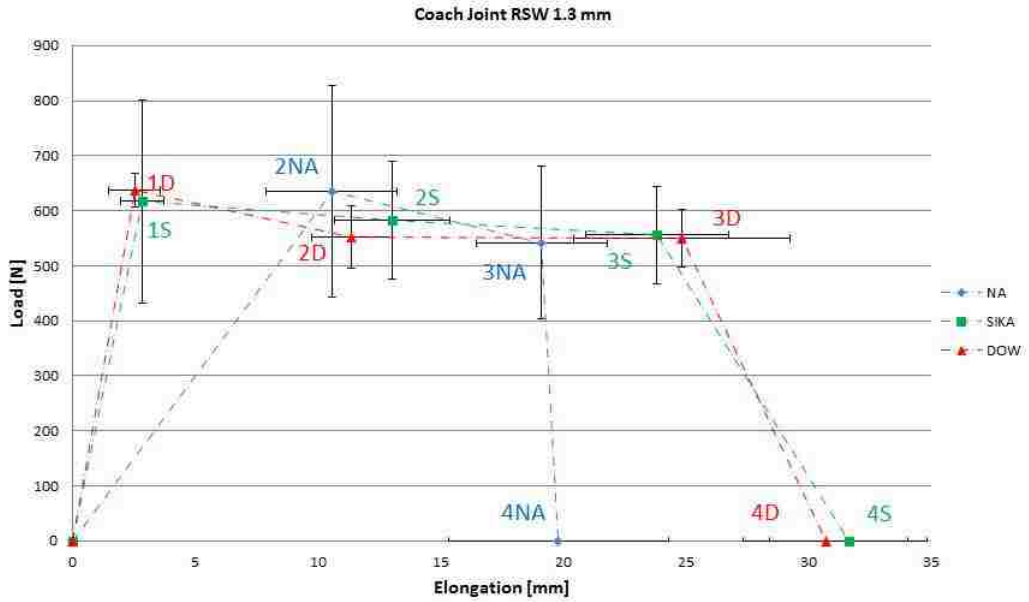

Figure 4-5. Schematic representation of the Load - Displacement curves for the RSW Coach Joint 1.3 mm thick.

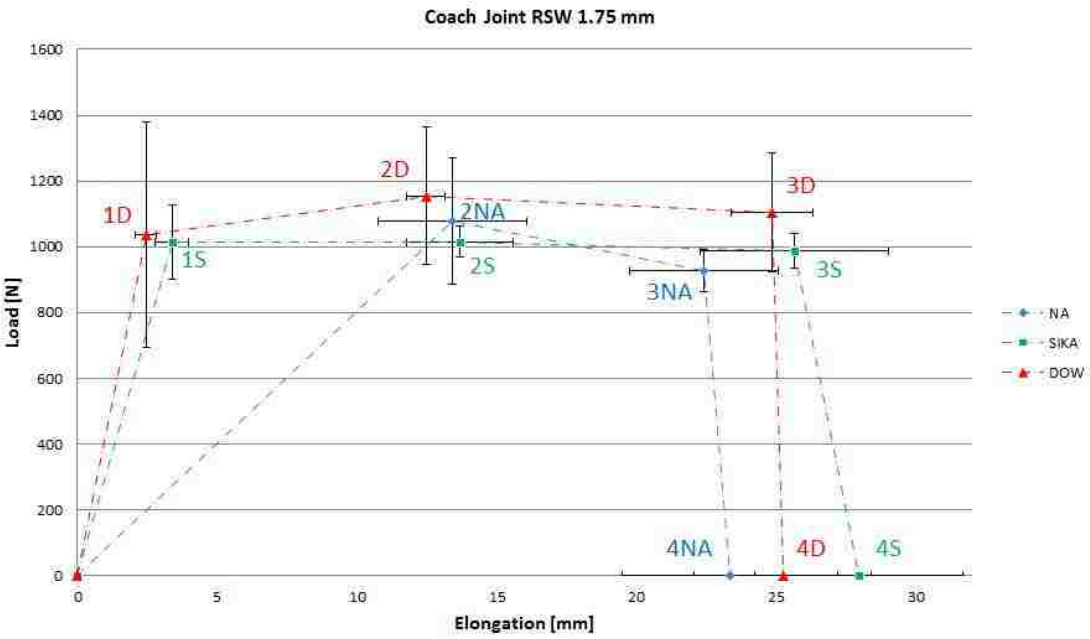

Figure 4-6. Schematic representation of the Load - Displacement curves for the RSW Coach Joint 1.75 mm thick.

Table 4-1. Load at the indicated peaks; RSW Coach Joints.

Load [N]										
RSW Coach Joint 1.3mm vs 1.75mm		NA		SIKA		DOW		Sika vs Na	Dow vs Na	Dow vs Sika
		mean	st.dev	mean	st.dev	mean	st.dev			
1st peak	1.3 mm	-	-	617	30%	637	5%	-	-	3.1%
	1.75 mm	-	-	1013	11%	1037	33%	-	-	2.4%
				64%		63%				
2nd peak	1.3 mm	635	30%	583	19%	552	10%	-8.1%	-13.1%	-5.4%
	1.75 mm	1078	11%	1015	5%	1155	18%	-5.8%	7.1%	13.8%
		70%		74%		109%				
3rd peak	1.3 mm	542	26%	556	16%	551	10%	2.6%	1.7%	-0.8%
	1.75 mm	926	7%	988	5%	1104	16%	6.6%	19.2%	11.8%
		71%		78%		100%				

Table 4-2. Elongation at the indicated peaks; RSW Coach Joints.

Elongation [mm]										
RSW Coach Joint 1.3 vs 1.75		NA		SIKA		DOW		Sika vs Na	Dow vs Na	Dow vs Sika
		mean	st.dev	mean	st.dev	mean	st.dev			
1st peak	1.3 mm	-	-	2.8	31%	2.5	42%	-	-	-11.0%
	1.75 mm	-	-	3.4	17%	2.5	15%	-	-	-27.3%
				18.6%		-3.1%				
2nd peak	1.3 mm	10.6	25%	13.1	18%	11.4	15%	23.6%	7.9%	-12.7%
	1.75 mm	13.4	20%	13.7	14%	12.5	6%	2.0%	-7.0%	-8.9%
		27.0%		4.8%		9.5%				
3rd peak	1.3 mm	19.1	22%	23.8	12%	24.8	18%	24.6%	29.9%	4.3%
	1.75 mm	22.4	15%	25.7	13%	24.8	6%	14.5%	10.8%	-3.2%
		17.3%		7.7%		0.0%				
joint failure	1.3 mm	19.8	23%	31.6	10%	30.7	11%	59.7%	55.0%	-3.0%
	1.75 mm	23.4	17%	28.0	13%	25.2	13%	19.7%	8.0%	-9.7%
		17.9%		-11.6%		-17.8%				

4.1.1.3 Energy– Coach Joint RSW

The "peak-by-peak" calculation approach illustrated in the previous sections has been applied also to the calculation of the energy absorbed by the joint during the deformation. The benefit obtained by the adoption of this method for the energy calculation is probably much greater compared to the load measurement, as shown by the following example. The literature indicates that the energy absorbed by the joint at the point of maximum load is the critical variable to be calculated [33]. This approach, however, could lead to an erroneous conclusion, as shown in Figure 4-7. The curve on the left registered the maximum load at the first peak and a lower load at the second peak; while the curve on the right exhibits the opposite behaviour. Equation 4.1 states clearly the dependency of the energy on the displacement; as such the energy absorbed at maximum load by the joint represented on the right (6 J) is much greater than the joint shown on the left (1 J), even though at each point the load carried by the sample on the left was higher.

$$Energy = \int Load * Displacement \qquad (4.1)$$

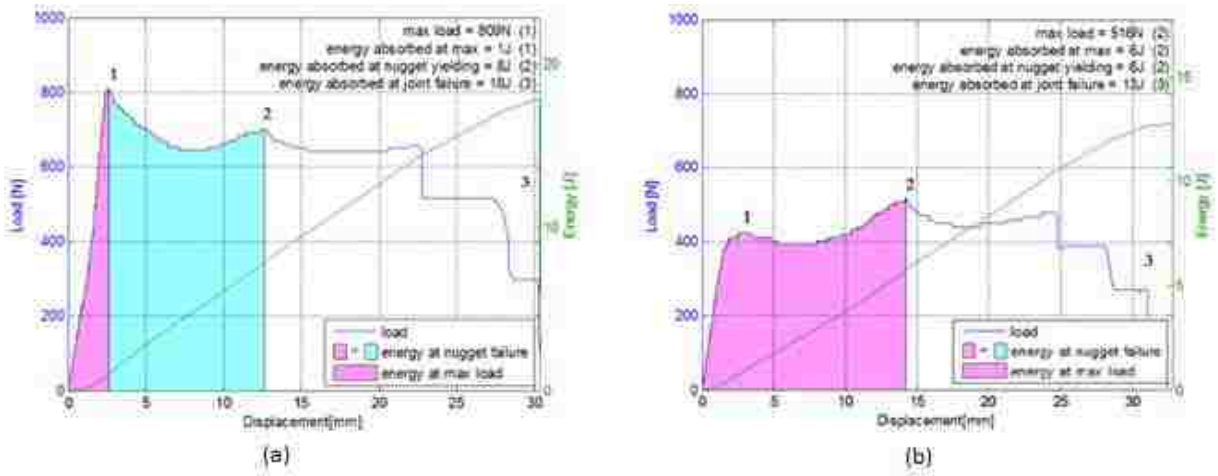

Figure 4-7. Load vs. Displacement curves for 1.3mm Coach Joint Weld + Sika, sample # 5 (a) and sample #4 (b). The area under the curve (equal to the absorbed energy) until maximum load and nugget yielding has been highlighted with different colors.

By adopting the "peak-by-peak" approach shown in the previous sections, this problem is overcome because the energy is always calculated in the same conditions, namely at the yielding of the adhesive, the yielding of the nugget, and the final failure.

The results obtained with RSW Coach Joints are summarized in Figure 4-8, Figure 4-9 and in Table 4-3. As explained for the load calculation in Section 4.1.1.2 the lines connecting the points in Figure 4-8 and Figure 4-9 do not represent the average cumulative energy absorption but rather are just for connecting the points in the diagram. The first peak is located after a few millimeters of displacement thus the energy absorbed at the first peak is relatively low; at this peak the two adhesive showed a similar behavior. The energy absorbed by the adhesive prior to the second peak is responsible for the greater average value of energy absorbed by the hybrid joints compared to the no-adhesive samples. However all the cases showed a high variability of the results (especially the weld-only case) that does not allow drawing any definitive conclusion on the performance of the joints.

The same trend is noticeable also in the last section of the curves, from the third peak to the joint final failure. As mentioned in Section 4.1.1.2, the presence of adhesive allows for more gradual breakage, thus a higher displacement at failure and consequently higher energy absorption. Thus, while the welded only samples showed a very small increase in energy from the third peak to final failure, a remarkable increment was shown instead by the hybrid samples. This piece of information is important when studying the crashworthiness of the joints, where the energy absorption until the final failure of the joint is considered as useful

energy. Both the 1.3 mm hybrid samples showed similar energy absorption at final failure. Considering the thicker stack, Sika samples absorbed on average the highest value of energy at fracture, followed by Dow and lastly by the NA samples. As mentioned in the previous Section, in the Dow samples the load dropped almost vertically, with virtually no additional displacement and energy absorption from the third peak to final failure. On the other side the Sika samples showed an additional elongation after the third peak that led to a higher final elongation and a higher average absorbed energy at failure. Once again the large variability of the results must be emphasized.

Analyzing the impact of the increment in blank thickness it can be noticed that the energy absorbed at the second peak, third peak and at final failure increased more significantly for the no-adhesive samples. This is ascribable to the different trend of the elongation observed for the thin and thick stacks with the hybrid joints; as mentioned, the adhesive significantly improved the elongation at fracture for the 1.3 mm joints while it had a much reduced effect on the 1.75 mm joints. Thus the difference in energy absorption between the no-adhesive samples and the hybrid samples is reduced for the 1.75 mm joints compared to the 1.3 mm joints, especially the energy at final failure (Table 4-3).

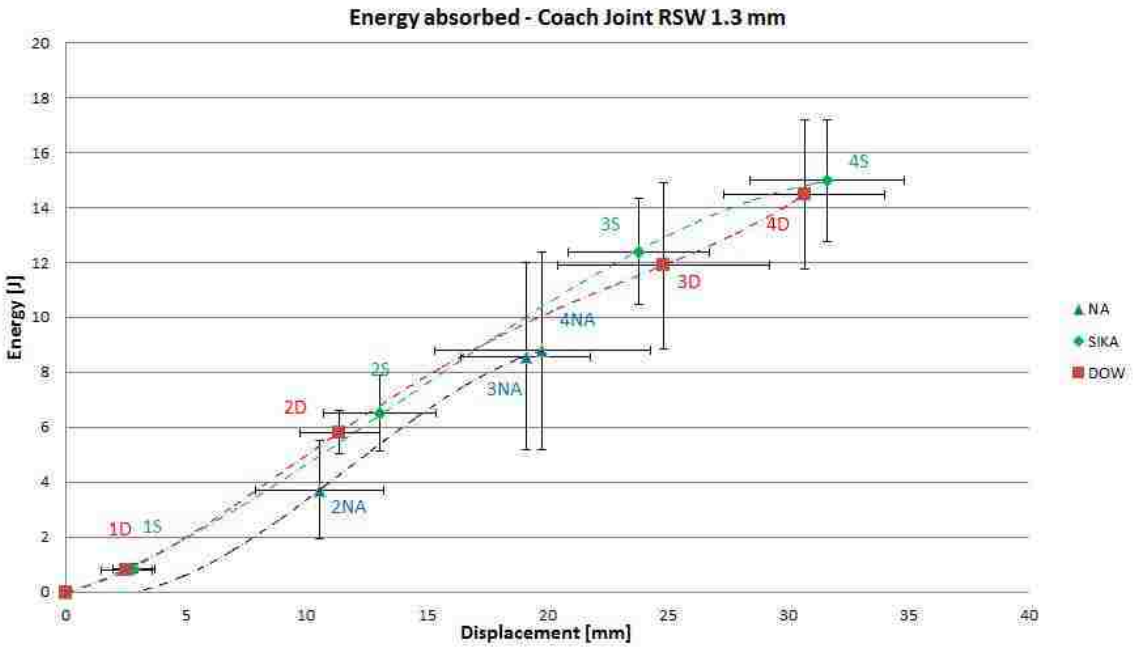

Figure 4-8. Energy absorbed by the joint as function of the displacement; Coach Joint 1.3 mm RSW.

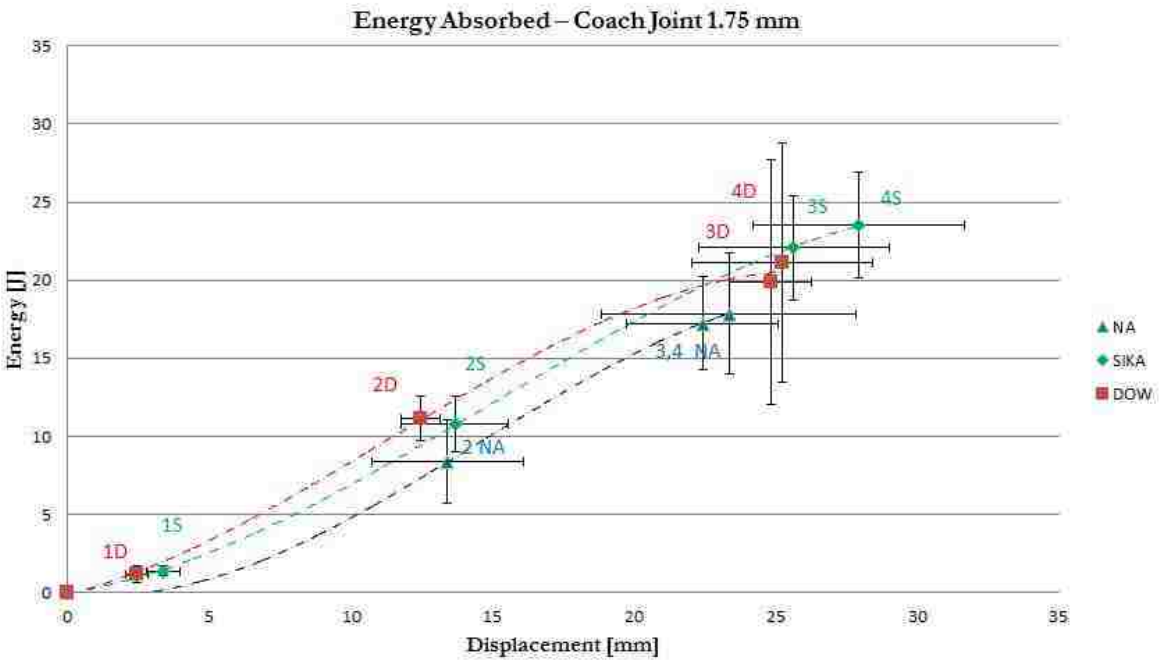

Figure 4-9. Energy absorbed by the joint as function of the displacement; Coach Joint 1.75 mm RSW.

Table 4-3. Energy at the indicated peaks; RSW Coach Joints.

Energy [J]										
Coach Joint Weld 1.3 mm vs. 1.75 mm		NA		SIKA		DOW		Sika vs NA	Dow vs NA	Dow vs. Sika
		mean	st.dev	mean	st.dev	mean	st.dev			
1st peak	1.3 mm			0.9	20%	0.8	26%			-9.2%
	1.75 mm			1.4	25%	1.2	46%			-14.3%
				63%		54.2%				
2nd peak	1.3 mm	3.7	48%	6.5	21%	5.8	13%	75.4%	56.8%	-10.6%
	1.75 mm	8.4	22%	10.8	16%	11.1	13%	28.6%	32.1%	2.8%
		126%		65.9%		90.8%				
3rd peak	1.3 mm	8.6	40%	12.4	16%	11.9	25%	44.4%	38.5%	-4.1%
	1.75 mm	17.3	17%	22.1	15%	19.8	40%	27.9%	15.0%	-10.1%
		101%		78.1%		66.9%				
joint failure	1.3 mm	8.8	41%	15.0	15%	14.5	19%	70.6%	65.0%	-3.3%
	1.75 mm	17.9	18%	23.5	14%	21.1	36%	31.3%	17.9%	-10.2%
		104%		56.9%		45.7%				

4.1.1.4 Stiffness– Coach Joint RSW

The stiffness of the joint can be calculated as the slope at the origin of the load displacement curves. Due to in-homogeneities in the sample preparation the load-displacement line often showed a transient at the beginning of the test (i.e. in Figure 4-1 the

line of the RSW + Dow sample has a much lower slope at the origin compare to RSW + Sika). The transient is probably due to possible misalignments of the sample in the testing machine frame and grips and not rather to the effective performance of the joint and consequently the initial transient is discarded and the slope is calculated in the section pd the curve following it.

The results obtained with the RSW coach joints are reported in Table 4-4. The addition of the glue guaranteed a remarkable increase in stiffness to the joint, from 73 N/mm for the no-adhesive joints up to 437 N/mm and 432 N/mm respectively for Sika and Dow hybrid joints. The increment obtained with the 1.75 mm joints was more limited, namely equal to 269% and 347% respectively for Sika and Dow hybrid joints. This difference is not to be ascribed to the performance of the adhesive itself; both the 1.3 mm and the 1.75 mm hybrid joint showed in fact a very similar stiffness. For the no-adhesive samples the stiffness increased by 53% when thickness changed from 1.3 mm to 1.75 mm. Thus the relative increase in stiffness due to the adhesive obtained with the thicker joint is lower.

In order to explain this behavior the interpretation of the tensile test should be recalled. Figure 4-3 (a) and (b) show that the portion of the curve where the stiffness of the joint is measured corresponds to the deformation of the adherends that are progressively separating starting from the fillet. As mention in Section 4.1.1.2 the increase in the cross section of the adherends requires a higher load to be applied for the same deflection and thus causes an increase in the stiffness between the 1.3 mm thick and the 1.75 mm thick welded-only samples. On the other side Figure 4-4 (a) and (b) show that in the first portion of the elastic line of a hybrid joint the adhesive is being loaded almost in pure tension with no significant differences between the two thicknesses. The stiffness of the hybrid joint is thus function of the elastic modulus of the adhesive and is quite independent of the thickness of the coupons.

Table 4-4. Stiffness of the RSW Coach Joint group.

Stiffness at initial load application [N/mm]									
Coach Joint RSW	NA		SIKA		DOW		Sika vs NA	Dow vs NA	Dow vs Sika
	mean	st.dev	mean	st.dev	mean	st.dev			
1.3 mm	73	36%	437	53%	423	20%	500%	481%	-3%
1.75 mm	111	27%	411	18%	498	44%	269%	347%	17%
	52.9%		-5.8%		17.7%				

4.1.1.5 Nugget Size– Coach Joint RSW

A common practice, both at the academic and the industrial level is to correlate the variation in load with the variation in the weld nugget size. Examples of this analysis can be found in the research by Darwish [30], Darwish et al. [42] and Radakovic and Tumuluru [31]. All these authors agree that the bigger the nugget size, the higher the load that a welded joint is able to hold.

The same kind of analysis is carried out here. In addition, the measurement of the nugget size allows investigating if a difference in the weld nugget dimension of hybrid joints exists, due to interactions of the adhesive with the welding process itself. In Figure 4-10 the white arrows show the measurement of the nugget diameter. The nugget thickness was measured as well to enable the calculation of the lateral surface of the weld nugget, approximated as a cylinder. For both the cases, 3 measurements were performed and the average value and the standard deviation were calculated and reported in Table 4-5

The table indicates that no large differences in the nugget diameter exist between the welded-only samples and the hybrid samples (the difference between the averages is always smaller than the variability of those averages). This indicates that the preheating cycle used in the welding process of the hybrid joints has removed effectively the adhesive and allowed a sound process (see Section 6.1). The difference between the nugget diameter in the thin and thick configuration is reduced as well. This result is not surprising since the same electrode dimensions and weld parameters have been used for both the thicknesses (Section 0). This datum indicates that relatively to the sheet thickness the nugget in the thinner stack is actually bigger. Expressing the nugget size as[8]

$$d = n\sqrt{t} \tag{4.2}$$

where d is the nugget diameter and t the sheet thickness, the coefficient n takes the values of respectively 6.02 for the welded-only 1.3 mm and 5.29 for the 1.75 mm thick coach joints. Table 4-6 shows that the increase in thickness of the weld nugget for the 1.75 mm joints is significant, namely in between 37.5% for the welded only samples and about 50% for the Sika and Dow hybrid samples.

[8] See also Section 2.5.1.3

Figure 4-10. Measurement for the weld nugget size.

Table 4-5. Weld nugget diameter for the studied joints.

Nugget diameter [mm]								
Coach Joint	No Adhesive		SIKA		DOW		Sika vs NA	DOW vs NA
	mean	st.dev	mean	st.dev	mean	st.dev		
1.3 mm	6.86	0.29	6.70	0.10	6.73	0.44	-2.3%	-1.9%
1.75 mm	7.00	0.25	7.14	0.27	6.95	0.47	1.9%	-0.7%
	2.1%		6.5%		3.2%			

Table 4-6. Weld nugget thickness for the studied joints.

Nugget thickness [mm]								
Coach Joint	No Adhesive		SIKA		DOW		Sika vs NA	DOW vs NA
	mean	st.dev	mean	st.dev	mean	st.dev		
1.3weld	1.75	0.12	1.71	0.10	1.57	0.18	-2.2%	-10.3%
1.75weld	2.41	0.11	2.60	0.15	2.43	0.25	8.1%	1.1%
	37.5%		52.0%		54.9%			

The correlation between the nugget dimensions and the load held by the joint at the nugget yielding peak (second peak) is shown in Figure 4-11 - Figure 4-16.

Following the examples of the literature, trend lines were added to the graphs. However, the equations of the trend line and the correlation coefficients were not indicated in the presented studies. In the analyses reported in the literature [30, 31, 42] the welding parameters were intentionally varied with the purpose of getting highly different nugget sizes (i.e. nugget diameter ranging from 2.5mm to 5.5 mm [30]); the correlation then obtained with the load was quite good and robust. In this study the welding parameters are not changed and the differences in dimension are more reduced (especially in this case for the Sika samples, Figure 4-13) and caused by factors like inhomogeneity of the surface

conditions. The obtained scatter was considered too high for a reliable calculation of the trend line.

The following general observations:

- The larger the nugget size, the higher the load that the joint is able to hold
- The smaller the variation between the dimensions of the nuggets, the more the correlation in the previous point is overshadowed by the variability associated with the process. A clear example is represented here by the Sika joints in Figure 4-13 and Figure 4-14.

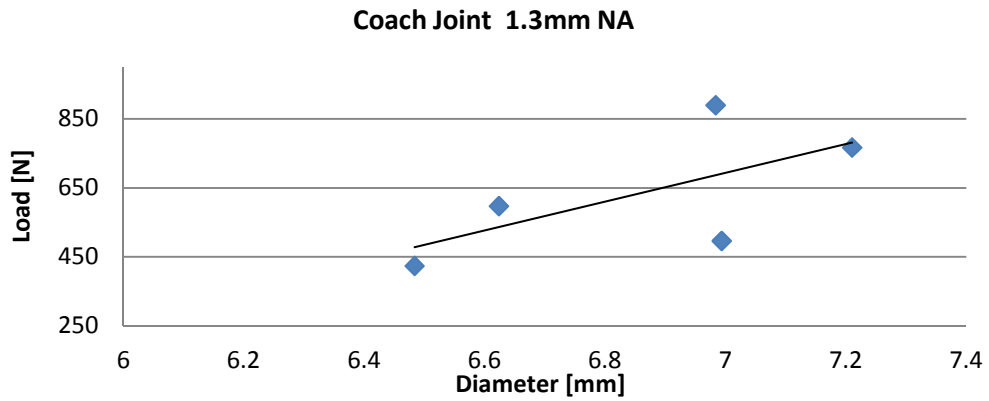

Figure 4-11. Load vs. Nugget Diameter Coach Joint RSW 1.3 mm No Adhesive.

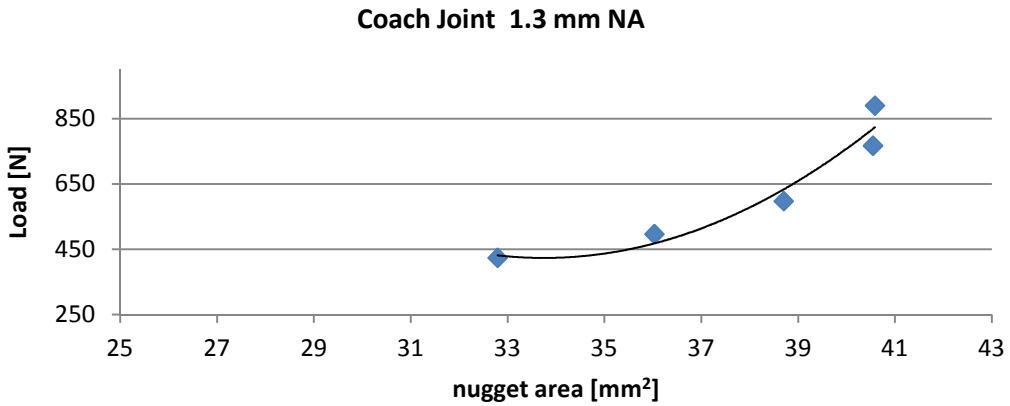

Figure 4-12. Load vs. Nugget Lateral Area Coach Joint RSW 1.3 mm No Adhesive.

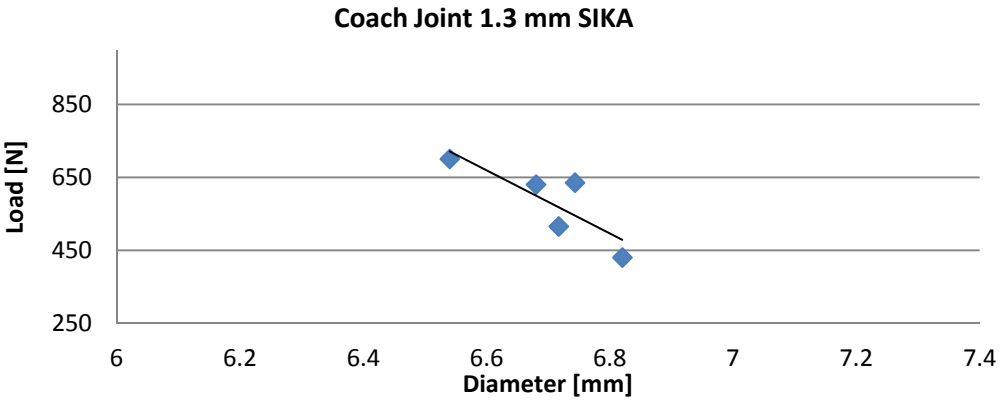

Figure 4-13. Load vs. Nugget Diameter Coach Joint RSW 1.3 mm Sika.

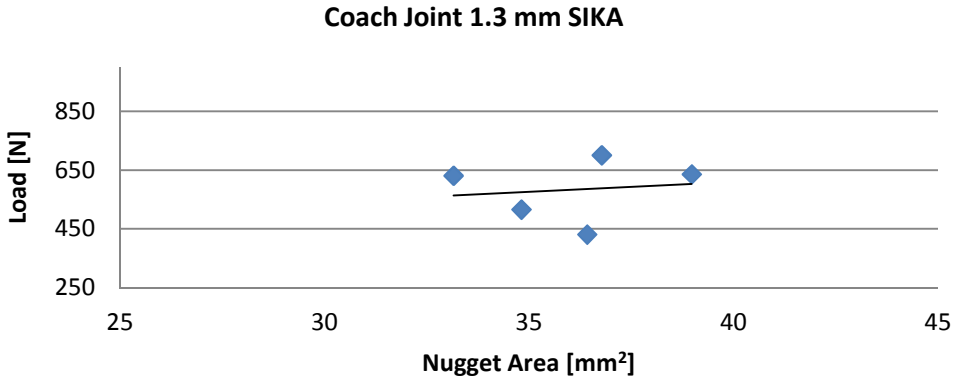

Figure 4-14. Load vs. Nugget Lateral Area Coach Joint RSW 1.3 mm Sika.

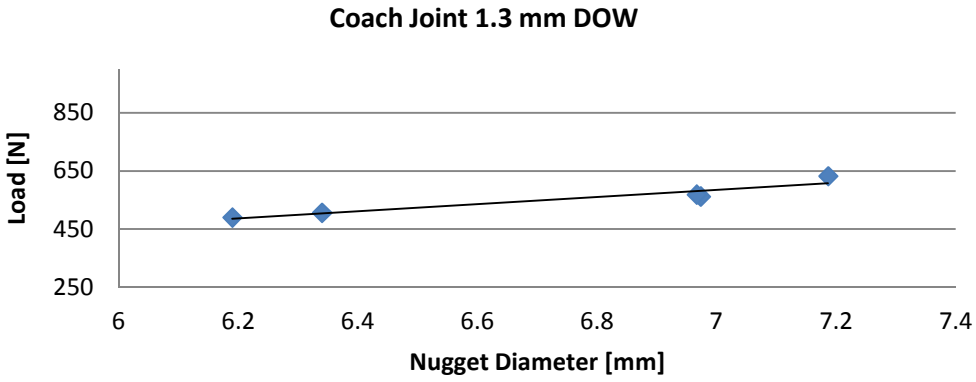

Figure 4-15. Load vs. Nugget Diameter Coach Joint RSW 1.3 mm Dow.

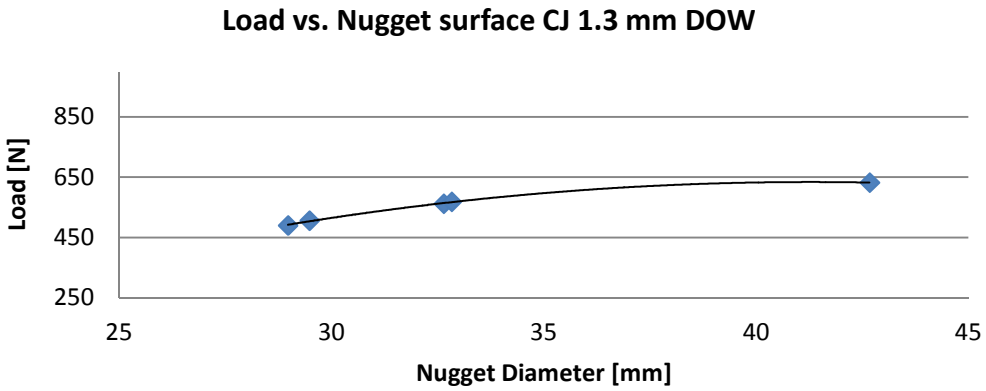

Figure 4-16. Load vs. Nugget Lateral Area Coach Joint RSW 1.3 mm Dow

Similar results have been obtained with the 1.75 mm thick stack.

4.1.1.6 Failure modes analysis – Coach Joint RSW

The most common failure modes and the importance of the failure mode analysis have been introduced in the literature review in Section 2.5.3. The present section attempts to explain the test results in terms of failure modes.

The weld nugget failure for both the thin and thick stack is analyzed first followed by the failure of the adhesive.

For all the RSW coach joints the nugget was pulled out of one of the sheets (in accordance with Han et al. [33]). In all the analyzed samples weld expulsion[9] was noticed (Figure 4-17); weld expulsion has a number of contributing factors (part fit, gun alignment, weld force, coating, contaminants, oxide layer thickness, schedule parameters, etc.). In particular the observed expulsion takes the name of "interfacial flash" (at the weld interface) and is not noticeable until the welds are pulled apart. Resistance spot welding of aluminum alloys in general has a high probability of showing weld flash based on the fact that it requires extremely high weld currents along with short weld times.

Some of samples showed a lip on one side of weld nugget; matching with this lip, the opposite sheet was partially torn (Figure 4-17). The samples showing this phenomenon usually gave also a higher value of load, elongation and absorbed energy. A better understanding was gained by comparing the two samples shown in Figure 4-18. The sample on the left shows the aforementioned characteristics while the one on the right does not

[9] See also Section 2.1.1

show any lip on the nugget but rather a partially failed nugget. This latter sample had a high value of maximum load but a very small elongation and consequently a very small absorbed energy. Thus it can be concluded that the integrity of the nugget and the presence of the lip on the nugget that caused a tearing of the opposite sheet influenced the elongation and the energy absorbed but not the maximum load. This hypothesis is confirmed in the study done by Sun et al. [51].

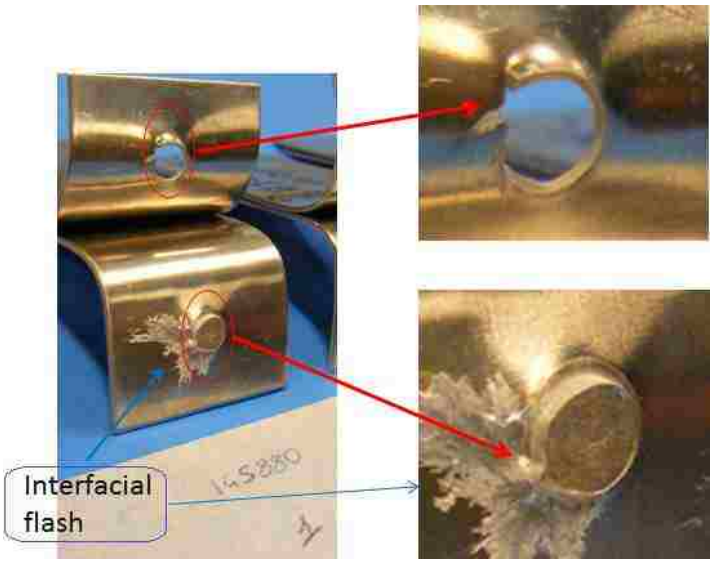

Figure 4-17. Failure mode analysis of RSW coach joints; highlighted in red the lip on the nugget and the corresponding tearing of the material on the opposite sheet and in blue the interfacial flash (weld expulsion).

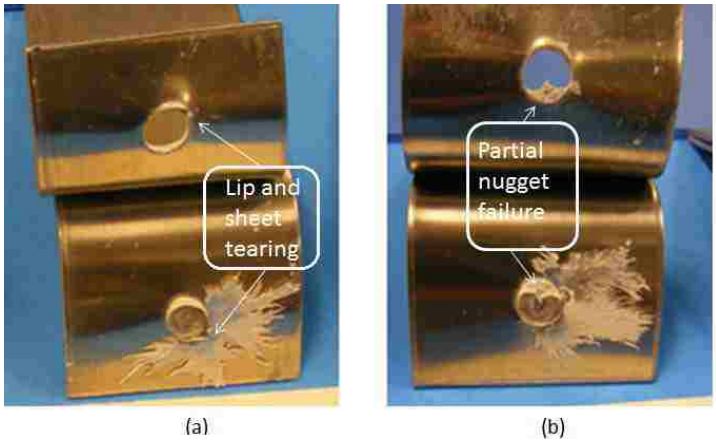

Figure 4-18. (a) Integer nugget showing a lip; (b) partially fracture nugget.

The failure of the adhesive layer can be a very complicated phenomenon and thus not always a complete prediction of the joint strength can be based on this analysis. Some relevant pictures showing some of the observed phenomenon are presented here.

In Section 4.1.1.1 it was shown that during the first portion of the tensile test the load is held by the adhesive in the portion of the overlap close to the radius and that the failure starts from there and propagates inward. The area close to the radius is then to be analyzed to understand the behavior at the adhesive yielding peak. The region of interest is highlighted with two red boxes in Figure 4-19.

The 1.3 mm thick Sika samples showed a high variability at the adhesive yielding peak (see Section 4.1.1.2). Figure 4-19 (a) and (b) show respectively the strongest and weakest samples, based on the adhesive yielding peak. Both samples showed a mixed failure mode, combination of adhesion and cohesion failure. In Figure 4-19 (a) an almost complete line of cohesive failure can be distinguished at the loaded portion of the overlap; the adhesive in weakest sample (Figure 4-19 (b)) presents numerous voids, which drastically reduce the actual area over which the force can be exchanged.

All the samples of the 1.75 mm RSW+Sika coach joints show characteristics close to the sample shown in Figure 4-19 (a). This could be a valid explanation for the much reduced variability at the adhesive peak with the latter group of joints.

Most of the samples glued with Dow showed the typical characteristics of purely adhesive failure, namely complete de-bonding of the glue from one of the two adherends (Figure 4-20). As explained in Section 2.5.3 this failure mode is usually undesirable as it indicates inadequate surface preparation that leads to poor bonding of the glue to the adherends, which makes this failure mode inconsistent on the strength level. This observation however was not sufficient to explain the different behavior noticed with the thin and thick RSW + Dow Coach Joints, which showed a very low variability at the adhesive yielding peak with the thinner stack but a significantly higher variability with the thicker stack.

Figure 4-19. Adhesive failure mode analysis, RSW + Sika 1.3 mm (a) sample #5, (b) sample #1.

Figure 4-20. RSW and Dow coach joint 1.3 mm showing adhesive failure.

4.1.2 Coach Joint SPR

4.1.2.1 Tensile test data interpretation - Coach Joint SPR

Examples of the load-displacement curves for no-adhesive, Sika and Dow coach joints SPR 1.3 mm thick are shown in Figure 4-21.

The no-adhesive sample (black line) shows a similar behavior to the welded no-adhesive sample, even though in this case the peak registered at a higher displacement and the plateau following the load peak is no longer present; instead, after a small load decrease the point of catastrophic failure is reached at the load drops vertically.

The video recording of the tensile test is helpful for the understanding of the failure mode. Figure 4-23 (b) closely resembles Figure 4-3 (c), where the tip of the slit that started at the leftmost portion of the overlap has moved rightwards until it reaches the rivet or weld nugget rivet. In the welded sample the maximum load was reached at this point and the fracture started from the tip of the nugget and propagated around it. In the riveted sample the rivet is able to maintain its integrity and its vertical position. Thus even though the two sheets keep on separating the slit does not propagate further rightward until the maximum load is reached, as shown in Figure 4-23 (c). Figure 4-23 (d) shows a brief instant before the final failure. Just to the left of the rivet a small protrusion is observed. It indicates the onset of the material failure that will soon lead to the final fracture; the rivet is made out of steel and the aluminum of the coupons will be the failing element.

Some similarities between the rivet bonded and the weld-bonded joints can be observed too. The three-peaks nature of the load-deflection curve is still recognizable, even though in

this case the first and the third peak are less evident (Figure 4-21 and Figure 4-22). The third peak in particular could be better described as a change of the slope of the line, or a temporary delay of the final drop enabling a few additional millimeters of elongation. For a matter of consistency this third point of the curve will be taken into account in the calculation of the load also for the rivet samples, even though it has only a limited impact on the joint performance. The only exception is constituted by the no-adhesive line, for which the load was calculated only at the maximum peak. The displacement instead will be measured as final failure as well.

Two main reasons lie behind the reduced impact of the adhesive on the performance of the riveted joint. Firstly, as it will be shown in Section 4.1.2.2, the rivet is able to hold a higher load compared to the weld nugget and reaches the maximum load at a higher value of elongation; thus assuming that the adhesive shows the same performance when combined with RSW or SPR, the higher peak shown by the rivet "overshadows" the peak of the adhesive. In addition, it will also be shown that the adhesive performed worse when combined with SPR than when combined with RSW. This latter phenomenon will be analyzed in Section 4.1.2.5 and 4.1.3.

Figure 4-22 shows three curves for the riveted 1.75 mm thick coach joints. The described trends are now further evident; the first and the third peaks of the hybrid joint are hardly recognizable as the rivet yielding peak[10] became highly predominant, making all the three curves resemble each other quite closely.

[10] For a matter of simplicity, the second peak will be referred to as the "rivet yielding peak" even though it has been illustrated that the component actually failing is the aluminum sheet at the rivet interlock and not the rivet itself.

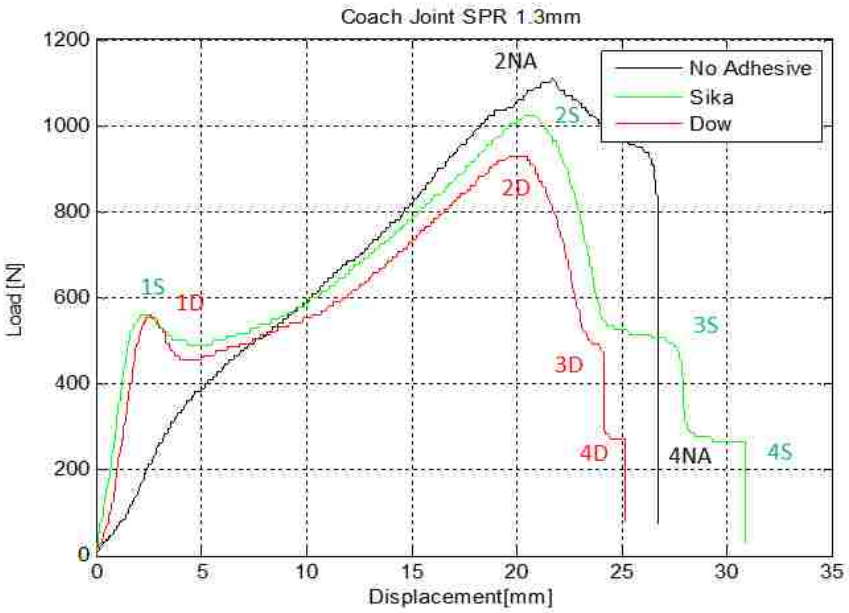

Figure 4-21. Results Interpretation; Curve superimposition Coach Joint SPR 1.3mm.

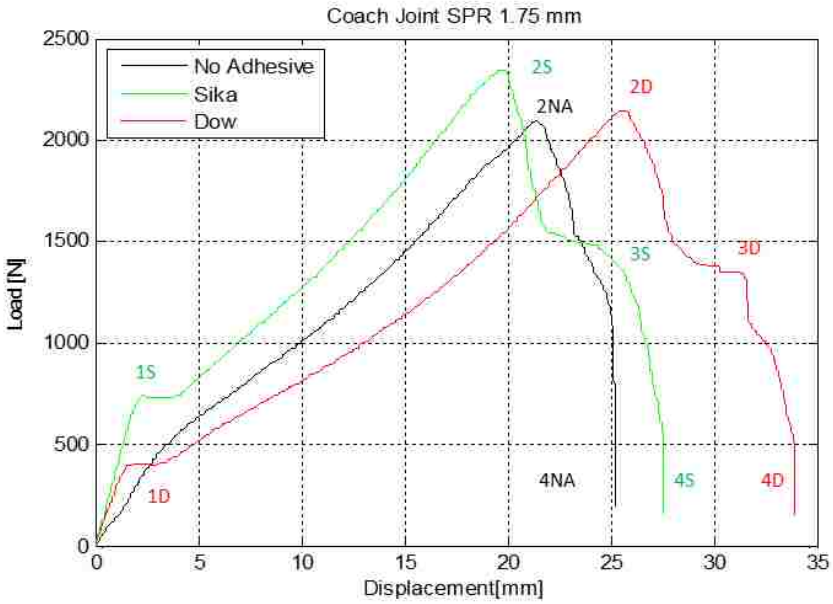

Figure 4-22. Results Interpretation; Curve superimposition Coach Joint SPR 1.75 mm.

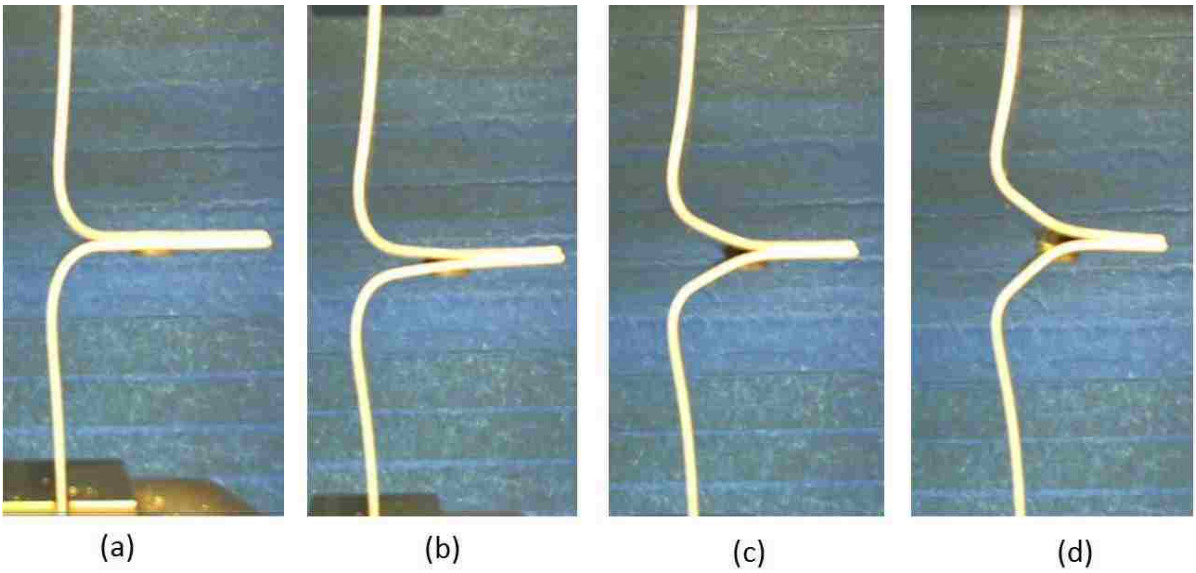

Figure 4-23. Tensile test of a 1.3 mm thick riveted coach joint, No adhesive; un-deformed shape (a), progressive deformation before peak load (b) and (c) and onset of material yielding before final failure (d).

4.1.2.2 Load vs. Displacement - Coach Joint SPR

The load and displacement at the previously described peaks for the riveted coach joint are represented and summarized in Figure 4-24, Figure 4-25, Table 4-7 and Table 4-8.

1.3 mm thick SPR Sika and Dow samples showed a similar value of load at the first peak, with Sika outperforming on average Dow (533N for Sika vs. 464N for Dow). 1.75 mm Sika samples held on average a higher load than the corresponding Dow samples (640 N vs. 508N). However, in the thicker stack the adhesive peak is overshadowed by the rivet yielding peak that on average exceeded 2000N for all the tests (see Figure 4-22). All the analyzed samples showed the same elongation at the first peak. A load increment of 20% for Sika samples and 9% for Dow samples was recorded at the first peak as function of the increment in thickness. The reasons behind the considerably reduced rise in strength compared to the equivalent welded joints will be explained in the Section 4.1.2.5 analyzing the failure mode of the glue in the riveted joints.

1.3 mm thick NA samples showed a higher load at the second peak (1107 N) compared to both the hybrid samples (954 N were reached for Sika samples and 912 N for Dow samples); in a similar manner, NA samples showed the highest average elongation at the second peak, followed by Sika and Dow samples. Considering the thicker stack it can be noticed that NA and Dow samples showed the same load at the second peak (2051N and 2052 N) while Sika samples were on average stronger (2322 N). In addition, NA and Sika

samples showed the same elongation (21 mm) while Dow averaged a displacement of about 5 mm higher than the other two joint types. A very significant increase in load due to joint thickness increase can be noticed at the second peak, especially for Sika (+143%) and Dow (+125%). The possibility of using a longer rivet associated with the higher thickness allowed to achieve a better interlock resulting in a much higher strength. The elongation at the second peak did not vary significantly for Sika and no-adhesive samples; Dow samples instead registered an increase in the elongation at second peak of 34 %.

As already mentioned in the previous section the third peak is actually in this case just a small variation in the slope of the line, as can be seen from Figure 4-24. However, even though no clear third peak was noticeable after the rivet yielding, the elongation obtained during the final drop in load is higher for the hybrid joints; while the no-adhesive samples fail dramatically soon after the sheet at the rivet interlock yields (or at the rivet head, depending on the failure mode, Section 4.1.2.5) the adhesive layer remaining at the tip of the overlap is able to hold some load thus delaying the final failure and allowing for some further elongation. As a result the average final elongation for Sika and Dow samples is respectively 18% and 8% greater than the no-adhesive sample for the 1.3 mm SPR joints and 30.5% and 9.8% greater for the 1.75 mm stack.

Differently from the welded coach joints the maximum load for the riveted coach joints has been measured invariably at the rivet yielding peak. In addition, while the NA SPR samples showed the highest maximum load among the 1.3 mm joints, the 1.75 mm hybrid joints outperformed the NA samples. The different impact of the presence of adhesive on the second peak will be analyzed in Section 4.1.2.5

In summary the adhesive has an impact on the initial and final portions of the load-displacement diagram represented respectively by the first peak and by the greater final elongation of the joint. At the second peak, where the strength of the rivet interlock is the predominant factor the presence of the adhesive seems to have a detrimental effect with the thinner stack but a beneficial effect with the thicker stack. In addition it is worth noting how the variability at the second peak is considerably lower compared to RSW joints. A similar observation was made by Han et al. [33] and reported in the chapter dedicated to the Literature review.

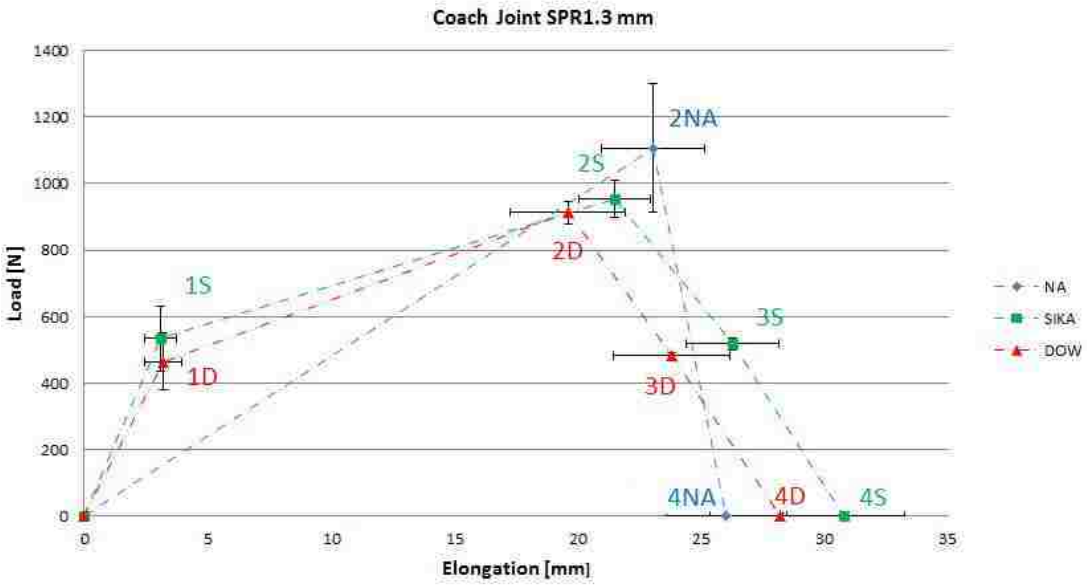

Figure 4-24. Schematic representation of the Load-Displacement curves for the Coach Joint SPR 1.3 mm group.

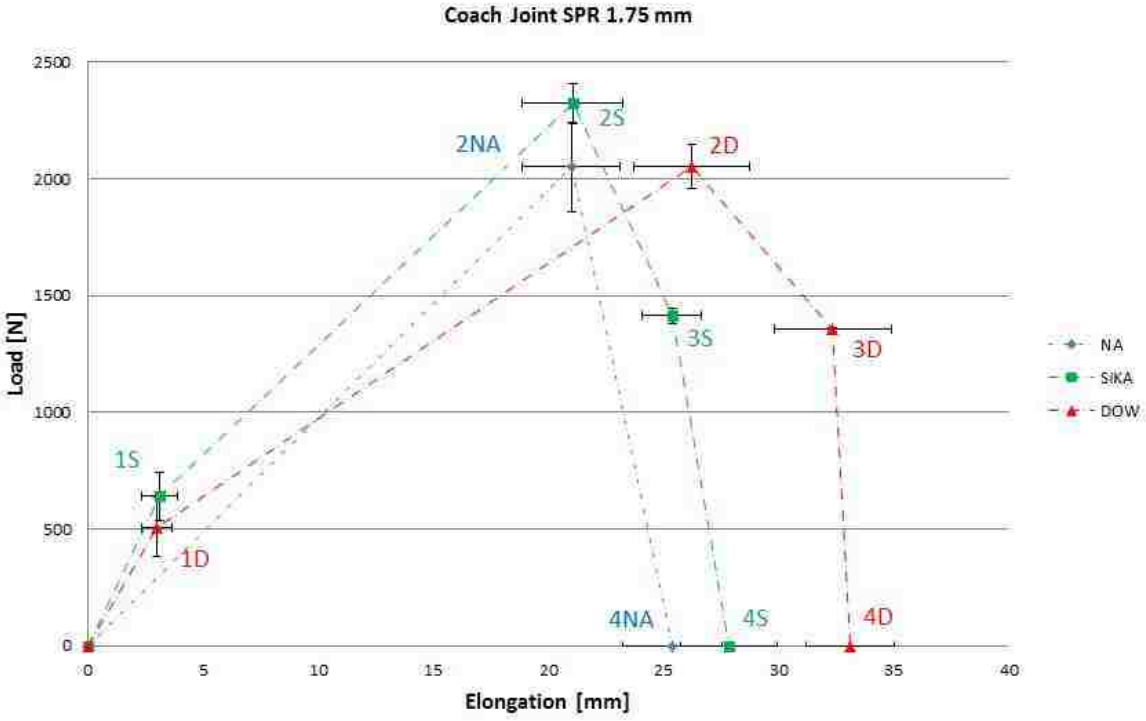

Figure 4-25. Schematic representation of the Load-Displacement curves for the Coach Joint SPR 1.75 mm group.

Table 4-7. Load at the indicated peaks; SPR Coach Joints.

Load [N]										
SPR Coach Joint 1.3mm vs 1.75mm		NA		SIKA		DOW		Sika vs Na	Dow vs Na	Dow vs Sika
		mean	st.dev	mean	st.dev	mean	st.dev			
1st peak	1.3 mm	-	-	533	19%	464	19%	-	-	-12.9%
	1.75 mm	-	-	640	16%	508	25%	-	-	-20.6%
				20%		9%				
2nd peak	1.3 mm	1107	7%	954	6%	912	4%	-13.9%	-17.6%	-4.4%
	1.75 mm	2051	5%	2323	4%	2052	5%	13.2%	0.0%	-11.7%
		85%		143%		125%				
3rd peak	1.3 mm	-	-	518	3%	482	2%	-	-	-7.0%
	1.75 mm	-	-	1414	2%	1355	1%	-	-	-4.1%
				173%		181%				

Table 4-8. Elongation at the indicated peaks; SPR Coach Joints.

Elongation [mm]										
SPR Coach Joint 1.3 vs 1.75		NA		SIKA		DOW		Sika vs Na	Dow vs Na	Dow vs Sika
		mean	st.dev	mean	st.dev	mean	st.dev			
1st peak	1.3 mm	-	-	3.1	21%	3.2	23%	-	-	4.1%
	1.75 mm	-	-	3.1	26%	3.0	12%	-	-	-3.9%
				0.3%		-7.3%				
2nd peak	1.3 mm	23.0	9%	21.5	7%	19.6	12%	-6.7%	-14.9%	-8.8%
	1.75 mm	21.0	10%	21.1	10%	26.2	10%	0.3%	25.0%	24.6%
		-8.9%		-2.0%		33.8%				
3rd peak	1.3 mm	-	-	26.3	7%	23.8	10%	-	-	-9.4%
	1.75 mm	-	-	25.4	5%	32.4	8%	-	-	27.6%
				-3.5%		36.0%				
joint failure	1.3 mm	26.0	9%	30.8	8%	28.2	423%	18.3%	8.3%	-8.4%
	1.75 mm	25.4	7%	27.8	8%	33.1	265%	9.8%	30.5%	18.9%
		-2.6%		-9.6%		17.5%				

4.1.2.3 Energy - Coach Joint SPR

The problem of the uncertainty on the position of the maximum load in the calculation of the energy absorbed by the joint introduced in Section 4.1.1.4 does not apply to this group of joints; it was shown in the previous section that the maximum load is always measured at the rivet yielding peak. Nevertheless the same methodology for the calculation of the energy was followed to compare the results obtained with riveted and welded joints and with the purpose of indicating the contribution of each joining component (adhesive and rivet in case of hybrid joints) to the final energy result.

The calculation of the energy at the third peak was neglected for this group of joints; it has been demonstrated that the only impact of the adhesive on the final portion of tensile test is to allow for a higher displacement at failure thus its effect on the energy absorption can be estimated using the energy at final failure.

The energy absorbed at the adhesive yielding peak is comparable for Sika and Dow samples for both the stack thicknesses and in both cases its impact is quite limited, being on average less than 1 J (Table 4-9).

The vast majority of the energy is instead absorbed in the deformation of the material necessary to cause the rivet pull-out (second peak); in particular the 1.3 mm NA samples absorbed on average the highest value of energy (13.8 J). At the rivet yielding peak on average 1.3 mm Sika samples outperformed the corresponding Dow samples (12.7 J vs. 10.6 J). At final failure the trend is partly inverted; the additional elongation granted by the presence of the adhesive gave to the hybrid joints a higher energy absorption from the second peak to final failure thus reducing the gap between the Dow and no-adhesive samples and even making the Sika samples the joint configuration with the highest average energy absorption at final failure.

As already mentioned in the analysis of the load and displacement (Section 4.1.2.2) the 1.75 mm hybrid joints on average outperformed the riveted-only joints; Dow samples in particular absorbed 13% more energy than the no-adhesive samples and 10% more than the Sika samples. The trend is still present in the portion of the curve from the second peak to final failure, where thanks to a higher elongation the gap between the hybrid samples and the traditional ones was further incremented.

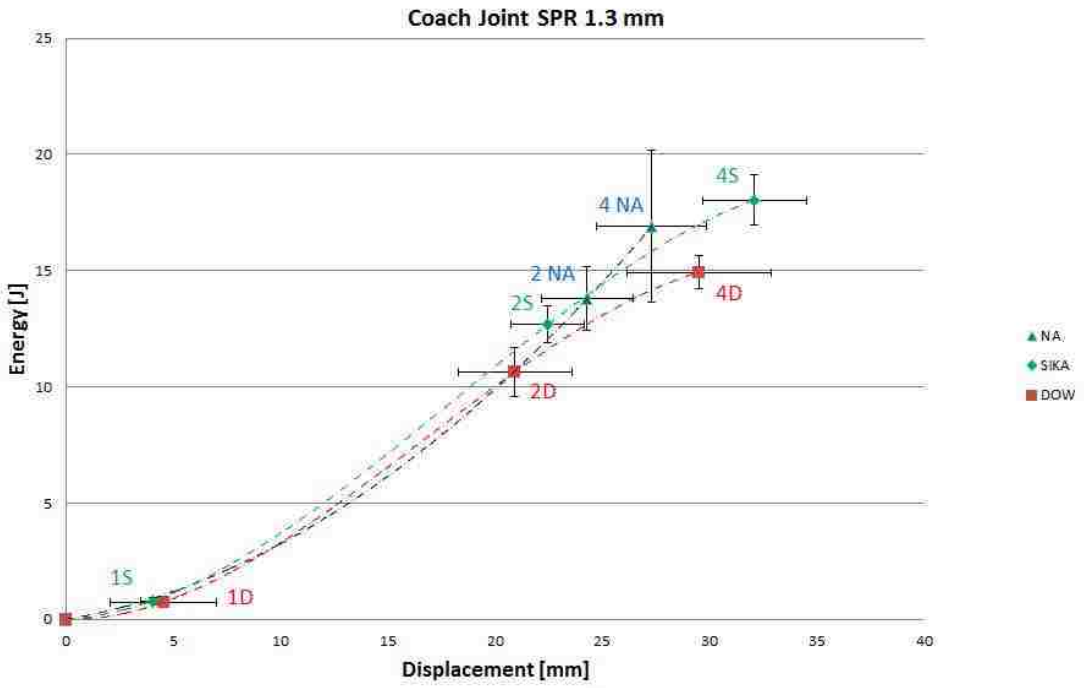

Figure 4-26. Energy absorbed by the joint as function of the displacement; Coach Joint SPR 1.3 mm.

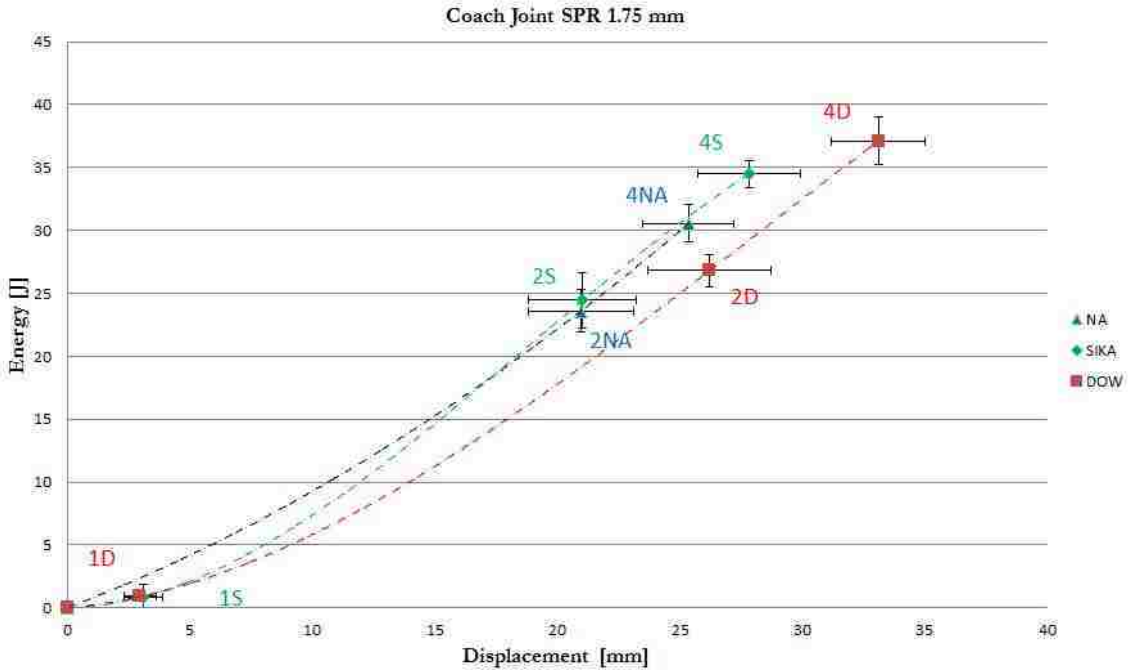

Figure 4-27. Energy absorbed by the joint as function of the displacement; Coach Joint SPR 1.75 mm.

Table 4-9. Energy at the indicated peaks; SPR Coach Joints.

Energy [J]										
Coach Joint Weld 1.3 mm vs. 1.75 mm		NA		SIKA		DOW		Sika vs NA	Dow vs NA	Dow vs. Sika
		mean	st.dev	mean	st.dev	mean	st.dev			
1st peak	1.3 mm			0.8	14%	0.7	18%	-	-	-7.7%
	1.75 mm			0.9	40%	0.9	38%	-	-	2.2%
				8.9%		20.6%				
2nd peak	1.3 mm	13.8	10%	12.7	6%	10.6	10%	-8.1%	-22.9%	-16.2%
	1.75 mm	23.6	7%	24.5	4%	26.8	5%	3.6%	13.5%	9.6%
		71.0%		92.6%		156%				
joint failure	1.3 mm	16.9	19%	18.0	6%	14.9	5%	6.7%	-11.6%	-17.2%
	1.75 mm	30.6	5%	34.5	6%	37.1	5%	12.9%	21.5%	7.6%
		80.9%		91.3%		149%				

4.1.2.4 Stiffness - Coach Joint SPR

The stiffness of the group of joints under analysis is summarized in Table 4-10. The presence of adhesive increased the stiffness of the joint 1.3 mm thick SPR coach joints from 84 N/mm to 250 N/mm (Sika) and 211 N/mm (Dow) respectively. Comparing to the 1.3 mm thick RSW coach joint it can be noticed that the increase in stiffness given by the presence of adhesive is much reduced, due to a lower value achieved with the rivet bonded joints compared to the weld bonded. This trend is even more apparent with the 1.75 mm thick joints where almost no difference is registered between Sika and the no-adhesive samples while Dow samples on average proved to be 18% stiffer than the no adhesive ones.

Comparing the results obtained with the two thicknesses it can be observed that the stiffness achieved with the hybrid joints is lower for the thicker samples by 37% for Sika samples and 14% for Dow samples.

The no-adhesive samples showed instead a significant stiffness increase, from 84 N/mm (1.3 mm) to 154 N/mm (1.75 mm). As already explained is Section 4.1.1.4 this increase is ascribable to the greater load needed for deflecting a beam of increased cross-section. This results will be further analyzed in Section 4.1.2.5.

Table 4-10. Stiffness of the SPR Coach Joint group.

Stiffness at initial load application [N/mm]									
Coach Joint SPR	NA		SIKA		DOW		Sika vs NA	Dow vs NA	Dow vs Sika
	mean	st.dev	mean	st.dev	mean	st.dev			
1.3 mm	84	22%	250	24%	211	49%	198%	152%	-18%
1.75 mm	154	18%	156	41%	182	67%	1%	18%	14%
	84.4%		-37.4%		-14.0%				

4.1.2.5 Failure mode analysis - Coach Joint SPR

As introduced in Section 2.5.3 the two typical failure modes for a riveted joint are "rivet–tail pull out" and "rivet–head pull out". The SPR coach joints showed both the phenomena.

The 1.3 mm SPR no adhesive samples showed three cases of rivet tail pull-out (Figure 4-28(a)) and two cases of rivet head pull out (Figure 4-28(b)). The simultaneous presence of both the failure modes indicates that the interlocking strength achieved for the 1.3 mm SPR no adhesive is comparable to the sheet tearing strength on the head side. Interestingly, for all the hybrid samples 1.3 mm thick rivet tail pull-out was observed. Combining this information with the data shown in Section 4.1.2.2 that indicate that the maximum measured load for the hybrid samples was lower than for the rivet-only samples it can be concluded that the presence of the adhesive has weakened the mechanical interlocking of the rivet.

With the thicker stack the head of the rivet was pulled through the upper sheet for all the samples. The interlocking strength achieved with the longer rivet used for the thicker stack was then always greater than the sheet tearing strength, independent of the presence of adhesive. The strength of the thick stack joint thus depends only on the rivet head diameter and on the sheet tearing strength.

To explain the increase in strength highlighted in Section 4.1.2.2 for the 1.75 mm hybrid coach joints it has to be kept in mind that the adhesive layer completely surrounds the rivet and it is loaded simultaneously to it. While for the thinner stack the benefit from the simultaneous presence of the two joining methods is cancelled by the weakening of the rivet interlock, in the thicker stack the strength of the rivet is independent of the adhesive, and thus the latter can have only a beneficial effect.

Figure 4-28. Rivet failure mode analysis, (a) rivet tail pull-out. (b) rivet head pull-out.

The failure of the adhesive layer in the SPR + Sika coach joints is shown in Figure 4-29; numerous voids can be seen in the area close to the end of the coach peel specimen curvature, especially for the 1.75 mm sample (Figure 4-29 (b)) where the presence of a consistent quantity of adhesive is limited to some narrow stripes. Similar observations were made with SPR + Dow samples. This large presence of voids could be the explanation for the low strength and stiffness of the SPR hybrid joints mentioned in Sections 4.1.2.2 and 4.1.2.4.

The highly uneven distribution of the adhesive and void formation has likely taken place during the sample preparation. The force needed to punch the rivet through the upper sheet and to deform it into the bottom sheet is large and can have cause the dishing of the two aluminum component; in particular it is likely that at the edge of the overlap the two components tend to separate from each other. Since the adhesive is not cured yet during the riveting process, this relative movement can cause the displacement of the adhesive and the void formation.

Figure 4-29. Adhesive layer failure mode analysis, SPR + Sika coach joint (a) 1.3 mm , (b) 1.75 mm.

4.1.3 RSW vs. SPR

4.1.3.1 Load vs. Displacement - RSW vs. SPR

The results obtained with RSW and SPR are summarized and compared in Table 4-11 - Table 4-14.

Ideally the strength of the joint at the adhesive yielding peak (first peak) should be independent of the utilization of SPR or RSW. In Section 4.1.2.5 though the main reasons for the weakest behavior noticed when the adhesive is combined with SPR have been already explained thank to the failure mode analysis. As already anticipated the gap at the adhesive peak is the biggest for the 1.75 mm stack, where the SPR + Dow sample where 52% weaker than the corresponding RSW samples. The elongation at the adhesive peak was consistently 20% greater for SPR samples when Dow adhesive was used while SPR + Sika samples showed an increase of 8% with the thinner stack and a decrease of the same magnitude with the thicker stack. These variations however cannot be considered as significant due to the high variability registered.

The highest difference between RSW and SPR has been registered at the second peak, for both the load and the elongation. The significant gap in load between the two joining methods noticed with the 1.3 mm stack is even further enlarged with the thicker stack, thanks probably to the longer rivet used. The main reason lying behind the difference in elongation is the different failure mode; as explained in Sections 4.1.2.1 the crack does not propagate around the nugget showing a plateau in the load-displacement curve, but rather the rivet is able to hold the joint in position up to a much higher elongation where catastrophic failure then happens.

The load at third peak showed a non-constant behavior, being slightly lower for the rivet joint with the thinner stack but quite significantly higher for the thicker stack, especially for Sika (+43%).

When no adhesive was used SPR joints elongated at failure 31.4% more than RSW joint with the thinner stack but only 8.6% more with the thicker stack. Similar elongation at failure is obtained with SPR + Sika and RSW + Sika for both the stack thicknesses and for the 1.3 mm SPR and RSW + DOW samples, while 1.75 mm SPR + Dow samples elongates 31.2% more than the corresponding RSW samples.

Table 4-11. Load at the indicated peaks; RSW 1.3 mm vs. SPR 1.3 mm.

Load [N]							
Coach joint Weld vs SPR 1.3mm		NA		SIKA		DOW	
		mean	st.dev	mean	st.dev	mean	st.dev
1st peak	RSW	-	-	617	30%	637	5%
	SPR	-	-	533	19%	464	19%
				-13.6%		-27.1%	
2nd peak	RSW	635	30%	583	19%	552	10%
	SPR	1107	7%	954	6%	912	4%
		74.5%		63.6%		65.3%	
3rd peak	RSW	-	-	556	16%	551	10%
	SPR	-	-	518	3%	482	2%
				-6.9%		-12.6%	

Table 4-12. Load at the indicated peaks; RSW 1.75 mm vs. SPR 1.75 mm.

Load [N]							
Coach joint RSW vs SPR 1.75 mm		NA		SIKA		DOW	
		mean	st.dev	mean	st.dev	mean	st.dev
1st peak	RSW	-	-	1013	11%	1037	33%
	SPR	-	-	640	16%	508	25%
				-36.8%		-51.0%	
2nd peak	RSW	1078	11%	1015	5%	1155	18%
	SPR	2051	5%	2323	4%	2052	5%
		90.3%		129%		77.6%	
3rd peak	RSW	-	-	988	5%	1104	16%
	SPR	-	-	1414	2%	1355	1%
				43.1%		22.8%	

Table 4-13. Elongation at the indicated peaks; RSW 1.3 mm vs. SPR 1.3 mm.

Elongation [mm]							
Coach Joint RSW vs SPR 1.3mm		NA		SIKA		DOW	
		mean	st.dev	mean	st.dev	mean	st.dev
1st peak	RSW	-	-	2.8	31%	2.5	42%
	SPR	-	-	3.1	21%	3.2	23%
				8.5%		26.9%	
2nd peak	RSW	10.6	25%	13.1	18%	11.4	15%
	SPR	23.0	9%	21.5	7%	19.6	12%
		118%		64.7%		72.1%	
3rd peak	RSW	-	-	23.8	12%	24.8	18%
	SPR	-	-	26.3	7%	23.8	10%
				10.2%		-4.2%	
elongation at failure	RSW	19.8	23%	31.6	10%	30.7	11%
	SPR	26.0	9%	30.8	8%	28.2	10%
		31.4%		-2.7%		-8.2%	

Table 4-14. Elongation at the indicated peaks; RSW 1.75 mm vs. SPR 1.75 mm.

Elongation [mm]							
Coach Joint RSW vs SPR 1.75 mm		NA		SIKA		DOW	
		mean	st.dev	mean	st.dev	mean	st.dev
1st peak	RSW	-	-	3.4	17%	2.5	16%
	SPR	-	-	3.1	26%	3.0	22%
				-8.2%		21.3%	
2nd peak	RSW	13.4	20%	13.7	14%	12.5	6%
	SPR	21.0	10%	21.1	10%	26.2	10%
		56.5%		53.9%		110%	
3rd peak	RSW	-	-	25.7	13%	24.8	6%
	SPR	-	-	25.4	5%	32.4	8%
				-1.2%		30.3%	
elongation at failure	RSW	23.4	17%	28.0	13%	25.2	13%
	SPR	25.4	7%	27.8	8%	33.1	6%
		8.6%		-0.4%		31.2%	

4.1.3.2 Energy - RSW vs. SPR

The energy absorbed at the indicated peaks for the RSW coach joints and the SPR coach joints has been summarized and compared in Table 4-15 and Table 4-16. As mentioned in Section 4.1.2.3 the energy at the third peak has not been calculated for the riveted coach joints; thus the energy measured at the third peak for the welded coach joints has been neglected in this analysis.

As mentioned in the previous sections the trend of energy is closely correlated to the trend of load and displacement. Thus the presented results will be commented in the form of a bullet list, since the considerations made in the previous sections apply for the analysis of the energy as well.

- The energy absorbed at the first peak is larger for the welded coach joints, especially for the thicker stack.
- At the second peak the riveted joints largely outperform the welded joints
- The energy at final failure is bigger for the rivet joints, even though the gap is educed compared to the second peak. This behavior is a further proof of the different failure modes of these two joints; while the welded joints after the peak load still show a significant elongation (and thus energy absorption) the failure for riveted joints happens soon after the peak load (with consequently less additional energy absorption).

Table 4-15. Energy at the indicated peaks, RSW 1.3 mm vs. SPR 1.3 mm.

Energy [J]							
Coach Joint RSW vs. SPR 1.3 mm		NA		SIKA		DOW	
		mean	st.dev	mean	st.dev	mean	st.dev
1st peak	RSW			0.9	20%	0.8	26%
	SPR			0.8	14%	0.7	18%
				-5.8%		-4.3%	
2nd peak	RSW	3.7	48%	6.5	21%	5.8	13%
	SPR	13.8	10%	12.7	6%	10.6	10%
		272%		95.1%		82.9%	
joint failure	RSW	8.8	41%	15.0	15%	14.5	19%
	SPR	16.9	19%	18.0	6%	14.9	5%
		92.5%		20.4%		3.1%	

Table 4-16. Energy at the indicated peaks, RSW 1.75 mm vs. SPR 1.75 mm.

Energy [J]							
Coach Joint RSW vs. SPR 1.75 mm		NA		SIKA		DOW	
		mean	st.dev	mean	st.dev	mean	st.dev
1st peak	RSW			1.4	25%	1.2	46%
	SPR			0.9	40%	0.9	38%
				-37.2%		-23.6%	
2nd peak	RSW	8.4	22%	10.8	16%	11.1	13%
	SPR	23.6	7%	24.5	4%	26.8	5%
		182%		127%		141%	
joint failure	RSW	17.9	18%	23.5	14%	21.1	36%
	SPR	30.6	5%	34.5	6%	37.1	5%
		71.1%		46.6%		75.7%	

4.1.3.3 Stiffness - RSW vs. SPR

As can be seen in Tables Table 4-17Table 4-18 the stiffness greatly increased the stiffness of the welded coach joints while the impact on the riveted coach joints was quite reduced, particularly for the thicker stack.

When the adhesive is not used instead the rivet coach joint proves to be higher compared to the welded coach joint (by 13% with the 1.3 mm stack and 27.9% with the 1.75 mm stack).

Table 4-17. Stiffness of the coach joints; RSW vs. SPR 1.3 mm.

Stiffness at initial load application [N/mm]						
Coach Joint RSW vs. SPR 1.3 mm	NA		SIKA		DOW	
	mean	st.dev	mean	st.dev	mean	st.dev
RSW	73	36%	437	53%	423	20%
SPR	84	22%	250	24%	211	49%
	13.0%		-74.9%		-100%	

Table 4-18. Stiffness of the coach joints; RSW vs. SPR 1.75 mm.

Stiffness at initial load application [N/mm]						
Coach Joint RSW vs. SPR 1.75 mm	NA		SIKA		DOW	
	mean	st.dev	mean	st.dev	mean	st.dev
RSW	111	27%	411	18%	498	44%
SPR	154	18%	156	41%	182	67%
	27.9%		-163%		-174%	

4.1.4 Deviation from ideal conditions

Numerous times throughout this chapter it has been mentioned that the results shown have been influenced by the sample preparation. Gilchrist and Smith [38] investigated the impact of the distance between the loading line and the edge of the adhesive layer. By reducing this distance the stress concentration in the adhesive layer drops dramatically, increasing the maximum strength of the joint. Similarly, the offset between the load line and the weld nugget (or the rivet) represents the lever arm of the pulling force.

The manual sample preparation of the coach joints described in Section 3.3 does not allow a perfect control on the radius of curvature of the components; as a results the curvature were quite variable from sample to sample, being on average close to 6 mm.

Additional samples have been prepared by SIKA engineers to test the strength of an adhesively bonded coach joint in ideal conditions, namely:

- Minimized radius of curvature (Figure 4-30)
- Utilization of glass bead of constant diameter as spacers to keep the adherends at constant distance and thus keeping the adhesive layer thickness constant.
- Full clamping of the samples before and during the curing process to avoid any possible movement.

As a result purely cohesive fracture was observed for all the tested samples (Figure 4-30) and the load hold at the adhesive yielding peak ranged in between 2226N and 2900N

depending on the adhesive layer thickness, more than double compared to the maximum load registered at the adhesive yielding peak with the studied samples.

Figure 4-30. Adhesively bonded coach joint prepared in "ideal conditions"; prepared by SIKA engineers.

4.2 Lap Joint

In this section the results obtained with the lap joints are assessed.

The testing methodology adopted with the lap joints is partly different than that applied to the coach joints. In the original test program design the peak-by-peak approached was not developed yet and the targets of the investigation were simply maximum load and the energy at maximum load. Thus after testing one hybrid joint batch (namely the Lap Joints RSW + Dow 1.75 mm) and observing that in lap shear test adhesive bonding is the strongest joining method, the tests that followed on hybrid samples were performed only until fracture of the adhesive layer. Since the adhesive layer was the first element to fail, the tensile tests of the hybrid joints were stopped before the nugget or rivet failure (Figure 4-31). Thus in the present study the peak-by-peak approach cannot be fully applied to all the lap-joints test samples.

4.2.1 Lap Joint RSW

4.2.1.1 Tensile test data interpretation - Lap Joint RSW

Examples of the load-displacement curves for no-adhesive and hybrid Sika and Dow lap joints RSW 1.3 mm thick and 1.75 mm are shown in Figure 4-32 and Figure 4-33. Analyzing Figure 4-33 all the features of the load-displacement curves of these group of joints can be

understood; the shown batch include in fact welded-only samples, hybrid samples tested until adhesive failure (Sika) and hybrid joints tested until final failure (Dow). The welded-only sample (black line) shows one peak, corresponding to the weld nugget failure (point 1NA). Sika sample shows also just one peak, corresponding in this case to the adhesive layer failure, labeled as point 2S (as mentioned, the test was stopped before the nugget failure (Figure 4-31)). In the Dow test two peaks can be distinguished: the first is attributable to the adhesive yielding failure (point 2D) due to the similarity with the peak shown by Sika, while the second is attributable to the nugget failure (point 3S). This last peak resembles closely the last portion of the load-displacement curve of the welded only sample.

Both the hybrid joints show a characteristic point where the slope of the load – displacement line changes (points 1S and 1D). As explained by Campilho et al. [23] this point corresponds to the onset of the plastic deformation of the aluminum adherends.

Figure 4-31. Lap Joint RSW + Sika; the test was stopped after the adhesive layer failure and before the nugget failure.

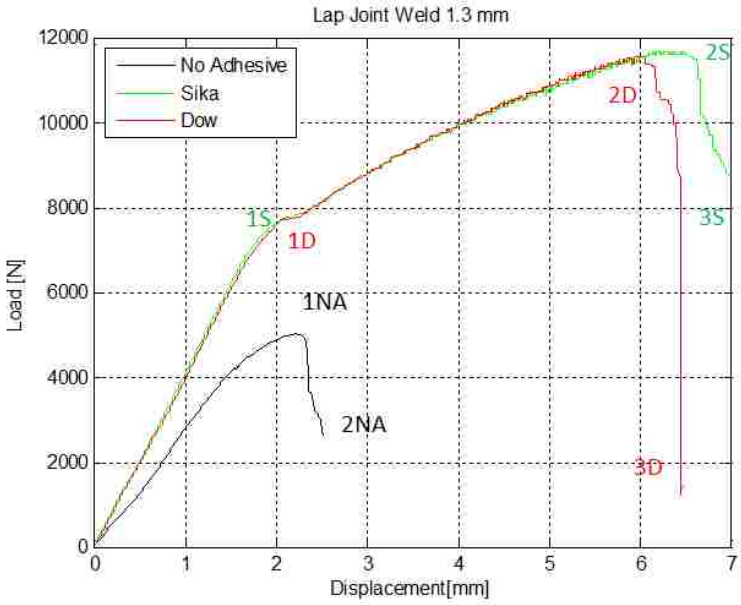

Figure 4-32. Results Interpretation; Curve superimposition Lap Joint RSW 1.3mm.

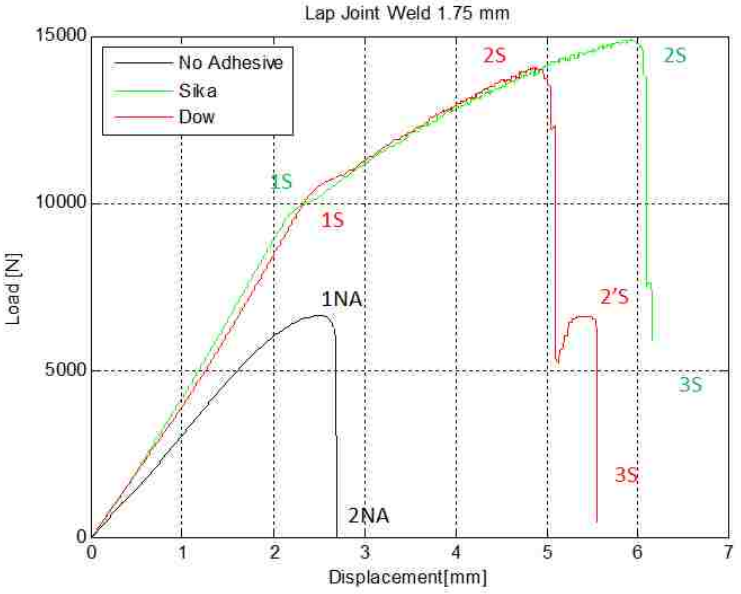

Figure 4-33. Results Interpretation; Curve superimposition Lap Joint RSW 1.75 mm.

4.2.1.2 Load vs. Displacement - Lap Joint RSW

Due to the interruption of the tensile tests of the hybrid joints before the failure of the weld nugget the "peak-by-peak" comparison of the welded only and of the hybrid joints is not possible. A graphical representation of the obtained results is nevertheless provided in Figure 4-34 and Figure 4-35 and the numerical results are tabulated in Table 4-19-Table 4-22.

The welded-only samples registered a peak load of 5121N and 6536 N respectively for the thin and thick stack, thus showing an increase of 28%. The elongation at the maximum load peak of the thicker stack was 11% greater while almost no difference is noticeable at final failure. This behaviour is due to a different failure mode, which will be described in Section 4.2.1.6.

The onset of plastic deformation of the aluminum adherends is indicated by the points "1D" and "1S" in Figure 4-34 and Figure 4-35 and as "first peak" in the following tables. The load and elongation at this point depend on the properties of the material and of the geometry of the coupons; this explains the very low variability of the results, the small difference observed between Sika and Dow, and the increase in load and elongation obtained when the thickness of the stack is increased from 1.3 mm to 1.75mm.

Sika samples outperformed on average Dow samples at the adhesive yielding peak (second peak) both in the thinner and in the thicker stack. However, in both cases the high variability of the results does not allow drawing definitive conclusions regarding either the load or the displacement. The same observation applies for the elongation at final failure.

The increment of the stack thickness had a beneficial impact on the load at the adhesive yielding peak (2D, 2S) while on the other hand both at the adhesive yielding peak and final failure of the 1.75 mm thick hybrid joints showed a reduced elongation.

Table 4-22 compares the maximum load obtained with the RSW lap joints. The addition of adhesive has increases the lap joint maximum load by more than a factor of two.

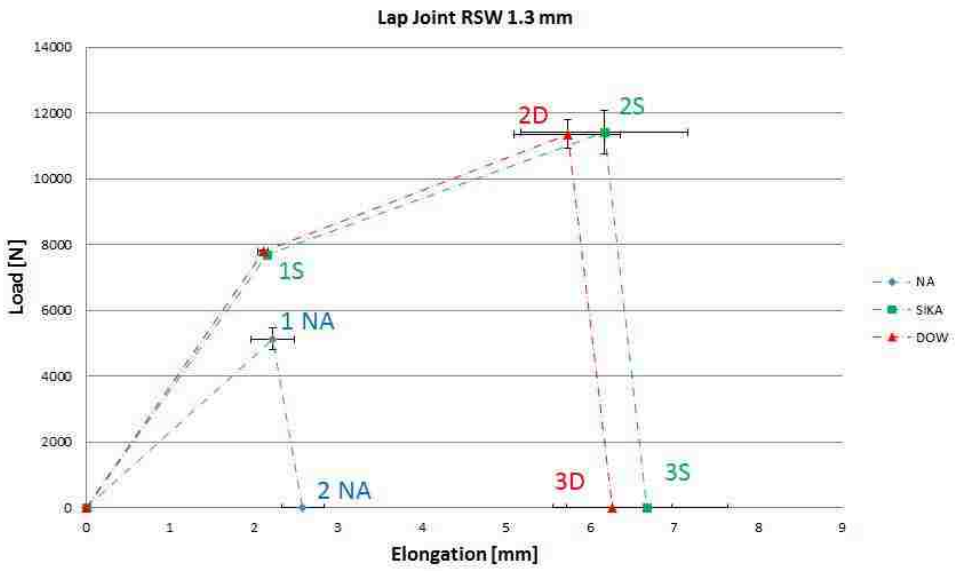

Figure 4-34. Schematic representation of the Load-Displacement curves for the Lap Joint RSW 1.3 mm group.

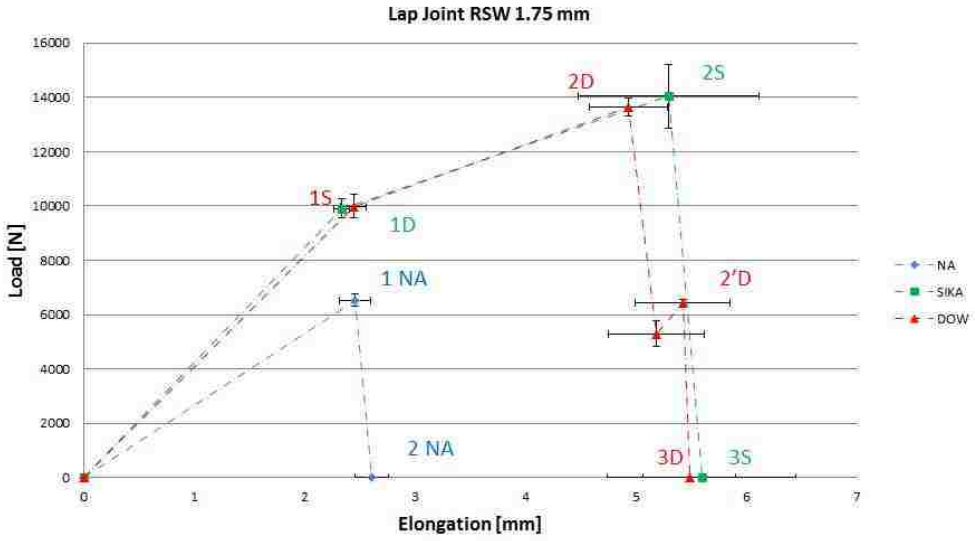

Figure 4-35. Schematic representation of the Load-Displacement curves for the Lap Joint RSW 1.75 mm group.

Table 4-19. Load and elongation RSW Lap Joints No Adhesive.

Load [N]			
Lap Joint RSW		NA	
		mean	st.dev
	1.3 mm	5121	6%
	1.75 mm	6536	13%
		28%	

Elongation [mm]				
Lap Joint RSW			NA	
			mean	st.dev
	elongation at max load	1.3 mm	2.22	11%
		1.75 mm	2.46	6%
			11%	
	elongation at failure	1.3 mm	2.58	10%
		1.75 mm	2.61	6%
			1%	

Table 4-20. Load at the highlighted points RSW Lap Joints Sika and Dow.

Load [N]						
Lap Joint RSW 1.3 mm vs 1.75 mm		SIKA		DOW		Dow vs. Sika
		mean	st.dev	mean	st.dev	
1st peak	1.3 mm	7709	0%	7784	1%	1%
	1.75 mm	9907	4%	9995	4%	1%
		29%		28%		
2nd peak	1.3 mm	11421	6%	11362	4%	-1%
	1.75	14040	8%	13654	2%	-3%
		23%		20%		

Table 4-21. Elongation at the highlighted points; RSW Lap Joints Sika and Dow.

Elongation [mm]						
Lap Joint RSW 1.3 mm vs 1.75 mm		SIKA		DOW		Dow vs. Sika
		mean	st.dev	mean	st.dev	
1st peak	1.3 mm	2.2	2%	2.1	3%	-2%
	1.75 mm	2.3	3%	2.4	5%	5%
		9%		16%		
2nd peak	1.3 mm	6.2	16%	5.7	11%	-7%
	1.75	5.3	15%	4.9	7%	-7%
		-14%		-14%		
Final elongation	1.3 mm	6.7	14%	6.3	11%	-6%
	1.75	5.6	15%	5.5	8%	-2%
		-16%		-12%		

Table 4-22. Maximum load RSW Lap Joints

Maximum Load [N]								
	NA		SIKA		DOW		Sika vs. Na	Dow vs. Na
	mean	st.dev	mean	st.dev	mean	st.dev		
1.3 mm	5121	6%	11421	6%	11362	4%	123%	123%
1.75 mm	6536	10%	14040	8%	13653	2%	115%	109%
	28%		23%		20%			

4.2.1.3 Energy - Lap Joint RSW

The energy absorbed during the deformation of the RSW lap joints is illustrated as function of the displacement in Figure 4-36 and Figure 4-37. In addition the results obtained with the two different thicknesses are compared in Table 4-23.

From the calculation of the energy the following conclusion can be drawn:

- The addition of the adhesive significantly increased the energy absorbed by the joint.
- On average Sika samples outperformed Dow samples; however the results are highly variable.
- The increase in thickness increased the energy at maximum load of the welded only samples by 17%. At final failure the welded-only 1.75 mm samples absorbed only 0.6J more than the 1.3 mm.
- The energy absorbed at the adhesive yielding peak by the hybrid joints did not vary with the increase in thickness; the elongation at the adhesive yielding peak for the thicker stack was lower than the thicker stack and counterbalanced the increase in load.

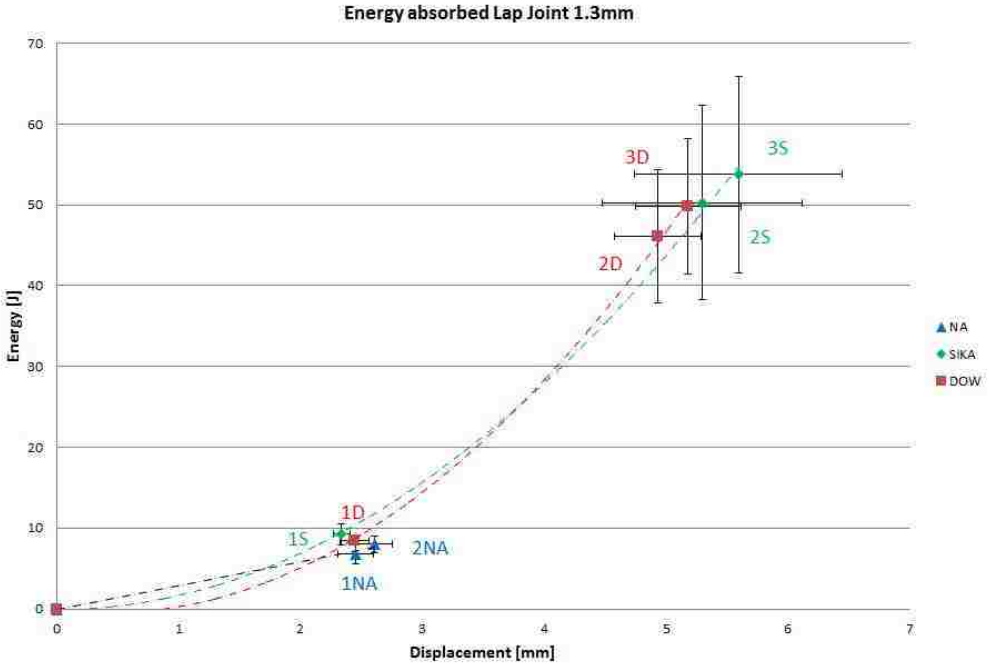

Figure 4-36. Energy absorbed by the joint as function of the displacement; Lap Joint 1.3 mm RSW.

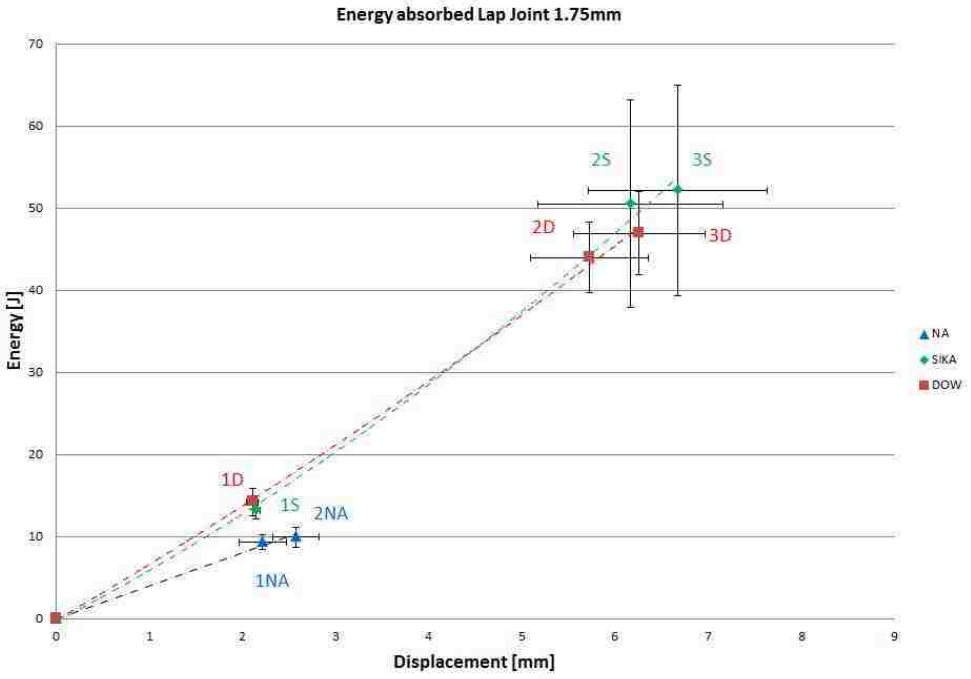

Figure 4-37. Energy absorbed by the joint as function of the displacement; Lap Joint 1.75 mm RSW.

Table 4-23. Energy at the indicated peaks; RSW Lap Joints

Energy NA samples [J]			
Lap Joint RSW 1.3 mm vs. 1.75 mm		NA	
		mean	st.dev
1st peak	1.3 mm	6.9	9%
	1.75 mm	8.0	18%
		17%	
Joint failure	1.3 mm	9.4	12%
	1.75 mm	10.0	13%
		7%	

Energy hybrid samples [J]						
Coach Joint SPR		SIKA		DOW		Dow vs Sika
		mean	st.dev	mean	st.dev	
1st peak	1.3 mm	9.2	14%	8.5	7%	-8%
	1.75 mm	13.3	8%	14.3	12%	8%
		44%		68%		
2nd peak	1.3 mm	50.3	24%	46.1	18%	-8%
	1.75 mm	50.6	25%	44.0	10%	-13%
		1%		-5%		
Adhesive failure	1.3 mm	53.8	23%	49.8	17%	-7%
	1.75 mm	52.2	24%	47.0	11%	-10%
		-3%		-6%		

4.2.1.4 Stiffness - Lap Joint RSW

The stiffness of the RSW lap joints as computed from the initial loading slope is tabulated in Table 4-24.

Both Sika and Dow hybrid joints showed an increase in stiffness compared to the welded-only joints between 40% and 45% for both the thin and the thick stack. The only

exception is the RSW + Dow 1.75 mm thick batch whose increase was equal to 33%. As mentioned in the Literature Review, the loading path during the tensile test of lap joints is not collinear with the two components of the joint [21]. This causes a bending moment and results in a rotation of the two components. The welded-only samples are constrained only by the nugget and the coupons can deform freely elsewhere. When adhesive is added it keeps together the entire overlap area and makes the joint stiffer.

The increase in the aluminum sheet thickness did not have any significant impact on the stiffness of the joint.

Table 4-24. Stiffness of the RSW lap joints.

Stiffness at initial load application [N/mm]									
Lap Joint RSW	NA		SIKA		DOW		Sika vs NA	Dow vs NA	Dow vs Sika
	mean	st.dev	mean	st.dev	mean	st.dev			
1.3 mm	2839	15%	4031	4%	4124	4%	42%	45%	2%
1.75 mm	2959	5%	4229	6%	3949	7%	43%	33%	-7%
	4.2%		4.9%		-4.3%				

4.2.1.5 Nugget Size - Lap Joint RSW

The importance of the analysis of the weld nugget size has been introduced in Section 4.1.1.5.

Differently from the coach joints, two failure modes were noticed with the lap joints, namely nugget pull out with the 1.3 mm stack and nugget shearing with the 1.75 mm stack. In addition, because of the testing methodology, it was not possible to measure the nugget size for the hybrid joints because the sheets were not separated.

The weld nugget dimensions increased more significantly in thickness than in diameter when the thicker sheet was welded (Table 4-25).

Chao et al. [40] proposed an analytic correlation between the nugget size and the failure mode of the joint; in particular they defined a critical diameter d_{cr} as function of the sheet thickness as

$$d_{cr} = 3.65t^{4/3} \qquad (4.3)$$

where t is the sheet thickness. When the nugget diameter is larger than the critical diameter nugget pull-out will be the preferred failure mode. Vice versa, a smaller nugget will be sheared.

The critical diameter for the sheet thicknesses under investigation was calculated using Equation 3.3 and the results were compared with the experimental measurements (Figure 4-38). The points corresponding to the nuggets of the thin stack are below of the calculated critical diameter (blue line) thus the measured diameter is bigger than the critical and nugget pull-out is expected. On the other hand the nugget dimension for the thicker stack is on average smaller than the critical diameter and so nugget shearing is the preferred failure mode. These predictions matched with the observed failure mode and verified the validity of the d_{cr} model.

Table 4-25. Nugget diameter and thickness; RSW lap joints.

Nugget Diameter [mm]		
Lap Joint	NA	
	mean	St.dev
1.3 mm	6.68	21%
1.75 mm	7.50	2%
	12%	

Nugget thickness [mm]		
Lap Joint	NA	
	mean	St.dev
1.3 mm	1.71	8%
1.75 mm	2.70	5%
	58%	

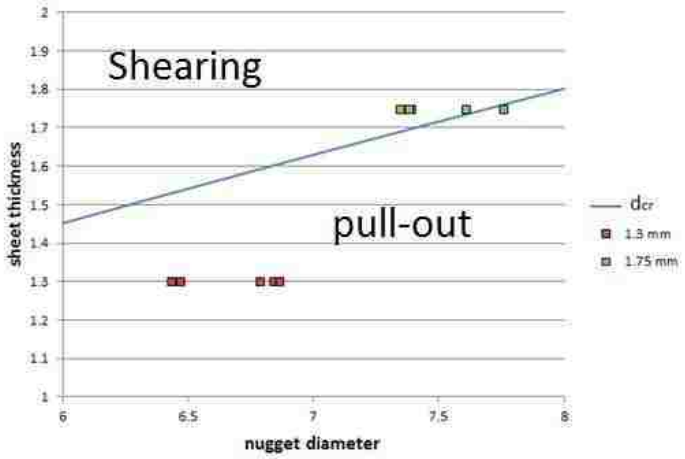

Figure 4-38. Calculation of the critical nugget diameter [40] and comparison with the experimental data.

Figure 4-39 shows the correlation between the load held by the 1.3 mm thick RSW NA lap joint and the measured nugget diameter; as highlighted for the coach joints, it can be observed that the increase in nugget diameter corresponds to an increase in the nugget failure load.

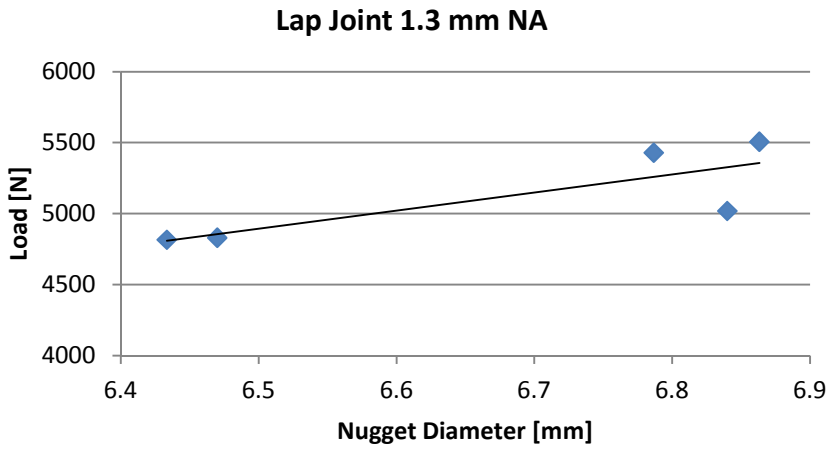

Figure 4-39. . Load vs. Nugget Diameter Lap Joint RSW 1.3 mm No Adhesive.

4.2.1.6 Failure mode analysis - Lap Joint RSW

As anticipated in the previous section, nugget pull out was observed for the 1.3 mm thick RSW NA lap joints (Figure 4-40 (a)) while in the thicker stack the nuggets were always sheared (Figure 4-40(b)). The impact of these different failure modes on the load displacement curve can be noticed in Figure 4-32 and Figure 4-33, where the NA samples are represented by the black lines. In the thinner stack, after the nugget starts yielding, the crack has to propagate around the nugget before the nugget is pulled put. This is reflected by a small additional elongation after the peak load before final failure (Figure 4-32). On the other hand, when the nugget is sheared the fracture propagates almost instantaneously and the load drops vertically with no additional elongation (Figure 4-32).

The failure mode of the adhesive layer could be analyzed only for the 1.75 RSW + Dow samples, because the adherends in the other hybrid joints remained together by the weld nugget (Figure 4-31). Adhesive failure was noticed in all these samples, as proved by the complete absence of glue on one of the two matching surfaces (Figure 4-41).

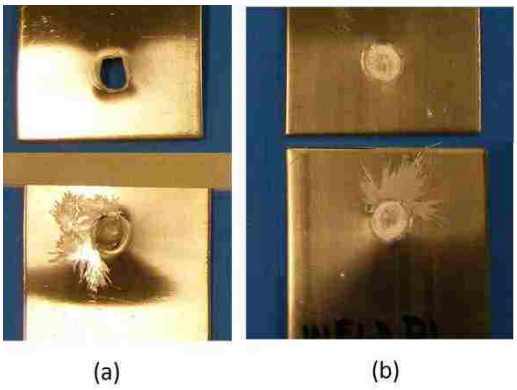

Figure 4-40. Failure modes observed with RSW lap joints; (a) 1.3 mm sheets, nugget pull-out, (b) 1.75 mm sheets, nugget shearing.

Figure 4-41. Adhesive layer failure mode, 1.75 mm Lap Joints RSW + Dow.

4.2.2 Lap Joint SPR

4.2.2.1 Tensile test data interpretation - Lap Joint SPR

Figure 4-42 and Figure 4-43 show three typical load-displacement curves for the SPR lap joint 1.3mm and 1.75 mm thick.

The hybrid joints load-displacement lines show the same characteristics observed for the weld-bonded joints. The riveted-only sample (black line) is characterized by a region of constant load elongation at the point of maximum load after which the load drop and the joint eventually fails. This drop in particular is more severe for the 1.75 mm thick stack (Figure 4-43). This difference will be assessed in Section 4.2.2.5

In the following sections dedicated to the data processing by means of the "peak-by-peak" approach both the beginning and the end of the described plateau will be taken into account to better represent the shape of the load-displacement curve.

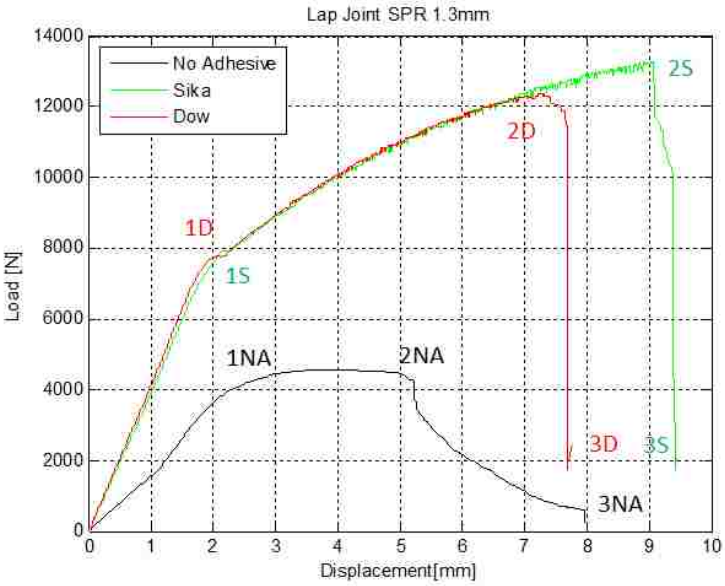

Figure 4-42. Results Interpretation; Curve superimposition Lap Joint SPR 1.3 mm.

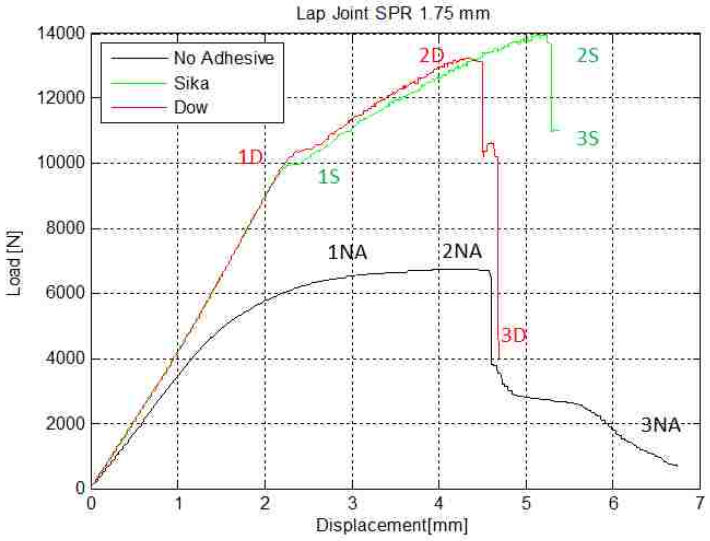

Figure 4-43. Results Interpretation; Curve superimposition Lap Joint SPR 1.75 mm.

4.2.2.2 Load vs. Displacement - Lap Joint SPR

The results obtained with the SPR lap joints are shown in Figure 4-44 and Figure 4-45. As previously explained, the testing of the hybrid joints was stopped before rivet failure thus no direct "peak-by-peak" comparison is allowed between the hybrid and the simple lap joints.

The results show that:

- The load at the first and second peak for the riveted only samples is the same; by increasing the stack thickness the load increased significantly (about 55%)
- The flat portion of the load-displacement line between the two peaks (previously referred to as "plateau") is longer for the thinner stack. The elongation obtained at failure is comparable.
- The maximum load held by the hybrid joints is significantly higher compared to the rivet-only joints (Table 4-29). In particular, given the reduced increment in strength as function of the increase in thickness experience by the hybrid joints compared to the rivet-only joints, the difference between the load held by the NA samples and Sika and Dow is lower for the thicker stack.
- The elongation of both the hybrid joints dropped dramatically with the increase in stack thickness.
- Sika 1.3 mm samples significantly outperformed Dow 1.3 mm samples. No significant difference is noticeable with the thicker stack.

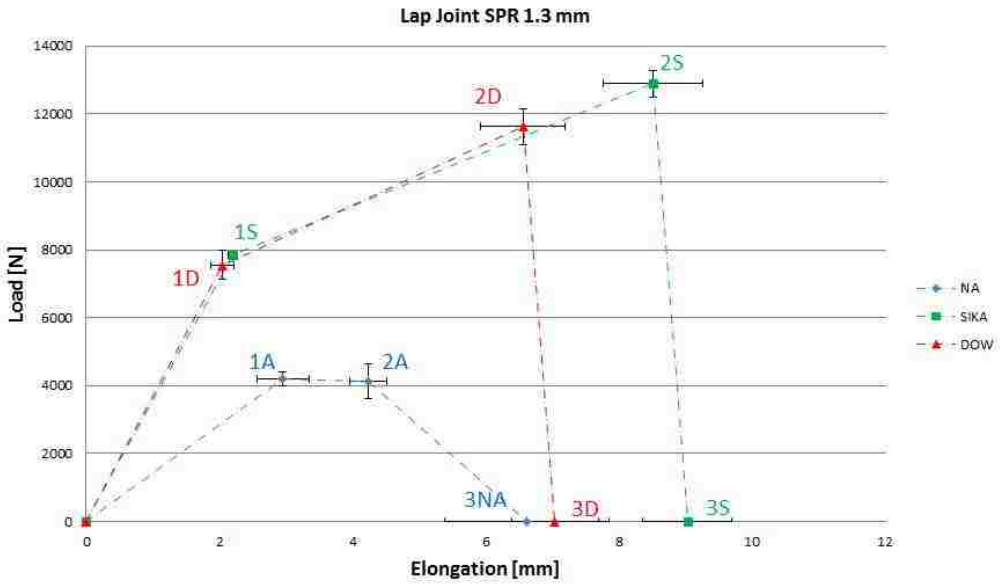

Figure 4-44. Schematic representation of the Load-Displacement curves for the Lap Joint SPR 1.3 mm group.

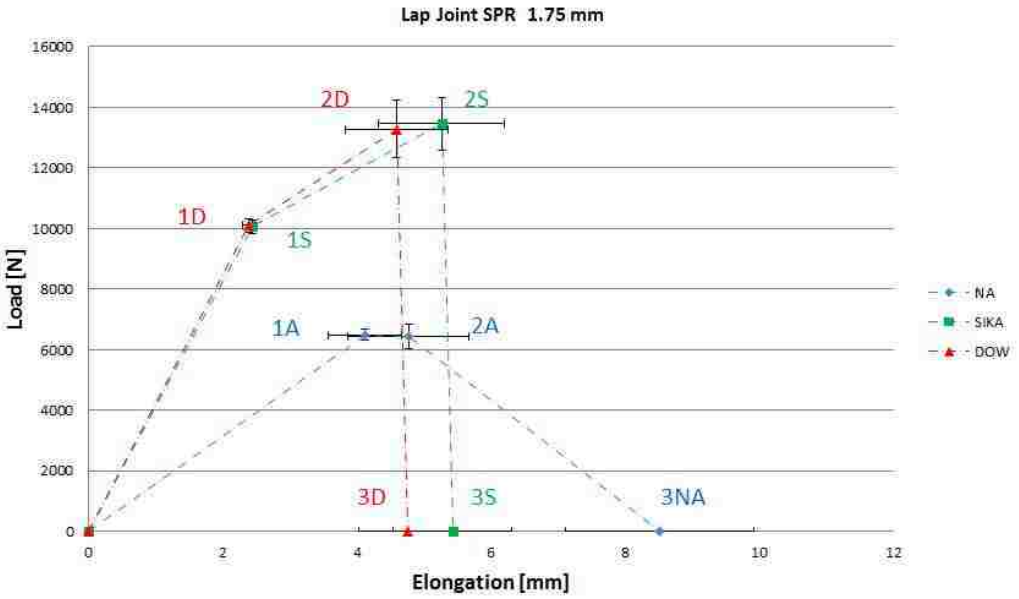

Figure 4-45. Schematic representation of the Load-Displacement curves for the Lap Joint SPR 1.75 mm group.

Table 4-26. Load and elongation at the highlighted points; SPR Lap Joints No Adhesive.

Load [N]			
Lap Joint SPR		NA	
		mean	st.dev
1st peak	1.3 mm	4195	5%
	1.75 mm	6496	3%
		55%	
2nd peak	1.3 mm	4142	12%
	1.75 mm	6446	6%
		56%	

Elongation [mm]			
Lap Joint SPR		NA	
		mean	st.dev
1st peak	1.3 mm	2.2	18%
	1.75 mm	4.1	13%
		87%	
2nd peak	1.3 mm	8.5	3%
	1.75 mm	4.8	19%
		-44%	
failure	1.3 mm	9.0	14%
	1.75 mm	8.5	16%
		-6%	

Table 4-27. Load at the highlighted points; SPR Lap Joints Sika and Dow.

Load [mm]						
Lap Joint SPR 1.3 vs 1.75		SIKA		DOW		Dow vs. Sika
		mean	st.dev	mean	st.dev	
1st peak	1.3 mm	7840	49%	7557	6%	17%
	1.75 mm	10058	2%	10108	2%	1%
		28%		34%		
2nd peak	1.3 mm	12884	3%	11622	4%	-10%
	1.75	13454	6%	13283	7%	-1%
		4%		14%		

Table 4-28. Elongation at the highlighted points; SPR Lap Joints Sika and Dow.

Elongation [mm]						
Lap Joint SPR 1.3 vs 1.75		SIKA		DOW		Dow vs. Sika
		mean	st.dev	mean	st.dev	
1st peak	1.3 mm	2.2	3%	2.1	8%	-7%
	1.75 mm	2.5	2%	2.4	4%	-2%
		11%		17%		
2nd peak	1.3 mm	8.5	9%	6.6	10%	-23%
	1.75	5.3	18%	4.6	17%	-13%
		-38%		-30%		
failure	1.3 mm	9.0	7%	7.0	9%	-22%
	1.75	5.4	16%	4.8	15%	-12%
		-40%		-32%		

Table 4-29. Maximum load SPR Lap Joints.

Maximum Load [N]								
	NA		SIKA		DOW		Sika vs. Na	Dow vs. Na
	mean	st.dev	mean	st.dev	mean	st.dev		
1.3 mm	4194.8	5%	12884	3%	11622	4%	207%	207%
1.75 mm	6496	3%	13454	6%	13283	7%	107%	104%
	55%		4%		14%			

4.2.2.3 Energy - Lap Joint SPR

The results of the calculation of the energy absorbed by the riveted lap joints during the tensile test are shown in Figure 4-46 and Figure 4-47, and Table 4-30.

Most of the observations made in the previous section regarding load and displacement are applicable also to energy:

- The energy absorbed by the rivet-only samples showed a significant increase at all the considered points as function of the increment in stack thickness.
- The 1.3 mm thick hybrid joints absorbed a much higher energy compared to the 1.3 mm thick riveted only; in particular, Sika samples showed the highest energy absorption.
- Both the difference between the two hybrid joints and the difference between the hybrid joints and the riveted-only is greatly reduced considering the thicker stack. This is due mainly to the reduced elongation noticed with the 1.75 mm thick hybrid joints.

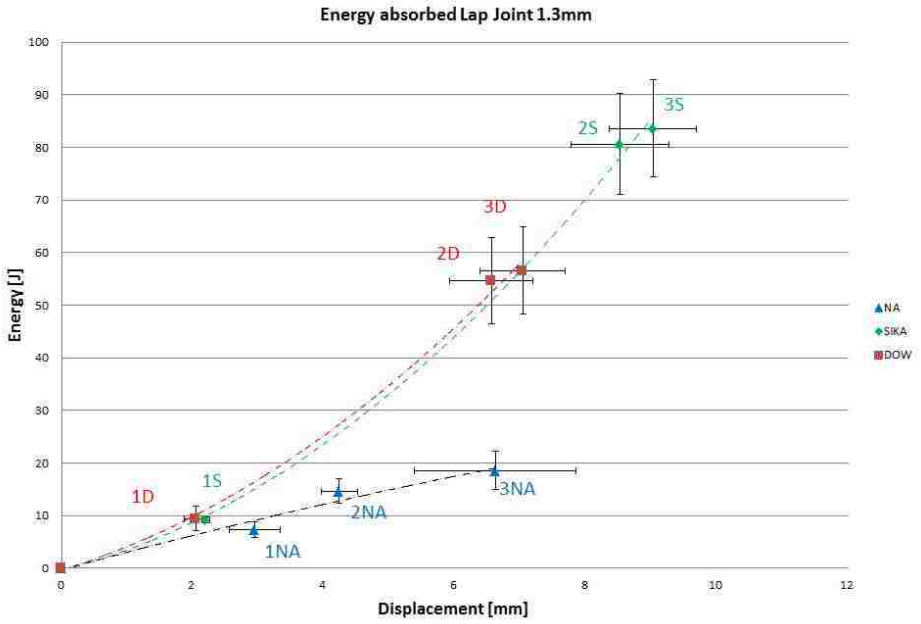

Figure 4-46. Energy absorbed by the joint as function of the displacement; Lap Joint 1.3 mm SPR.

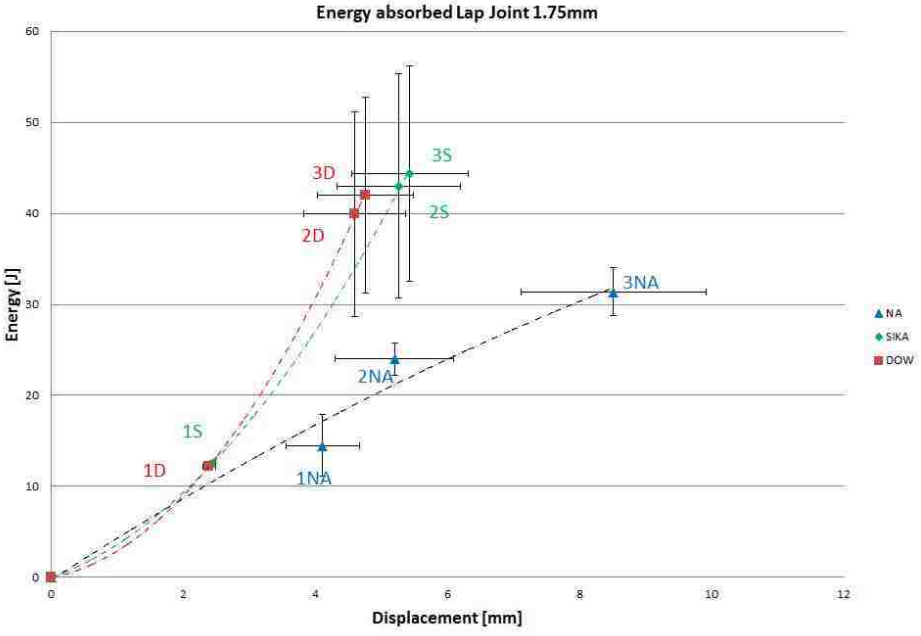

Figure 4-47. Energy absorbed by the joint as function of the displacement; Lap Joint 1.75 mm SPR.

Table 4-30. Energy at the indicated peaks; SPR Lap Joints .

Energy NA samples [J]			
Lap Joint SPR		NA	
		mean	st.dev
1st peak	1.3 mm	7.4	20%
	1.75 mm	13.7	24%
		86%	
2nd peak	1.3 mm	14.6	16%
	1.75 mm	24.1	7%
		65%	
Joint failure	1.3 mm	18.6	20%
	1.75 mm	31.4	8%
		69%	

Energy hybrid samples [J]						
Lap Joint SPR		SIKA		DOW		Dow vs Sika
		mean	st.dev	mean	st.dev	
1st peak	1.3 mm	9.2	6%	9.4	24%	3%
	1.75 mm	12.5	1%	12.2	3%	-3%
		36%		29%		
2nd peak	1.3 mm	80.7	12%	54.6	15%	-32%
	1.75 mm	43.0	29%	39.9	28%	-7%
		-47%		-27%		
adhesive failure	1.3 mm	83.6	11%	56.6	15%	-32%
	1.75 mm	44.4	27%	42.0	26%	-5%
		-47%		-26%		

4.2.2.4 Stiffness - Lap Joint SPR

The initial loading stiffness of the SPR lap joints is tabulated in Table 4-31.

The presence of the adhesive gave a higher stiffness. The stiffness of the rivet only joints increased significantly with the increase in thickness, from 1925N/mm to 2823 N/mm. On the other hand the impact of the increase in thickness on the stiffness of the hybrid joints was more limited, especially for the Sika samples. Thus, similarly to the behavior highlighted for the energy absorption, the gap between the stiffness of the hybrid joints and the riveted-only joints is much reduced, namely from 105% to 48% when NA samples and compared to Sika samples and from 85% to 46% when compared with Dow.

Table 4-31. Stiffness of the SPR lap joints.

Stiffness at initial load application [N/mm]									
Lap Joint SPR	NA		SIKA		DOW		Sika vs NA	Dow vs NA	Dow vs Sika
	mean	st.dev	mean	st.dev	mean	st.dev			
1.3 mm	1925	14%	3946	5%	3564	9%	105%	85%	-11%
1.75 mm	2823	25%	4168	8%	4124	4%	48%	46%	-1%
	46.7%		5.6%		15.7%				

4.2.2.5 Failure mode analysis - Lap Joint SPR

Due to the adopted testing methodology the failure mode of the adhesive layer could not be investigated thus only the analysis of the SPR NA samples is presented in this section.

The failure mode of SPR lap joints have been studied by Atzeni et al. [43]; in their research they proved that a rotation of the rivet around a transverse axis is induced by the misalignment between the joint components and the loading path. This rotation causes the steel rivet head to penetrate into the softer aluminum blank and partially shear it.

Figure 4-48 proves the applicability of these observations to the samples under analysis in this research. Figure 4-48 (a) is a frame of the video recording of the tests just before the final failure of the joint and shows the rotation of the rivet axis (black dashed line); additionally, the video-recording of the tensile tests proved that the plateau observed in the load – displacement line of the SPR lap joints corresponds to the period during which the rivet rotates and starts shearing the upper sheet.

Figure 4-48 (b) and (c) shows the partial shearing of the upper sheet caused by the rivet rotation. In particular it can be noticed that with the thinner stack (Figure 4-48(b)) the fracture propagates into the sheet, away from the rivet head circumference, while in the thicker stack the fracture followed precisely the rivet head (Figure 4-48(c)). These different fracture propagation modes could be the reason for the different behavior of the load displacement curves after the second peak observed with the two sheet thicknesses (Figure 4-42 and Figure 4-43). The comparison of the black lines (NA samples) shows a more severe load drop after the second peak for the thicker stack.

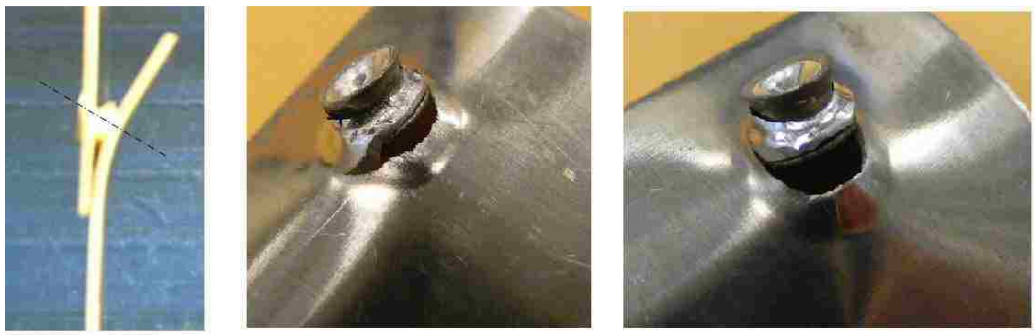

Figure 4-48. (a) Rivet rotation before final joint failure; picture from video-recording of the tensile tests. Upper sheet shearing due to rivet rotation in (b) 1.3 mm and (c) 1.75 mm SPR NA lap joints.

4.2.3 RSW vs. SPR

4.2.3.1 Load vs. Displacement - RSW vs. SPR

The loads and displacements observed with the RSW lap joints and SPR lap joints are summarized and compared in Table 4-32 Table 4-35[11].

- The 1.3 mm welded-only samples are 18% stronger than the 1.3 mm rivet only sample. This different is completely cancelled when the thicker stack is considered.
- At all the considered points the performance obtained with the riveted and welded hybrid joints are comparable. The only exception is represented by the 1.3 mm SPR + Sika samples that held 1463 N more than the corresponding RSW joints.
- Substantial differences are noticeable analyzing the elongation of the no adhesive sample. The SPR NA elongated significantly more than the RSW NA especially when the thicker stack is considered. In particular the largest gap was noticed considering the elongation at final failure.
- The hybrid joints showed similar values of elongation except for the 1.3 mm SPR + Sika that outperformed the RSW + Sika 1.3 mm thick.

Table 4-32. Load at the indicated peaks; RSW lap joints 1.3 mm vs. SPR lap joints 1.3 mm.

Load [N]							
RSW vs SPR 1.3mm		NA		SIKA		DOW	
		mean	st.dev	mean	st.dev	mean	st.dev
1st peak	Weld	5121	6%	7709	0%	7784	1%
	SPR	4195	10%	7840	2%	7557	6%
		-18%		2%		-3%	
2nd peak	Weld	-	-	11421	6%	11362	4%
	SPR	4142	12%	12884	3%	11622	4%
				13%		2%	

[11] In the following tables the results for the NA samples and the hybrid samples are represented together to reduce the number of tables and the space occupied. However the results obtained with and without adhesive must not be compared "peak by peak", as the peaks represent different physical phenomena (Section 4.2.1.1)

Table 4-33. Load at the indicated peaks; RSW lap joints 1.75 mm vs. SPR lap joints 1.75 mm.

Load [N]							
RSW vs SPR 1.75mm		NA		SIKA		DOW	
		mean	st.dev	mean	st.dev	mean	st.dev
1st peak	Weld	6536	4%	9907	4%	9995	4%
	SPR	6496	6%	10058	2%	10108	2%
		-1%		2%		1%	
2nd peak	Weld	-	-	14040	8%	13654	2%
	SPR	6446	6%	13454	6%	13283	7%
				-4%		-3%	

Table 4-34. Elongation at the indicated peaks; RSW lap joints 1.3 mm vs. SPR lap joints 1.3 mm.

Elongation [mm]							
RSW vs SPR 1.3 mm		NA		SIKA		DOW	
		mean	st.dev	mean	st.dev	mean	st.dev
1st peak	Weld	2.2	11%	2.2	1.9%	2.1	3%
	SPR	3.0	13%	2.2	2.9%	2.1	8%
		33%		2%		-3%	
2nd peak	Weld	-		6.2	16.1%	5.7	11%
	SPR	4.2	6%	8.5	8.8%	6.6	10%
				38%		14%	
failure[12]	Weld	2.6	10%	6.7	14.4%	6.3	11%
	SPR	6.6	19%	9.0	7.4%	7.0	9%
		157%		35%		12%	

Table 4-35. Elongation at the indicated peaks; RSW lap joints 1.75 mm vs. SPR lap joints 1.75 mm.

Elongation [mm]							
RSW vs SPR 1.75 mm		NA		SIKA		DOW	
		mean	st.dev	mean	st.dev	mean	st.dev
1st peak	Weld	2.5	6%	2.3	3%	2.4	5%
	SPR	4.1	13%	2.4	2%	2.4	4%
		68%		5%		-2%	
2nd peak	Weld	-		5.3	15%	4.9	7%
	SPR	4.8	19%	5.3	18%	4.6	17%
				-1%		-7%	
failure	Weld	2.6	6%	5.60	15%	5.48	8%
	SPR	8.5	16%	5.43	16%	4.76	15%
		227%		-3%		-13%	

[12] Note: failure corresponds to the joint final failure for NA while to the failure of the adhesive layer for the hybrid joints.

4.2.3.2 Energy - RSW vs. SPR

The comparison of the energy absorbed during the tensile testing of the RSW and SPR lap joints is shown in Table 4-36 and Table 4-37.

Summarizing it can be said that:

- The NA samples were more influenced by the joining method used. Since the hybrid joints have been tested until adhesive failure the results should be independent of the use of RSW or SPR and the measured differences represent actually different performances of the adhesive layer in the investigated batches.
- Similarly to the observations made for the load and elongation, the 1.3 mm thick SPR + Sika significantly outperformed the corresponding welded batch.
- SPR NA samples outperformed RSW NA samples, especially considering the thicker stack.

Table 4-36. Energy at the indicated peaks, RSW 1.3 mm vs. SPR 1.3 mm.

Energy [J]							
Coach Joint RSW vs. SPR 1.3 mm		NA		SIKA		DOW	
		mean	st.dev	mean	st.dev	mean	st.dev
1st peak	Weld	6.9	9%	9.2	14%	8.5	7%
	SPR	7.4	20%	9.2	6%	9.4	24%
		7%		0%		11%	
2nd peak	Weld	-	-	50.3	24%	46.1	18%
	SPR	14.6	16%	80.7	12%	54.6	15%
				60%		18%	
failure	Weld	9.4	12%	53.8	23%	49.8	17%
	SPR	18.6	20%	83.6	11%	56.6	15%
		98%		56%		14%	

Table 4-37. Energy at the indicated peaks, RSW 1.75 mm vs. SPR 1.75 mm.

Energy [J]							
Coach Joint RSW vs. SPR 1.75 mm		NA		SIKA		DOW	
		mean	st.dev	mean	st.dev	mean	st.dev
1st peak	Weld	8.0	18%	13.3	8%	14.3	12%
	SPR	13.7	24%	12.5	1%	12.2	3%
		71%		-6%		-15%	
2nd peak	Weld	-	-	50.6	25%	44.0	10%
	SPR	24.1	7%	43.0	29%	39.9	28%
				-15%		-9%	
failure	Weld	10.0	13%	52.2	24%	47	11%
	SPR	31.4	8%	44.4	27%	42.0	26%
		214%		-15%		-11%	

4.2.3.3 Stiffness - RSW vs. SPR

The stiffness of the riveted and welded lap joints and of the corresponding hybrid joints are compared in Table 4-38 and Table 4-39.

It can be noticed that the 1.3 mm RSW NA samples were significantly stiffer than the 1.3 mm SPR NA samples. In all the other joints under analysis the variation in stiffness was more limited and often lower than the variability of the measured values.

Table 4-38. Stiffness of the lap joints; RSW vs. SPR 1.3 mm.

Stiffness at initial load application [N/mm]						
Lap Joint RSW vs. SPR 1.3 mm	NA		SIKA		DOW	
	mean	st.dev	mean	st.dev	mean	st.dev
RSW	2839	15%	4031	4%	4124	4%
SPR	1925	14%	3946	5%	3564	9%
	-47.5%		-2.2%		-15.7%	

Table 4-39. Stiffness of the lap joints; RSW vs. SPR 1.75 mm.

Stiffness at initial load application [N/mm]						
Lap Joint RSW vs. SPR 1.75 mm	NA		SIKA		DOW	
	mean	st.dev	mean	st.dev	mean	st.dev
RSW	2959	5%	4229	6%	3949	7%
SPR	2823	25%	4168	8%	4124	4%
	-4.8%		-1.5%		4.3%	

4.3 Cross tension

The last subsection of this chapter is dedicated to the cross tension geometry. The same testing method used for the coach joints was adopted so the samples were tested until final failure of all the joining elements and complete separation of the two coupons composing the joint.

4.3.1 Cross Tension RSW

4.3.1.1 Tensile test data interpretation - Cross Tension RSW

Examples of the load-displacement curves for no-adhesive, Sika and Dow coach joints RSW 1.3 mm thick and 1.75 mm thick are shown in Figure 4-49 and Figure 4-50.

The No-Adhesive samples showed a progressive increase of load until the point of maximum load is reached, after which the load drops vertically, with no significant additional

elongation. The hybrid joints are characterized by a steeper load increase in the first portion of the load-displacement diagram followed by a plateau of constant load elongation. The load starts then to increase again until the point of maximum load and finally the joint failure are reached. It has to be noted however that many hybrid samples failed after the constant load elongation, without any additional increase in load (an example is represented by the Sika sample in Figure 4-49).

Comparing the described lines it can be said that the effect of the adhesive addition appears in the first portion of the load-displacement line, where the slope of the line is higher compared to welded-only samples. On the other hand, the load increment until final failure is similar independently of the presence of adhesive and thus can be ascribed to the joining force given by the weld nugget.

The video recording the tensile tests both confirmed the aforementioned hypothesis and helped explain the behavior noticed with the Sika sample in Figure 4-49.

Figure 4-51 shows the progressive deformation of the aluminum coupons until the nugget is pulled out and the joint fails. Figure 4-51 (c) shows the deformation an instant before the joint failure. The onset of the nugget extraction from one of the two components can be seen. The behavior of a RSW + Dow joint is show in Figure 4-52. Figure 4-52 (a) represents the deformation of the components during the first portion of the line, where the hybrid joints proved to be stiffer. It can be seen that the adhesive layer keeps the two components together over the entire area of the overlap and that the deformation of the coupons is limited to the ends of the adherends at or under the bolt washers. The end of the steep load rise corresponds to the yielding of the adhesive layer at the edge of the overlap and the subsequent plateau corresponds to the inward propagation of the adhesive fracture (Figure 4-52 (b)). In many samples the adhesive yielding proved to be asymmetric, starting from one of the two sides of the overlap (on the right in Figure 4-52 (b)). Two highly different situations can develop afterwards: if no significant difference exists between the adhesive bonding strength on the two sides of the overlap the entire adhesive layer will fail and the weld nugget will remain as the last load-carrying element. From this point onward the joint will behave as a welded-only joint and will eventually fail after nugget yielding. An example is the red curve (Dow) in Figure 4-49. Alternatively, in some samples the adhesive layer yields first on one side and then on the other; when this phenomenon happens an asymmetric loading condition of the weld nugget is created (Figure 4-52 (c)). In

particular the nugget is now partly loaded in peeling mode. This could then cause the nugget to yield at a much lower load at the end of the plateau, as shown by Sika sample in Figure 4-49.

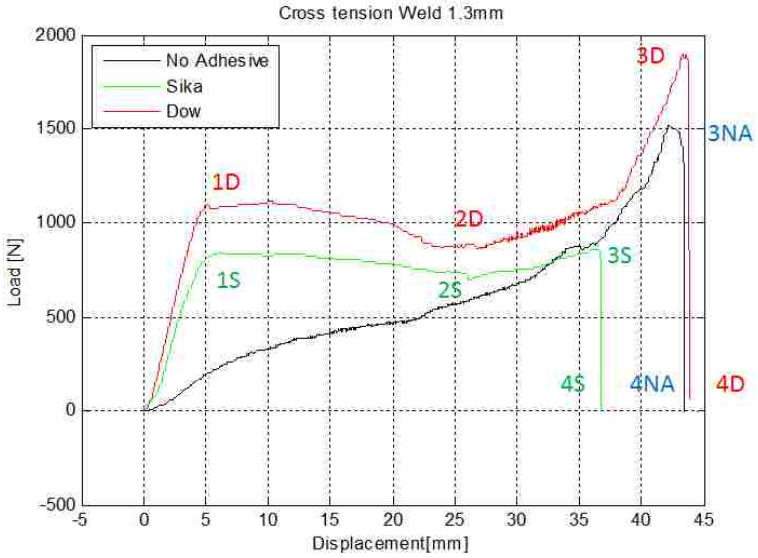

Figure 4-49. Results Interpretation; Curve superimposition Cross Tension RSW 1.3mm. The numbered points will be considered in the calculation of the Load and displacement reported in Section 4.3.1.2.

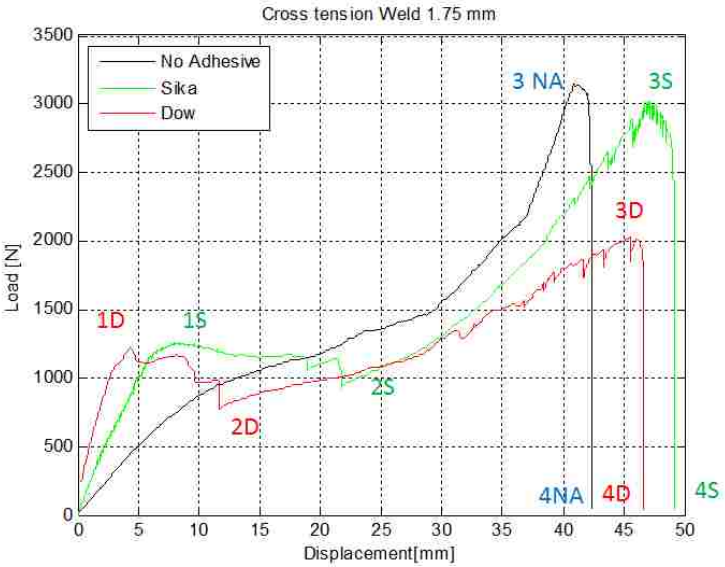

Figure 4-50. Results Interpretation; Curve superimposition Cross Tension RSW 1.75mm. The numbered points will be considered in the calculation of the Load and displacement reported in Section 4.3.1.2.

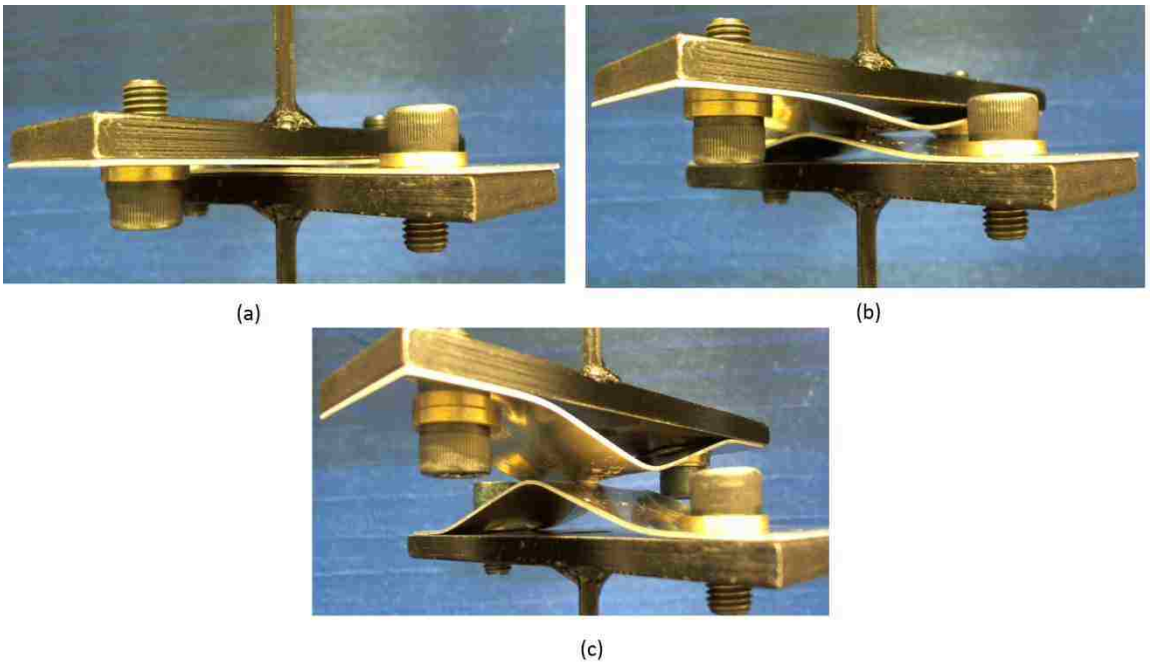

Figure 4-51. Tensile test of a 1.3 mm thick RSW cross tension joint, No adhesive; un-deformed shape (a), progressive deformation of the coupons (b) until nugget pull-out and final failure (c).

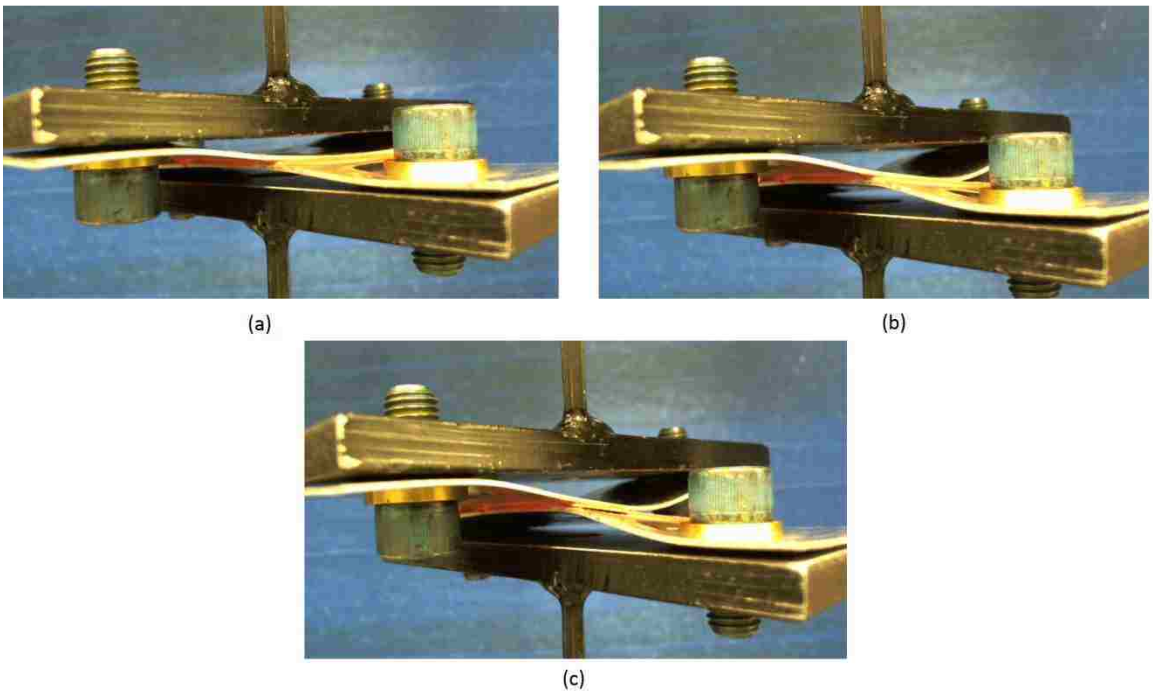

Figure 4-52. Tensile test of a 1.3 mm thick RSW + Dow cross tension joint; deformation before the first peak (a); crack propagation in the adhesive layer after the first peak (b); asymmetric loading of the weld nugget due to the one sided failure of the adhesive layer (c).

4.3.1.2 Load vs. Displacement - Cross Tension RSW

The load and displacement of the samples under analysis have been calculated in the points indicated in Figure 4-49 and Figure 4-50. In particular, the end of the plateau noticed in the hybrid joints has been indicated by points "2S" and "2D". These points has been reported in the schematic representation of the load-displacement curves for improving the visual resemblance of the schematic lines to the experimental ones (Figure 4-53 and Figure 4-54); its load and displacement however have not been tabulated in Table 4-40 and Table 4-41.

The "peak-by-peak" approach is used to analyze and compare the results.

Sika and Dow showed a comparable adhesive yielding load (1D and 1S in Figure 4-53 and "first peak" in Table 4-40) for both the stack thicknesses; in particular Dow was on average stronger than Sika with the thinner stack and vice versa Sika outperformed Dow on average in the thicker stack. In both cases however the results variability was greater than the difference between the averages. No significant difference in elongation was noticed at the first peak with the thinner stack while Sika samples outperformed Dow samples in the thicker stack. The increment in sheet thickness gave the joints a significant increase in load at the first peak, especially for Sika samples (+66%). The impact of the thickness increase on the elongation at the first peak was beneficial for Sika samples and detrimental for Dow samples.

The results at the nugget yielding peak ("second peak" in Table 4-40) were highly influenced by the failure mode of the adhesive layer, as explained in the previous section. All the 1.3 mm RSW + Sika samples failed at the end of the constant-load plateau (3S), with no increment in load, as can be seen in Figure 8-26 in Appendix A; thus the obtained load at nugget yielding was significantly lower compared to NA and Dow samples. Figure 8-27 shows instead that two 1.3 mm RSW + Dow samples had an increase in load after the plateau while the three remaining samples failed with no load increment. This is the reason for the high variability of the load at nugget yielding measured with Dow samples. Finally, the 1.3 mm welded – only samples showed the highest average load at nugget yielding for the 1.3 mm cross tension joints. Even though no adhesive was present, the variability of the results was considerably high. An explanation for this behavior will be given in Section 4.3.4.

Increasing the sheet thickness proved to increase the weld nugget dimension and consequently the nugget strength; thus the weld nugget was able to sustain possible asymmetries of the loading condition due to the "one-sided" failure of the adhesive layer. Consequently 1.75 mm Dow samples showed a nugget yielding load comparable to the 1.75 mm NA samples, while 1.75 mm Sika samples had, on average, the highest failure load.

Unlike the coach joint tests the addition of adhesive to cross tension samples does not result in higher elongation between the third peak and final failure; all the analyzed cross tension tests showed a similar load drop following the nugget yielding.

With the exception of a few 1.3 mm Sika samples, the maximum load of the cross tension joints was always registered at the nugget yielding peak.

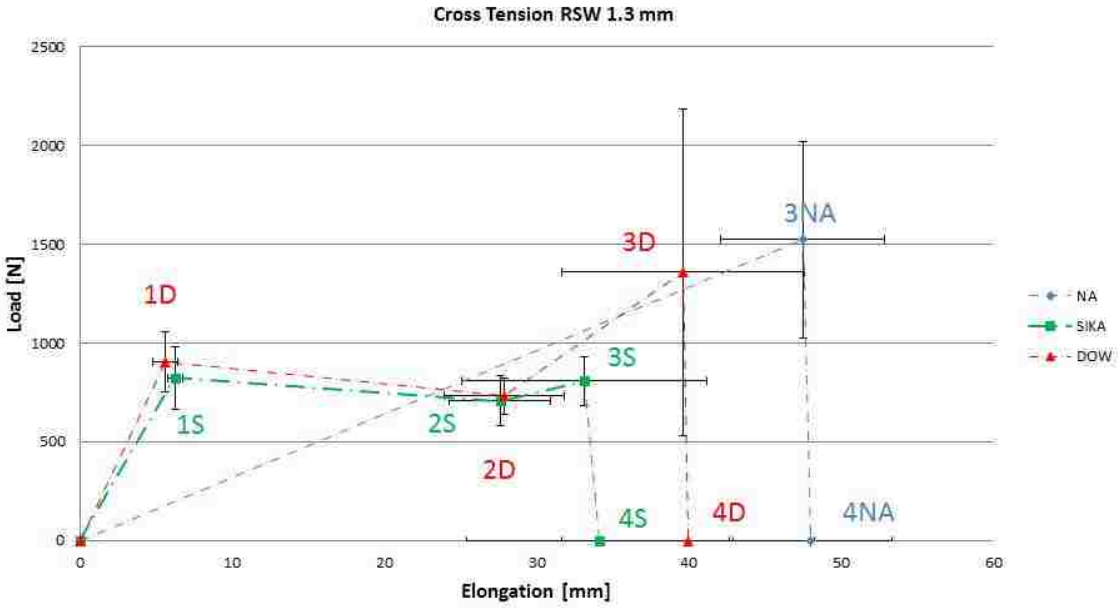

Figure 4-53. Schematic representation of the Load - Displacement curves for the RSW Cross Tension joints 1.3 mm thick.

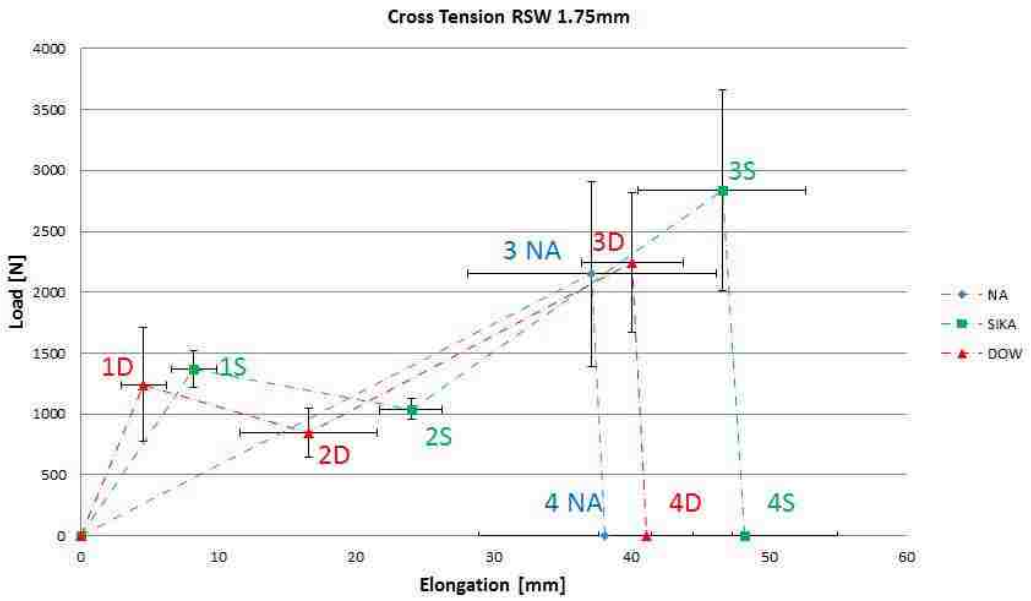

Figure 4-54. Schematic representation of the Load - Displacement curves for the RSW Cross Tension joints 1.75 mm thick.

Table 4-40. Load at the indicated peaks; RSW Cross Tension joints.

Load [N]										
Cross Tension RSW		NA		SIKA		DOW		Sika vs Na	Dow vs Na	Dow vs Sika
		mean	st.dev	mean	st.dev	mean	st.dev			
1st peak	1.3 mm	-	-	824	19%	904	17%			9.8%
	1.75 mm	-	-	1368	11%	1241	38%			-9.3%
				66.0%		37.2%				
2nd peak	1.3 mm	1523	33%	808	16%	1358	61%	-47.0%	-10.8%	68.2%
	1.75 mm	2151	35%	2838	29%	2244	25%	32.0%	4.3%	-20.9%
		41.2%		251%		65.2%				

Table 4-41. Elongation at the indicated peaks; RSW Cross Tension joints.

Elongation [mm]										
Cross tension RSW		NA		SIKA		DOW		Sika vs Na	Dow vs Na	Dow vs Sika
		mean	st.dev	mean	st.dev	mean	st.dev			
1st peak	1.3 mm	-	-	6.2	8.0%	5.6	14.3%			-9.8%
	1.75 mm	-	-	8.2	20.2%	4.6	35.2%			-44.2%
				32.3%		-18.2%				
2nd peak	1.3 mm	47.5	11.4%	33.1	24.2%	39.6	20.2%	-30.2%	-16.6%	19.6%
	1.75 mm	37.2	24.2%	46.6	13.1%	40.1	9.2%	25.5%	7.8%	-14.1%
		-21.7%		40.8%		1.2%				
Failure	1.3 mm	48.0	11.1%	34.1	25.6%	39.9	20.7%	-28.9%	-16.7%	17.1%
	1.75 mm	38.1	24.2%	48.3	14.0%	41.1	8.4%	26.5%	7.7%	-14.9%
		-20.5%		41.5%		2.8%				

4.3.1.3 Energy - Cross Tension RSW

The energy absorbed by the RSW cross tension joints is schematically represented in Figure 4-55 and Figure 4-56 and the numerical results are reported in Table 4-42. The energy at the end of the plateau (points 2D and 2S) has not been reported.

The figures show clearly that the energy absorbed at the nugget yielding (3NA, 3S, 3D) is largely dominant and almost equal to the energy at final failure (4NA, 4S, 4D).

All the phenomena described in the previous section had an impact also on the energy absorption of the joint. For example, considering the thinner stack, the Sika samples showed lower energy absorption compared to Dow samples because of the low values of load at nugget yielding. Alternatively when analyzing the thicker stack it can be noticed that the high load and elongation experienced by the 1.75 mm Sika samples corresponds to high energy absorption. Sika samples showed then the highest increase in energy with the increase in sheet thickness, as reported in Table 4-42. On the other hand, the increment in energy as function of the sheet thickness experienced by Dow samples was the smallest among the analyzed conditions.

The presence of adhesive proved to have a more beneficial impact on the energy absorption than on the load carried by the joints. Even though 1.3 mm Sika samples had a lower nugget yielding load (3S, 3D) compared to 1.3 mm NA samples, the energy absorbed during the adhesive yielding caused the energy at final failure of the two conditions to be comparable. Similarly, 1.3 mm Dow samples gave a lower load at nugget yielding (3D) compared to 1.3 mm NA samples (3NA) but at that point they had absorbed a higher energy.

It should be also noted that the high variability in load and elongation caused the variability of the energy to be significantly high as well.

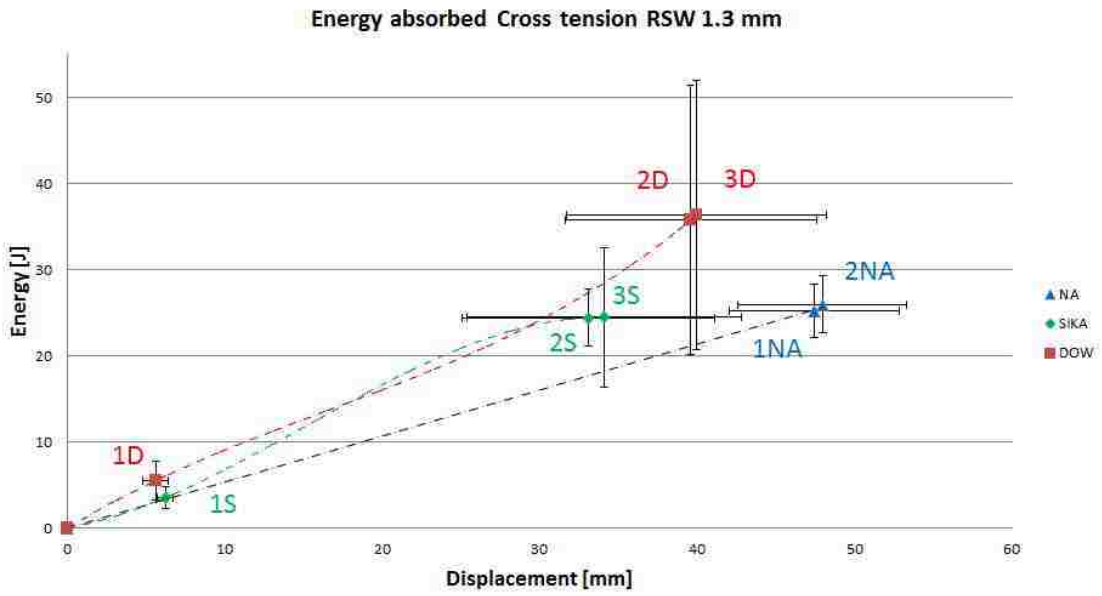

Figure 4-55. Energy absorbed by the joint as function of the displacement; Cross Tension 1.3 mm RSW.

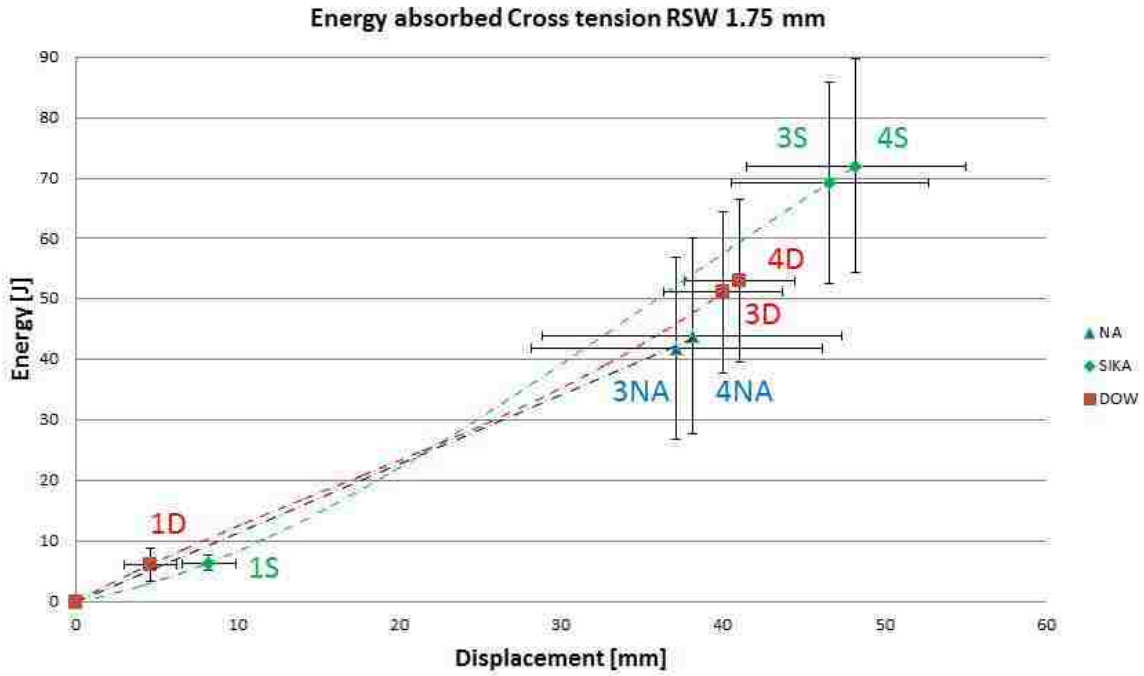

Figure 4-56. Energy absorbed by the joint as function of the displacement; Cross Tension 1.75 mm RSW.

Table 4-42. Energy at the indicated peaks; RSW Lap Joints.

Energy [J]										
Coach Joint Weld 1.3 mm vs. 1.75 mm		NA		SIKA		DOW		Sika vs NA	Dow vs NA	Dow vs. Sika
		mean	st.dev	mean	st.dev	mean	st.dev			
1st peak	1.3 mm			3.6	35%	5.5	42%			54.8%
	1.75 mm			6.4	19%	6.1	44%			-5.5%
				80.6%		10.3%				
2nd peak	1.3 mm	25.2	12%	24.4	13%	35.8	44%	-3.0%	42.1%	46.5%
	1.75 mm	41.9	36%	69.2	33%	51.2	26%	65.2%	22.1%	-26.1%
		66.4%		183%		42.9%				
joint failure	1.3 mm	26.0	13%	24.5	33%	36.3	43%	-5.8%	39.8%	48.4%
	1.75 mm	44.0	37%	72.0	25%	53.1	25%	63.8%	20.7%	-26.3%
		69.2%		194%		46.2%				

4.3.1.4 Stiffness - Cross Tension RSW

The initial loading stiffness of the RSW cross tension joints is summarized in Table 4-43.

As already anticipated in the previous sections, the addition of adhesive causes the increase of the slope of the load-displacement curve until the adhesive yielded and thus increases the initial stiffness of the joint. This phenomenon is particularly evident in the thinner stack, where the stiffness increased from 29 N/mm for the NA samples to 212 N/mm and 246 N/mm respectively for Sika and Dow. By constraining the entire area of overlap, the adhesive layer allows the adherends to deform only in the portion between the edge of the overlap and the washer on the loaded end. This corresponds to a reduction of the lever arm and thus a lower deflection for the same load, which means a higher stiffness.

The increase in thickness of the aluminum blank had a dramatic impact on the stiffness of the NA samples; in this case the greater stiffness corresponds to a higher moment of inertia of the cross section which leads to a lower deflection for the same load. The stiffness of the hybrid joints instead showed a more limited increase.

Table 4-43. Stiffness of the RSW Cross Tension joints.

Stiffness at initial load application [N/mm]									
Cross Tension RSW	NA		SIKA		DOW		Sika vs NA	Dow vs NA	Dow vs Sika
	mean	st.dev	mean	st.dev	mean	st.dev			
1.3 mm	29	23%	212	23%	246	20%	632%	749%	14%
1.75 mm	107	15%	273	20%	332	10%	154%	209%	18%
	271%		28.7%		34.9%				

4.3.1.5 Nugget size - Cross Tension RSW

The results of the measurements of the nugget size diameter and thickness are reported in Figure 4-57. The considerations made with the previously analyzed geometry are valid also in this case. Summarizing:

- The presence of adhesive did not impact significantly neither the nugget diameter nor the thickness.
- The increase in thickness had a larger impact on the nugget thickness that on the nugget diameter. In particular, if the nugget diameter is normalized with respect to the thickness, a bigger nugget is obtained for the 1.3 mm stack.

In Figure 4-58 the load at nugget yielding for the 1.3 mm NA samples is plotted versus the nugget lateral area. The increase is area was in general matched to an increase in load.

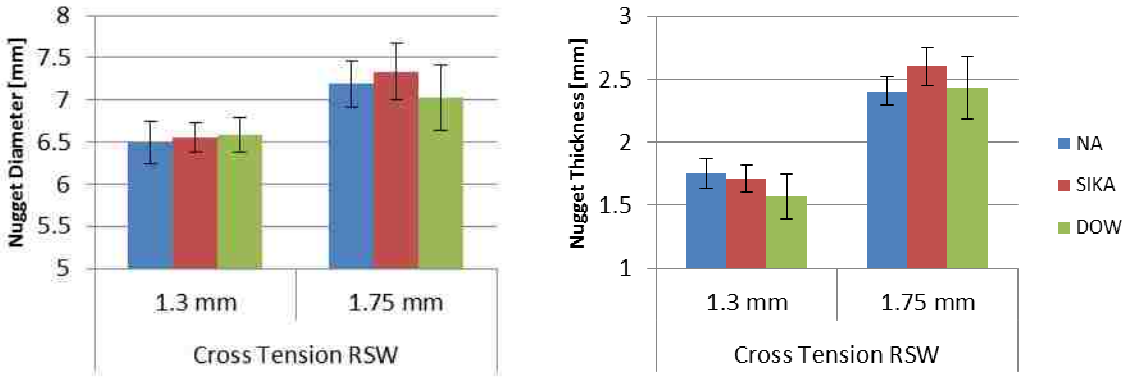

Figure 4-57. Nugget diameter and thickness, RSW Cross Tension Joints.

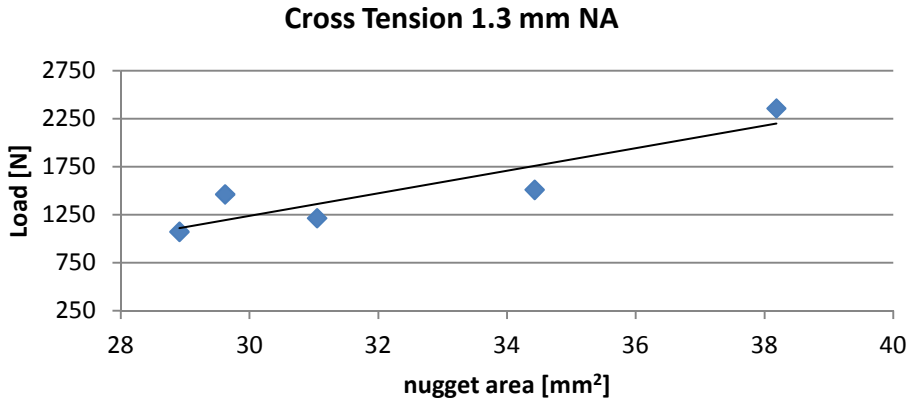

Figure 4-58. Load vs. Nugget Diameter 1.3 mm RSW Cross Tension No Adhesive.

4.3.1.6 Failure Mode - Cross Tension RSW

Radakovic and Tumuluru [31] studied the failure mode of RSW cross tension joints. Their results show that the preferred failure mode is nugget pull out and they attributed this behavior to the characteristic loading mode of a cross tension joint. Due to the constraining of the ends of the aluminum coupons (Figure 4-69 shows how the samples are bolted to the fixture used for the tensile test), the lateral movement is constrained which caused an horizontal force perpendicular to the pulling direction in addition to the vertical traction force and the bending moment. According to [31] this transversal force is the main cause of the nugget pull out failure mode.

The results obtained in this study are in agreement with the quoted research, as all the analyzed RSW samples failed in nugget pull-out mode (Figure 4-59(a)).

In numerous samples a tilting of the nugget was noticed (Figure 4-59(b)). This could be attributed to the asymmetric loading condition caused by the non-homogeneous failure of the adhesive layer. In Section 4.3.4 it will be shown that also the imperfect sample preparation caused asymmetries in the loading condition.

The adhesive layer of all the analyzed RSW hybrid samples showed adhesive failure as preferred failure mode. The observed variability of the adhesive layer failure load (first peak) is thus intrinsic in the failure mode itself, which usually is observed when the bonding of the glue with the substrate is not optimal. Additional reasons for the observed variability are reported in Section 4.3.4.

Figure 4-59. RSW cross tension joints failure mode. (a) nugget pull-out; (b) tilting of the nugget induced by the asymmetric loading conditions.

4.3.2 Cross Tension SPR

4.3.2.1 Tensile test data interpretation - Cross Tension SPR

Figure 4-60 and Figure 4-61 show three typical load-displacement curves for the SPR cross tension joint 1.3 mm and 1.75 mm thick. All the plotted curves resemble closely the results obtained with the 1.75 mm RSW Cross Tension shown in the previous section (see Figure 4-50). Thus it can be said that the rivet was able to withstand the loading induced by the asymmetric failure of adhesive layer and to guarantee an increase in load after the complete delamination of the adhesive layer (Figure 4-62).

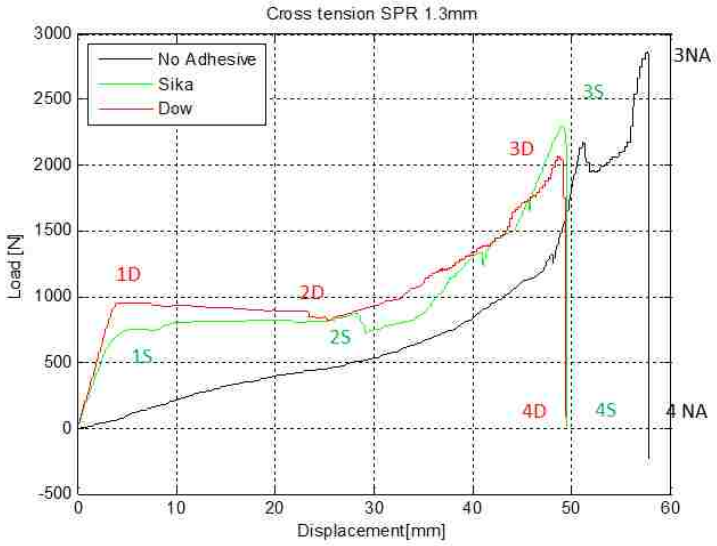

Figure 4-60. Results Interpretation; Curve superimposition, 1.3 mm SPR Cross Tension.

3

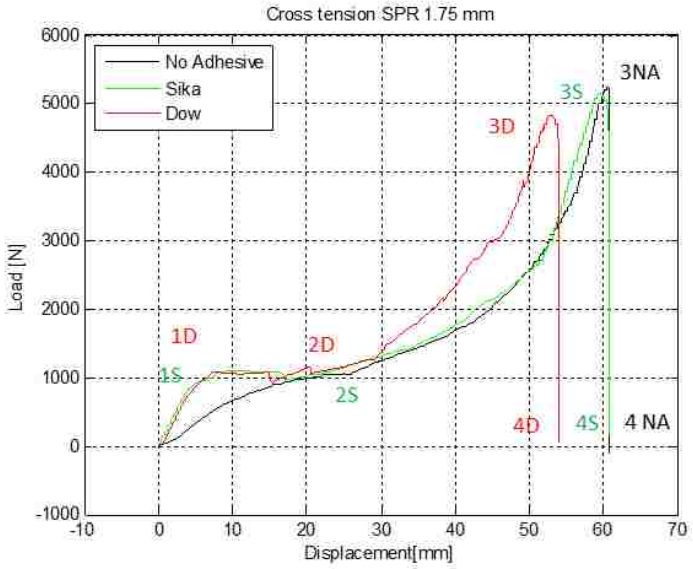

Figure 4-61. Results Interpretation; Curve superimposition, 1.75 mm SPR Cross Tension.

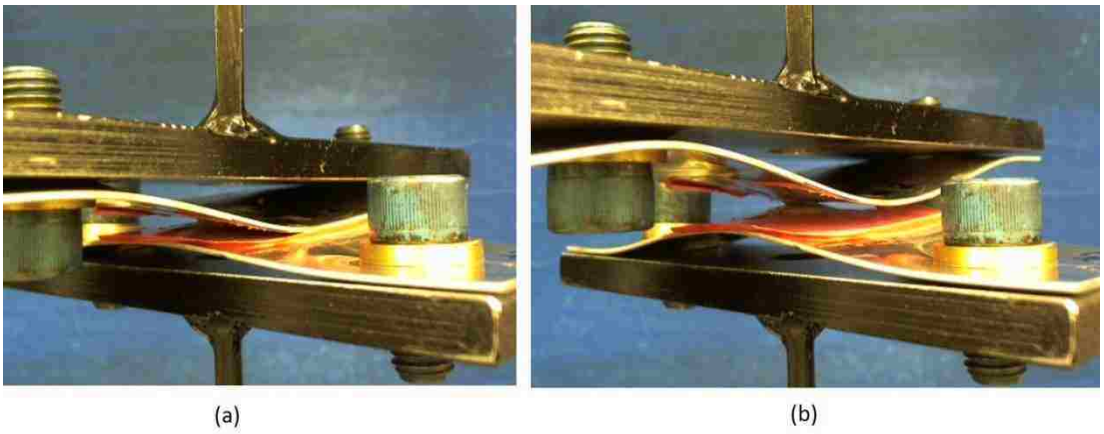

Figure 4-62. Tensile test of a 1.3 mm thick SPR cross tension joint. Crack propagation in the adhesive layer and asymmetric loading of the rivet (a); complete failure of the adhesive layer, rivet intact still holding load (b).

4.3.2.2 Load vs. Displacement - Cross Tension SPR

The results obtained with the SPR cross tension joints are schematically represented in Figure 4-63 and Figure 4-64 and tabulated in Table 4-44 and Table 4-45.

The two adhesives showed similar performance at the adhesive yielding peak, especially considering the 1.75 mm stack. In the thinner stack Dow samples gave a higher average load while Sika samples gave a higher average elongation; in both cases however the difference between the averages was smaller than the variability of the results. The increase in sheet thickness allowed a partial load increase at the first peak (17% for Dow samples and 27% for Sika samples) and a significant increment in deflection at the same peak (1D) for Dow samples (97%).

The NA samples held a higher load at the second peak (3NA, 3S, and 3D, corresponding to rivet yielding) than the hybrid specimens for both the analyzed thicknesses; in particular this difference was more significant in the thinner stack, where the NA samples registered an average load of 2654 N, versus 2207 N and 2028 N respectively for Sika and Dow. These results suggest that the presence of the adhesive weakened the rivet interlock, especially in the 1.3 mm stack. Further investigation of the impact of the presence of adhesive on the rivet interlock will be presented in Section 6.2. The hybrid joints showed the highest relative increment in load at the second peak when the two thicknesses are compared. Both Sika and Dow samples' peak loads increased by more than a factor of two the while NA samples experienced an increase of 96% due to the thickness difference.

The elongation at the rivet yielding peak showed the same trend of the load, with NA samples showing a higher elongation of the hybrid samples, especially considering the thinner stack. The increase in deflection as function of the increase in thickness was however not substantial as the increase in load.

As for the RSW cross tension joints the elongation measured after the second peak was almost null.

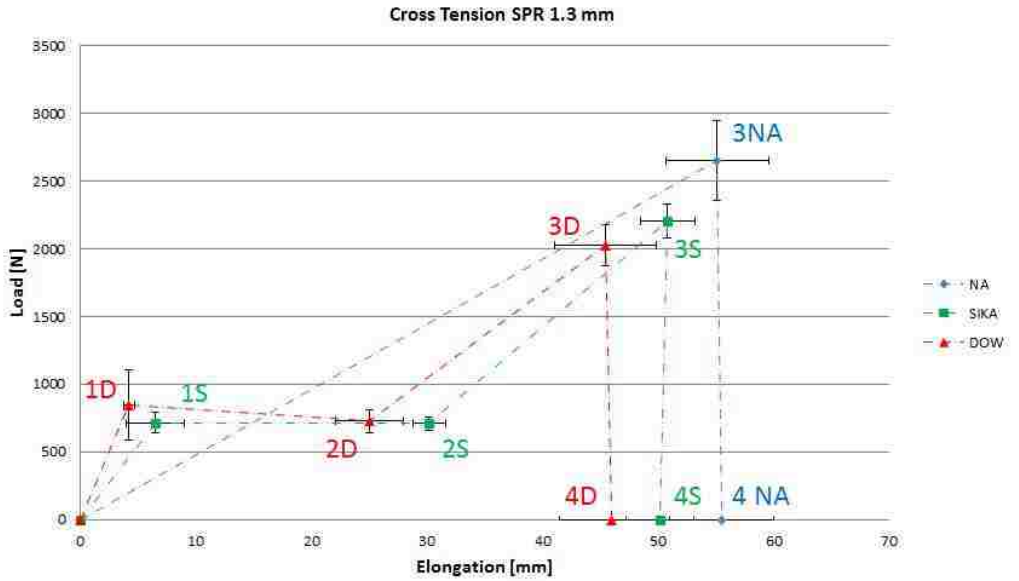

Figure 4-63. Schematic representation of the Load - Displacement curves for the SPR Cross Tension joints 1.3 mm thick.

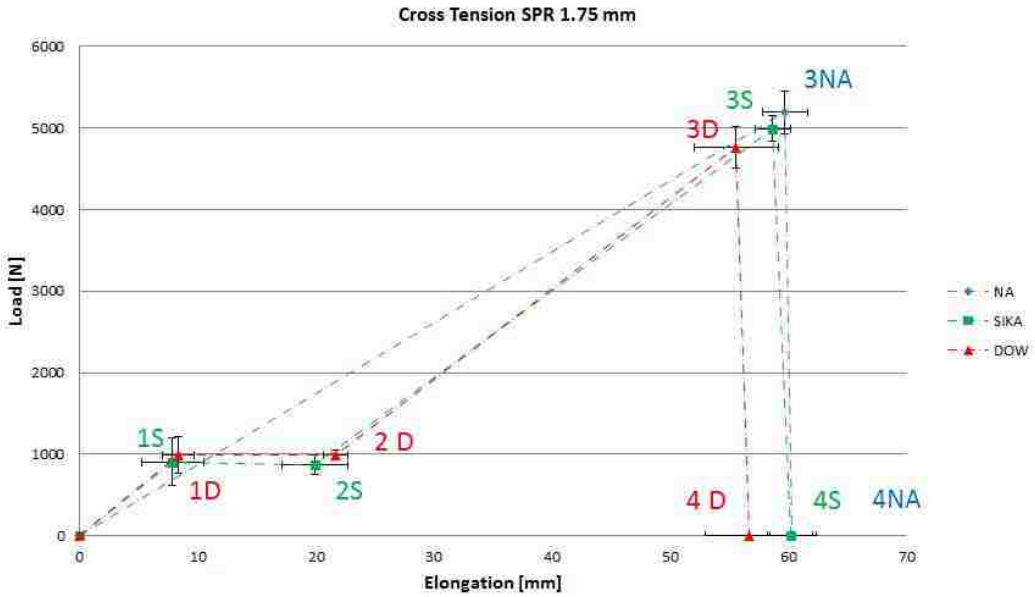

Figure 4-64. Schematic representation of the Load - Displacement curves for the SPR Cross Tension joints 1.3 mm thick.

Table 4-44. Load at the indicated peaks; SPR Cross Tension joints.

Load [N]										
Cross Tension RSW		NA		SIKA		DOW		Sika vs Na	Dow vs Na	Dow vs Sika
		mean	st.dev	mean	st.dev	mean	st.dev			
1st peak	1.3 mm	-	-	714	11%	846	30%			18.4%
	1.75 mm	-	-	905	32%	990	23%			9.4%
				26.7%		17.1%				
2nd peak	1.3 mm	2654	11%	2207	6%	2028	7%	-16.8%	-23.6%	-8.1%
	1.75 mm	5194	5%	4996	3%	4762	5%	-3.8%	-8.3%	-4.7%
		95.7%		126%		135%				

Table 4-45. Elongation at the indicated peaks; SPR Cross Tension joints.

Elongation [mm]										
Cross tension RSW		NA		SIKA		DOW		Sika vs Na	Dow vs Na	Dow vs Sika
		mean	st.dev	mean	st.dev	mean	st.dev			
1st peak	1.3 mm	-	-	6.5	39.2%	4.2	11.7%			-34.4%
	1.75 mm	-	-	7.9	33.4%	8.3	15.9%			6.2%
				21.7%		97.1%				
2nd peak	1.3 mm	55.1	8.1%	50.8	4.6%	45.5	9.7%	-7.8%	-17.5%	-10.6%
	1.75 mm	59.7	3.2%	58.7	2.6%	55.6	6.4%	-1.8%	-6.9%	-5.3%
		8.3%		15.4%		22.3%				
failure	1.3 mm	55.5	8.1%	50.2	5.8%	46.0	9.7%	-9.6%	-17.2%	-8.4%
	1.75 mm	60.3	3.4%	60.2	3.0%	56.7	6.6%	-0.1%	-6.0%	-5.9%
		8.6%		20.0%		23.3%				

4.3.2.3 Energy - Cross Tension SPR

The results of the calculation of the energy absorbed by the SPR cross tension joints can be summarized as follow:

- The presence of adhesive reduced the difference between riveted-only and hybrid samples noticed in load and elongation, and made the energy absorbed at rivet yielding and final failure in the three configurations comparable, especially with the thicker stack (Figure 4-65Figure 4-66).
- Both Sika and Dow showed very similar energy absorption in all the analyzed points.
- The increase in sheet thickness was particularly beneficial for the energy at rivet yielding and at final failure. All the analyzed conditions showed at these points an increment of about 120% (Table 4-46).

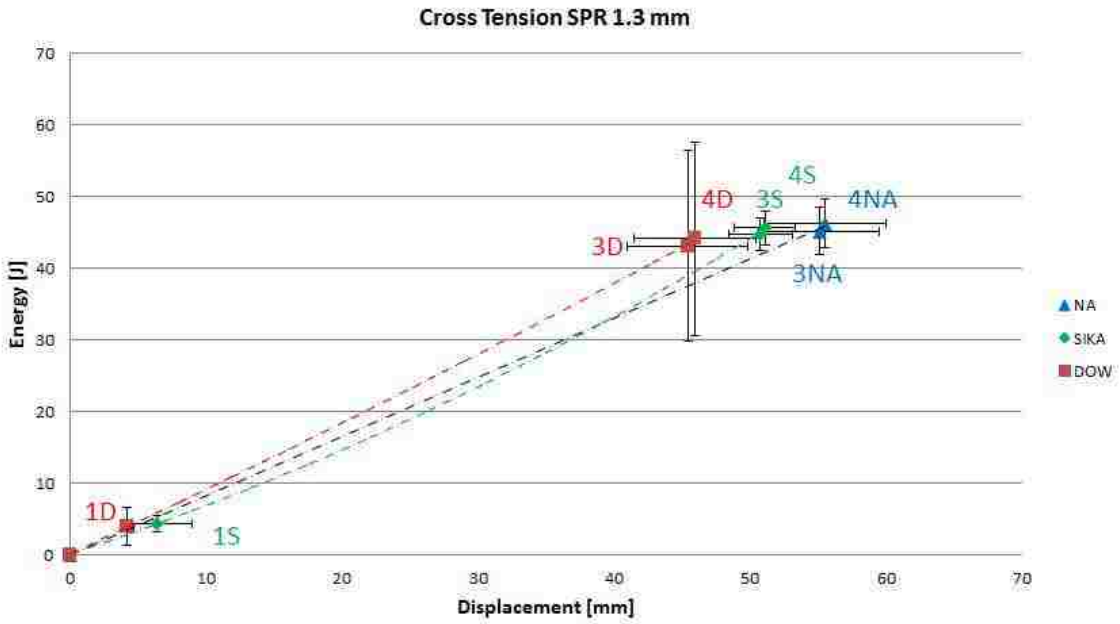

Figure 4-65. Energy absorbed by the joint as function of the displacement; Cross Tension 1.3 mm SPR.

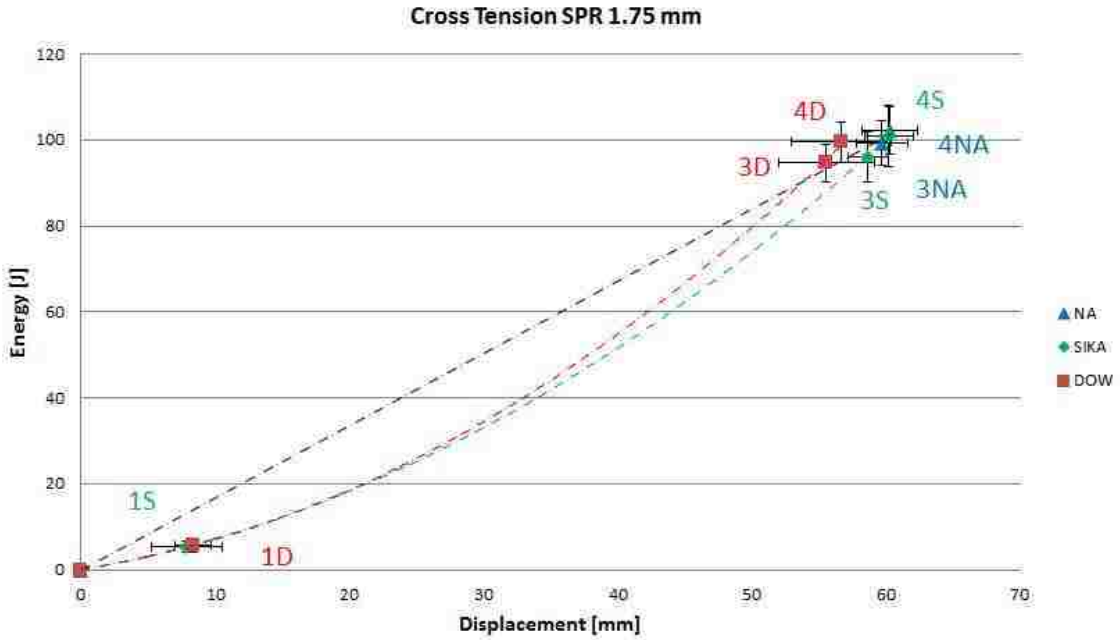

Figure 4-66. Energy absorbed by the joint as function of the displacement; Cross Tension 1.75 mm SPR.

Table 4-46. Energy at the indicated peaks; SPR Lap Joints.

Energy [J]										
Cross Tension SPR		NA		SIKA		DOW		Sika vs NA	Dow vs NA	Dow vs. Sika
		mean	st.dev	mean	st.dev	mean	st.dev			
1st peak	1.3 mm			4.3	27%	3.8	54%			-10.1%
	1.75 mm			5.5	25%	5.7	26%			4.7%
				27.9%		48.9%				
2nd peak	1.3 mm	45.2	7%	44.7	5%	43.0	14%	-1.0%	-4.7%	-3.7%
	1.75 mm	99.3	5%	96.1	6%	94.7	5%	-3.3%	-4.7%	-1.4%
		120%		115%		120%				
joint failure	1.3 mm	46.2	7%	45.6	5%	44.1	14%	-1.5%	-4.6%	-3.2%
	1.75 mm	102	5%	101	7%	99.5	5%	-1.1%	-2.6%	-1.5%
		121%		122%		125%				

4.3.2.4 Stiffness - Cross Tension SPR

The initial loading stiffness of the RSW joints is summarized in Table 4-47.

It can be noticed a behavior similar to the RSW coach joints (section 4.3.1.4). In particular:

- The presence of adhesive significantly increases the stiffness of the joint. In particular, the increment is more pronounced with the thinner stack than with the thicker stack.
- The two adhesives showed an opposite trend, with Dow outperforming Sika in the thinner stack and Sika outperforming Dow in the thicker stack.
- The increase in stack thickness was highly beneficial for the NA samples (+132%) while Sika samples showed a more limited increment, equal to 22.4%. On the other hand, the stiffness of Dow samples decreased as the thickness of the stack was increased.

Table 4-47. Stiffness of the SPR Cross Tension joints.

Stiffness at initial load application [N/mm]									
Cross Tension SPR	NA		SIKA		DOW		Sika vs NA	Dow vs NA	Dow vs Sika
	mean	st.dev	mean	st.dev	mean	st.dev			
1.3 mm	42	43%	167	39%	272	8%	301%	551%	-18%
1.75 mm	97	20%	205	34%	174	26%	112%	80%	14%
	132%		22.4%		-36.0%				

4.3.2.5 Failure mode - Cross Tension SPR

All the 1.3 mm SPR samples, both NA and hybrid, experienced rivet tail pull out failure mode. The difference with the observations made with coach joints, where rivet head pull out was noticed in same of the thinner stack joints (section 4.1.2.5) can be ascribed to the loading mode, as described in Section 4.3.1.6.

Four out of five 1.75 mm SPR NA samples failed in head pull-out mode, indicating that the strength of the interlock has overcome the tearing strength of the material. On the other hand only one hybrid 1.75 mm SPR joint failed in head pull-out mode, while all the other failed in tail pull-out mode. This indicates that the presence of adhesive has a negative impact on the strength of the interlock.

Similarly to the RSW hybrid samples, the SPR hybrid samples show adhesive failure mode of the adhesive layer (Figure 4-67 (c)). No clear evidence of any possible difference in the adhesive yielding load between RSW and SPR joints was then found by means of the failure mode analysis.

Figure 4-67. Failure mode Cross Tension SPR joints. (a) Rivet tail pulled out from the bottom sheet. (b) Rivet head pulled out the top sheet; rivet still stuck in the bottom sheet. (c) Adhesive failure of the adhesive layer.

4.3.3 RSW vs. SPR

4.3.3.1 Load vs. Displacement - RSW vs. SPR

The load and displacement measured with the RSW and SPR cross tension joints are compared in Table 4-48 -Table 4-51.

- The load at the adhesive yielding peak was higher for the RSW samples, especially when the thicker stack is considered. This same phenomenon was noticed with the coach joints and it was explained by analyzing the adhesive failure mode. As shown in Section 4.3.2.5 the load difference noticed with the cross tension geometry cannot be successfully explained with the failure mode analysis.
- The elongation at the first peak of the SPR + Sika and RSW + Sika sample was comparable for both the stack thicknesses. On the other hand SPR + Dow samples showed an elongation 24.7% lower than RSW + Dow with the thinner stack and 81.4% greater with the thicker stack.
- The load at the second peak is always higher for the riveted joints and with the exception of Sika samples, the gap between SPR and RSW joints increases with the thickness. The opposite trend noticed with Sika samples is due to the low load at the weld nugget yielding peak registered with the thin stack samples; the load difference with the corresponding SPR joints is thus considerably large (221%).
- The SPR joints experience a larger deflection at failure than the corresponding RSW joints in all the analyzed condition. As noticed for the load, the difference in deflection between riveted and welded joints increased with the increase of the stack thickness, with the exception of Sika samples.

Table 4-48. Load at the indicated peaks; RSW 1.3 mm vs. SPR 1.3 mm.

Load [N]							
1.3mm Cross Tension RSW vs SPR		NA		SIKA		DOW	
		mean	st.dev	mean	st.dev	mean	st.dev
1st peak	RSW	-	-	824	19.1%	904	16.7%
	SPR	-	-	714	10.8%	846	30.3%
				-13.3%		-6.5%	
2nd peak	RSW	1523	32.8%	688	55.9%	1358	60.8%
	SPR	2654	11.2%	2207	5.6%	2028	7.4%
		74.2%		221%		49.3%	

Table 4-49. Load at the indicated peaks; RSW 1.75 mm vs. SPR 1.75 mm.

Load [N]							
Weld vs. SPR 1.75 mm		NA		SIKA		DOW	
		mean	st.dev	mean	st.dev	mean	st.dev
1st peak	RSW	-	-	1368	10.8%	1241	37.8%
	SPR	-	-	905	32.0%	990	23.0%
				-33.8%		-20.2%	
2nd peak	RSW	2151	35.4%	2838	29.1%	2244	25.4%
	SPR	5194	5.0%	4996	3.2%	4762	5.4%
		141%		76.0%		112%	

Table 4-50. Elongation at the indicated peaks; RSW 1.3 mm vs. SPR 1.3 mm.

Elongation [mm]							
1.3 mm Cross TensionRSW vs. SPR		NA		SIKA		DOW	
		mean	st.dev	mean	st.dev	mean	st.dev
1st peak	RSW	-	-	6.23	8.0%	5.62	14.3%
	SPR	-	-	6.45	39.2%	4.23	11.7%
				3.5%		-24.7%	
2nd peak	RSW	47.5	11.4%	33.1	24.2%	39.6	20.2%
	SPR	55.1	8.1%	50.8	4.6%	45.5	9.7%
		16.1%		53.5%		14.8%	
failure	RSW	48.0	11.1%	34.1	25.6%	39.9	20.7%
	SPR	55.5	8.1%	50.2	5.8%	46.0	9.7%
		15.8%		47.1%		15.1%	

Table 4-51. Elongation at the indicated peaks; RSW 1.75 mm vs. SPR 1.75 mm.

Elongation [mm]							
1.75 mm Cross Tension RSW vsv SPR		NA		SIKA		DOW	
		mean	st.dev	mean	st.dev	mean	st.dev
1st peak	Weld	-	-	8.24	20.2%	4.596	35.2%
	SPR	-	-	7.85	33.4%	8.3375	15.9%
				-4.7%		81.4%	
2nd peak	Weld	37.2	24.2%	46.6	13.1%	40.1	9.2%
	SPR	59.7	3.2%	58.7	2.6%	55.6	6.4%
		60.7%		25.8%		38.7%	
failure	Weld	38.1	24.2%	48.3	14.0%	41.1	8.4%
	SPR	60.3	3.4%	60.2	3.0%	56.7	6.6%
		58.1%		24.8%		38.0%	

4.3.3.2 Energy - RSW vs. SPR

The results of the calculation of the energy absorbed by the riveted and welded joints are reported and compared Table 4-52 and Table 4-53. As highlighted for the other geometries,

the results obtained for the energy calculation are a direct consequence of the trends observed for load and elongation. Summarizing:

- The energy absorbed at the adhesive yielding peak is higher for the RSW joints, with the only exception of 1.3 mm Sika samples.
- The energy absorbed at rivet yielding and final failure is significantly higher for the riveted joints, and this difference between SPR and RSW increases with the thickness. In particular, the 1.75 SPR NA samples absorbed more than double the energy than that absorbed by the welded joints. Again, the only exception is represented by the Sika samples, which showed a greater difference in energy with the RSW joints considering the thinner stack.

Table 4-52. Energy at the indicated peaks, RSW 1.3 mm vs. SPR 1.3 mm.

Energy [J]							
1.3 mm Cross Tension RSW vs. SPR		NA		SIKA		DOW	
		mean	st.dev	mean	st.dev	mean	st.dev
1st peak	Weld			3.6	35%	5.5	42%
	SPR			4.3	27%	3.8	54%
				19.6%		-30.6%	
2nd peak	Weld	25.2	12%	24.4	13%	35.8	44%
	SPR	45.2	7%	44.7	5%	43.0	14%
		79.3%		82.9%		20.2%	
failure	Weld	26.0	13%	24.5	33%	36.3	43%
	SPR	46.2	7%	45.6	5%	44.1	14%
		78.0%		86.3%		21.5%	

Table 4-53. Energy at the indicated peaks, RSW 1.75 mm vs. SPR 1.75 mm.

Energy [J]							
1.75 mm Cross Tension RSW vs. SPR		NA		SIKA		DOW	
		mean	st.dev	mean	st.dev	mean	st.dev
1st peak	Weld			6.4	19%	6.1	44%
	SPR			5.5	25%	5.7	26%
				-15.4%		-6.3%	
2nd peak	Weld	41.9	36%	69.2	24%	51.2	26%
	SPR	99.3	5%	96.1	6%	94.7	5%
		137%		38.7%		85.1%	
failure	Weld	44.0	37%	72.0	25%	53.1	25%
	SPR	102	5%	101	7%	99.5	5%
		132%		40.2%		87.5%	

4.3.3.3 Stiffness - RSW vs. SPR

Table 4-54Table 4-55 report and compare the stiffness of the cross tension joints as calculated from the initial loading slope. Only Dow samples showed a significant difference in stiffness between the SPR and RSW joints, with the latter proving to be 90.7 % stiffer.

In all the other analyzed cases the differences between the average stiffnesses were lower than the variability of the results so no definitive conclusion can be drawn.

Table 4-54. Stiffness of the Cross Tension joints; 1.3 mm RSW vs. 1.3 mm SPR.

Stiffness at initial load application [N/mm]						
Cross Tension RSW vs. SPR 1.3 mm	NA		SIKA		DOW	
	mean	st.dev	mean	st.dev	mean	st.dev
RSW	29	23%	212	23%	246	20%
SPR	42	43%	167	39%	272	8%
	30.6%		-26.7%		9.5%	

Table 4-55. Stiffness of the Cross Tension joints; 1.75 mm RSW vs. 1.75 mm SPR.

Stiffness at initial load application [N/mm]						
Cross Tension RSW vs. SPR 1.75 mm	NA		SIKA		DOW	
	mean	st.dev	mean	st.dev	mean	st.dev
RSW	107	15%	273	20%	332	10%
SPR	97	20%	205	34%	174	26%
	-11.0%		-33.2%		-90.7%	

4.3.4 Deviation from ideal condition

One of the factors that contributed to the remarkable variability of the results is the non-ideality of the samples preparation and of the testing conditions.

The fixture used for riveting and welding of the cross tension samples has been described in Section 3.3. The difference in diameter between the holes in the coupons and the pins of the fixture allowed some relative movement between the coupons and the grip fixtures. As a consequence, the weld nuggets (or the rivets) were often offset from the center of the coupon (see Figure 4-68 (a)). This caused secondary bending moments to arise and to influence the performance of the joint.

The adhesive layer was applied manually to the coupons; the amount of glue applied on the samples is in some cases visibly different (i.e the amount of glue applied to the samples in Figure 4-68 (b) is considerably higher than in Figure 4-68 (c)).

As far the testing of the samples is concerned, some issues were caused by the clamping of the sheets to the testing machine plates. Figure 4-69 (a) shows the fixture used to conduct the tensile tests[13]. In some cases the coupons moved relatively to the fixture during the test, as proved by the scratches left on the surface of the blank by the washers (Figure 4-69 (b)). The component of the force transverse to the loading direction mentioned is Section 4.3.1.6 is highly influenced by this slippage and can have a significant impact on the final strength of the joint.

(a) (b) (c)

Figure 4-68. (a) Offset position of the weld nugget; (b) and (c) different quantities of glue applied to the samples.

(a) (b)

Figure 4-69. (a) fixture used for the tensile tests of the cross tension joints. (b) Scratches left by the washer on the surface of the blank because of the inward movement of the blank.

[13] Figure 4-69 (a) shows the set up used for the tests synchronized with the video camera and not the one used for the testing of the samples which results are reported in this Chapter.

Chapter 5

Stress Analysis

The comparison of the experimental results shown in the previous section highlights the impact of the joint geometry on the analyzed parameters (e.g. the maximum energy absorbed by SPR cross tension joints is larger than the energy absorbed by the SPR coach joints by more than a factor of two). The sheet thickness was shown to also have a significant role.

The calculation of the stress at failure of the various joining elements (weld nuggets, rivets and adhesive layer) enables the normalization of the results obtained and investigates if a unique failure criterion exists for all the RSW, SPR and adhesively bonded joints. In Section 2.5.4 has been already introduced the importance of a methodology for assessing the properties of a structural joint and in particular Figure 2-44 classifies the definition of a failure criterion as one of the four fundamental steps in the process of design of a structural joint.

5.1 RSW Joints

The calculation of the failure stress at the weld nugget of RSW joints will be performed, by using the formulae proposed by Zhang [47]. As reported in Section 2.5.4.2, Zhang approximated the weld nugget as a circular rigid inclusion and found the following analytical expressions to approximate the nominal stress.

$$\sigma_{lj} = \frac{4F}{\pi dt} \tag{5.1}$$

$$\tau_{lj} = \frac{F}{\pi dt} \tag{5.2}$$

$$\sigma_{ct} = \frac{3cF}{4\pi dt^2} \tag{5.3}$$

$$\sigma_{cp} = \frac{6eF}{\pi dt^2} \tag{5.4}$$

where d is the nugget diameter, t the sheet thickness, F the tensile-shear force, T the cross - tension force, c the distance between the two applied forces in cross-tension loading, P the coach-peel load, e is the load eccentricity in coach peel (Figure 5-1). σ_{lj}, σ_{ct}, and σ_{cp} are the maximum radial normal stress at the weld nugget respectively in lap joint, cross

tension and coach joint and τ_{lj} is the circumferential shear stress at the weld nugget in lap joint.

In a first trial, the nugget thickness has been used in the calculations instead of the sheet thickness in an attempt to account for the indentation left by the welding gun electrodes in the aluminum coupons. However the obtained stresses reached values considerably higher than the stress at fracture of the parent material; this methodology was thus abandoned and the sheet thickness was used.

Figure 5-1. Geometrical quantities considered for the stress calculation at the weld nugget in lap joints (a), cross-tension(b) and coach joints(c) [47].

As the stresses computed with Equations 5.1 – 5.4 are elastic stresses and are often greater than the aluminum yield stress, the "Neuber method" was applied to correct the results and account for the plasticization of the materials [53].

This method equates the "elastic energy", calculated as the elastic stress S times the elastic strain e to the "plastic energy" obtained as the product of the plastic stress σ and plastic strain ε (Figure 5-2).

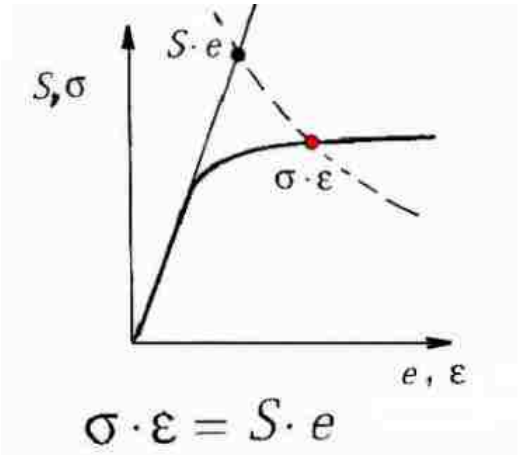

Figure 5-2. Neuber method for plasticity correction [53].

The calculation of the stress in the RSW joints under analysis in this thesis can be summarized with the following steps:

- Calculation of the elastic stresses at the weld nugget using Equations 5.1 – 5.4. The weld nugget yielding loads were used for the calculation.
- Knowing the slope of the elastic portion of the stress-strain curve, the elastic strain was calculated. The elastic energy was then found as the product of elastic stress and elastic strain.
- By using the Neuber method the plastic stress and strain have been calculated.

The obtained results have been plotted on the true stress-true strain curve of AA5182-O; in particular, in Figure 5-3, Figure 5-4 and Figure 5-5 each joints geometry average Neuber corrected stress-strain have been plotted. All the results have been then superimposed in Figure 5-6.

Figure 5-3 shows the results obtained with the RSW coach joints. The calculated stresses are all concentrated between 199MPa and 231MPa, for both the stack thicknesses. In a

similar manner, the stresses at failure of the lap joints are comparable for both the thicknesses (Figure 5-4). Figure 5-6 indicates that the obtained results are also comparable between the two geometries. A similar failure criterion seems then to exist for the coach joint and the lap joint geometry. In particular, the critical stress is slightly higher than 200MPa, about 70% of the true ultimate tensile stress of the base material σ_f (equal to 340MPa[14]).

The cross tension joints showed a slightly different behavior. Significant differences exist between the calculated stresses at failure of the cross-tension joints, especially with the thinner stack. In this regard it must be recalled that 1.3 mm RSW + Sika samples showed a significantly low value of load at nugget yielding because of the loading asymmetries caused by the one-sided failure of the adhesive layer. Interestingly, the stress at failure of this batch of samples is quite comparable to the results obtained with the coach joint geometry, and lower than the other stresses calculated for the cross tension samples. The thicker stack was less influenced by the loading asymmetries and the stresses calculated for the NA and hybrid samples are in closer agreement compared to the thinner stack. On average the calculated failure stresses were higher than coach and lap joint, and centered around 300 MPa, so close to 90% of the true ultimate tensile stress.

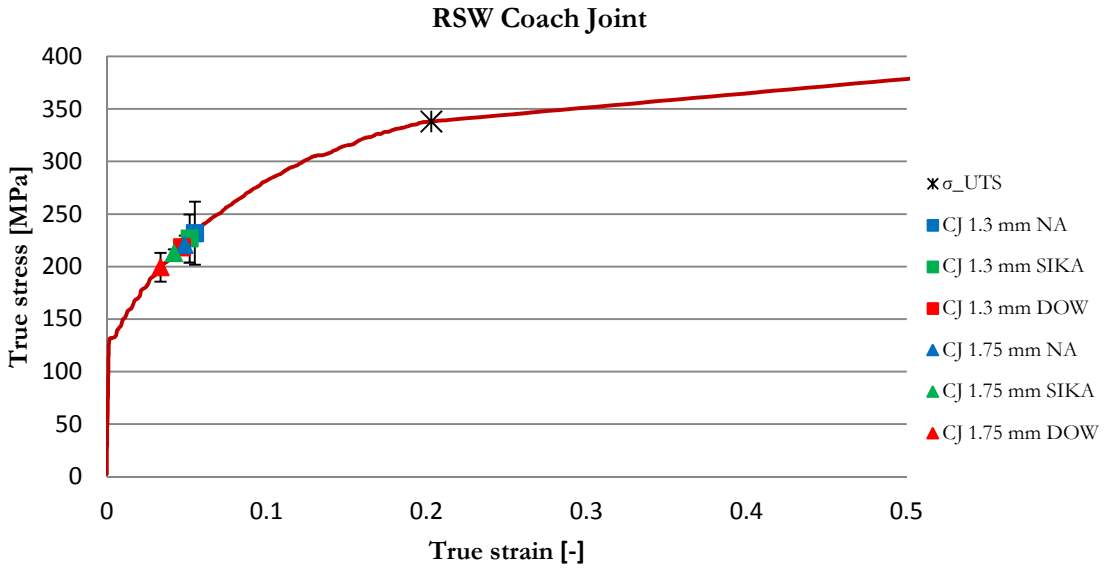

Figure 5-3. Stress at nugget yielding plotted on true stress-true strain tensile curve of base material; RSW Coach joints.

[14] Calculated from the engineering ultimate tensile stress reported in Table 3-3

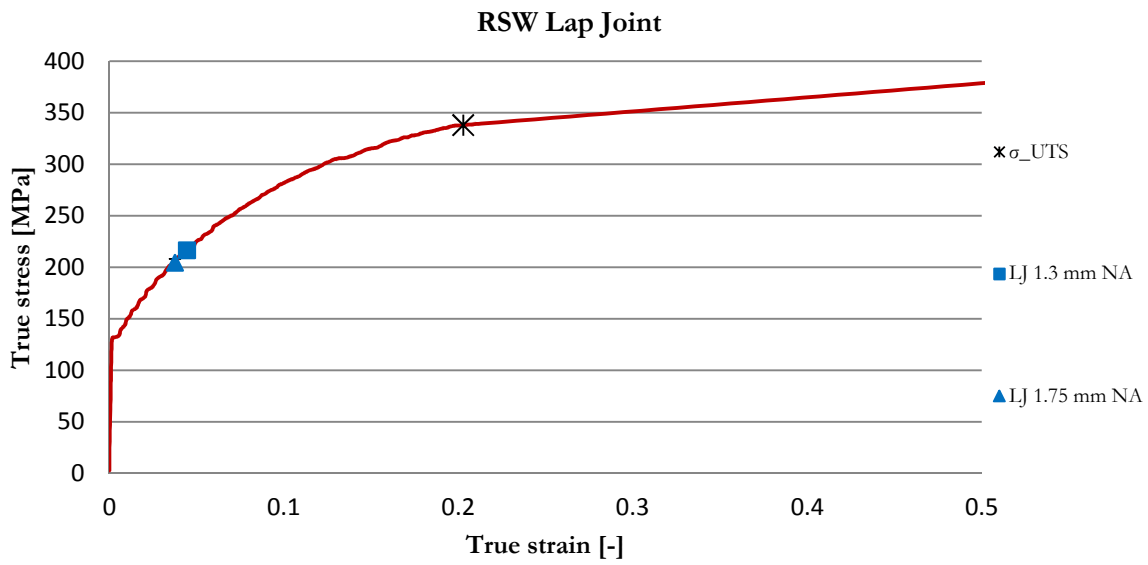

Figure 5-4. Stress at nugget yielding plotted on true stress-true strain tensile curve of base material; RSW Lap Joints.

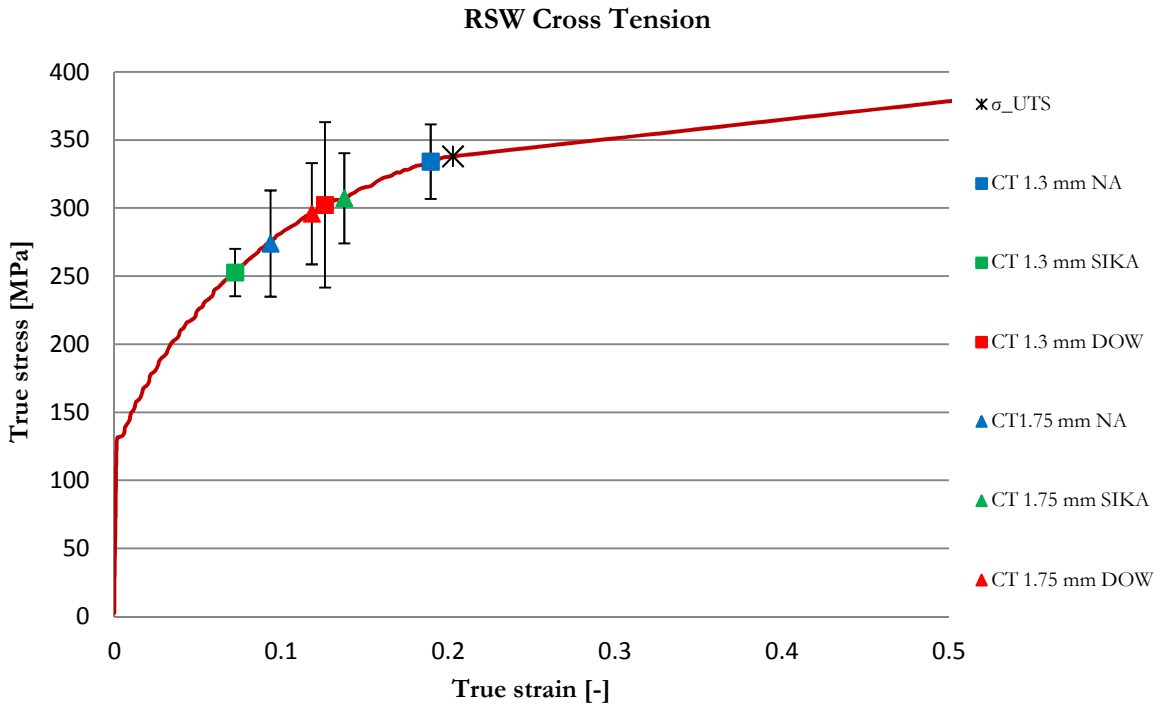

Figure 5-5. Stress at nugget yielding plotted on true stress-true strain tensile curve of base material; RSW Cross Tension Joints.

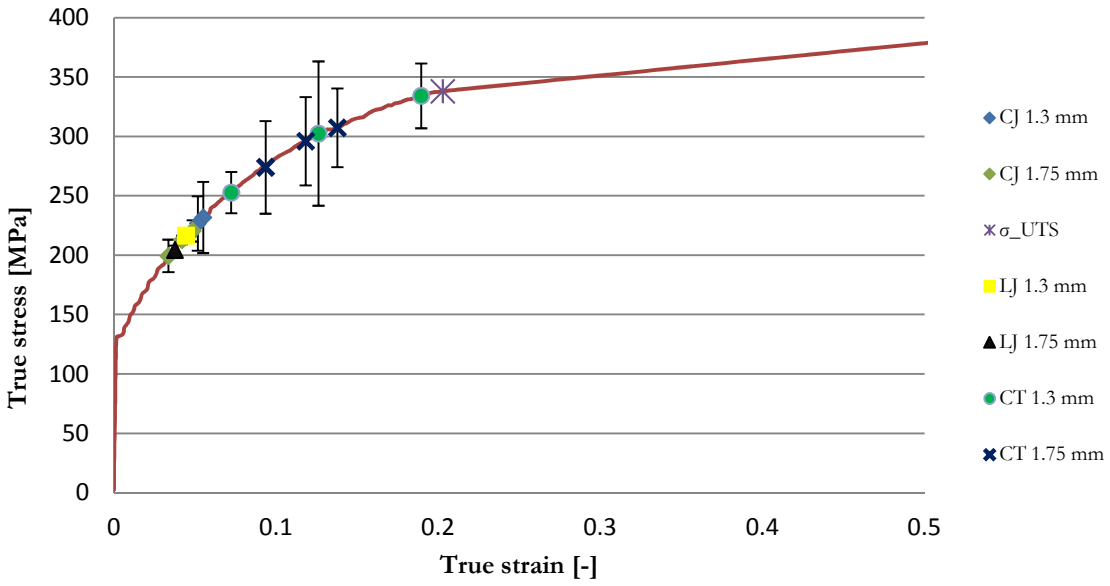

Figure 5-6. Stress at nugget yielding plotted on true stress-true strain tensile curve of base material; RSW Joints, superimposition of the obtained results.

5.2 SPR Joints

No analytical formula for calculating the stress at the rivet of an SPR joint has been found in the literature. A model is proposed and evaluated here. The cross tension joint will be analyzed first, followed by the coach and the lap joint.

Differently from a weld nugget, a self-piercing rivet is a separate entity from the aluminum sheet; the load between the sheets and the rivet thus cannot be transmitted in tension or in shear along the lateral surface of the rivet, but rather just in compression, due to the mechanical interference between the aluminum sheets and the rivet legs and head.

The SPR can be represented schematically as a "pi" as pictured in Figure 5-7

When the joint is loaded in cross tension mode, the bottom sheet will push on the legs of the "pi" while the top sheet will push on the head of rivet (Figure 5-8). The square element of parent material represented in Figure 5-8 will experience both compressive stress and shear stress due respectively to the force distributed over the ring area formed by the rivet foot and to the shearing reaction force caused by the rivet foot tip.

The normal compressive stress σ_r $[MPa]$ and the shear stress $\tau_r[MPa]$ can thus be calculated as

(5.5)

(5.6)

where is the load at the rivet yielding peak (values reported in Chapter 4), and are the outer and inner radius of the ring formed by the rivet skirt (or the rivet head) is the sheet thickness and k is a corrective coefficient to account for variation of the effective load carrying area.

SPR joints fail in "rivet-tail pull out" mode or in "rivet head pull-out mode"; the diameters and thicknesses used in Equation 5.5 and 5.6 must be chosen according to the failure mode; the dimensions relative to the head of the rivet (labelled with sub index "h" in Figure 5-7) must be used when calculating the stress in joints that showed rivet head pull-out. Vice versa when the joint shows tail pull-out the dimensions relative to the rivet tail, labelled with sub index "t" in Figure 5-7, should be used. The utilized[15] values for the mentioned geometrical quantities are reported in Table 5-1.

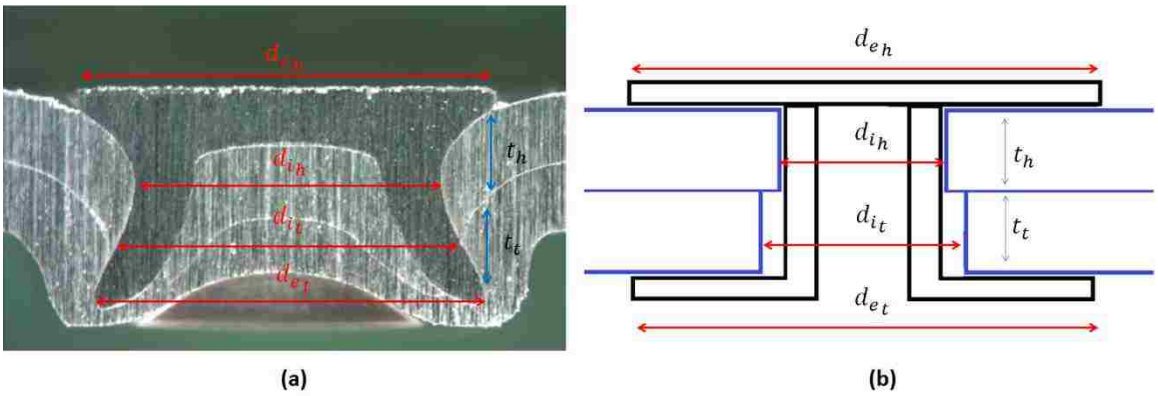

Figure 5-7. Schematic representation of a self-piercing rivet.

[15] i.e. (1.3 mm) was not reported since the 1.3 mm SPR joints failed in tail pull-out.

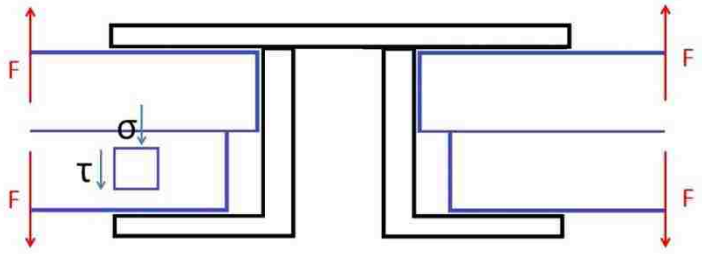

Figure 5-8. Cross tension loading of a self-pierce rivet.

Table 5-1: Rivet dimensions used in the joint stress calculation.

d_{e_t} **(1.3 mm)**	7.1 mm
d_{i_t} **(1.3 mm)**	6.4 mm
t_t **(1.3 mm)**	1.55 mm
d_{e_h} **(1.3 mm & 1.75 mm)**	7.5 mm
d_{e_t} **(1.75 mm)**	7.3 mm
t_t **(1.75 mm)**	2.4 mm
t_h **(1.75 mm)**	2.3 mm

The bending moment induced in cross tension loading condition causes the material surrounding the rivet to deform. Figure 5-9 (a) shows that the joint button has assumed an elliptical shape (whose longer axis is aligned with the y axis in figure). Four points have been highlighted in Figure 5-9; in correspondence of points 2 and 4, the deformation of the joint button can significantly reduce the mechanical interference between the rivet skirt or head and the aluminum sheets; consequently the load carrying area is reduced too. Additional proof of this phenomenon comes from the presence of shearing lips only at points 1 and 3, while at points 2 and 4 no evident sign of shearing is noticeable (Figure 5-9 (b)). To account for this reduction of the effective load carrying area the coefficient k in Equation 5.5 and 5.6 is set equal to two.

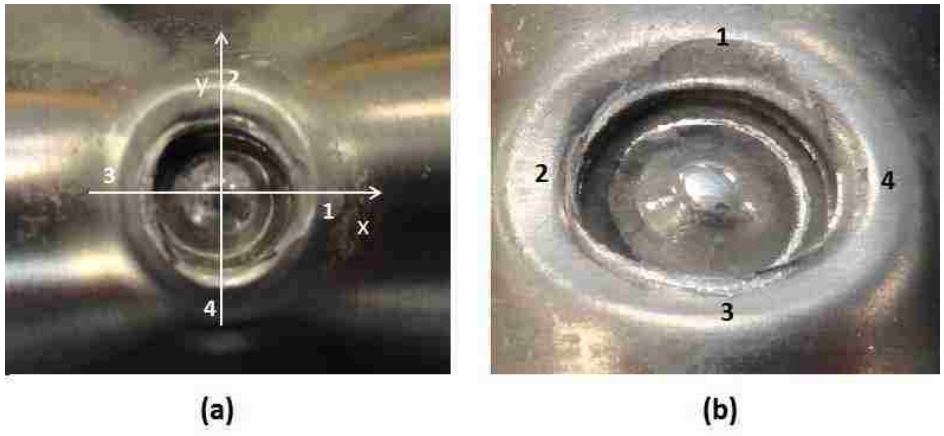

Figure 5-9. Deformation (a) and shearing (b) of the SPR joint button loaded in cross tension mode.

The results of the calculations showed that an extremely high value of compressive stress σ_r, in the gigapascal range, because of the considerably small area over which the load is distributed. The failure mode shown in Figure 5-9 (b) however showed clearly that the critical quantity determining the strength of the joints is the shear stress at points 1 and 3. The compressive stress σ_r will be then disregarded in the presented results. Summarizing, the following methodology will be followed for the stress calculation of cross tension joints:

- The shearing stress τ_r is calculated as from Equation 5.5, with $k = 2$
- The equivalent axial stress is calculated as [54]

$$\bar{\sigma} = \sqrt{3}\tau_r \tag{5.7}$$

The coach joint loading mode is, for the purpose of this analysis, simplified with the same scheme presented in Figure 5-7 and Figure 5-8 for the cross tension geometry. In a coach joint however the forces are considered applied only to one side of the overlap. This in turn translates into a reduction of the effective load carrying area, as ideally only half of the rivet is carrying load. Taking into account also the considerations made for the cross tension joint regarding the ovalization of the joint button a value of the coefficient k equal to 4 was used in Equation 5.5. Equation 5.7 was then used to calculate the equivalent axial stress.

In lap joints the external load is applied perpendicularly to the rivet legs, as shown in Figure 5-10. In particular, due to the two forces being non-coaxial, a force couple is generated. Two reaction forces have then to arise to counteract this couple and assure the rivet equilibrium. In particular, the force on the rivet tail R_t has been drawn in the middle of

the rivet skirt while the force on the head side R_h is at two third of the radius head from the center of the rivet. The following reasons lie behind this choice: as mentioned before, the ovalization of the joint button significantly reduces the mechanical interference of the rivet with the aluminum sheet at the tip of the rivet foot while it allows for the load to be held at the center of the rivet (points 1 and 3 in Figure 2-8). Figure 5-10 clearly shows two shearing lips in the central portion of the joint button while no shearing is visible on the left hand side of the button. Differently from Figure 5-9 the shearing lips are in this case tilted, clearly indicating that the rivet has rotated during the joint deformation around an axis perpendicular to the joint axis, as explained by Atzeni et al. [43].

The reacting force on the head side of the rivet is distributed on the right hand side of the rivet head and it linearly increases from the center to the tip of the rivet head, in a triangular manner (Figure 5-10 (a)); thus, the average force can be placed at two thirds of the distance between the rivet head center and tip.

Based on the failure mode shown in Figure 5-10 (b), a value of area correction coefficient n equal to 2 was chosen.

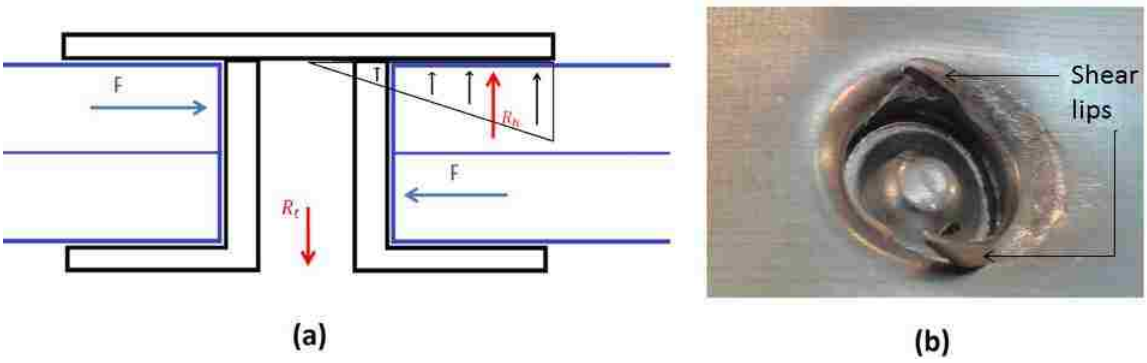

Figure 5-10. (a) schematic representation of a rivet under lap shear loading mode. (b) Detail of the failure mode of an SPR lap joint.

The results of the calculation are plotted in Figure 5-11, Figure 5-12, Figure 5-13 and Figure 5-14.

Analyzing the results it can be concluded that:

- The stress predicted by the proposed model is comparable for all the joint geometries when considering the same stack thickness; in particular all the 1.3 mm SPR joints showed a stress at failure on average around 250 MPa while for the thicker stack the stress at failure was generally higher, close to 300MPa for

lap and coach joints and in between 300MPa and 350 MPa for cross tension joints.

- The highlighted differences in the results obtained with the two stack thicknesses seems to suggest that the model is not able to fully account for the impact of the increase in stack thickness.
- The geometrical quantities reported in Table 5-1 were measured from the cross section of a 1.3 mm SPR NA and a 1.75 mm SPR NA samples. Possible variations induced by the presence of the adhesive have not been taken into account; this could be the reason for the differences in the stress predicted between the NA and the hybrid samples (often higher for the NA samples).

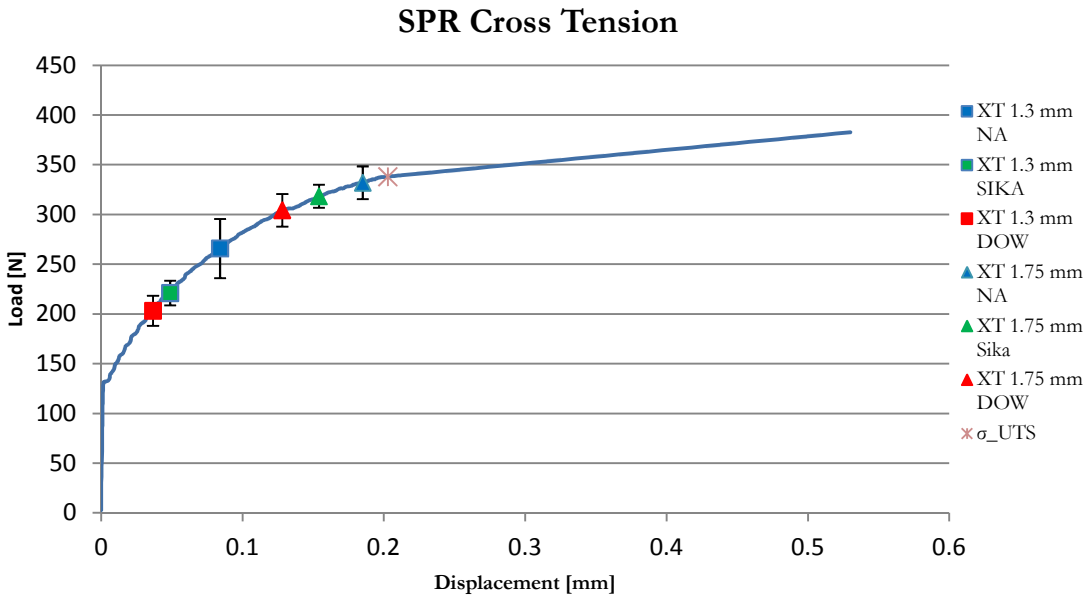

Figure 5-11. Stress at rivet yielding plotted on true stress-true strain tensile curve of base material; SPR cross tension.

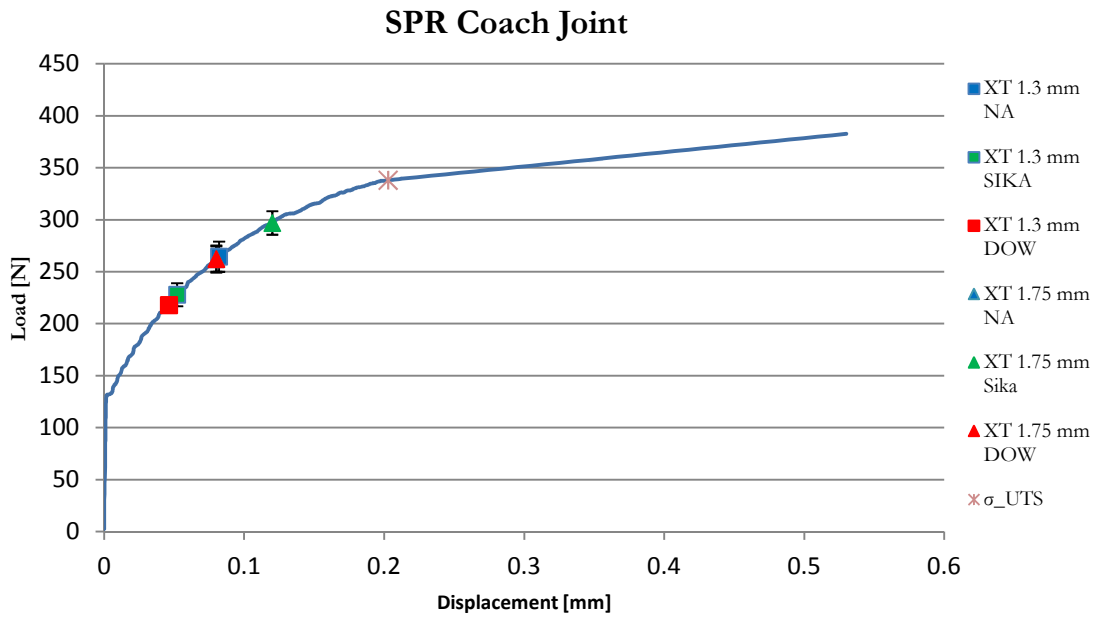

Figure 5-12. Stress at rivet yielding plotted on true stress-true strain tensile curve of base material; SPR coach joint.

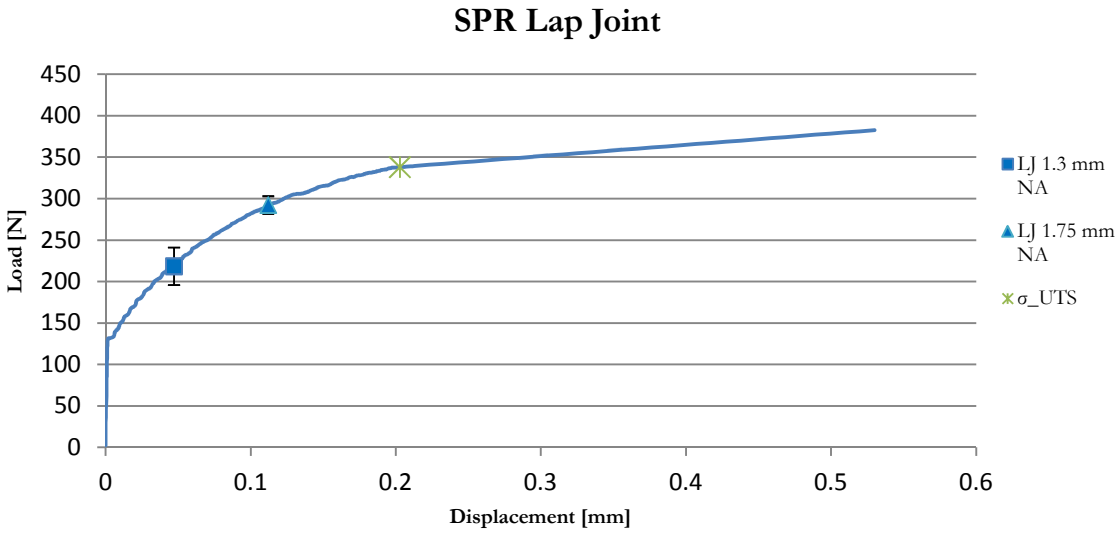

Figure 5-13. Stress at rivet yielding plotted on true stress-true strain tensile curve of base material; SPR lap joint.

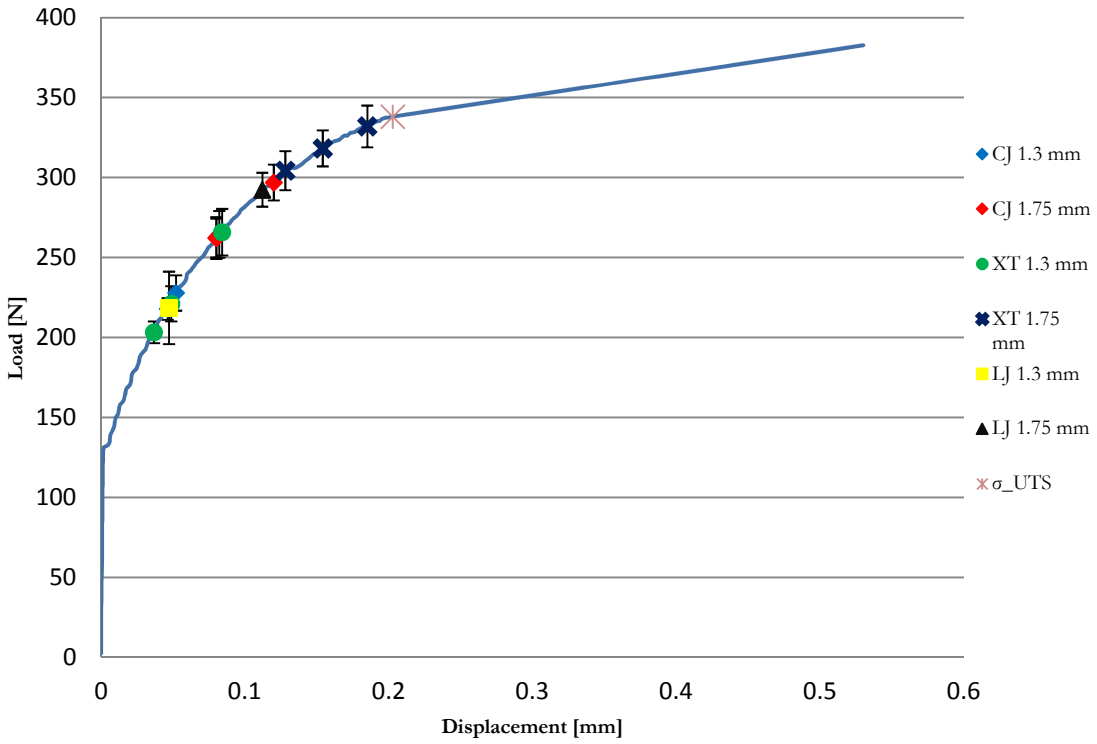

Figure 5-14. Stress at rivet yielding plotted on true stress-true strain tensile curve of base material; SPR Joints, superposition of the obtained results.

5.3 Adhesively bonded joints

The calculation of the stresses in the adhesive layer will be performed using the model proposed by Bigwood and Crocombe [46], which has been already introduce in Section 2.5.4.1. The material properties and the geometrical dimensions of the joint used for the calculation are summarized in Table 5-2.

Table 5-2. Adhesive overlap data used for the calculation of the stresses in the adhesive layer[16].

Young modulus (aluminum)	69600 MPa
Young Modulus (adhesive)	1942 MPa
Poisson ratio (aluminum)	0.33
Thickness adhesive layer	0.5 mm
Overlap Length	25 mm
Overlap width	40 mm

[16] The same mechanical properties have been used for both the adhesives

Figure 5-15, Figure 5-16 and Figure 5-17 represent the distribution of the shearing and peeling stress in the adhesive layer as function of the position on the overlap; in particular, the origin of the position axis corresponds to the edge of the overlap.

In all the analyzed cases the peak stress is registered at the edge of the overlap. In coach-peel loading mode the adhesive layer is subjected to peeling stress only. The stress drops dramatically and becomes negative within few millimeters of distance from the edge of the overlap. After rising to zero again, its value is maintained constant and equal to zero over the rest of the overlap. In lap shearing loading mode both the components of stress are non-zero and they assume very similar values at the edges of the overlap. The stress distribution in the adhesive layer of cross tension joints share similarities with both coach and lap joints; at the overlap edge both the stress components are different from zero and the peeling stress is about double compared to the shearing stress. In addition, the peeling stress shows a symmetric distribution with respect to the center of the overlap while the shearing stress assumes opposite values on the two sides of the overlap (Figure 5-17).

Goglio et al. [45] performed a similar study and obtained the same shape as in the mentioned Figures for the stress distribution. In addition, they varied the characteristic joint dimensions (overlap length, adherends and adhesive thickness) in order to create a wide combination of shearing and peeling stress. The obtained results suggest that the failure criterion, defined as the envelop enclosing the stresses at failure, assumes a rectangular shape.

The peak adhesive stresses for the hybrid RSW lap and coach joints investigated in this study are reported in Figure 5-18. Even though the combinations of shear and peel stress analyzed are not sufficient to infer the shape of the failure envelop, the peak stresses reported in Figure 5-18 could be enclosed inside a rectangular of 50 MPa in peel mode and 35 MPa in shear mode.

A similar analysis has been conducted for the rivet-bonded lap and coach joints and the results have been plotted in Figure 5-19. The peak stresses calculated for the lap joint are highly comparable to the one obtained with the weld-bonded lap joints. The coach joints showed a lower value of stress, which could be attributed to the failure mode of the hybrid SPR coach joints, as explained in Section 4.

The peak stresses in cross tension loading mode are significantly higher both compared to the results obtained with the other geometries and with the fracture stress of the adhesive

itself (about 40 MPa). As the stress at the edge of the overlap overcomes the yielding point of the adhesive, it redistributes on a wider area and thus allows for a load increase before final fracture. This phenomenon however cannot be taken into account with the proposed model thus the numerical results for the cross tension joints have not been plotted.

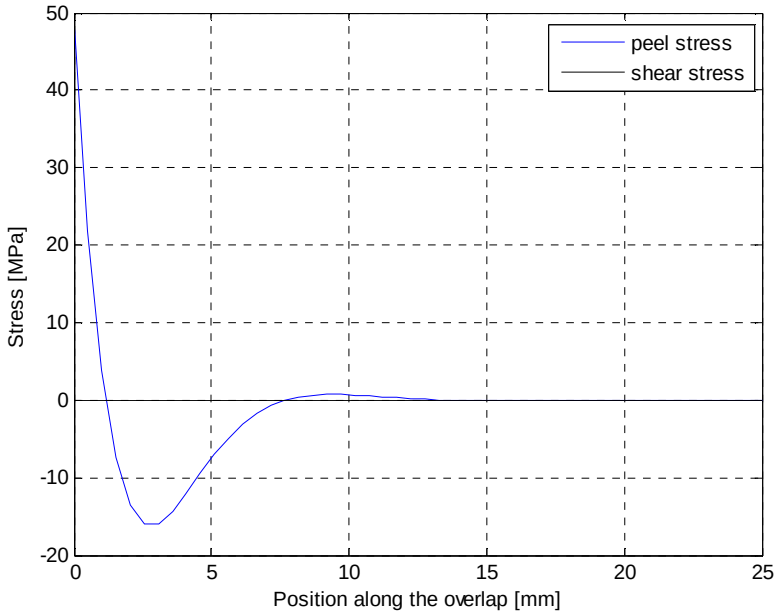

Figure 5-15. Peel and shear stress distribution in coach joint.

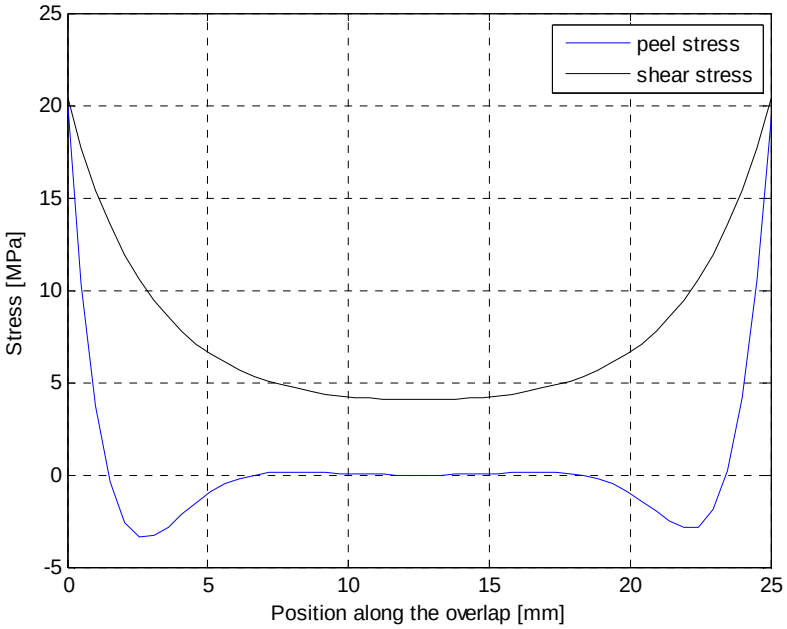

Figure 5-16. Peel and shear stress distribution in lap joint.

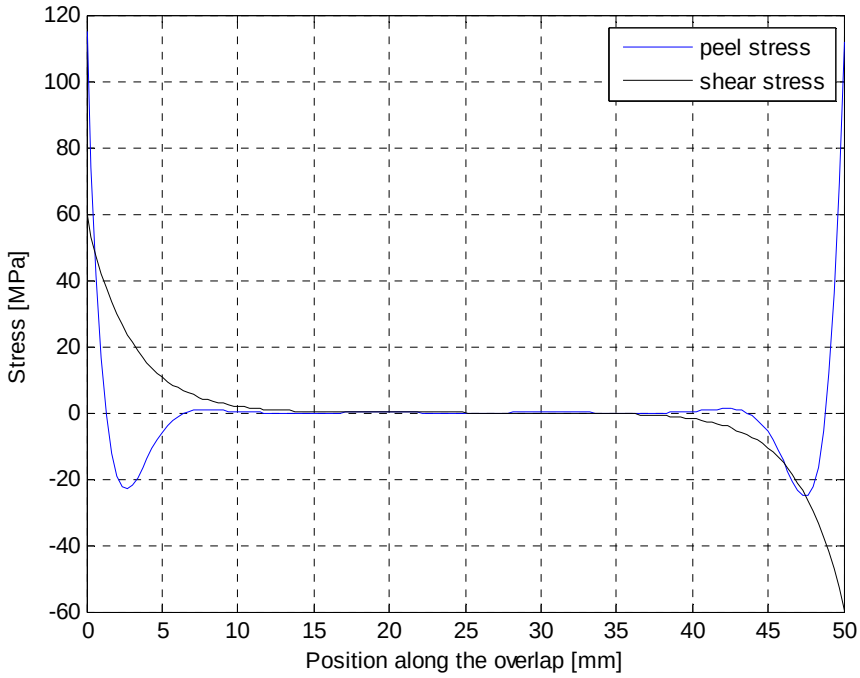

Figure 5-17. Peel and shear stress distribution in cross tension joint.

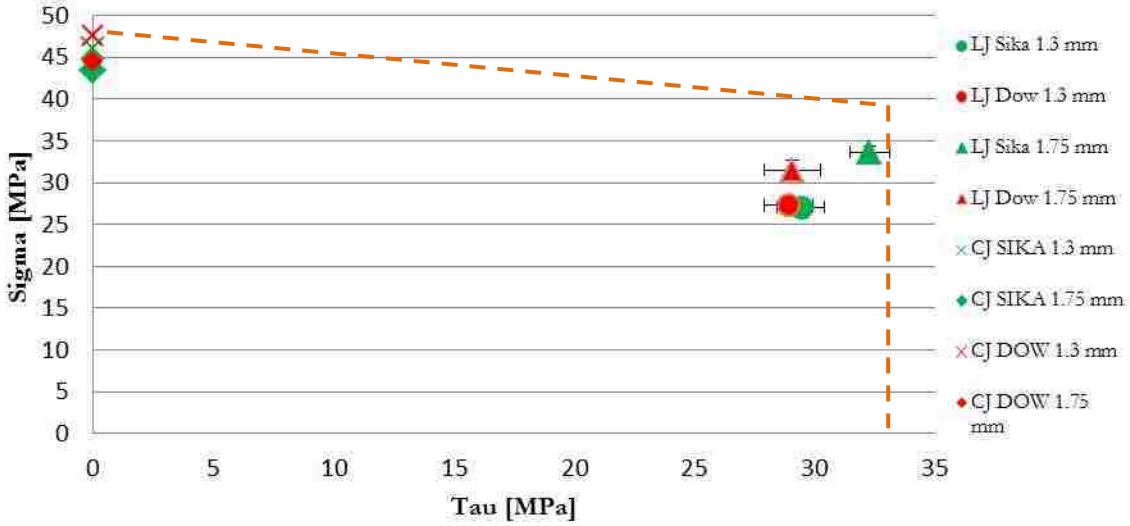

Figure 5-18. Peak stress of the adhesive layer in hybrid RSW lap and coach joints showing theoretical stress combination limit line.

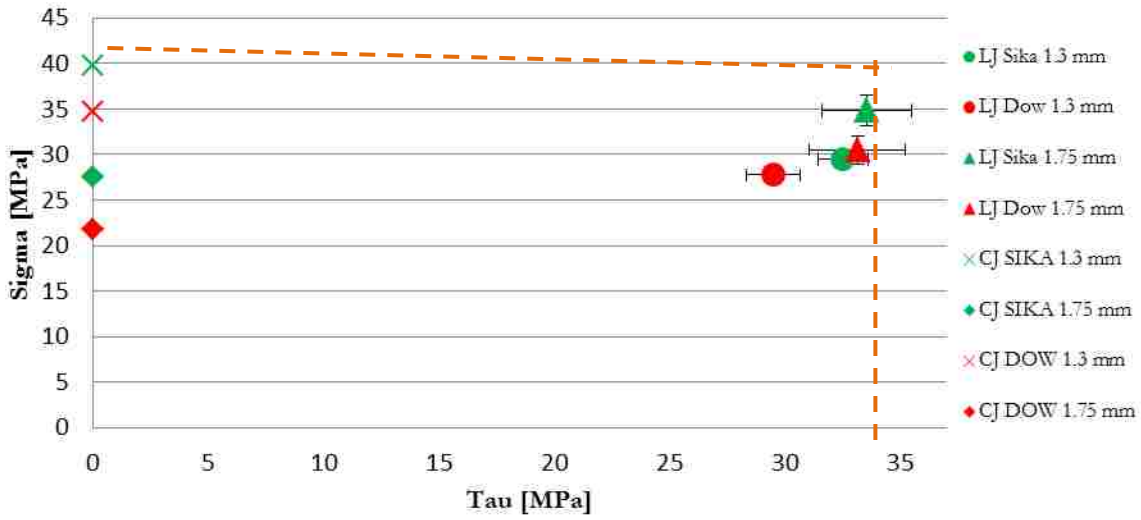

Figure 5-19. Peak stress of the adhesive layer in hybrid SPR lap and coach joints showing theoretical stress combination limit line.

5.4 Design rules for the studied joints

The results of the stress analysis can be summarized in a set of design rules for the structural joints studied. The design rules are grouped by joining method

5.4.1 Tentative design rules for RSW joints

The design criteria for the RSW joints can be summarized as follow

1. The nominal elastic critical stress can be calculated using the model proposed by Zhang [47] (Equations 5.1-5.4).

$$\sigma_{lj} = \frac{4F}{\pi dt} \tag{5.1}$$

$$\tau_{lj} = \frac{F}{\pi dt} \tag{5.2}$$

$$\sigma_{ct} = \frac{3cF}{4\pi dt^2} \tag{5.3}$$

$$\sigma_{cp} = \frac{6eF}{\pi dt^2} \tag{5.4}$$

2. Calculate the plasticity corrected stress σ_{RSW} using the Neuber method
3. The allowable stress in RSW joints then is

$$\sigma_{RSW} \leq 0.7\ \sigma_f \tag{5.8}$$

for lap and coach joint and

$$\sigma_{RSW} \leq 0.9\,\sigma_f \tag{5.9}$$

for cross-tension joints

4. The study of an appropriate safety factor has not been carried out in the present work. However, a higher safety factor is recommended with cross tension joints to account for the wider scatter of the obtained results.

5.4.2 Tentative design rules for SPR joints

The calculation of the stresses in SPR joints have been achieved by means of a new methodology, based on the schematic representation of a rivet as shown in Figure 5-7

1. From cross-sectioned sample measure the quantitiesd_{e_h}, d_{e_t}, t_h and t_t indicated in Figure 5-7.
2. Compute the shearing force F^* and the corrective coefficient n to account for the reduction in the effective load carrying area.
   (a) Lap shear:
      i. $F^* = R_t$ (see Figure 5-10)
      ii. n=2
   (b) Cross tension
      i. $F^* = F$ (tensile test load)
      ii. n=2
   (c) Coach joint
      i. $F^* = F$ (tensile test load)
      ii. n=4
3. Calculate the shear stress τ_r using Equation 5.6

$$\tau_r = \frac{F^*}{\pi n d_e t} \tag{5.6}$$

4. Calculate the equivalent axial stress $\bar{\sigma}$ using Equation 5.7

$$\bar{\sigma} = \sqrt{3}\tau_r \tag{5.7}$$

5. Depending on the thickness of the material the allowable SPR stress then in

$$\bar{\sigma} \leq 0.7\ \sigma_f \tag{5.8}$$

when t = 1.3 mm

$$\bar{\sigma} \leq 0.9\ \sigma_f \tag{5.8}$$

when t=1.75 mm

5.4.3 Tentative design rules for adhesively bonded joints

1. The peak elastic stresses in the adhesive layer are calculated using the method proposed by Bigwood and Crocombe [46] (Equations 2.7 and 2.8; see also Section 2.5.4.1).

$$\tau_{yx} = B_1 \cosh(K_6 x) + B_2 \sinh(K_6 x) + B_3 \tag{2.7}$$

$$\sigma_y = A_1 \cos(K_5 x)\cosh(K_5 x) + A_2 \cos(K_5 x)\sinh(K_5 x) + A_3 \sin(K_5 x)\cosh(K_5 x) + A_4 \sin(K_5 x)\sinh(K_5 x) \tag{2.8}$$

2. The allowable elastic peak stresses in the adhesive layer are:
    a. Lap joint and coach joints

$$\sigma_y \leq 50MPa$$

$$\tau_{yx} \leq 35\ MPa$$

No design rule can be inferred for the cross tension joints based on the obtained results; further studies are recommended.

5.4.4 Tentative design rules for hybrid joints

In Chapter 4 it has been illustrated that the hybrid joints show two clearly distinct peaks, corresponding to the yielding of the adhesive layer and of the nugget or the rivet. Thus, in the design of a hybrid joints the design rules proposed for the adhesively bonded and the RSW or SPR joints can be simply adopted simultaneously, to take into account of the two

joining method used. It is important though to keep into account of the failure sequence of the joining elements used. For example, if a hybrid joint has to be designed such that the stress does not cause the failure of any joining element, the failure stress in the adhesive layer becomes the crucial designing parameter, as the adhesive layer is the first joining element to yield in all the analyzed geometries.

Chapter 6

Impact of the adhesive layer on the RSW and SPR process

This chapter details the investigation into the impact of the adhesive layer on the RSW and SPR processes. For the RSW process, two parameters are considered: the porosity of the weld nugget, and the microhardness of the various areas of the weldment (parent material, HAZ and fused nugget).

The cross section of some riveted joints will be shown afterward and the influence of the adhesive layer will be analyzed.

6.1 Impact of the adhesive on the RSW joints

As mentioned in Chapters 2 and 4, the strength of a RSW joint is highly influenced by the quality of the weld nugget and the strength of the HAZ. These two characteristics are often assessed by studying the porosity of the weld nugget, and by measuring the variation in microhardness from the parent material to the HAZ and into the fused zone of the weld nugget [41] [42] [55].

In this thesis in particular, both analyses have been conducted to compare the RSW NA joints with the hybrid joints, and thereby to determine whether the presence of the adhesive layer has introduced any kind of modification in the welded area, i.e., increased weld nugget porosity or a different HAZ hardness.

6.1.1 Weld nugget porosity

For the analysis of the weld nugget porosity, nine samples (3 NA, 3 Sika and 3 Dow) were cross sectioned through the weld nugget and prepared metallographically. They were analyzed on an optical microscope using the image analysis software Image-Pro Plus.

A weld nugget cross section is shown in Figure 6-1(a). The sample shows both porosity and a crack through the lower central portion of the nugget. Similar cracks where often noticed in the other samples. Figure 6-1(b) shows a screenshot of Image-Pro Plus; the software is able to recognize the darker areas corresponding to the pores, highlighted in red, and allows for the calculation of the area fraction of the pores. In order to consider only the "macropores" and to avoid the erroneous inclusion in the calculation of second phase

particles and impurities, a filter was set to disregard all the recognized elements smaller than $50\mu m^2$.

The results are reported in Table 6-1. The results have been normalized with respect the area of the nugget. Sika samples showed the highest level of porosity and Dow samples the lowest; however, the difference between the measured values was less than 0.5%, thus proving that the welding process of the hybrid joints was accomplish effectively.

Table 6-1. Calculation of the porosity in the weld nugget.

	NA	SIKA	DOW
Normalized pores area	1.47%	1.92%	1.45%

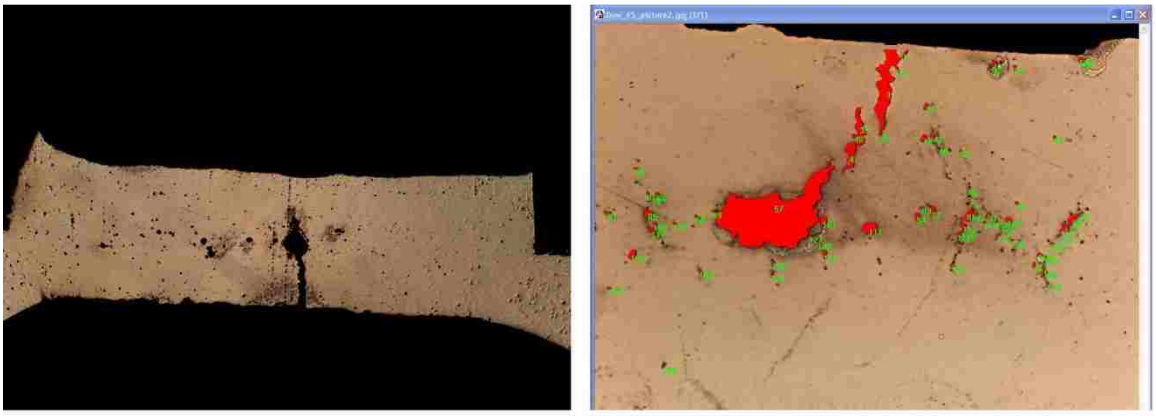

Figure 6-1. Analysis of the weld nugget porosity; (a) cross section of a weld nugget, (b) screenshot of the image analysis software.

6.1.2 Microhardness

One sample per condition (NA, Sika and Dow) was used for the Vickers microhardness test. A load of 25 grams was applied for ten seconds on the pyramidal shaped diamond indenter. The position of the indentations is shown in Figure 6-2 (a). For each point shown in the figure, three measurements were taken; the average and the standard deviation were calculated.

The microhardness can be calculated from the measurement of the diagonals of the pyramidal indentation as

$$HV = 1854\frac{L}{d^2} \tag{6.1}$$

where L is the load applied in gram-force (gf) and d is the arithmetical average of the length of the two diagonals measured in micrometers.

The results of the measurements of the three samples are superimposed in Figure 6-3. It can be concluded that

- No significant difference between the three analyzed samples is evident; thus the presence of the adhesive did not influence the microstructure of the aluminum.
- A slight increase in hardness is noticeable at the borders of the weld nugget that correspond to the heat affected zone. The hardness of the parent material and of the weld nugget is instead slightly lower. Based on these considerations the points in Figure 6-3 are divided into three main regions: parent material, HAZ, and weld nugget. Similar results have been obtained in [41].

It should be mentioned that microhardness measurements of welded joints is usually carried out on cross sections of non-tested samples. The deformation caused during the tensile test can induce strain hardening of the aluminum and can bias the results of the measurements; however no non-tested welded samples were available. The previously made considerations can be anyway considered as valid as all the compared cases has undergone the same deformation.

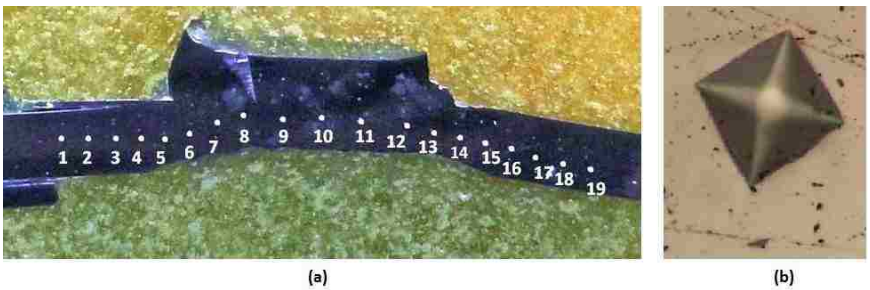

Figure 6-2. Microhardness measurement; (a) position of the indentations; (b) enlargement of an indentation.

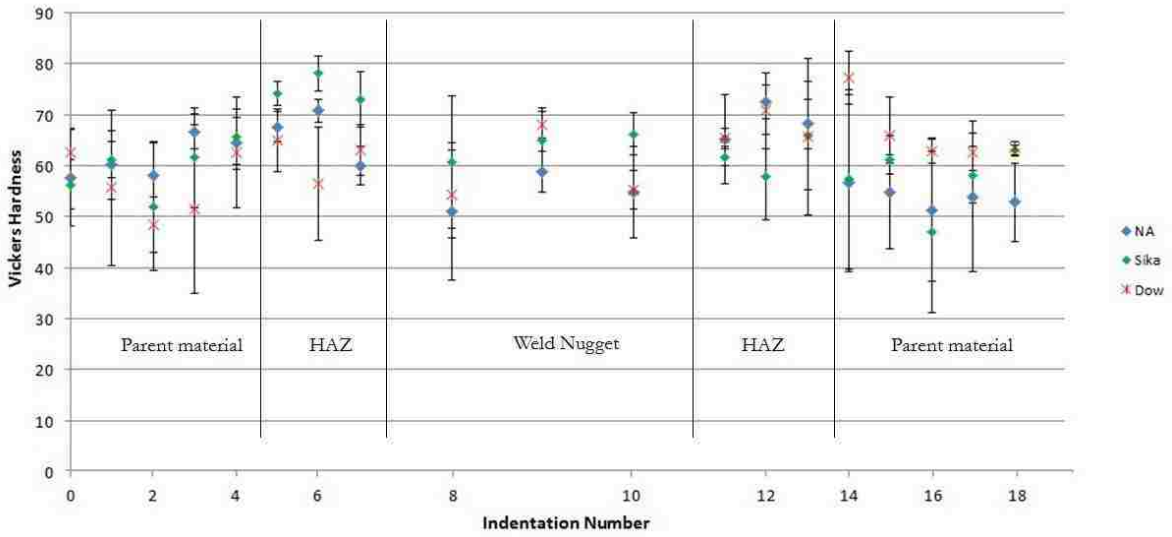

Figure 6-3. Results of the microhardness measurements.

6.2 Impact of the adhesive on the Self Pierce Riveting joints

Numerous times in Chapter 4 a lower rivet yielding load has been noticed for the hybrid joints compared to the NA joints. In particular, this difference in load is larger for the thinner joints. Figure 6-4 compares the cross section of 1.3 mm thick SPR NA and hybrid joints and reports the values for the interlock at the rivet legs. Both hybrid samples show a lower value of interlock, which means a lower anchoring strength of the rivet in the bottom sheet. This observation clearly explains the behavior noticed in Chapter 4.

Figure 6-5 compares the cross section of a 1.3 mm thick and a 1.75 mm thick SPR + Sika joints. The two joints differ not only in sheet thickness, but also in the rivet length and the die profile. In particular a DP09-175 die has been used for the thinner stack while a DZ09-025 die has been used for the thicker stack. The DP09-175 die is characterized by a higher pip while the DZ09-025 has a lower pip. As a consequence most the adhesive remains trapped between the rivet legs after the riveting of the 1.75 mm joints while a larger quantity of adhesive is pushed away from the rivet in the thinner stack. This different displacement of the adhesive layer from the area involved in the riveting process may explain the different impact of the presence of adhesive on the joint strength.

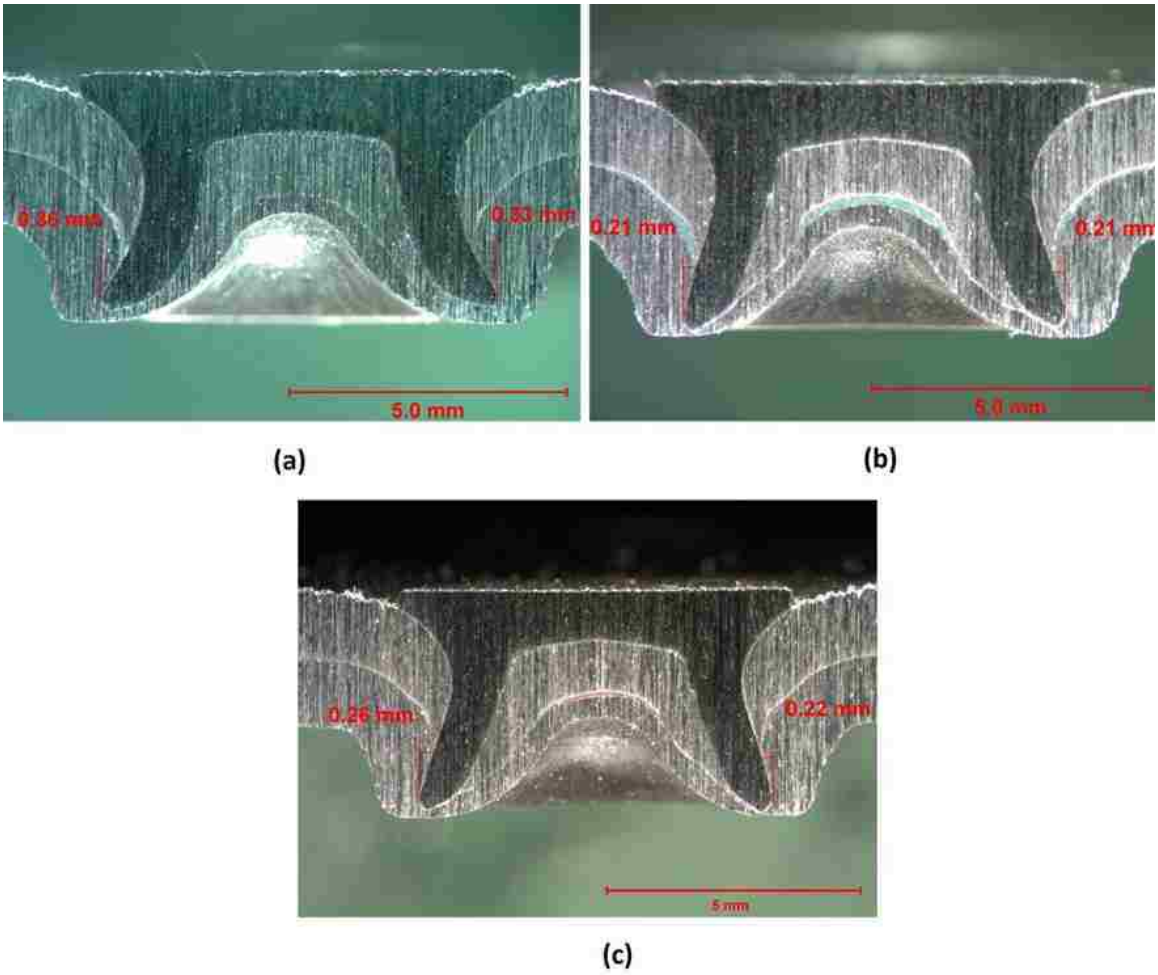

Figure 6-4. Riveted joint cross section; (a) 1.3 mm NA, (b) 1.3 mm Sika, (c) 1.3 mm Dow [Source: Henrob].

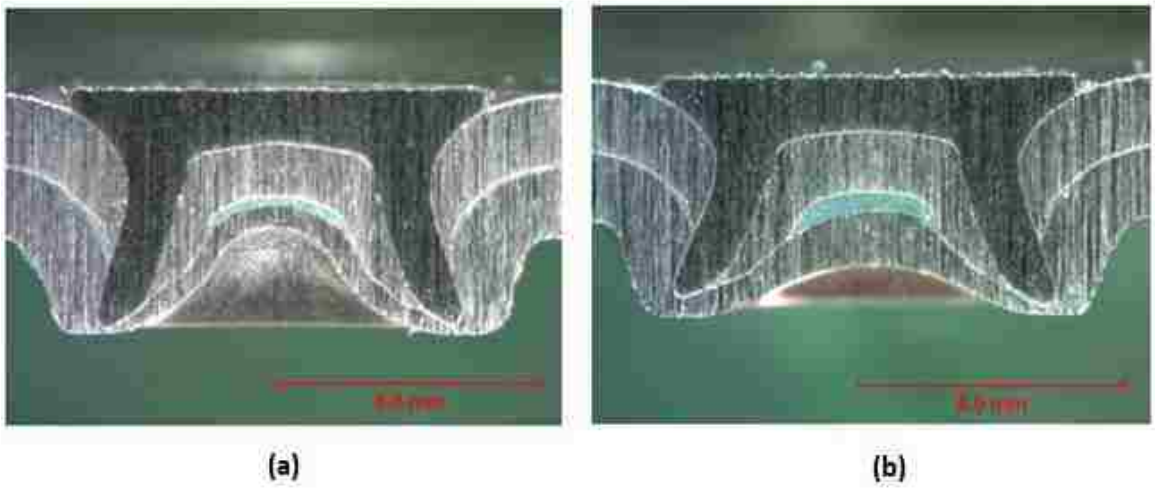

Figure 6-5. Riveted joint cross section; (a) Ø5 x 5 rivet with DP09-175 die (used for 1.3 mm stack), (b) Ø5 x 6 rivet with DZ09-025 die (used for 1.75 mm stack) [Source: Henrob].

Chapter 7

Summary and Recommendations

The tensile test results of aluminum alloy structural joints have been studied throughout this thesis. Resistance spot welded joints have been compared to self-piercing riveted joints. Additionally the effect of adding two types of adhesives, SIKAPOWER497 and DOW BETAMATE 1620US to both the welded and the riveted joints was investigated to determine the potential benefits of using hybrid joining techniques. The impact of the variation in thickness of the aluminum blanks was also analyzed too. The results of the tensile tests, in particular the load, were then used for the analytical calculation of the stress at failure of the joining elements. Finally, a metallographic analysis investigated the impact of the presence of the adhesive layer on the quality of the RSW and SPR joints.

7.1 Summary

7.1.1 Tensile test results.

The results of the tensile tests can be summarized as follow:

1. The superimposing of the load-displacement curves together with the video recording of the tests proved to be useful for the interpretation of the behavior of the joints during the tests.
2. The "peak-by-peak" approach, which segments the specimen fracture into specific events such as adhesive failure, nugget failure or SPR failure, allowed for the determination of the contribution of the different factors, i.e. joining method, sheet thickness to the final shape of the load-displacement curves.
3. A universal optimal joining solution appears not to exist, because the strength of each analyzed joining method was noted to be highly dependent on the joint geometry and on the blank thickness.
4. The addition of adhesive is highly beneficial in lap shearing loading mode, where the adhesive yielding peak showed the highest load; in coach peel and cross tension loading modes, the adhesive yielding load is comparable or lower than the nugget or rivet yielding load.

5. The presence of the adhesive often showed a negative impact on the nugget and rivet yielding load. In particular, the 1.3 mm rivet bonded hybrid joints exhibited lower loads compared to the 1.3 mm riveted-only joints.
6. Different from the failure load, both the energy absorbed by the joints during the deformation as well as the stiffness at initial loading of the joint generally increased when the adhesive was added. This increment was less evident for the rivet-bonded coach and cross tension joints.
7. Increasing the thickness of the aluminum blank from 1.3 mm to 1.75 mm had a positive impact on the performance of all of the analyzed joining methods. The greatest impact was noticed at the rivet yielding peak, for both load and energy; and the smallest impact was seen at the adhesive yielding peak.
8. The addition of adhesive generally had a higher impact on improving the performance of the thinner joints compared to the thicker joints.
9. The two adhesives showed comparable performance.
10. Rivet yielding load and energy were higher compared to the nugget yielding load and energy in coach and cross tension joints, especially for the 1.75 mm thickness. In lap joining mode, the nugget yielding load was higher than the rivet yielding load for the thinner stack while comparable loads were measured with the thicker stack. In all the analyzed cases, riveted joints were benefitted more by the increment in thickness.
11. In contrast with point 10, the adhesive yielding load in t-peel and cross tension loading mode was higher for the weld-bonded joints than the rivet-bonded joints. This gap in load was larger for the 1.75 mm joints. A similar trend was observed for the stiffness at initial loading of the joints.
12. The energy at final failure of the SPR and rivet-bonded coach and cross-tension joints was always larger than the energy absorbed by the corresponding RSW and weld-bonded joints. This observation is due to the higher deformation needed before rivet final failure.
13. The variability of the obtained results was in general considerably larger at the nugget yielding peak and at final failure of welded and weld-bonded joints compared to the rivet yielding peak and final failure of riveted and rivet-bonded

joints. The variability in the performance of the adhesive layer did not follow a clear trend.

14. A direct correlation between the weld nugget size and the load at nugget yielding has been shown. No significant difference in the nugget size of the hybrid joints compared to the welded-only joints was noticed. The nugget dimension compared to square root of the sheet thickness is larger for the thinner stack. It indicates that a larger nugget could have been used with the thicker stack, and as such explains the reduced benefit obtained by the increment in thickness of the aluminum sheet compared to the SPR joints.
15. The severe impact of the non-ideal preparation of the samples has been highlighted for the coach and the cross tension joints. Consistency in the test sample preparation is noted as a primary factor for future testing.
16. All the measured results of the tensile tests showed a significant variability, especially the RSW joints. A better consistency of the results was obtained with the SPR joints.

7.1.2 Optimal joining solution

As previously mentioned, a universal optimal joining solution does not exist; the results of the three joint geometries are thus analyzed separately.

- In lap-shearing loading mode, the adhesive layer is considerably stronger than the rivet or the weld nugget. The use of adhesively bonded or hybrid lap joints is therefore highly recommended. The results for the weld-bonded and the rivet-bonded joints are comparable.
- An optimal joining solution for the coach and cross tension joints depend on the chosen designing criteria.
    1) If maximum load is considered, SPR joints outperform RSW joints, in particular when the thicker stack is considered. Furthermore, the addition of adhesive is not recommended.
    2) If the energy at final failure is considered, rivet-bonded joints are to be used with 1.75 mm coach joints while riveted – only joints are recommended for 1.3 mm coach joints and for cross tension joints.

3) If the design criteria are based on the load at the adhesive yielding peak (first peak) or the stiffness at initial loading the RSW + adhesive is the most suitable solution.

7.1.3 Stress analysis

Three analytical methods have been used to calculate the stress at failure of the weld nugget, the rivet and the adhesive layer.

- The formulae proposed by Zhang [47] and the Neuber method for plasticity correction allowed the calculation of the stresses at failure of the weld nugget. Two failure criteria, one for lap and coach joints, and a second for cross tension joints seem to exist. The following tentative design rules have been proposed (detailed description in Section 5):

$$\sigma_{RSW\ lap\ \&\ coach\ joints} \leq 0.7\ \sigma_f \qquad \sigma_{RSW\ cross\ tension\ joints} \leq 0.9\ \sigma_f$$

- A new model for the calculation of the failure stress of the riveted joints has been proposed. The obtained results show a good agreement for all the joint geometries when considering a single stack thickness. However, the proposed model is not able to incorporate the impact of the stack thickness. The following tentative design rules have been proposed (detailed description in Section 5):

$$\bar{\sigma}_{1.3\ mm} \leq 0.7\ \sigma_f \qquad \bar{\sigma}_{1.75\ mm} \leq 0.9\ \sigma_f$$

- The model proposed by Bigwood and Crocombe [46] has been used for the analysis of the adhesive layer failure. A common failure criterion can be inferred for lap and coach joints, in accordance with Goglio et al. [45]. The following tentative design rules have been proposed (detailed description in Section 5):

$$\sigma_y \leq 50MPa \qquad \tau_{yx} \leq 35\ MPa$$

7.1.4 Impact of the adhesive layer on the RSW and SPR process

- No significant differences in weld porosity and microhardness between the welded-only joints and the hybrid joints have been noticed. The pre-heating cycle added for hybrid joints allowed for an effective process.
- The presence of the adhesive layer had a different impact on the 1.3 mm thick and the 1.75 mm thick SPR joints; namely, the former group is more negatively affected. This behavior has been attributed to the different die profile adopted for the riveting of the two stacks, which caused a different displacement of the adhesive layer during the riveting process.

7.2 Recommendations

This investigation into an optimal joining solution has been based on the tensile test behavior of selected joint geometries and configurations. The natural continuation of this research is then the analysis of the performance of the same joints in dynamic loading mode, i.e., the fatigue strength of the joints.

The detrimental impact of the non-ideal sample preparation and testing conditions have been mentioned throughout the analysis of the results, especially for the coach and cross-tension joints. The comparison of the results with those obtained by Sika for adhesively bonded coach joints prepared under nearly-ideal conditions gives a clear indication of the importance of the sample preparation process, especially when dealing with adhesive bonding. Further study aimed at defining an optimal sample preparation procedure and testing procedure is thus recommended.

Lastly, the stress analysis of the joints and the proposed design criteria are based on simple analytical calculations of the stresses, without consideration of the stress intensity factors at the weld nugget and the rivet, or of singularity points of the stress field in the adhesive layer at the edge of the overlap. Further investigation of the impact of these factors is thus recommended, particularly for the SPR joint, where the proposed model in fact failed to successfully assess the impact of the thickness of the aluminum blank. The possible utilization of a correlating coefficient between the geometrical dimensions of the riveted joints and the quantities to be used in the proposed model should be also studied. Validation of the proposed design rules by means of FEM analysis would be beneficial.

Bibliography

[1] "FEDERAL VEHICLE STANDARDS," Center for Climate and Energy Solutions, [Online]. Available: http://www.c2es.org/federal/executive/vehicle-standards#ldv_2012_to_2025. [Accessed 4 6 2014].

[2] E. A. Association, "Aluminum in cars," September 2008. [Online]. Available: http://www.alueurope.eu/pdf/Aluminium_in_cars_Sept2008.pdf. [Accessed 1 4 2014].

[3] A. Ambroziak and M. Korzeniowski, "Using resistance spot welding for joining alumiunum elements in automotive industry," 2010.

[4] R. W. J. Messler, Joining of Materials and structures, Burlington (MA) USA: Elsevier Inc., 2004.

[5] M. P. Groover, Fundamentals of modern manufacturing: materials, processes and systems, 4th ed., John Wiley & Sons, INC., 2010.

[6] "Joining - fusion welding," Aluminum Association European, 2002.

[7] "Developments toward high-volume resistance spot welding of aluminum automotive sheet component," International Automotive Research Center, Warwick Manufacturing Group, The University of Warwick.

[8] E. Crinon and J. T. Evans, "The effect of surface roughness, oxide film thickness and interfacial sliding on the electric contact resistance of aluminum," *Material Science and Engineering,* pp. 121-128, 1997.

[9] Welding Handbook – Welding Processes, Part 2, Ninth ed., vol. III, Miami, USA: American Welding Society, 2007.

[10] "Joining - Resistance Welding," European Aluminium Association, 2002.

[11] "WeldCor," WeldCor Supplies Inc., 2013. [Online]. Available: http://www.weldcor.ca/public/ckfinder/userfiles/files/FIGURE%20R-8.png. [Accessed 28 5 2014].

[12] Z. Li, C. Hao, J. Zhang and H. Zhang, "Effect of sheet surface conditions on electrode life in resistance welding aluminum," *Welding Journal,* pp. 81-89, 2007.

[13] X. He, I. Pearson and K. Young, "Self-pierce riveting for sheet materials: State of the art," *Journal of material processing technology,* pp. 27-36, 2008.

[14] R. Haque, J. H. Beynon and Y. Durandet, "Characterization of force-displacement curve

in self-piercing riveting," *Science and Technology of Welding and Joining,* vol. 17, no. 6, pp. 476-488, 2012.

[15] A. Salisbury, "Design, Evaluation and Inspection of Self-Pierce Riveted Joints," Henrob, 2011.

[16] N. H. Hoang, H. A. G, M. Langseth and R. Porcaro, "Structural behavior of aluminum self-piercing riveted joints: An experimental and numerical investigation," *International Journal of Solid and Structures,* vol. 49, pp. 3211-3223, 2012.

[17] J. J. Bikermann, The Science of Adhesive Joints, New York: Academic Press, 1961.

[18] M. J. Davis and D. A. Bond, "The Importance of failure mode indentification in adhesive bonded aircraft structure and repairs," Royal Australian Air Force, Melbourne.

[19] "Adhesive.org," Adhesives and Sealant Council, 2014. [Online]. Available: http://www.adhesives.org/adhesives-sealants/science-of-adhesion/adhesion-cohesion. [Accessed 30 5 2014].

[20] "Adhesive.org," Adhesives and Sealant Council, 2014. [Online]. Available: http://www.adhesives.org/adhesives-sealants/adhesives-sealants-overview/adhesive-technologies/chemically-curing#heat. [Accessed 31 5 2014].

[21] M. Lucic, A. Stoic and J. Kopac, "Investigation of aluminum single lap adhesively bonded joints," in *International Scientific Conference on Contemporary Achivements in Mechanics, Manufacturing and Material Science*, GLiwice-Zakopane, Poland, 2005.

[22] "Adhesives Design Toolkit," [Online]. Available: http://www.adhesivestoolkit.com/Docs/test/MECHANICAL%20TEST%20METHOD%201_files/image002.jpg. [Accessed 31 5 2014].

[23] R. D. S. G. Campilho, A. M. G. Pinto, M. D. Banea and L. F. M. da Silva, "Optimization Study of Hybrid Spot-Welded/Bonded Single - lap Joints," *International Journal of Adhesion & Adhesive,* pp. 86-95, 2012.

[24] A. Al-Samhan and S. M. H. Darwish, "Strength prediction of weld bonded joints," *International Journal of Adhesion and Adhesives,* pp. 23-28, 2003.

[25] F. Moroni, A. Pirondi and F. Kliener, "Experimental analysis and comparison of the strength of simple and hybrid structural joints," *International Journal of Adhesion & Adhesives,* pp. 367-379, 2010.

[26] B. Chang, Y. Shi and S. Dong, "Comparative studies on stresse in weld-bonded, spot-welded and adhesive-bonded joints," *Journal of Material Processing Technology,* pp. 230-236,

1999.

[27] B. H. Chang, Y. W. Shi and S. J. Dong, "A study on the Role of Adhesive in Weld-Bonded Joints," *Welding Research ,* pp. 275s-279s, 1999.

[28] S. Gomez, J. Onoro and J. Pecherroman, "A simple mechanical model of a structural hybrid adhesive/riveted single lap joint," *Internationl Journal of Adhesion and Adhesive,* pp. 263-267, 2007.

[29] R. Porcaro, A. G. Hanssen, M. Langseth and A. Aalberg, "The behaviour of a self-piercing riveted connection under quasi-static conditions," *International Journal of Solids and Structures,* pp. 5110-5131, 2006.

[30] S. M. Darwish, "Characteristics of weld-bonded commercial aluminum sheets (B.S. 1050)," *International Journal of Adhesion &Adhesives,* pp. 169-176, 2003.

[31] D. J. Radakovic and M. Tumuluru, "An Evaluation of the Cross-Tension Test of Resistance Spot Welds in High-Strength Dual-Phase Steel," *Welding Journal,* pp. 8s-15s, 2012.

[32] G. Booth, C. Oliver, S. Westgate, F. Liebrecht and G. Braunling, "Self-piercing reiveted joints and resistance spot welded joints in steel and aluminum," in *International Body Engineering Conference*, Detroit, MI, 2000.

[33] L. Han, M. Thorton and M. Shergold, "A comparison of the mechanical behaviour of self-piercing riveted and resistance spot welded aluminum sheets for the automotive industry," *Material and Design,* pp. 1459-1467, 2010.

[34] P. Briskham, N. Blundell, L. Han, R. Hewitt and Y. Ken, "Comparison of the self-pierce riveting, resistance spot welding and spot friction joining for aluminum automotive sheet," *SAE International,* 2006.

[35] B. Bartczak, J. Mucha and T. Trzepiecinski, "Stress distribution in adhesively-bonded joints and the loading capacity of hybrid joints of car body steels for the automotive industry," *International Journal of Adhesion & Adhesives,* vol. 45, pp. 42-52, 2013.

[36] Y. Liu, L. Zhang, W. Liu and P. Wang, "Single-sided piercing riveting for adhesive bonding in vehicle body assembly," *Journal of Manufacturing System,* vol. 32, pp. 498-504, 2013.

[37] S. M. Darwish and A. Al-Samhan, "Design rationale of weld-bonded joint," *International Journal of Adhesion & Adhesive,* pp. 367-377, 2003.

[38] M. D. Gilchrist and R. A. Smith, "Development of cohesive fatigue cracks in T-peel joints," *International Journal of Adhesion and Adhesive,* vol. 13, no. 1, pp. 53-57, 1993.

[39] S. M. Darwish and A. M. Al-Samhan, "Peel and Shear strength of spot-welded and weld-

bonded dissimilar thickness joints," *Journal of Material Processing Technology,* pp. 51-59, 2004.

[40] Y. J. Chao, "Failure mode of spot welds: interfacial versus pullout," *Science and Technology of Welding and Joining,* vol. 8, no. 2, pp. 133-137, 2003.

[41] X. Sun, V. Stephens, R. W. Davies, M. A. Khaleel and D. J. Spinella, "Effect of Fusion Zone Size on Failure Modes and Static Strength of Aluminum Resistance Spot Weld," *Welding Journal,* pp. 308-318, 2004.

[42] S. M. Darwish and S. D. Al-Dekhial, "Micro-hardness of spot welded (B.S. 1050) commercial aluminium as correlated with welding variables and strength attributes," *Journal of Material Processing Technology,* vol. 91, pp. 43-51, 1999.

[43] E. Atzeni and L. Settineri, "Experimental and numerica appraisal of self-piercing riveting," *Cirp Annals - Manufacturing Technology,* vol. 58, pp. 17-20, 2009.

[44] Y. J. Chao, "Ultimate Strength and Failure Mechanism of Resistance Spot Weld Subjected to Tensile, Shear or Combined Tensile/Shear Loads," *Journal of Engineering Materials and Technology,* vol. 125, pp. 125-133, 2003.

[45] L. Goglio, M. Rossetto and E. Dragoni, "Design of adhesive joints based on peak elastic stresses," *International Journal of Adhesion & Adhesives,* vol. 28, pp. 427-435, 2008.

[46] D. A. Bigwood and A. D. Crocombe, "Elastic analysis and engineering design formulae for bonded joints," *Internaltional Journal of Adhesion and Adhesive,* vol. 9, no. 4, pp. 229-242, 1989.

[47] S. Zhang, "Stress intensities at spot welds," *International Journal of Fracture,* vol. 88, pp. 167-185, 1997.

[48] J. W. van Ingen and A. Vlot, "Stress Analysis of Adhesively Bonded Single Lap Joints," Delft University of Technology, Delft, 1993.

[49] S. H. Lin, J. Pan, T. Tyan and P. Prasad, "A general failure criterion for spot welds under combined loading openingq," *Interntional Journal of Solids and Structures,* vol. 40, pp. 5539-5564, 2003.

[50] S. H. Lin, J. Pan, S. R. Wu, T. Tyan and P. Wung, "Failure Loads of spot welds under combined opening and shear static loading conditions," *International Journal of Solids and Structures,* vol. 39, pp. 19-39, 2002.

[51] X. Sun and M. A. Khaleel, "Strength estimation of self-piercing rivets using lower bound limit load analysis," *Science and Technology of Welding and Joining,* vol. 10, no. 5, pp. 624-635, 2005.

[52] "MatWeb-Material Property Data," [Online]. Available: http://www.matweb.com/search/datasheet.aspx?matguid=79cd55e17b2648409398393c4e47bb45. [Accessed 17 July 2014].

[53] F. A. Conle, "Plasticity Corrections for Elastic Analysis Results: Neuber Method," 2010 November 2010. [Online]. Available: http://fde.uwaterloo.ca/Fde/Notches.new/neuber.html. [Accessed 18 June 2014].

[54] "Create fatigue curves from torsion tests," [Online]. Available: http://fde.uwaterloo.ca/Fde/Calcs/tor2axial.gif. [Accessed 30 July 2014].

[55] S. Smith and J. Vrenken, "Structural performance of adhesive and weld bonded joints in AHSS," TATA, Bad Nauheim, 2011.

[56] E. A. Association, "Joining - fusion welding," *The Aluminum Automotive manual,* 2002.

[57] W. Hou, E. Mangialardi, E. Hu, S. J. Wang and R. Menassa, "Characterization for quality monitoring of a self-pierce riveting process," in *Sheet Metal Welding Conference XI* , Sterling Heights, MI, 2004.

APPENDICES

8.1 Appendix A

Load vs. Displacement curves

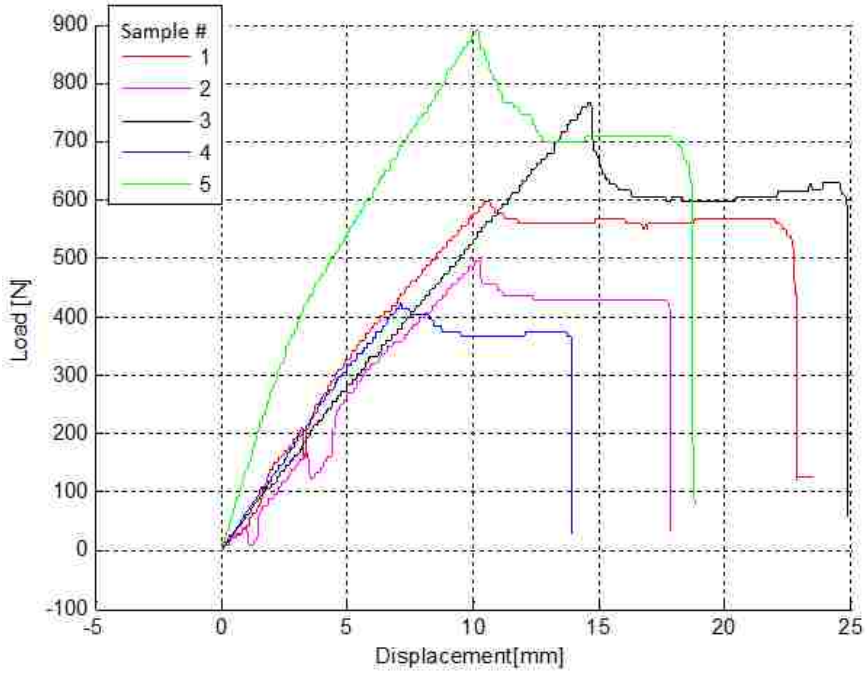

Figure 8-1. Load - displacement curves 1.3mm Coach Joint RSW no-adhesive

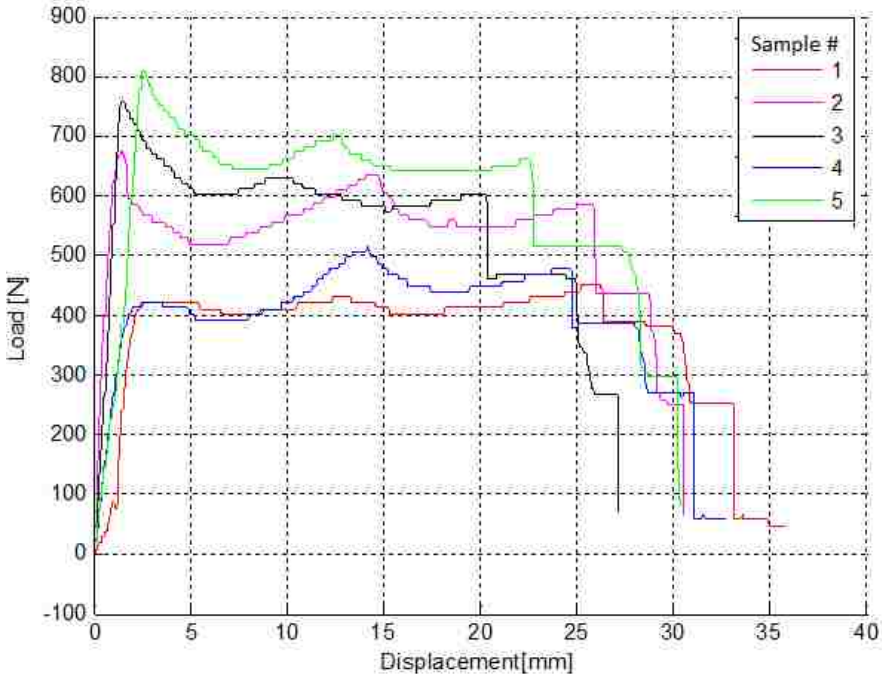

Figure 8-2. Load - Displacement curves 1.3 mm Coach Joint RSW + SIKAPOWER 497

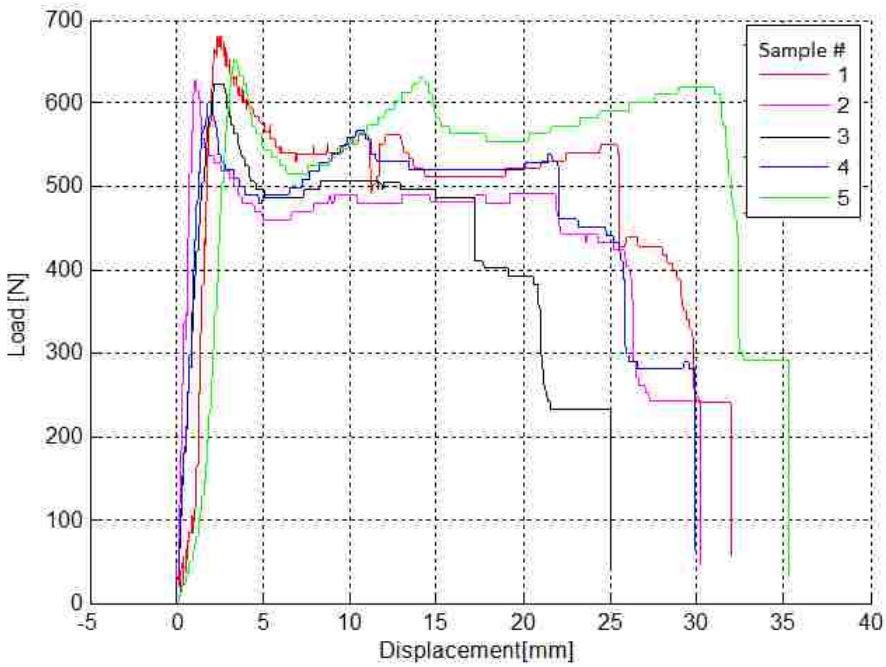

Figure 8-3. Load - Displacement curves 1.3 mm Coach Joint RSW + DOW Betamate 1620US

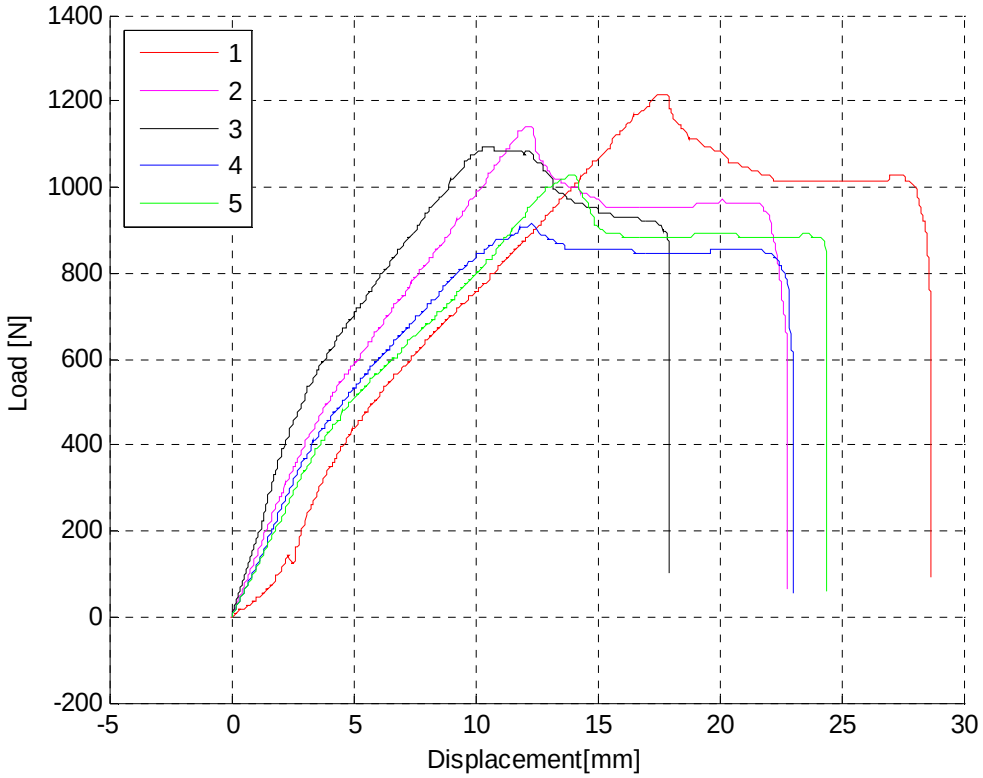

Figure 8-4. Load - displacement curves 1.75 mm Coach Joint RSW no-adhesive

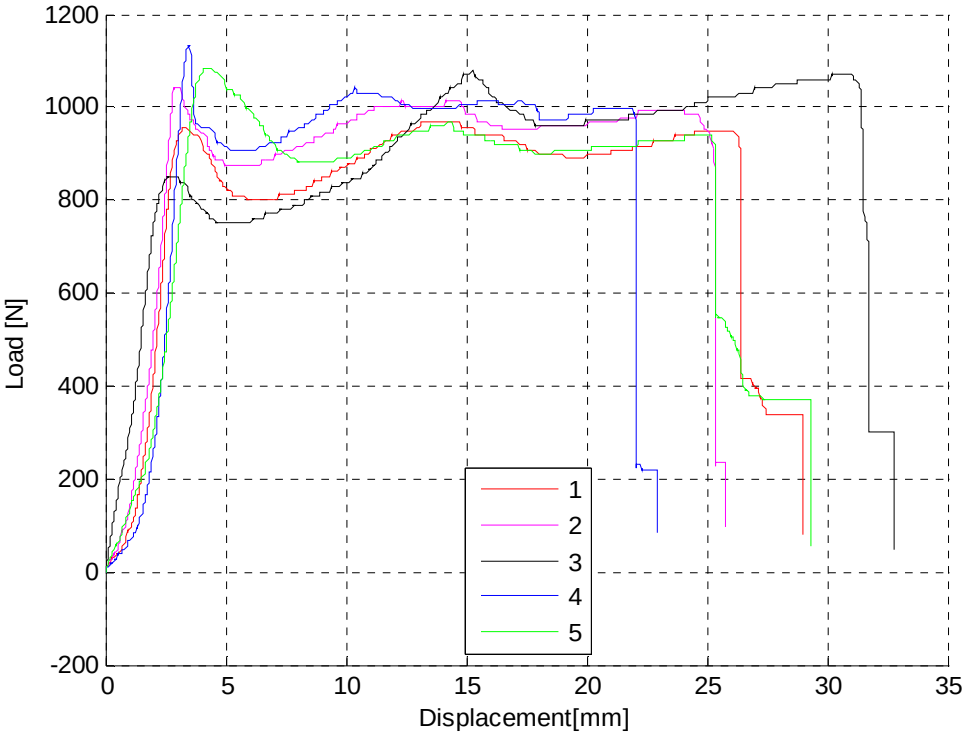

Figure 8-5. Load - Displacement curves 1.75 mm Coach Joint RSW + SIKAPOWER 497

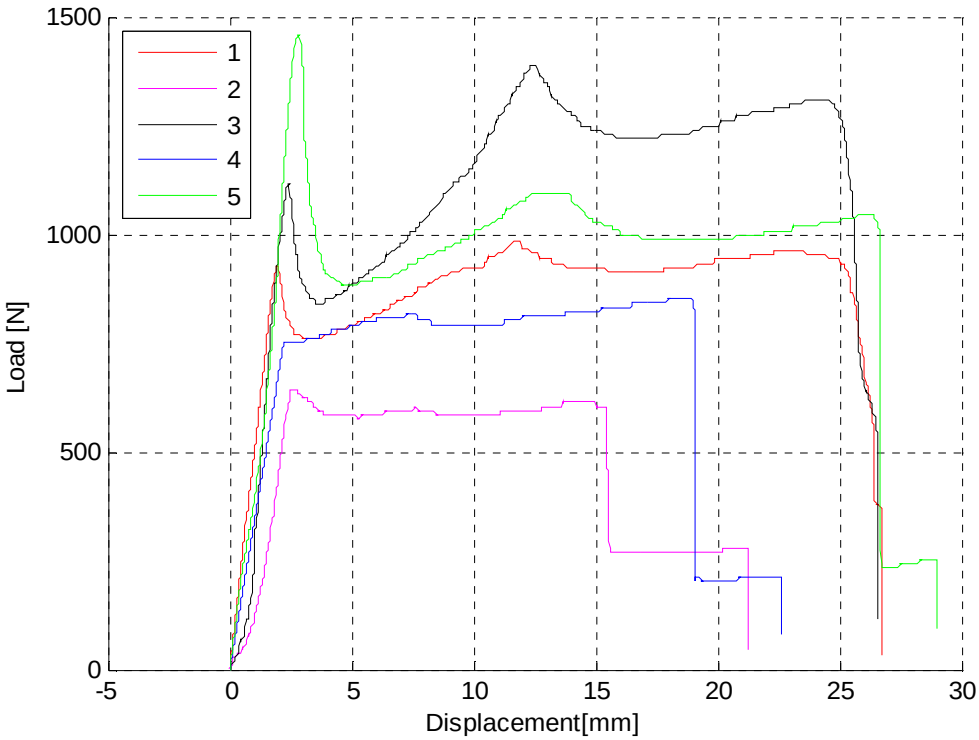

Figure 8-6. Load - Displacement curves 1.75 mm Coach Joint RSW + DOW Betamate 1620US

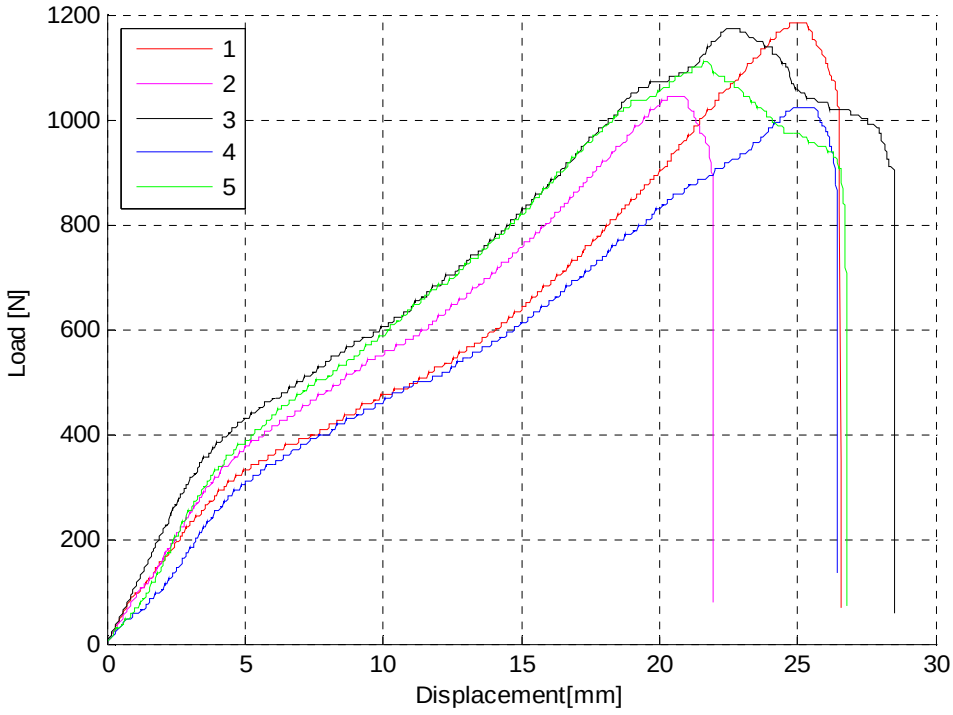

Figure 8-7. Load - Displacement curves 1.3 mm Coach Joint SPR + NA

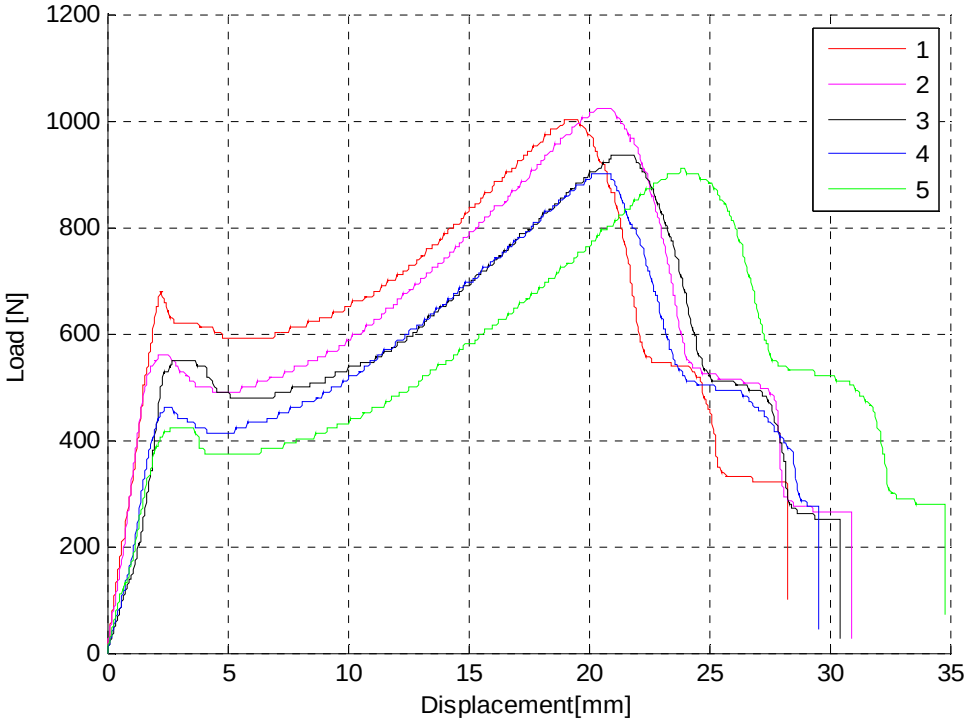

Figure 8-8. Load - Displacement curves 1.3 mm Coach Joint SPR + SIKAPOWER 497

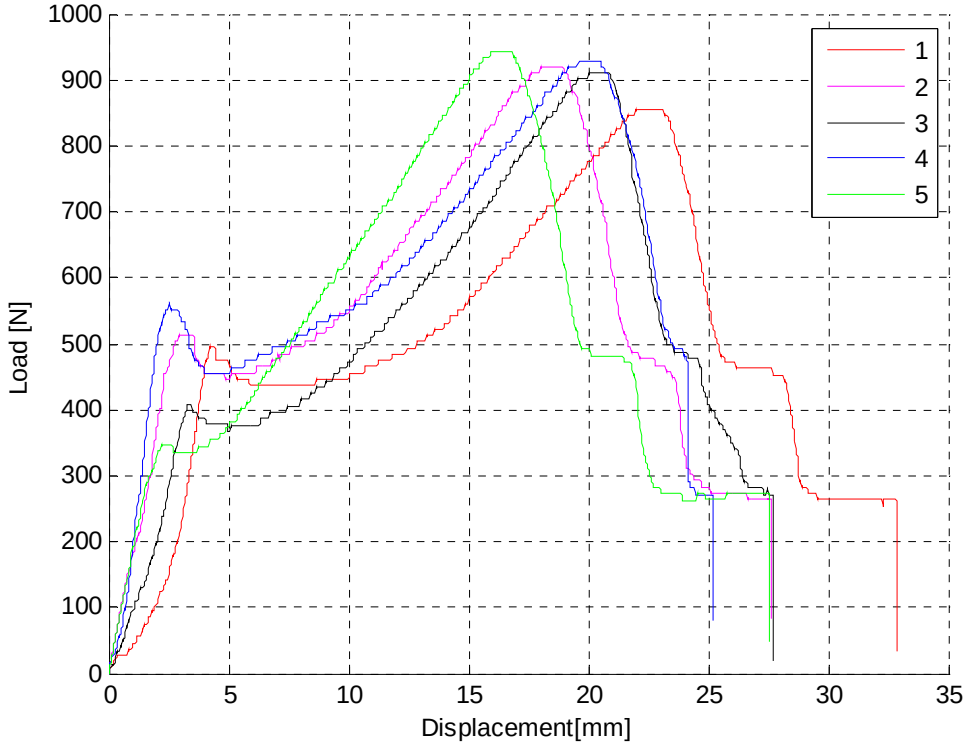

Figure 8-9. Load - Displacement curves 1.3 mm Coach Joint SPR + DOW Betamate 1620US

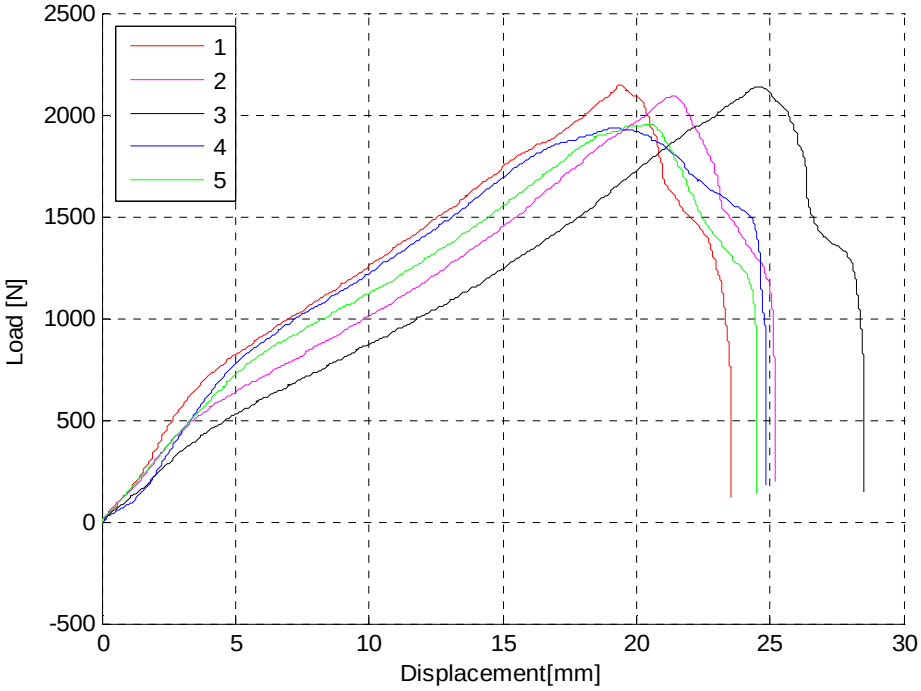

Figure 8-10. Load - Displacement curves 1.75 mm Coach Joint SPR + NA

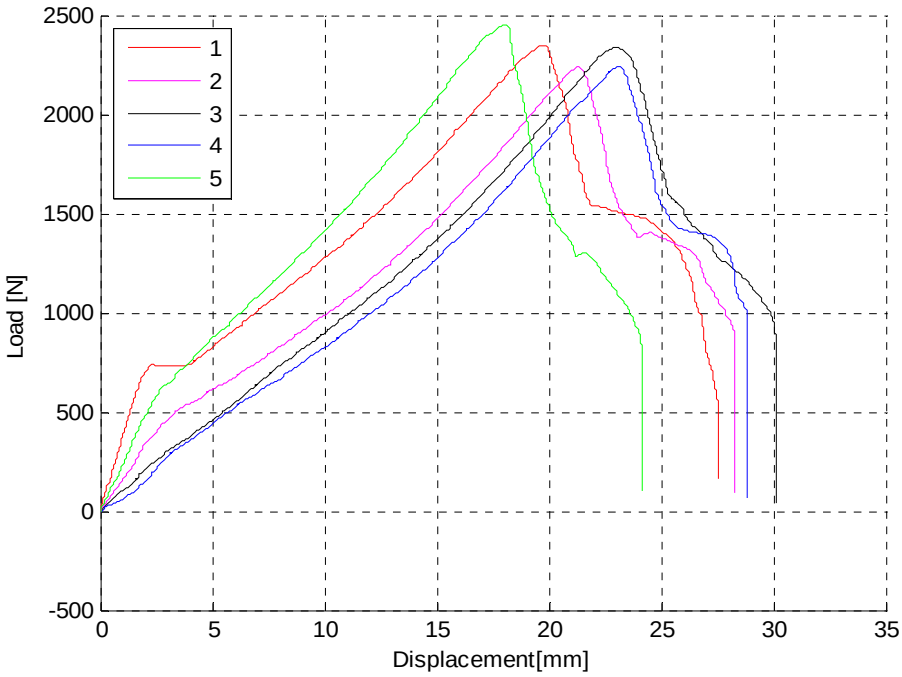

Figure 8-11. Load - Displacement curves 1.75 mm Coach Joint SPR + SIKAPOWER 497

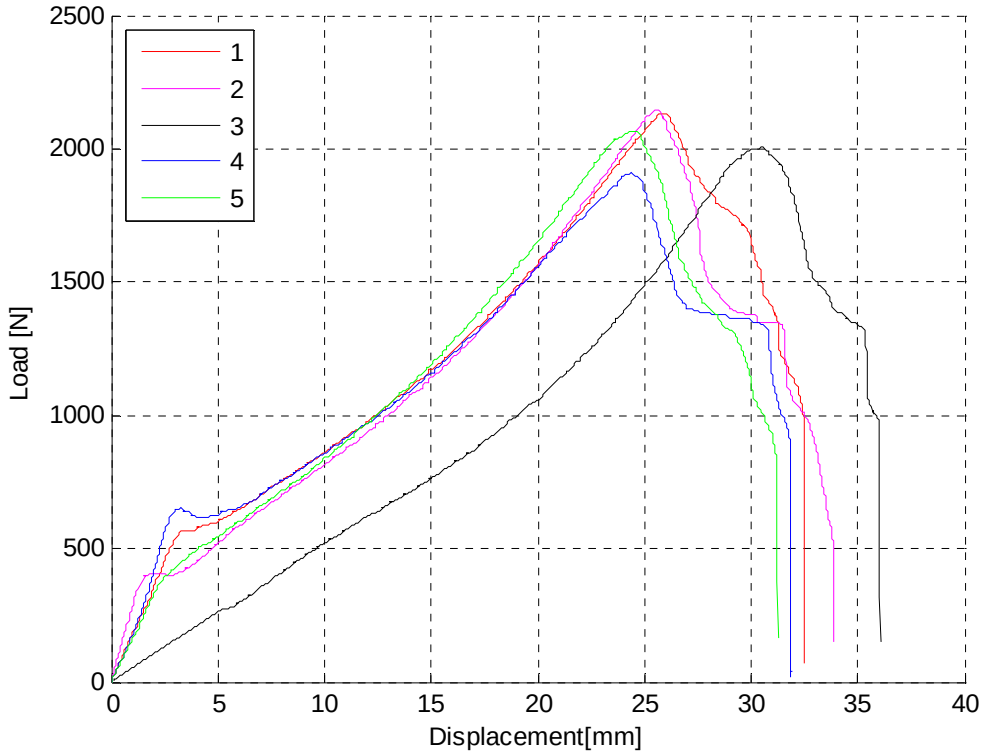

Figure 8-12. Load - Displacement curves 1.75 mm Coach Joint SPR + DOW Betamate 1620US

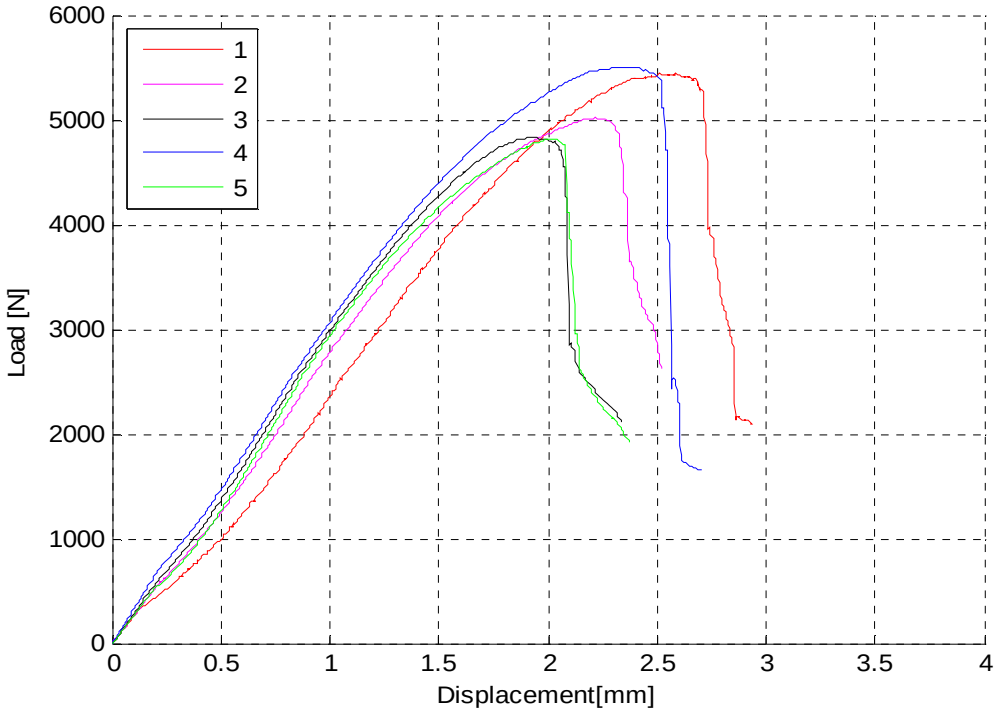

Figure 8-13. Load - Displacement curves 1.3 mm Lap Joint RSW Na

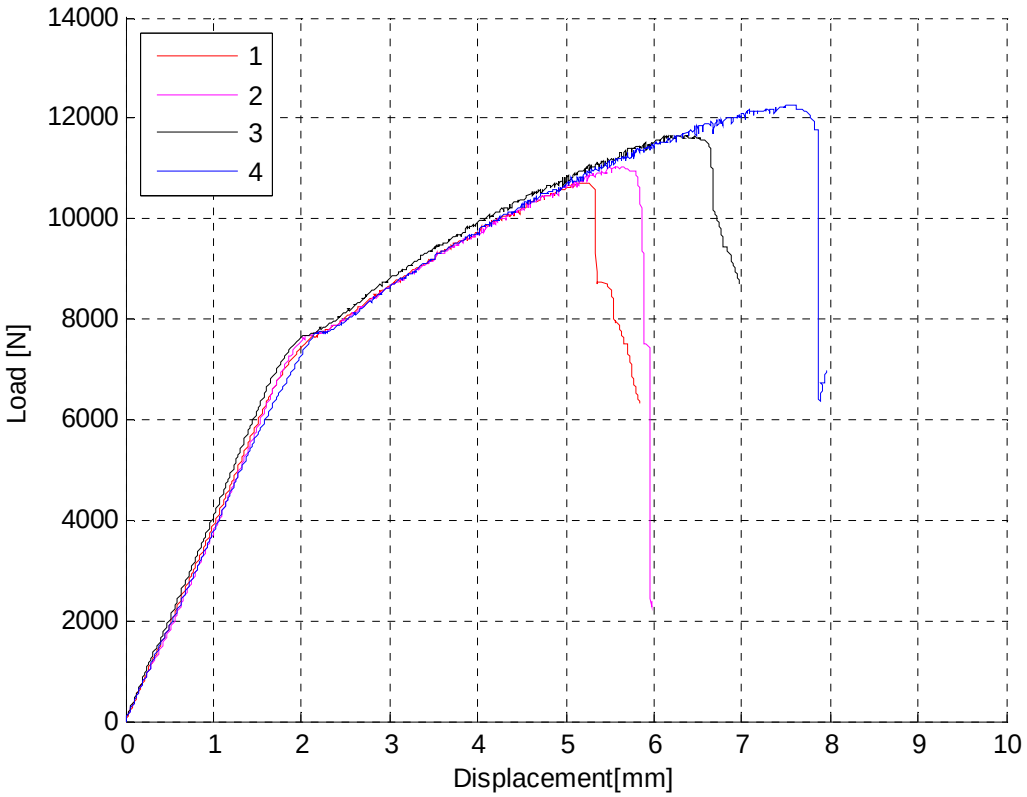

Figure 8-14. . Load - Displacement curves 1.3 mm :Lap Joint RSW + SIKAPOWER 497

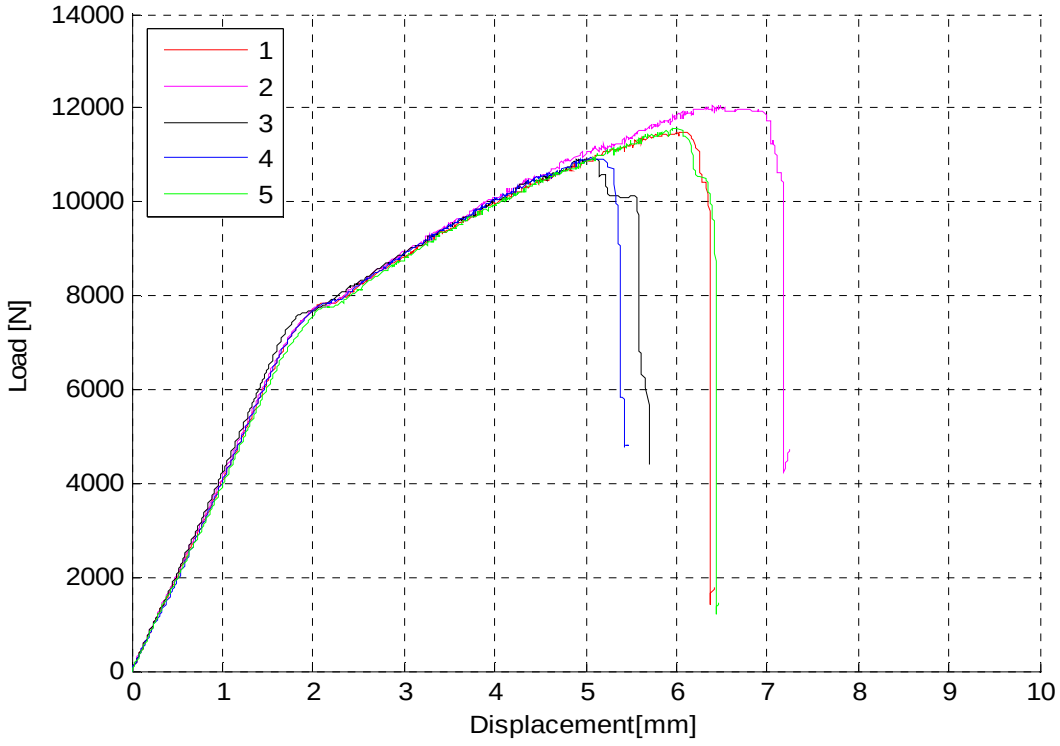

Figure 8-15. Load - Displacement curves 1.3 mm :Lap Joint RSW + DOW Betamate 1620US

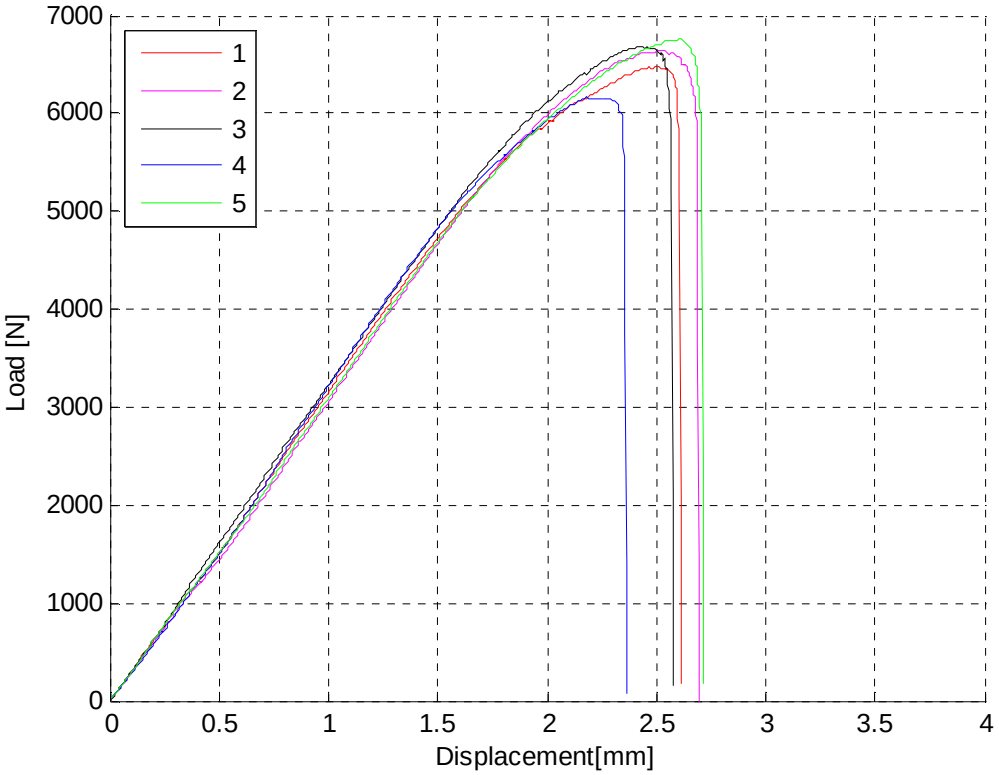

Figure 8-16. Load - Displacement curves 1.75 mm :Lap Joint RSW Na

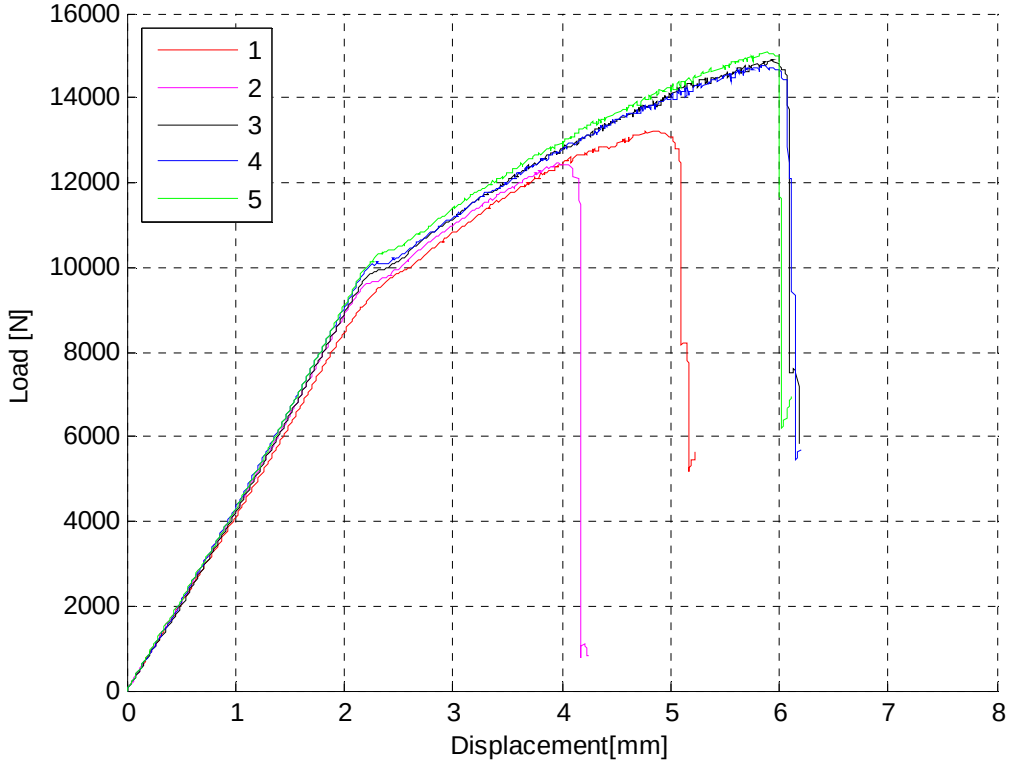

Figure 8-17. Load - Displacement curves 1.75 mm : Lap Joint RSW + SIKAPOWER 497

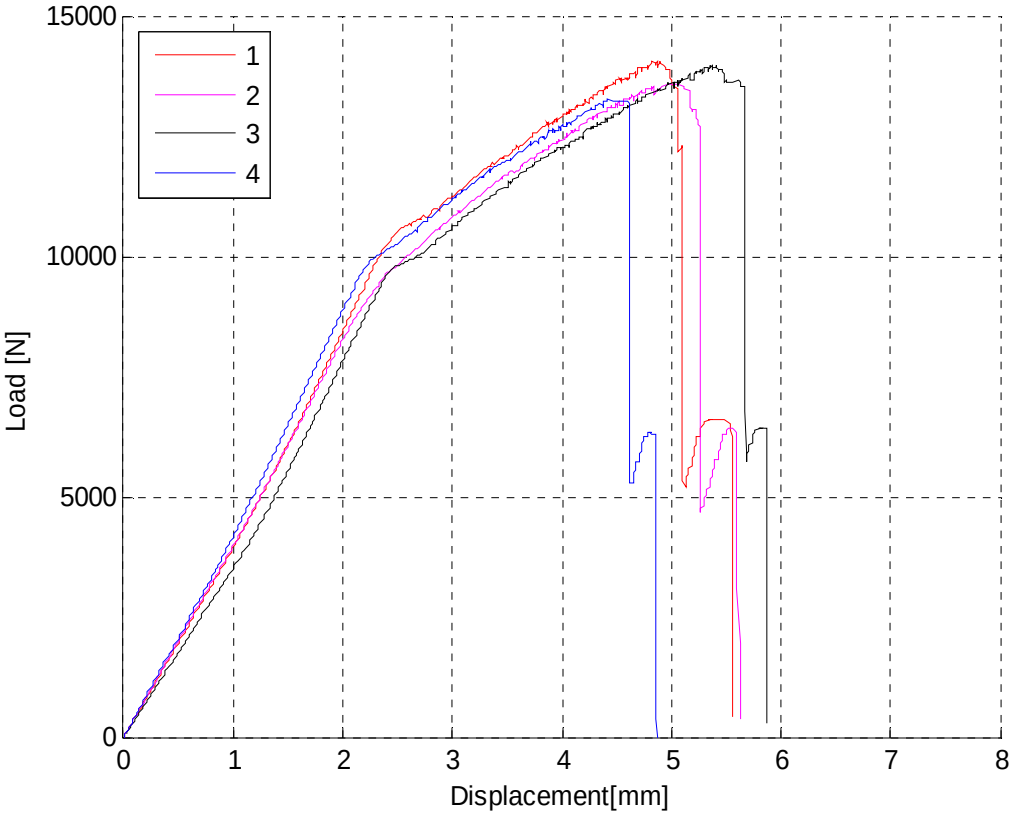

Figure 8-18. Load - Displacement curves 1.75 mm : Lap Joint RSW + DOW Betamate 1620US

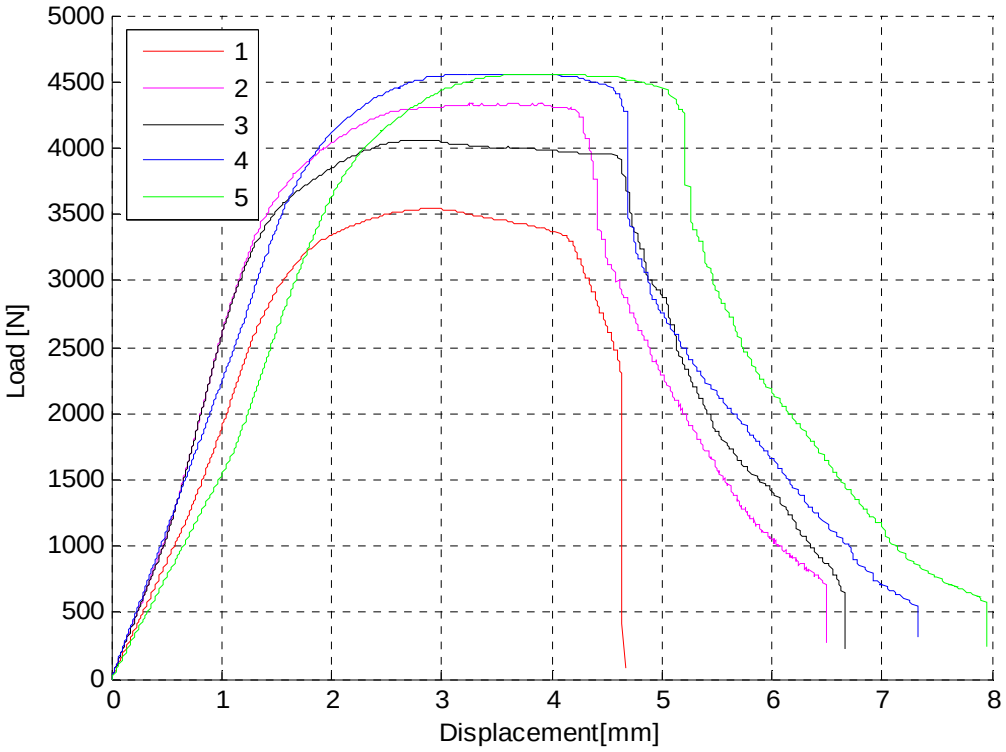

Figure 8-19. . Load - Displacement curves 1.3 mm Lap Joint SPR Na

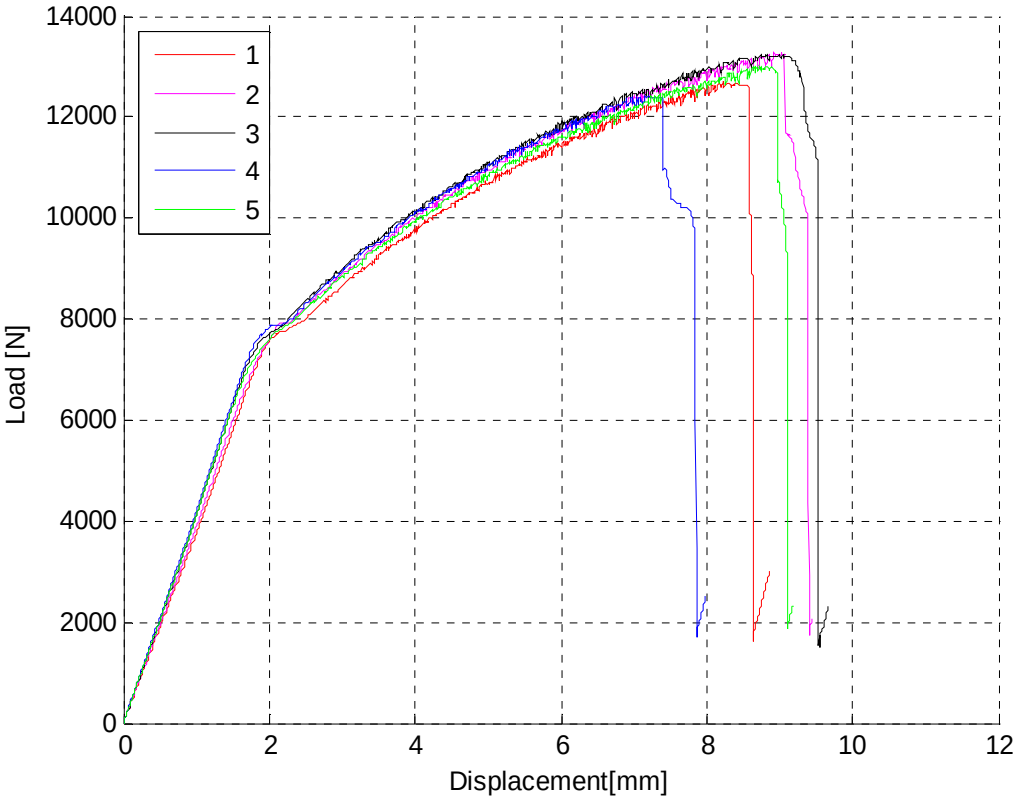

Figure 8-20. Load - Displacement curves 1.3 mm : Lap Joint SPR + SIKAPOWER 497

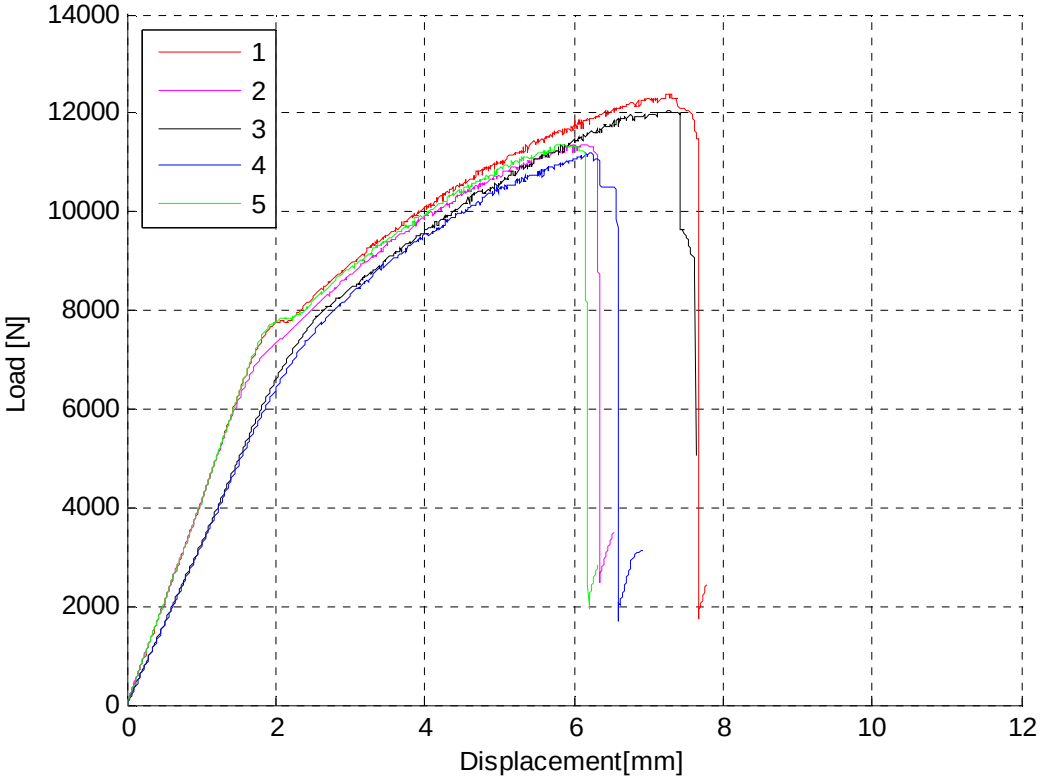

Figure 8-21. Load - Displacement curves 1.3mm Lap Joint SPR + DOW Betamate 1620US

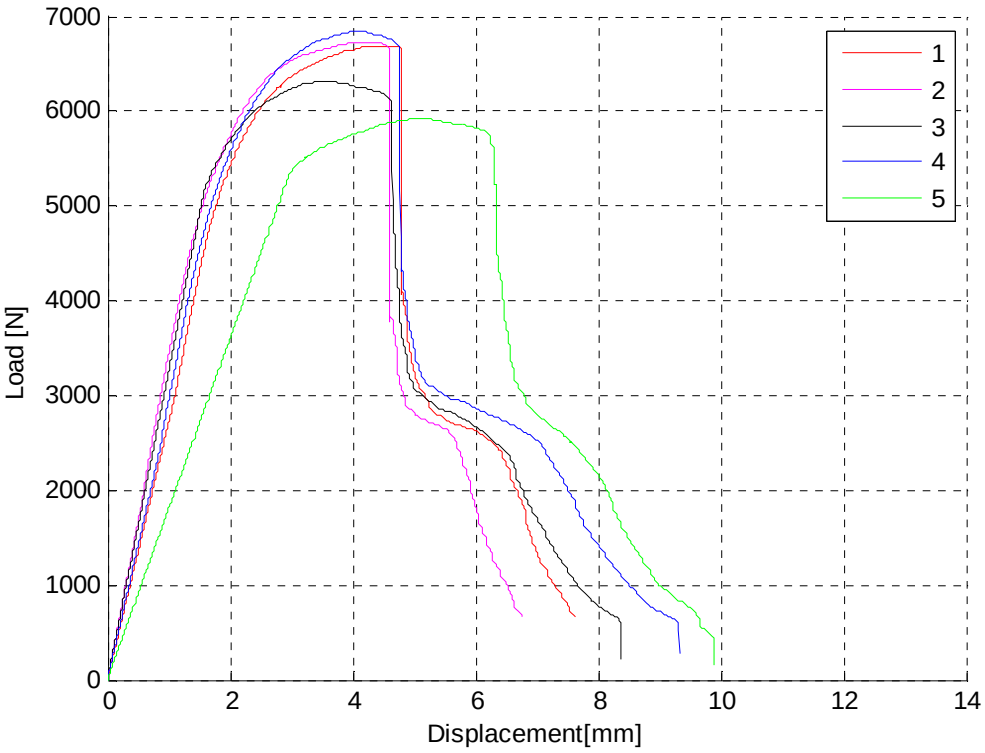

Figure 8-22. Load - Displacement curves 1.75 mm Lap Joint SPR Na

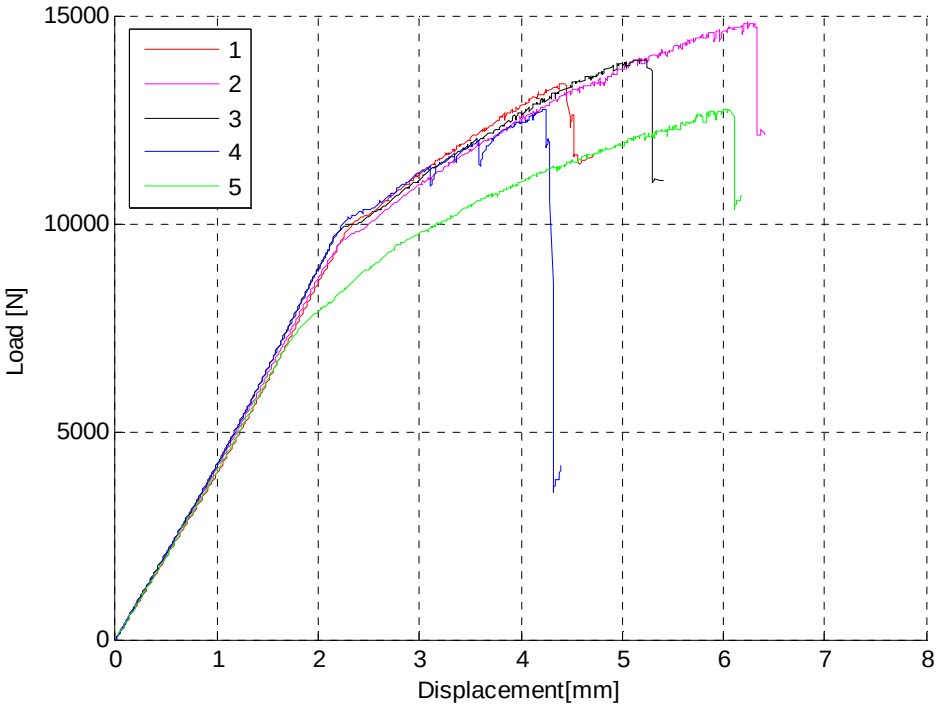

Figure 8-23. Load - Displacement curves 1.75 mm : Lap Joint SPR + SIKAPOWER 497

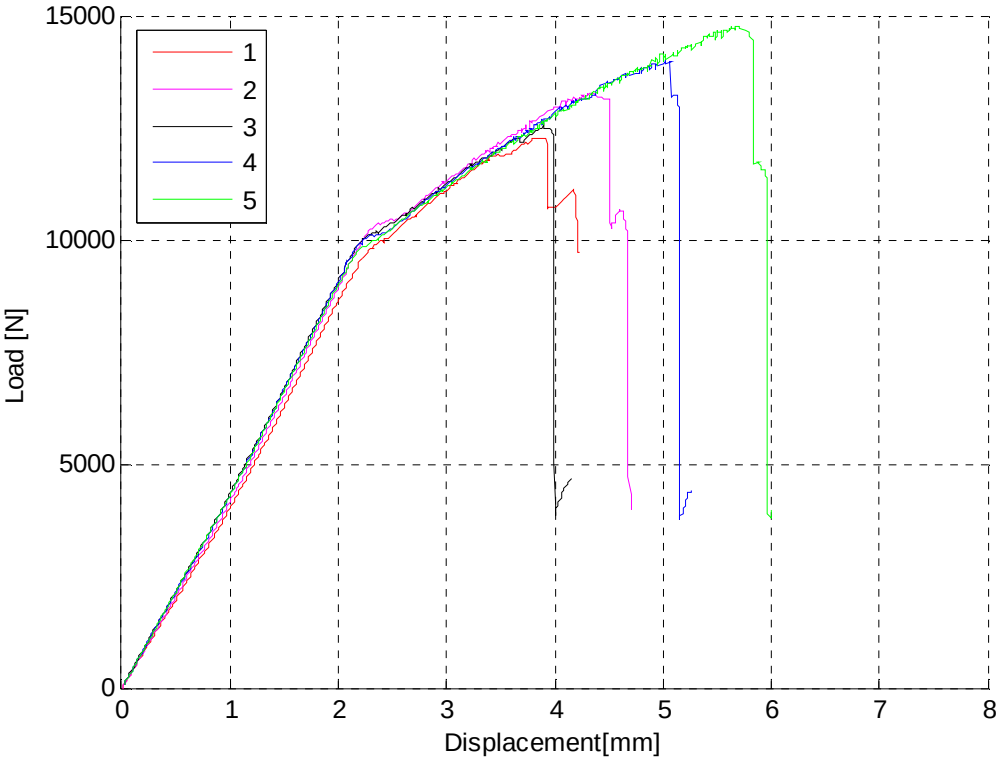

Figure 8-24. Load - Displacement curves 1.3mm Lap Joint SPR + DOW Betamate 1620US

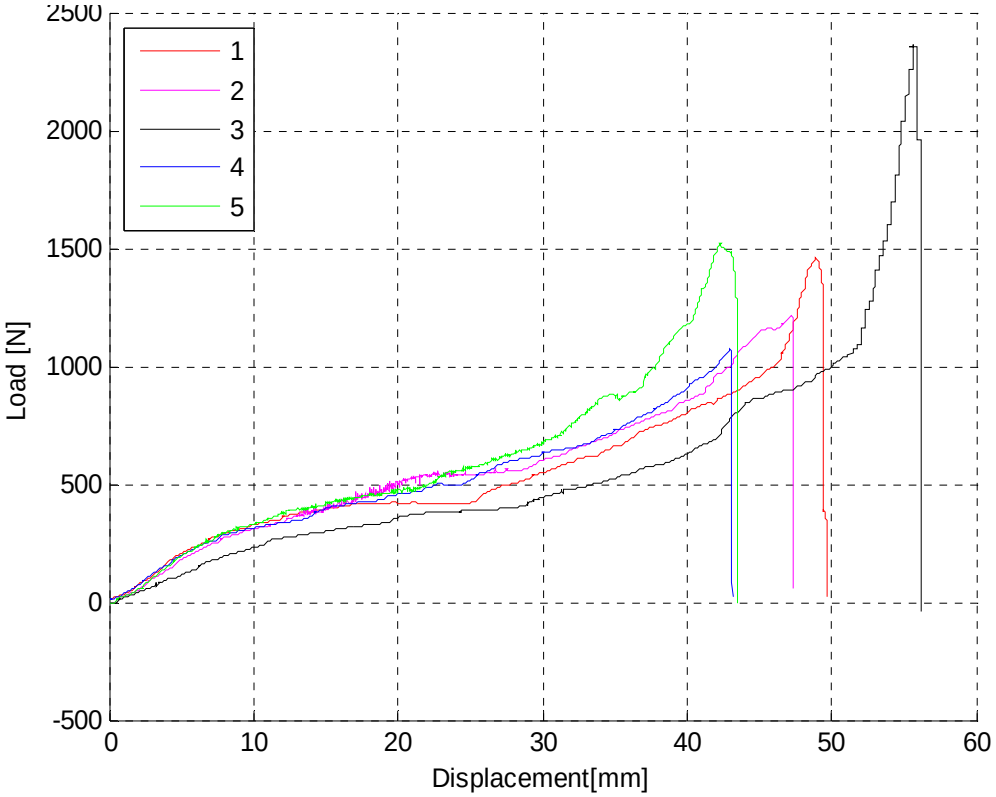

Figure 8-25. . Load - Displacement curves 1.3mm Cross Tension Joint RSW NA

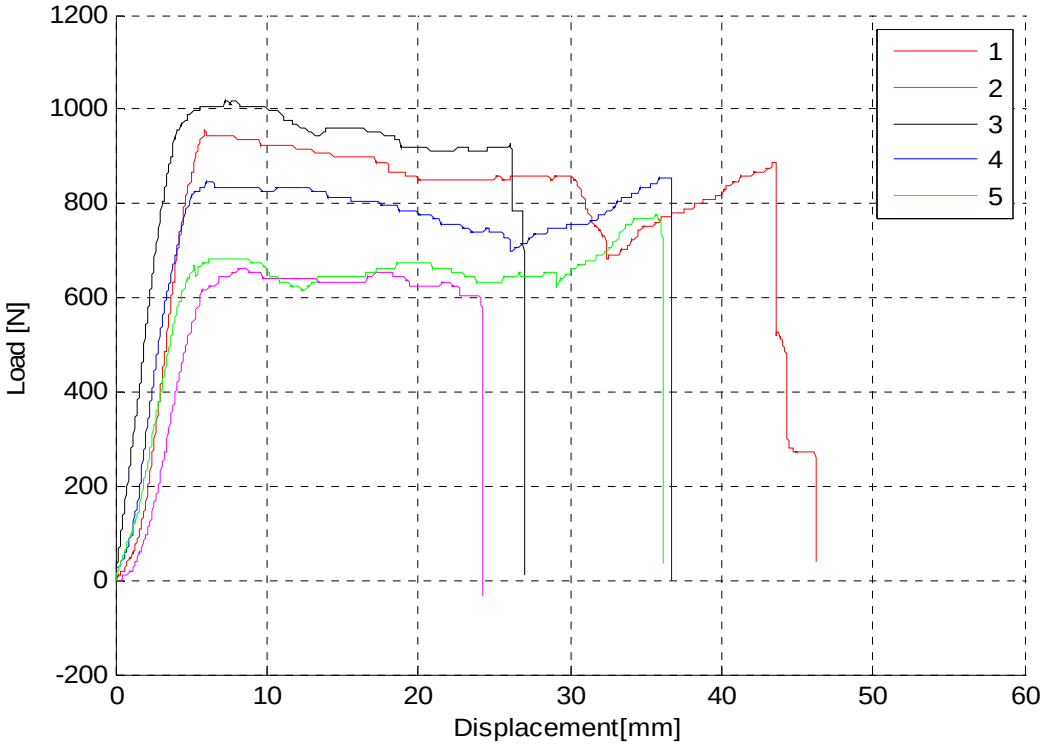

Figure 8-26. Load - Displacement curves 1.3mm Cross Tension Joint RSW + SIKAPOWER 497

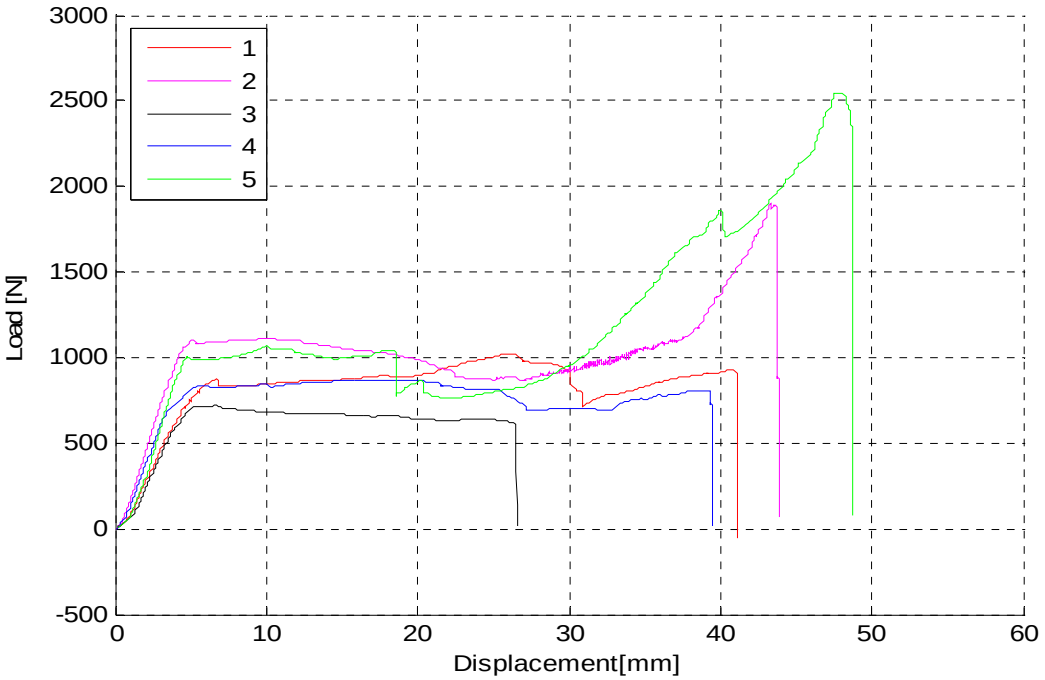

Figure 8-27. Load - Displacement curves 1.3mm Cross Tension Joint RSW + DOW Betamate 1620US

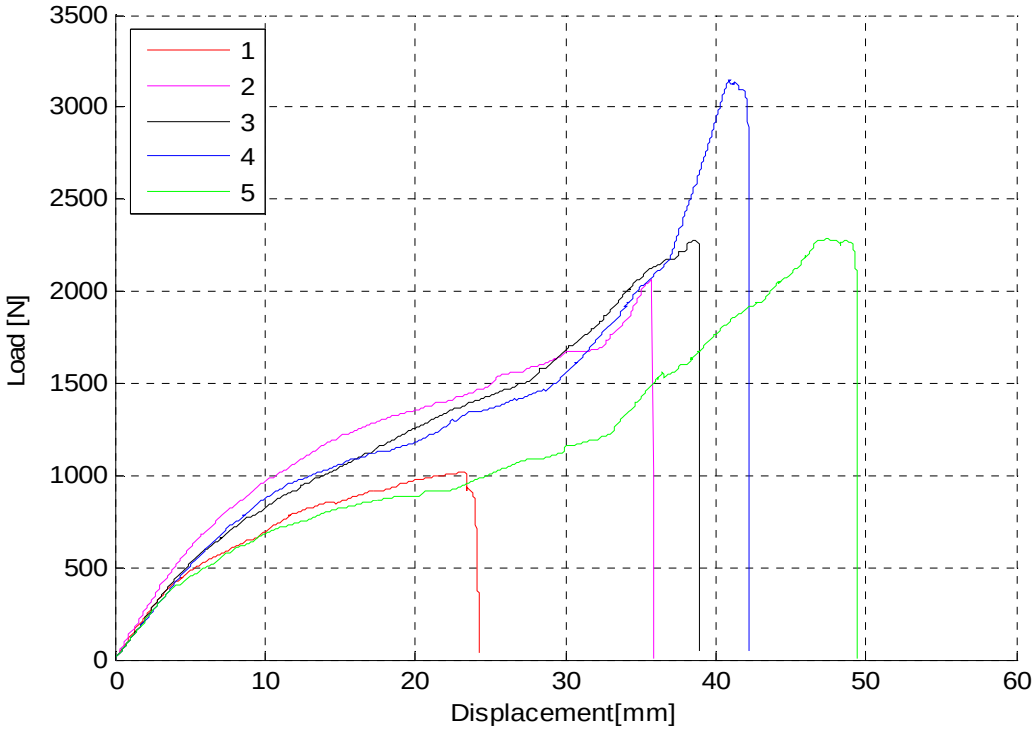

Figure 8-28. Load - Displacement curves 1.75 mm Cross Tension Joint RSW NA

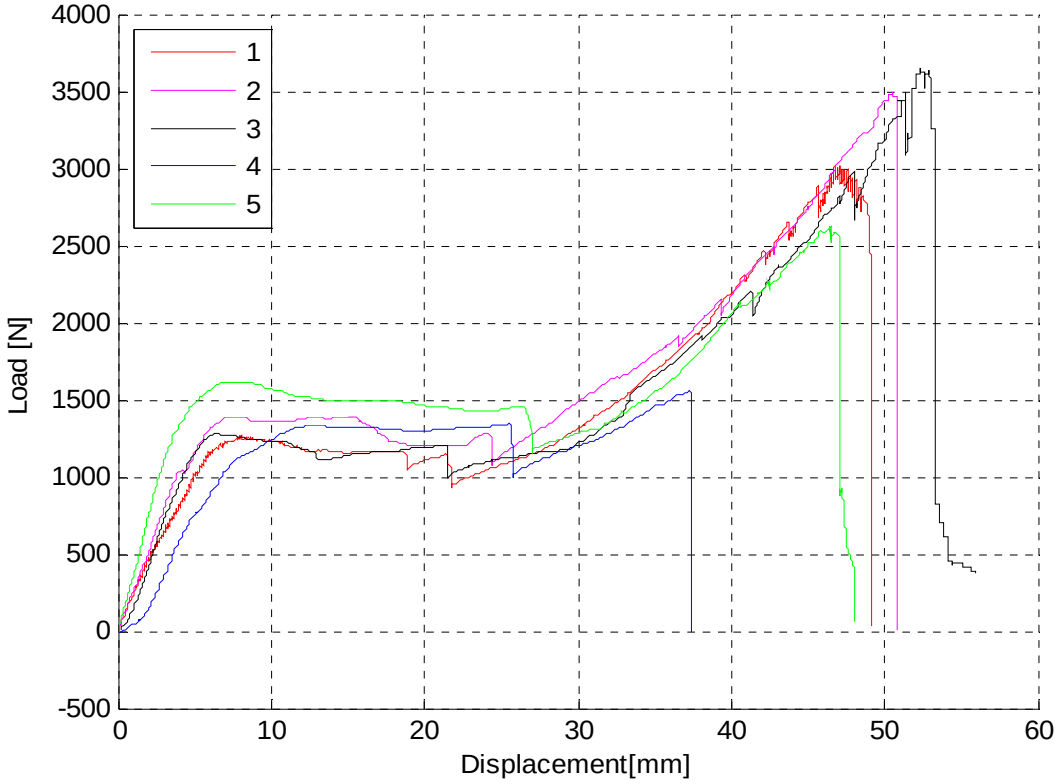

Figure 8-29. Load - Displacement curves 1.75 mm Cross Tension Joint RSW + SIKAPOWER 497

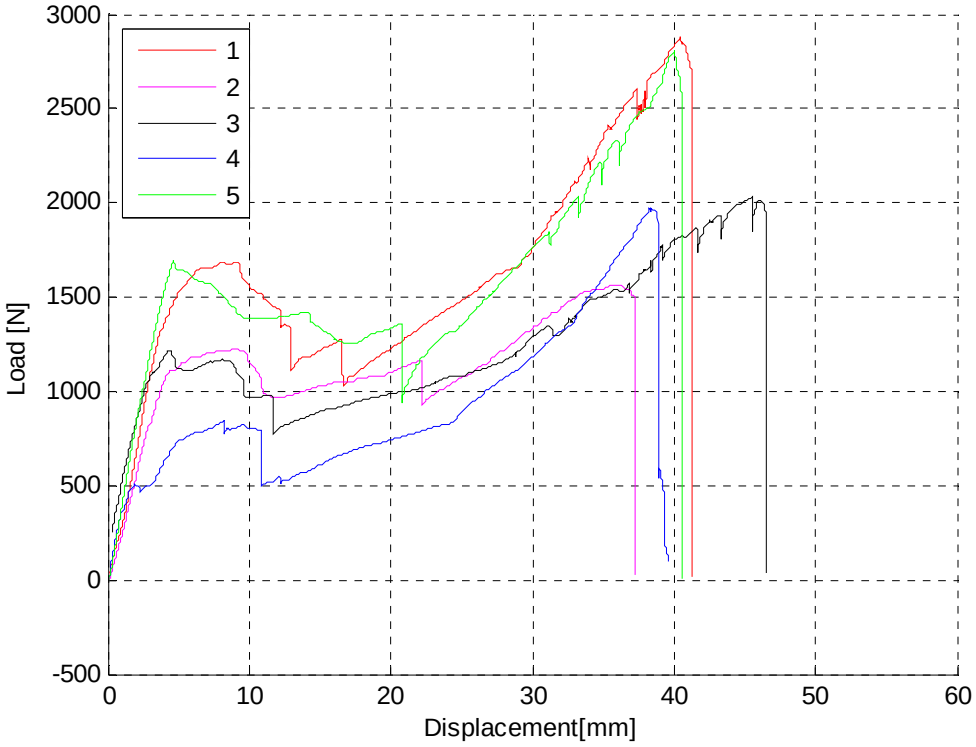

Figure 8-30. Load - Displacement curves 1.75 mm Cross Tension Joint RSW + DOW Betamate 1620US

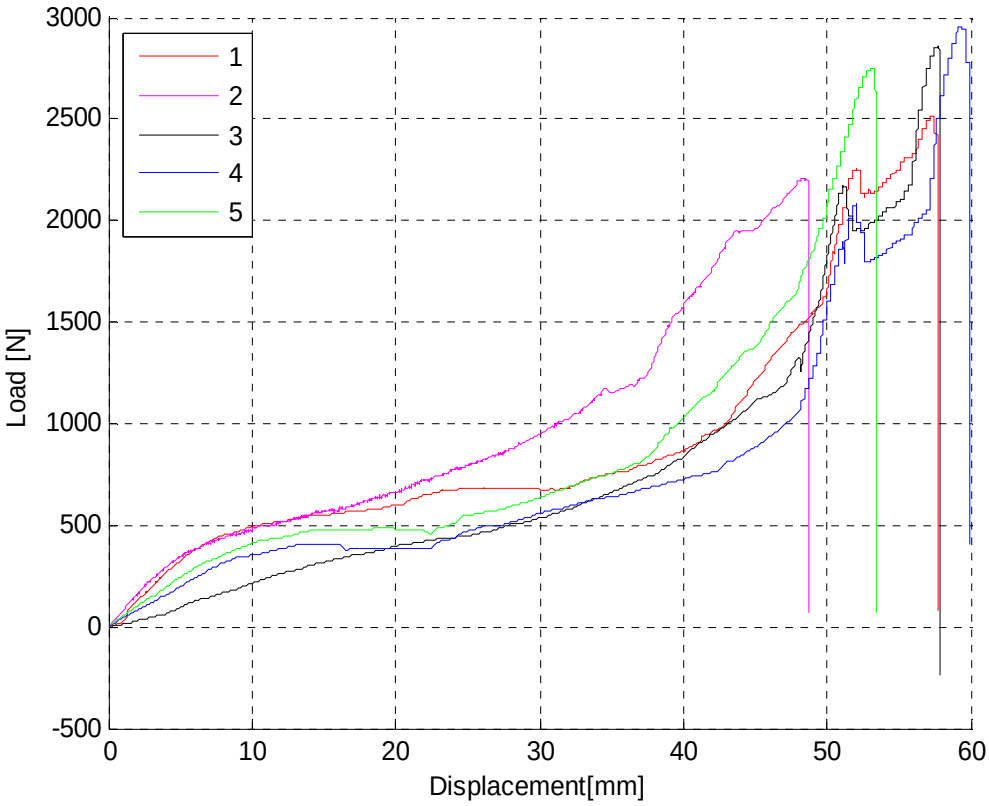

Figure 8-31. Load - Displacement curves 1.3 mm Cross Tension Joint SPR NA

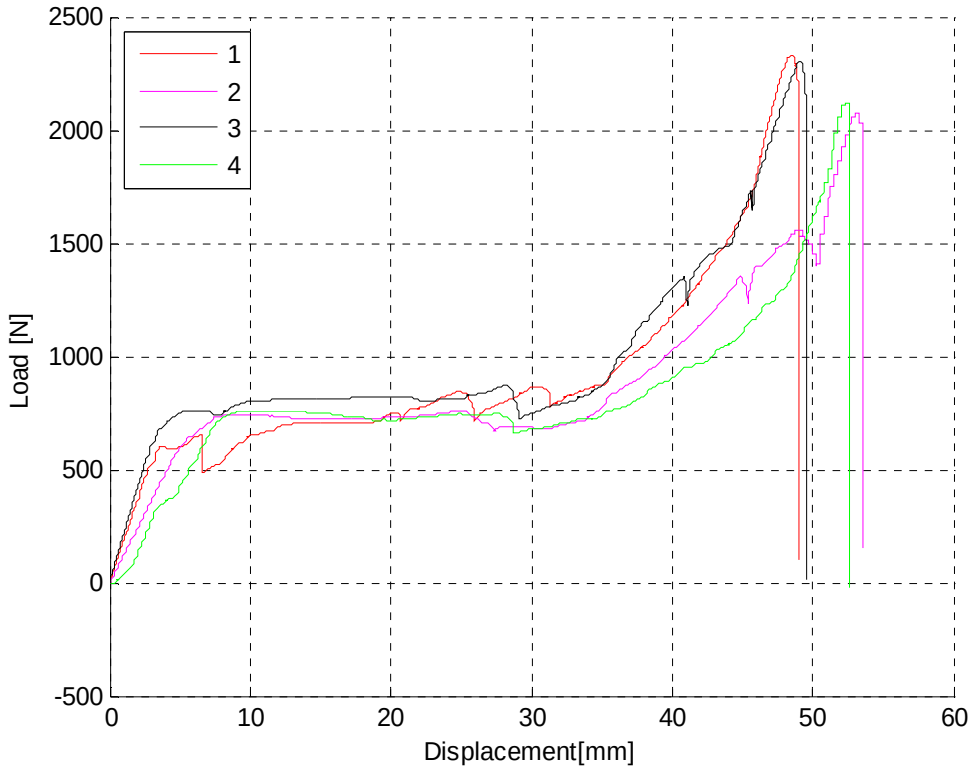

Figure 8-32. Load - Displacement curves 1.3 mm Cross Tension Joint SPR + SIKAPOWER 497

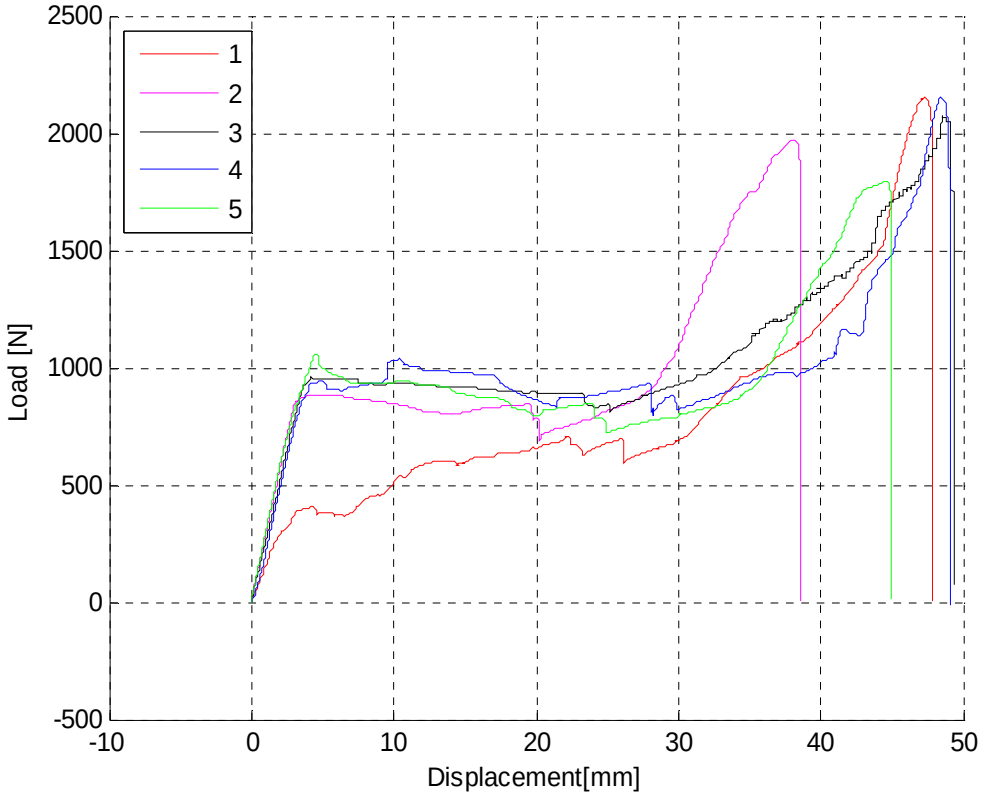

Figure 8-33. Load - Displacement curves 1.3 mm Cross Tension Joint SPR + DOW Betamate 1620US

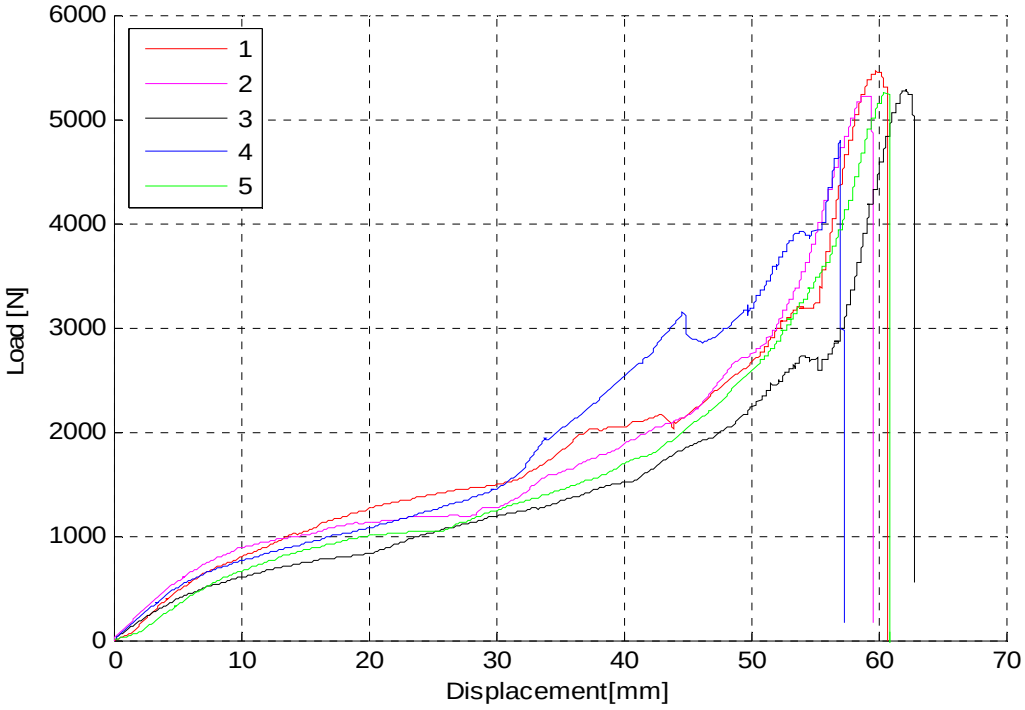

Figure 8-34. Load - Displacement curves 1.75 mm Cross Tension Joint SPR NA

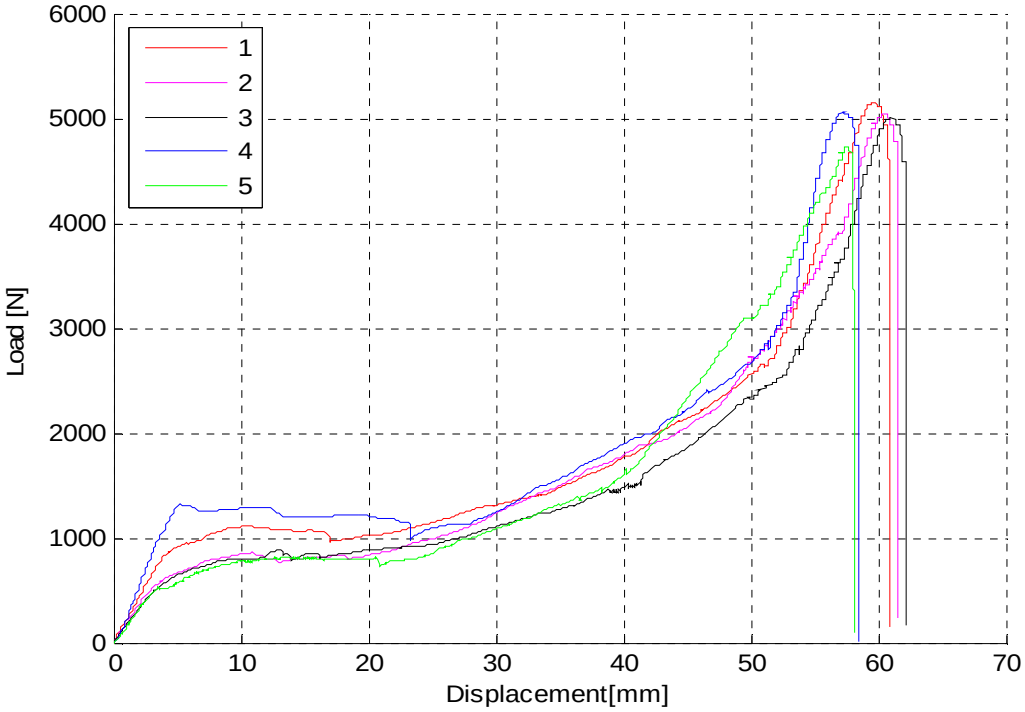

Figure 8-35. Load - Displacement curves 1.75 mm Cross Tension Joint SPR + SIKAPOWER 497

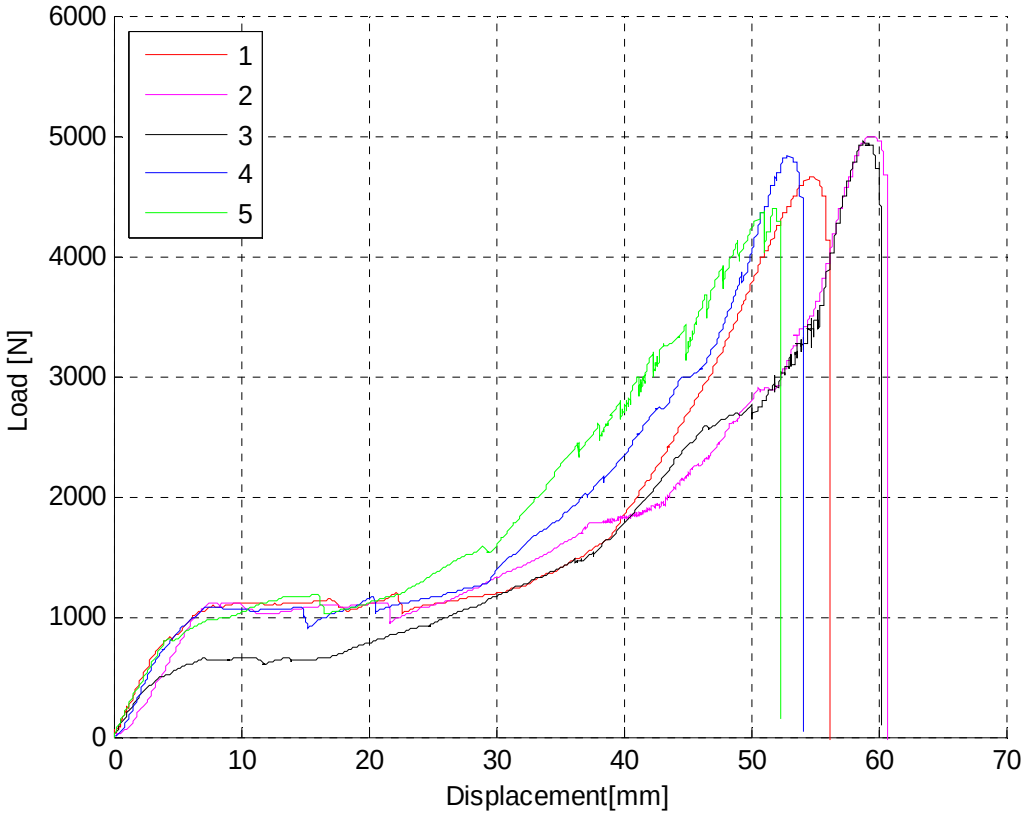

Figure 8-36. Load - Displacement curves 1.75 mm Cross Tension Joint SPR + DOW Betamate 1620US

VITA AUCTORIS

NAME:	Luca Bertin
PLACE OF BIRTH:	Torino, Italy
YEAR OF BIRTH:	1990
EDUCATION:	Politecnico di Torino, B.Sc. in Automotive Engineering, Torino, Italy, 2012.
	Politecnico di Torino, M.A.Sc. in Automotive Engineering, Torino, Italy, 2014.
	University of Windsor, M.A.Sc. in Mechanical Engineering, Windsor, On, Canada, 2014.